IRE Transactions

ON MILITARY ELECTRONICS

Volume MIL-5 October, 1961 Number 4

MISSILE AND SPACE RANGE INSTRUMENTATION

PUBLISHED BY THE
PROFESSIONAL GROUP ON MILITARY ELECTRONICS

IRE TRANSACTIONS® ON MILITARY ELECTRONICS

Published by The Institute of Radio Engineers, Inc., for the Professional Group on Military Electronics at 1 East 79 Street, New York 21, N. Y. Responsibility for the contents rests upon the authors, and not upon the IRE, the Group, or its members. Individual copies of this issue, and all available back issues, except Vol. MIL-4, Nos. 2, 3, and 4, may be purchased at the following prices: IRE members (1 copy) $2.25, libraries and colleges $3.25, all others $4.50. Annual subscription rate: non-members $17.00; libraries and colleges $12.75.

IRE Transactions

ON MILITARY ELECTRONICS

Volume MIL-5 **October, 1961** **Number 4**

MISSILE AND SPACE RANGE INSTRUMENTATION

A. G. Waggoner

Alvin G. Waggoner was born in Carlisle, Pa., on March 11, 1921. After receiving the B.S. degree in metallurgy from Massachusetts Institute of Technology, Cambridge, Mass., in 1942, he joined the Cramp Shipbuilding Company, Philadelphia, Pa. In his four years there, he was employed first as a Laboratorian in the experimental and test laboratory, and then as Supervisor and Company Metallurgist, working on metallurgical and materials problems and specifications, and the technical aspects of production methods, particularly welding. The results of two of these projects were published in the *Welding Journal*. Along with W. B. Brooks, the co-author of one of these projects, he patented alloy steel in 1949. During this time, he studied business administration at the Alexander Hamilton Institute, New York, N. Y.

After World War II, he joined the staff of the Applied Physics Laboratory of Johns Hopkins University, Silver Springs, Md. There, from 1946 to 1949, he served as an Associate Engineer and Administrative Assistant and as Secretary of the Bumblebee Guided Missiles Propulsion Panel.

In 1949 he began his career with the guided missiles and aeronautics groups of the research and development organization of the Office of the Secretary of Defense. He was with the Committee on Guided Missiles of the Research and Development Board until December, 1953, acting first as Panel Coordinator and Consultant to the committee in the fields of metallurgy and materials, and propulsion and fuels, and later as Deputy Executive Director. In 1954, he became Secretary of the Technical Advisory Panel on Aeronautics of the Office of the Assistant Secretary of Defense (Research and Development), where he served until he joined the missiles activity of the Office of the Secretary of Defense. From 1955 to 1959, with the exception of a short period he held the position of Executive Secretary of OSD Ballistic Missiles Committee, which he helped to organize. Also during 1956 to 1959, he was Executive Assistant to the Director of Guided Missiles. In 1959 he was appointed Special Assistant for Guided Missiles and Space Operations to the Director of Defense Research and Engineering. He was asked to organize the Office of the Assistant Director, Defense Research and Engineering (Ranges and Space Ground Support) in 1960, and was made Assistant Director. In 1961 he again became Special Assistant (Space) to the Director, Defense Research and Engineering. In June, 1961, he left the Department of Defense to join Airborne Instruments Laboratory as Executive Assistant to the Director, Research and Systems Engineering Division, the position he holds today.

Mr. Waggoner is a member of the American Society for Metals, the American Welding Society, the American Institute of Mining and Metallurgical Engineers, and the American Rocket Society. Among the various awards he has won for outstanding performance and leadership are the William A. Jump Memorial Award and the Department of Defense Distinguished Civilian Service Award.

Guest Editorial

THE magnitude of the range instrumentation job which arises from the demands of the Space Age is our challenge as this issue goes to press. The constantly changing, increasingly stringent, and varied support needs of the re-entry programs, the manned satellites, the rendezvous programs, and the deep-space-exploration programs impose a requirement for an unprecedented rate to increase in the technical capabilities of our ranges. Unless the planning and incorporation of new ideas and techniques are initiated now our range technology and capability will become the pacing factor in our missile and space programs. As one step, the already close working relationship of the Atlantic Missile Range, the Pacific Missile Range, and the White Sands Missile Range must be further directed toward such common advanced objectives as near-real-time communication and data handling for specific task operations on a unified world-wide basis.

To meet the needs of the foreseeable Space Age programs practicably requires certain actions and changes in attitude. 1) Because of the increasing lead times required for instrumentation development, research personnel responsible for future programs requiring range support must establish an earlier understanding with range personnel on range capabilities and program needs. 2) The three ranges, with the assistance of the users, must achieve the maximum standardization of instrumentation systems so that costs may be reduced, operational and maintenance programs simplified and a higher degree of compatibility among the three ranges attained. 3) Range program planners must be more receptive to new ideas that will advance the state-of-the-art and provide an increased capability with equivalent or, if possible, decreased instrumentation. 4) Recognizing the economics associated with the billion-plus-dollar investment in our national ranges, the users must insure that their test requirements not only are valid but also represent an optimized step toward advancing the state-of-the-art. The achievement of these objectives demands closer liaison between industry and the ranges.

For the United States "to take a clearly leading role in space achievement" is the stated intent of the President. The keystone of such achievement is the sophisticated instrumentation and use of our national ranges. To this end, the capabilities and growth potential of our ranges must be maintained and fully supported.

As Guest Editor, and on behalf of the officers and members of PGMIL, I thank the contributors to this issue of the TRANSACTIONS, as well as the many persons who submitted excellent papers that space limitations prevented us from publishing. We hope that subsequent issues highlighting this critical area may be published in the near future. I also wish to thank Commander F. P. Morrison, USN, Office of the Assistant Director (Ranges and Space Ground Support), ODDR&E, and W. H. Boone, Office of Electronics, ODDR&E, for their outstanding assistance in the preparation of this issue.

ALVIN G. WAGGONER

Microwave Telemetry at U. S. Missile Ranges*

G. F. BIGELOW†, MEMBER, IRE, T. B. JACKSON‡, SENIOR MEMBER, IRE, AND R. T. MERRIAM||, SENIOR MEMBER, IRE

Summary—An orderly plan has been prepared covering the implementation of UHF radio telemetry on the country's missile ranges. Requirements have been drafted for UHF systems to be developed by 1970. Programs have been launched to transfer the requirements into equipment. Preliminary standards have been established.

Today, UHF telemetry links are utilized for a limited number of projects. Currently a high-performance UHF link is expensive, large in size, and complex. One must use a transmitter that may weigh 12 to 50 pounds, that has a volume of 250 to 1000 cu in, and that has an over-all power efficiency of 2 per cent for an 8 to 10 watt output. Its cost may be 10 times that of a 5-watt VHF transmitter. Automatic tracking systems are required but are not generally available. Special preamplifier-converters are also necessary. Because of these factors, UHF telemetry is used, at present, only by a few missile projects.

Obviously, we must continue to advance the state-of-the-art until a spectrum of microwave devices is available to fill the needs of the majority of telemetry users. Economy, as well as technical capability and flexibility, will be the mark of these developments.

Introduction

VHF telemetry, operating in the 215–260-Mc band, is a well developed communications link. Effective and thorough standards control its use to the benefit of military as well as commercial testing programs. However, this band is shared by other users and will virtually exclude telemetry by 1970.

To accommodate telemetry in a protected band and to provide additional usable channels, allocations have been established in two UHF bands—1435 to 1535 Mc and 2200 to 2300 Mc.

This paper deals with problems and solutions to problems of implementing these UHF telemetry bands on Department of Defense test ranges. An attempt is made to clarify requirements and schedules for that effort.

Nontechnical features of the subject to be discussed will be divided into (1) range operator problems, (2) range user problems, and (3) equipment manufacturer problems. Detailed technical aspects are discussed first from a system standpoint. Airborne transmitters, antenna systems, and receivers will then be referred to separately.

Range Operator Problems

By official directive, the various Government ranges are faced with the problem of vacating the 215–260 Mc telemetry band by January 1, 1970. Very limited use of this band after 1970 may be permitted on a noninterference basis but hopes for any priority status in this area have been dispelled by repeated comments from those who control our frequency allocations.

Two areas in the UHF (300 to 3000 Mc) region have been assigned for telemetry occupation and, if no unforeseen technical obstacles prevent the move, most, if not all, range telemetry will be conducted in the 1435–1535-Mc and 2200–2300-Mc bands after the 1970 date. One basic nontechnical difference exists between these two bands: the 1435–1535-Mc band is a "Government/non-Government" assignment and is specifically planned for partial occupancy by manned aircraft telemetry service; the 2200–2300-Mc band is a "Government assignment," and it is subject to the same allocation procedures as the present 225–260-Mc band.

At the outset, the prospect of a major frequency shift presented the range operators with a host of new problems. No range had suitable ground-station equipment for use in the new bands; little or no practical experience was available for background reference; propagation anomalies were an unknown factor. In short, the RF link presented anew all of the problems which beset the telemetry industry in its shift to the 216–225-Mc band some twelve years ago.

It was felt from the beginning that the missile-borne equipment would offer serious problems, and that sophistication in ground receiving equipment could be more easily accomplished. Subsequent developments have proven this to be true.

As recently as three years ago, studies indicated that the 225-Mc band was an "optimum" band for telemetry. This was on the basis of all factors: transmitter, receiver, and antenna systems. One of the heavily contributing factors was the difficulty of manufacturing low-noise receivers above about 300 Mc. The advent of masers and parametric amplifiers provided the "breakthrough" that was needed to push the "optimum" band considerably higher than the 300-Mc figure and, today, there is little to choose between the proposed bands and our capability in the lower band one or two years ago. Further improvement through the use of phase-lock or correlation techniques is being rapidly carried forward.

We were also aware that further improvement could be expected through added complexity and refinement in our antenna systems. The bulk of antenna systems in use today have gains of from 8 to 17 db above isotropic. The truly deluxe installations such as the TLM-18 or similar antennas in use at larger ranges offer gains to 35 db. By incorporating aided or self-tracking features, and by narrowing beamwidth by element phasing or by the use of larger parabolic reflectors, it is a fairly easy matter to use presently known techniques to achieve 17 to 50

* Received by the PGMIL, May 29, 1961. This work was done in cooperation with the Telemetry Working Group of the Inter-Range Instrumentation Group, China Lake, Calif.

† White Sands Missile Range, White Sands, N. Mex.
‡ Naval Ordnance Laboratory, Corona, Calif.
|| Naval Ordnance Test Station, China Lake, Calif.

db or even higher gains in the antenna systems at the new frequencies. While the cost of these improvements will be greater than we now accept as "normal" for ground systems, we must balance the obvious advantages of improving the relatively few ground stations against the staggering cost of achieving these same gains in the missile-borne portion of the RF link.

Training operators for proficiency in the microwave regions will most likely be accomplished during the evaluation phases of the new hardware. Preliminary theoretical and practical studies do not forecast any insurmountable problems for propagation at the new frequencies. Flame attenuation and re-entry skin effect will undoubtedly offer difficulties, but the latter is apparently a factor with so many variables that no one frequency allocation can solve it. For the conventional missiles which are fired over relatively short ranges, the problems will probably be little different than those of today.

Range User Problems

As in the case of the range operator, the range user is also faced with a host of new problems. His, however, are of a very practical nature, if the telemetry design engineer and the range operators perform their tasks fully.

He is primarily concerned with size, weight, cost, and performance. In the mind of the missile manufacturer, for the ideal system a minimum in the first three factors and a maximum in the fourth are desirable. Because the present-day telemetry package has reached a high performance plateau from the standpoint of data return, the manufacturer will be satisfied with no less than currently obtainable performance, and he is already demanding higher performance systems to cut down on total development time.

The long time required to change from one missile antenna system to another is typical of the long lead time required for nearly all components. It is generally agreed that omni-directional or, at least, broad-beam patterns are essential. Design of the antenna itself should be straightforward. The very fact that the new frequencies will impose new dimensions on the antenna is the chief problem. It has been reliably estimated by missile manufacturers that given a new design of an antenna to be installed in a missile, it will require approximately three years before the missile with new antenna is rolling off the production line. Electronic engineers must design it; aeronautical engineers must position it and fabricate a new wing or compartment for it; draftsmen, Government project representatives, company management, funding and a host of related factors will add to the lead-time.

Another problem is that of cost. Current prototype transmitters which would meet requirements stated later cost from $10,000 to $30,000 each. While this might be acceptable for the large complex missile which costs many millions of dollars, it is out of the question for small, high-firing-rate missile projects. Industry must be encouraged to amortize engineering and design costs as quickly as possible, and to recognize that the design of a low-cost basic unit is one of the primary goals. It is estimated that the ceiling for this basic unit (the 2–5 watt output) must stay under $1000. Small missile programs with firing rates of 200 to 300 per year simply cannot afford transmitter costs that are in excess of the current costs for the entire telemetry package. If solid-state development bears fruit, it is conceivable that the present high-priced components will undergo rapid and drastic price reduction when production steps up.

Equipment Manufacturer Problems

In general, the telemetry equipment manufacturer is faced with several problems that either deter his entry into the UHF telemetry field or tend to impede developments that have been undertaken.

Perhaps the greatest problem that the typical manufacturer has to cope with today is that of determining what will be required in the way of telemetry transmitters, receivers, and antennas for the 1435–1535-Mc and 2200–2300-Mc bands during the next three to five years. Lack of published standards and time schedules for microwave-telemetry links, other than those recommended by the IRIG Telemetry and Frequency Coordination Working Groups, and, in some instances an unfamiliarity with the requirements for shifting to the UHF band has placed many manufacturers in the position of considering microwave telemetry as an unimportant problem that will not have to be faced for at least several years.

It appears that the needs of the manufacturer and user alike can best be served at this time by establishing realistic guidelines and design objectives that will eventually have to be attained if UHF telemetry user groups are to be provided with equipment to satisfy contemplated program requirements. This type of information would be particularly useful to manufacturers developing system components in the UHF telemetry field.

Last, but not least, of the problems faced by the manufacturer or any group involved in development of UHF telemetry equipment, is the high cost involved in designing and fabricating assemblies. Lumped constants are generally not applicable at these frequencies, and cavity or line-type configurations, which are more costly to design and manufacture, are required. Electron-tube devices that are useful at these frequencies become very special; size and shape factors become very important in design, and again result in more costly construction. High development cost, high cost to the user and the high cost involved in continually improving UHF equipment to prevent its becoming obsolete in terms of size, weight and performance, all have an adverse effect on the availability of equipment suitable for use in microwave telemetry systems.

Telemetry Working-Group Involvement

The TWG, since 1956, has been aware of the problem and has used various approaches toward coordinating efforts in development of UHF equipment to meet the 1970 deadline. At the present time, the Radio Links Committee of TWG is conducting an industry-wide survey of equipment availability. NASA members are conducting a survey of space and satellite developments which are pertinent, and frequent reports are being forwarded to the IRIG Steering Committee indicating progress and predicting bottle-necks. These reports have generated various development contracts, and progress has been made. The Air Force has been active in this because of the urgency of requirements in the 1435–1535-Mc band for high-performance manned aircraft, and because of a number of classified satellite programs. The Navy Bureau of Weapons sponsored a survey of "Design Objectives for Telemetry RF Transmission Links for the Period 1960–70."[1] If TWG does its work well, DOD and the ranges will be fully aware of the problems and the requirements during this development period.

System Requirements

An examination of system requirements suggests that a standard system should be established for some reasonable, minimum range. The standard system parameters could then be modified to accommodate extended ranges.

The popular method used for establishing any system with a particular range is to make range calculations and then draw conclusions as to how much transmitter power or antenna gain is required. Fig. 1 depicts the current and future performance characteristics of UHF and VHF radio links. Note that present day UHF links are much less reliable than VHF, because free-space loss between isotropic sources for 2200 Mc is 20 db greater than for 220 Mc. The advantage in gain shown by the 1970 UHF system will provide the much needed fade margin or additional gain depending on the application. Future users will have the prerogative of using this expected fade margin to reduce the power output of the transmitter and, therefore, its size and weight.

While range calculations are a useful tool, it is the factors primarily of cost and secondarily of size and component availability that determine ultimate system performance. With that as a reference, it is appropriate to discuss range requirements as a function of cost, with bandwidth as a common denominator. IRIG document 106-60 has standardized a maximum RF bandwidth of 1.5 Mc which is a useful figure for this case.

First, for a system that will perform over a 50- to 100-mile path, one would expect to use transmitters that are

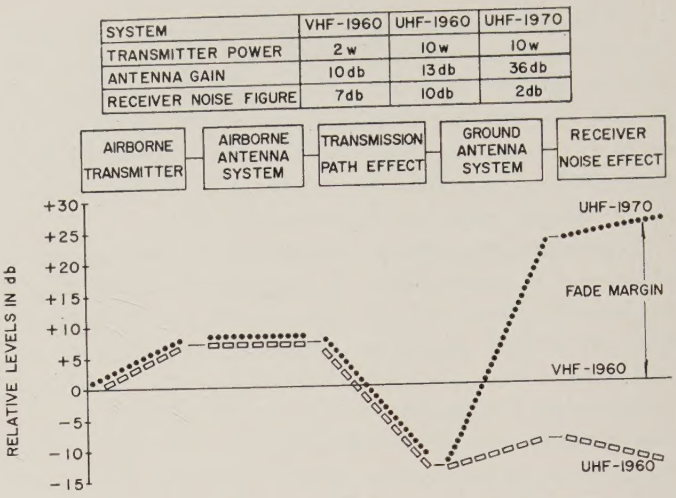

Fig. 1—UHF telemetry system normalized to a VHF system.

available today with an output power of 10 watts, a manually-directed antenna, a simple converter, and currently used VHF receivers. This system can be purchased for $10,000.

The next step in range is a large one, that is to about 3000 miles, which is mostly due to the high gain of automatic tracking antennas. For an improved transmitter, but with the same output power, a high-gain automatically directed antenna, a low-noise preamplifier, the same converter and an improved receiver, a cost of $100,000 is to be expected.

Finally the same system as above but with a power amplifier for the transmitter would cost only about $2000 more to provide whatever range is desired. The limiting factor here becomes the ability of the test vehicle to carry the additional weight. Larger antennas may be considered if a relatively unlimited budget is available.

It should be noted that none of the above range estimates accounted for a fade margin. Several factors tend to compensate for this point. As a long-range communication medium, the UHF band is fairly well located. Atmospheric, man-made, and extra-terrestrial noise sources combined are at a minimum in this band. Therefore, propagation anomalies are at a minimum, and the very low noise preamplifiers may be fully utilized.

Detailed technical requirements of the system are expressed in the following sections.

Transmitting Systems

Requirements for UHF telemetry systems have evoked a profusion of suggested designs for microwave transmitters, probably the weakest link in the RF transmission chain. While requirements have been easy to establish, their fulfillment is much more difficult.

As an example, consider several of the suggested schemes for generating the modulated UHF signals in the airborne system. These include 1) modulating an

[1] Survey results are contained in NAVWEPS rept. No. 7161/NOLC No. 538, January 1, 1961. This report is currently being updated.

exciter at a low frequency and afterwards multiplying to the UHF band; 2) modulating a UHF exciter directly; 3) translating a modulated low-frequency carrier to the UHF frequency. Even combinations of these schemes may be used. Complicating the problem are the intereffects of deviation linearity, stability, and use of solid-state devices or tubes in the circuitry. In addition, telemetry engineers are wont to talk in terms of traveling-wave tubes, magnetrons, klystrons, triodes, tetrodes, transistors, and diode multipliers as power output devices. While one or two of these are now workable, it will probably be 3 years before one is clearly optimum for telemetry usage.

Salient requirements are listed below for a typical 1970 FM transmitter:

Frequency
- Center: 2200–2300 Mc or 1435–1535 Mc
- Accuracy: ±0.001 per cent
- Stability: ±0.001 per cent

Deviation
- Modulation: dc to 1 Mc
- Total: ±1.5 Mc
- Linearity: ±0.5 per cent to ±250 kc, ±1 per cent to ±500 kc, ±5 per cent to 1 Mc or over

Incidental FM: ±5 kc maximum

Environment
- Vibration: ±15 g
- Temperature: −20°C to +150°C

Size: 50 cu in

Weight: 5 pounds

Over-all Power Efficiency: 25 per cent

Slot antennas are already available for transmission in this band and operate effectively.

Receiving Systems

The UHF telemetry receiving system in its simplest form may consist of a fixed, low-gain broad-beam antenna and a single receiver. However, such a system would serve adequately only as a pre-flight monitor or for recording very short-range test flights. At the other extreme, a requirement exists for a completely automatic UHF telemetry receiving system that will provide high-gain capabilities for long-range reception, fast acquisition of a target, and the ability to track the target at high angular velocities with automatic selection of the most suitable antenna beam pattern. These qualifications are to be satisfied with unattended operation of the system. In between these two extremes is a requirement for a general-purpose microwave-telemetry receiving system suitable for use on the test ranges in connection with the general flight testing of missiles and aircraft. A receiving system is proposed that satisfies the majority of these requirements as well as the requirements set forth in present IRIG Telemetry Standards or additions thereto now under consideration.

Antenna System Requirements

Radar systems development has provided an extensive background of technique and equipment directly applicable to automatic-telemetry tracking requirements. Very little need be added to adapt these systems to telemetry service. A statement of requirements is included in lieu of a discussion on techniques. Costs and auxiliary requirements will determine which technique is to be used in any particular situation. Major requirements for a general-purpose system are:

Tracking
- Acceleration: 30° per sec^2
- Velocity: 30° per sec
- Accuracy: ±1°

Size: 10 ft to 12 ft parabola or an array that will yield the gain of the 10 ft to 12 ft parabola

Frequency: Both UHF telemetry bands

Acquisition Capability: Must be determined on an individual Range basis.

Telemetry Receiver

If the additional propagation losses encountered in shifting from the 225-Mc band to the 1435- or 2200-Mc region are to be offset effectively, it becomes necessary to make improvements not only in radiated power and directional antenna characteristics but also in receiver sensitivity characteristics. Use of such new devices as parametric, maser, or low-noise traveling-wave tube amplifiers offers considerable possibilities for obtaining microwave receiver systems with improved sensitivity characteristics through reduction of front-end noise. If these devices are to be utilized to full advantage, however, it becomes necessary to mount them in close proximity to the antenna feed system, and to consider the receiver as made up of at least two major assemblies physically separated from each other. The receiver front-end or "preamplifier-converter," to be mounted as part of the receiving antenna assembly, consists of a low-noise amplifier, frequency converter, filters and related components. The main portion of the receiver or the "channel selector" provides the normal receiver functions of channel selection, amplification, bandwidth determination, and detection of desired signals. The proposed receiving system requires signals in the 1435–1535-Mc band or the 2200–2300-Mc band (or any other microwave band 100 Mc or less in width) to be converted at the antenna to the 200–300-Mc band. The use of a multicoupler or distribution amplifier between the converter output and the input to the main portion of the receiver provides for distribution of received signals to more than one channel selector, and thus permits simultaneous selection of several transmitter channels where more than one transmitter and/or more than one type of modulating signal is employed for a given flight test.

The basic receiver may be designed to handle FM/

FM, PDM/FM and PCM/FM signals without design modifications. Modular type plug-in or replaceable assemblies could be used as a means of accommodating any one of the various types of modulation specified.

It should be noted that the system as proposed will, in some cases, allow the use of existing telemetry receivers (which operate in the 225–260-Mc band) in place of the main portion of the receiver or channel selector. Good sensitivity characteristics can be obtained in the 225-Mc telemetry band by using a low-noise preamplifier ahead of the channel selector or main receiver. These features are particularly important during the transition period (1960–1970) when programs will be shifting from the VHF telemetry band to one of the UHF bands.

Main utilization of modular type construction will allow considerable flexibility of receiver characteristics through interchange of assemblies such as IF strips, filters, and other major circuit portions of the receiver.

A summary of required performance characteristics for the major units of the proposed telemetry receiver is outlined below.

Preamplifier-Converter

Frequency range: 1435–1535 Mc; 2200–2300 Mc

Noise figure: 4 db or less (initial objective); 2 db or less (final objective)

Local oscillator stability: ±0.001 per cent of received frequency (initial objective); ±0.0005 per cent of received frequency (final objective)

Preselector: A preselector unit designed to reject signals outside the designated bands of 1435–1535 Mc or 2200–2300 Mc should be provided ahead of the preamplifier, to prevent unwanted signals at the antenna output termination from causing nonlinear operation of the preamplifier. Some installations may require the use of additional rejection-type filters to minimize interference from specific high-power equipments located in close proximity to the telemetry receiving antenna.

Attenuator: The receiving system should be capable of linear operation with signal amplitudes up to 50 mv rms at the antenna output termination. An automatic attenuator may be required ahead of the preamplifier to prevent nonlinear operation with high-level signals within the passband.

Image rejection: Greater than 60 db

Gain: 20 db or more in the passband

Output: 200 to 300 Mc; 100-Mc bandwidth centered at 250 Mc

Main Receiver

Frequency tuning range: 200 to 300 Mc

Type of input signal: FM/FM, PDM/FM, PAM/FM, PCM/FM

Noise figure: Sufficient to maintain over-all system noise figure at approximately that specified for the preamplifier

IF rejection: Greater than 80 db

Image rejection: Greater than 60 db

First local oscillator: Stability ±0.001 per cent

Second local oscillator: Tunable ±175 kc from front panel

IF bandwidth: 12.5, 25, 50, 100, 300, 500, 1000 and 1500 kc, should be available as plug-in units

Discriminator: Linearity ±0.5 per cent or better to ±250 kc, 1 per cent or better to ±500 kc, 5 per cent or better to ±1 Mc or over.

Video bandwidth: Basic response of 10 cps to 1.5 Mc, maximally linear phase-response filters with slope of 36 db/octave to provide cutoff frequencies of 6.25, 12.5, 25, 50, 100, 200, and 400 kc, should be available as plug-in units.

Phase-lock capability: Provision should be made for receiver to employ phase-lock detection as an optional feature.

AFC: Normal automatic frequency control circuitry plus provisions for gated AFC when used with PAM/FM or PCM/FM signals.

Existing Systems

Little can be said for the capabilities of UHF telemetry systems available as standard items today. Transmitter development has received the most attention, and a 10-watt 12-pound FM/FM package is available having a volume of 250 cu in, including power supply, that meets most of the ultimate requirements. Frequency stability is 0.005 per cent. Programs are in progress to develop tracking antennas designed primarily for the UHF band. Preamplifier-converters are available.

The airborne antenna system may be considered to be an isotropic source. The receiving antenna is a single helix with 13-db gain. The preamplifier-converter receiver performs as follows:

Noise figure: 7 db,
Bandwidth: 500 kc,
S/N ratio required: 13 db.

With no fade margin this system will operate over a distance in excess of 100 miles. This may be termed the current capability of UHF telemetry. A quick reference compilation of this information is made in Table I.

Additional Effort Required

Because of the rapid pace of development activity in all phases of the microwave radio link, it is felt that by 1965 telemetry users may expect to utilize this new band with almost no restrictions. Small, efficient transmitters are currently being developed which will be satisfactory. In addition, solid-state devices are nearing feasibility and are being developed for this specified application. The major remaining problem is to miniaturize the airborne package. Microwave airborne antenna systems exist which are already an improvement over the

TABLE I
CHARACTERISTICS OF UHF TELEMETRY LINKS

Range Requirement	Transmitter	Ground Antenna	Receiver		Total Initial Cost	Expected Cost in 1970
			Converter	VHF Receiver		
50 to 100 miles	10 watts 0.01% stability $5000*	13-db gain $400	10-db N.F. $2100	$2500	$ 10,000	$ 4000
100 to 2500 miles	10 watts 0.001% stability $9000*	36-db gain $80,000	4-db N.F. $8500	$2500	$100,000	$90,000
2500 to 10^8 miles	710 watts $15,000*	50-db $500,000	2-db N.F. $15,000	$3000	$500,000	$90,000 and up (depending upon range)

* These prices should be drastically reduced with the advent of large production runs.
Note: Only a small fade margin is available in each case.

VHF types. Tracking antenna systems for UHF have been and are now under development, and are expected to be operative this year. All of the national ranges, and other ranges as well, have been active in procuring tracking antennas for VHF as well as microwave bands. Receiving capability exists to virtually the full extent since one may have the full capability of a VHF receiver at microwave frequencies with but just the addition of a preamplifier converter. Receiver manufactuers have made available receivers with almost full capability with respect to the IRIG-TWG standards. The major development required is the designing of receivers to accept inputs from 200 Mc to 300 Mc.

Between now and 1965, the variety of output power devices discussed earlier must be investigated and a decision made as to which is optimum for use in the typical telemetry system. There are also a number of modulation and mechanical design techniques to be refined. As previously mentioned, the basic configuration of the transmitter system requires further design. As yet it is not clear that any one method of achieving the required stability, output, and modulation is superior to all others.

Sustained and coordinated design and development will be needed to complete the task on time. The predicted date for field evaluation of prototypes during FY 63 is still valid. While final production prototypes will not be available at this time, many of the basic problems in propagation, field strength measurements, RF link gains, stability, and modulation will undergo actual field testing, and a background of experience will be built up.

During this period and not later than at the conclusion of field testing, firm engineering design must be fixed for the first limited production quantities of the critical hardware. The FY 64 and FY 65 period will be used in establishing ground-station equipment requirements and building up both range capability and production. It is estimated that ranges that have not already established a capability by 1967 will find "crash" programs in order. Missile programs starting up in the 1965–67 period, whose predicted life is over five years will find it advantageous to instrument for the new telemetry bands at the beginning in order that they not be faced with expensive and program-delaying changes in the middle of a program. Programs which are phasing out during this time undoubtedly will continue to use the current VHF band.

Frequency Allocation Problems

The major problem, that of securing a block of frequencies for development and future operations, has been taken care of by recent action of the frequency assignment agencies. Our only fear is that lack of sustained effort to shift into the new frequencies will result in encroachment by other services. The entire spectrum is at such a premium that those charged with allocations cannot allow large, unused portions of the spectrum to remain dormant for long.

Efforts are already underway to accommodate space and satellite telemetry in adjacent or nearby bands. The obvious advantage of such an arrangement would be in sharing hardware or design criteria. There are high-level international aspects which will govern these matters, however, and the telemetry industry can do little more than offer consultation and carry on active missionary effort in this regard.

The more practical aspects of allocation of specific frequencies at each range will be well controlled by the area and local frequency coordinators. Members of FCWG have been active in their planning for the telemetry shift since 1956 and have already published guidelines for operations in the 1400- and 2200-Mc bands in their "Parameters and Criteria." Close cooperation between FCWG and TWG will reduce these problems to the minimum.

It may be categorically stated at this time that frequency scrutiny and control will be much more stringent than that encountered by the telemetry industry over the past 14 years. Excessive band occupancy, drift, instability, and other evidence of poor design will not be tolerated in these bands and accurate test equip-

ment will be available at the ranges to monitor the RF link.

Conclusions

There are one or two obvious conclusions that can be drawn: the task is not an easy one, and everyone concerned will have to constantly keep the January 1, 1970 date in mind.

In design, the goal will have to be for small, efficient, low cost airborne equipment. Where the new modular or molecular techniques are applicable, they must be employed for reliability and size considerations. To fully utilize these, however, rapid strides will have to be made and production costs will have to be reduced drastically. Early prototypes will, undoubtedly, use more conventional techniques.

Management in both industry and government will recognize that such a major change will require funding in excess of that normal for the past years. A considerable amount of "in-house" funding by industry will have to be accepted, but to those firms with enlightened management, the returns will be great.

More careful use of the frequency spectrum and tighter controls over transmissions will be in effect, and all concerned must realize the importance of frequency conservation.

The present move will be carefully planned and supervised. Because a longer lead time has been given us than was true of the shift to the 220-Mc band, the shift should be far less painful.

The present outlook is that all goals will be met in time for an orderly shift to the new region with a minimum of confusion and lost data.

Information Bandwidth Problems in Instrumentation of Missile Flight Tests*

WILLIAM E. MIMMACK†

Summary—**The operation of missile flight-test instrumentation systems at minimum bandwidth is an important economic consideration. Design of instrumentation systems may become difficult or impossible unless intelligently chosen bandwidth parameters are specified. Since nearly all missile flight-test instrumentation systems operate as sampled data devices, the bandwidth parameter shows up as a sampling rate requirement.**

It can be shown, under fairly general conditions involving no highly restrictive assumptions, that the rate of information acquisition of a sampled-data instrumentation system, when considered as a function of sampling interval, has a maximum. This can be readily appreciated intuitively. For a position-measurement system, for instance, if the sampling interval is made very short, the amount of information gained with each subsequent sample is very small because of the large amount of prior information about the position of the object being measured. No information would be gained if a sample were taken an infinitesimally small time after an initial measurement. Also, a very long time interval between samples would permit considerable growth of ignorance about the object's position, but the logarithmic information-gain function would grow slowly compared with t^{-1}; so the information rate for long sampling intervals would also be a small number. Somewhere between these two cases lies at least one maximum in information rate.

The selection of a sampling rate corresponding to the maximum information rate is recommended as a good choice for many types of missile test instrumentation systems. General sampling-rate formulas are developed, as well as specific formulas for certain important types of instrumentation problems.

* Received by the PGMIL, June 29, 1961.

† Range Instrumentation Dev. Div., White Sands Missile Range, N. Mex.

I. Introduction

A RECURRENT problem in missile flight-test instrumentation is that of selecting an information bandwidth for the instrumentation system. The reason that this is a problem may perhaps be made clear by the following remarks.

1) The instrumentation engineer must design and apply instrumentation systems to a great variety of missile systems.

2) The amount of advanced information about missile-systems performance and requirements is always very scanty.

3) The instrumentation engineer often has no knowledge concerning the ways in which the data taken with the instrumentation system are to be used by the missile-system engineer; indeed, the missile-system engineer could probably not, in advance, specify all of the uses which are to be made of data supplied by the test ranges.

4) It is a fact of experience, at all the major test ranges of the country, that communications between missile-systems designers and range-instrumentation operators and designers are inadequate to permit selection of instrumentation-system parameters satisfactory to both.

5) There is normally a longer lead time in instrumentation developments than in missile-system developments, in spite of the often greater complexity of

the latter, because emphasis is not great on instrumentation-system development until it is realized that a deficiency exists in the case of some critical missile test.

These remarks apply to the selection of any basic parameter of an instrumentation system. With respect to the bandwidth parameter the following may be applicable:

1) The missile-systems test planner will normally urge use of large bandwidths, whereas the instrumentation engineer will urge use of minimum bandwidths.

2) Instrumentation bandwidth requirements are often very arbitrarily specified in test directives.

3) Information bandwidth may not be a familiar and important concept to instrumentation engineers who frequently specialize in instrument design in fields wholly unrelated to communications theory.

The problem, briefly, is this: to permit an instrumentation-system designer to specify an adequate minimal-information bandwidth for his system, on the basis of very limited data concerning the use of the product of the instrumentation system and the performance of the missile system and instrumentation system. The instrumentation-system designer must find the upper limit required for all of the various types of missile systems which are to be tested. The instrumentation-system operator must be able to operate in such a way that adequate minimal bandwidth is used on each particular test.

It is very important that the specification of instrumentation bandwidth be possible with a small amount of advance requirements information. Normally the only information of this type available is the accuracy required of all the measurements made by the test range instrumentation complex, and some few missile-performance data which may include expected flight path, thrust, maneuverability, times of important events, expected velocity characteristics, and perhaps one or two other data.

From the point of view of the operators of flight-test instrumentation systems, the use of these systems at minimum bandwidth is an important economic consideration. Since nearly all missile flight-test instrumentation systems operate as sampled-data systems in which the final output is a digital quantity, the information bandwidth parameter shows up as a sampling-rate requirement. The bandwidth used, therefore, affects directly the quantity of data taken, and thus the data processing time and cost are also directly influenced, except for a certain fixed cost entailed with the operational overhead of the primary data-gathering elements. The ultimate users of the data should also be influenced by the consideration that cost and time for extraction of required information will be in proportion to the instrumentation-system bandwidth.

Besides the cost and processing time considerations, there is the fact that design of instrumentation systems may become difficult or impossible unless reasonable and intelligently chosen bandwidth parameters are specified. As a simple example, if a permanent record is to be made by the instrumentation system, it may not be feasible to design a device which operates at a very high sampling rate and still provides adequate total record length considering the capacity of whatever data storage medium is used. Both instrumentation-system operator and designer have need of means for selecting minimum adequate bandwidth specifications.

It is the thesis of the present communication that for a particular measurement required of an instrumentation system the accuracy needed for the measurement (and perhaps other quantities related to the measured quantity as time integrals or derivatives), the missile-system performance, and bandwidth are interrelated. An attempt will be made to justify this statement and to explore ways to use information of this type to derive methods or formulas which may be used for instrumentation-system bandwidth specifications. This approach has several points in its favor, particularly that it is based on use of relatively few data which will almost always be available; it is oriented toward the missile system being tested rather than toward the capabilities or potential capabilities of the instrumentation system, and does not depend on the way the instrumentation data are to be used eventually. It depends only on missile performance characteristics and the manner of presentation of accuracy requirements. The question of whether this is an entirely adequate approach remains open; however, the arguments, when examined in detail, are convincing, and are intuitively acceptable immediately.

Sampling rates are often established, for a certain measurand, by considering the necessity for smoothing the primary data, in order that derivative data (velocities, etc.) of reasonable behavior may be obtained from the primary data. In the present discussion a sampling rate for each measurand will be obtained, without consideration of any data-smoothing processes, or the use of the data for obtaining derivatives. This is not to imply that the results will apply only to the primary measurements made by an instrumentation system, or that all derivative data must be measured directly. By whatever process derivative data are gotten, the bandwidth and sampling rate requirements established should apply. Thus, for example, if a position-measurement system is to be used to obtain velocity, it must have adequate bandwidth for the velocity-measurement requirement.

The emphasis in this discussion will be on missile flight-instrumentation systems for trajectory measurement. For other types of missile flight instrumentation, *e.g.*, telemetry systems, the situation is clearer, and there seems to be no need for discussion. It is expected that the results should apply to instrumentation systems for measurement of missile position, velocity, acceleration, *i.e.*, the basic trajectory elements, as well

as systems designed for measurement of rigid-body rotations of the missile, *i.e.*, pitch, yaw, roll, angle of attack, etc.

II. Relation of Bandwidth to Missile Performance and Instrumentation Accuracy

It has been stated above that the accuracy required for a particular measurement and the missile system performance are related in a way which determines an upper limit to the bandwidth required of the instrumentation system. This can, perhaps, be better appreciated in terms of the following heuristic discussion. Since frequency domain specifications are sought, suppose that the missile is exhibiting oscillatory behavior in one position coordinate so that the path is described by a sinusoidal function.

$$x = a \sin \omega t.$$

Suppose, also, that the agency conducting the test has stated a need for x position measurements to a one-sigma accuracy level of σ_x. As the amplitude of the oscillation becomes large, the forces become large due to the high acceleration required. Similarly, for high frequencies, in fact, the acceleration is

$$\ddot{x} = -\omega^2 a \sin \omega t,$$

which has a maximum value of

$$\ddot{x}(\max) = \omega^2 a.$$

If the quantity $\omega^2 a$ exceeds the structural capability of the missile for withstanding acceleration or the ability of the missile steering-control system to exert forces causing accelerations of this magnitude, then the missile will either break up or be unable to have oscillatory behavior at this amplitude and frequency. That is to say

$$\omega^2 a \leqq A,$$

where A is a maximum acceleration term connected with missile performance. If the amplitude a is small, the frequency ω can become very large. However, when the amplitude becomes less than σ_x, then it is no longer of any interest, because it is below the accuracy level required for measurements of x. Using σ_x as a lower limit for a, one obtains as an upper limit for the frequency

$$\omega \leqq \sqrt{\frac{A}{\sigma_x}}.$$

An instrumentation system with this bandwidth would be adequate for this particular (rather artificial) missile-test instrumentation problem.

III. Methods of Obtaining Frequency-Domain Specifications for Instrumentation Systems

Several different approaches to the problem of arriving at instrumentation-system bandwidth specifications will be considered, and some examples given. An outline of these methods will be given below.

The informal method of Section II has been used for trajectory-determination systems which measure position. It certainly establishes a band limit for the case of an oscillating missile. The validity of this band limit would depend on whether, among the ensemble of possible missile position functions, there are members which contain frequencies much higher than this limit. Since this is unlikely, the band limit is probably a pretty good one, and could be used as the basis for establishing instrumentation-system bandwidth. The method can also, with appropriate modifications, be applied to velocity measurements and attitude and attitude-velocity measurements. With slight modifications this method may be extended to include other data which apply to the bandwidth required for a certain measurement, such as time-derivative and time-integral data tolerances.

A technique which is sometimes fruitful when the various quantities pertinent to a problem are known is dimensional analysis. This method can be applied to the present problem, and will yield some formulas which may be compared numerically with other methods which do not yield analytical expressions for the bandwidth. The dimensional-analysis formulas can thus be scaled, and are considerably more convenient than some other purely numerical or trial and error methods for getting the bandwidth figure.

The possibility may also exist of representing the desired data in a form amenable to statistical correlation and power spectrum analysis. Unless an adequate statistical representation of the time functions can be obtained, very little progress can be made with this approach; however, some results can be derived.

A control-systems engineering approach merits consideration because there is considerable similarity between a control system and an instrumentation system, and because there is an immense development of control-system technology which may be directly applicable to the present problem. Unfortunately, analytic expressions for the pertinent parameters of a control system are not usually obtained in the course of design.

Finally, an information theory approach seems to lead, in a fairly straightforward way, directly to sampling-rate specifications. The use of information theory is based on the fact that for a fairly reasonable time after having made a measurement one has good prior information about a new measurement of the same quantity. For typical measurement situations, the growth of uncertainty in the expected value of a quantity operates in such a way that the information rate considered as a function of sampling interval exhibits a single maximum. The value of the sampling interval at this maximum is recommended as a good choice for operation of an instrumentation system.

IV. Extension of Heuristic Method

The heuristic discussion of Section II can be extended somewhat. First, it should be mentioned that each argument for the selection of a bandwidth parameter is an upper limit argument. The attempt is made to establish successively lower upper limits to the bandwidth.

Again, considering the missile to be behaving in an oscillatory manner, a certain measurand follows

$$x = a \sin \omega t,$$

and has the velocity

$$\dot{x} = a\omega \cos \omega t.$$

The velocity, of course, has an upper limit so that $\dot{\chi}\ (\max) = a\omega \leqq V$, where V is the maximum possible velocity. This leads to a bandwidth formula $\omega = V/\sigma_x$, where σ_x is the tolerable error. Such a formula has been suggested as a sampling-rate formula, but for a position measuring system it greatly overestimates the required sampling rate.

One could also consider the velocity characteristics of an oscillating measurand

$$x = b \sin \omega t,$$

which would have an acceleration of

$$\ddot{x} = b\omega \sin \omega t.$$

Following the argument of Section II this would lead to a bandwidth formula for measuring the velocity of the quantity x

$$\omega = \frac{A}{\sigma_v},$$

where A is the maximum possible acceleration and σ_v the tolerable velocity error. For trajectory measurement systems this is not such a bad estimate.

A formula can also be obtained for bandwidth in the case of measurements made on a quantity x with permissible position error of σ_x and permissible velocity error of σ_v. Proceeding in a fashion similar to that used before:

$$\ddot{x}(\max) = \sigma_x\omega + \sigma_v$$

$$\ddot{x}(\max) = \sigma_x\omega^2 + \sigma_v\omega \leqq A,$$

where A is the maximum possible acceleration. Using the equality in the last expression and solving for ω gives

$$\omega = 1/2 \left\{ \frac{\sigma_v}{\sigma_x} + \sqrt{\left(\frac{\sigma_v}{\sigma_x}\right)^2 + \frac{4A}{\sigma_x}} \right\}.$$

The signs of σ_v and σ_x have been arbitrarly chosen to give the largest value of ω. This expression reduces to the one obtained in Section II when $\sigma_v = 0$. The expression indicates that the effect of considering velocity error is to increase the required bandwidth and sampling rate. This will also appear in the bandwidth formulas derived by information theory conditions, in which case the reason for this effect is more readily appreciated.

V. Dimensional Analysis of Required Measurements Data

Considering that the factors affecting bandwidth are: tolerable errors in position σ_x, and in velocity σ_v, and the maximum possible acceleration A, some rather unspecific formulas for bandwidth may be obtained from a dimensional analysis using the method of Lord Rayleigh. The formulas are

$$\omega = \frac{\sigma_v}{\sigma_x} \times \psi_1(\zeta),$$

$$\omega = \frac{A}{\sigma_v} \times \psi_2(\zeta),$$

$$\omega = \sqrt{\frac{A}{\sigma_x}} \times \psi_3(\zeta),$$

where ζ is a dimensionless number

$$\zeta = \frac{A\sigma_x}{\sigma_v^2}.$$

When systems for measurement of the quantity x and the velocity of the quantity $\dot{x}$ are considered independently, as if error of one had no influence on the bandwidth required for measurement of the other, then, because both σ_x and σ_v appear in the number ζ, the only permissible functional form for the ψ's in this case is a constant. Bandwidth formulas which follow from this assumption are

$$\omega = k_1 \frac{A}{\sigma_v}$$

which would be appropriate for a velocity measurement system, and

$$\omega = k_2 \sqrt{\frac{A}{\sigma_x}}$$

which would be appropriate for a system measuring the quantity x. It has been indicated in Section IV that neglect of velocity error causes an underestimate of bandwidth, so the latter formula is of little interest. One cannot get very far with more general formulas; however, the form of the ψ functions could perhaps be obtained empirically, to sufficient accuracy, using other methods for bandwidth.

VI. Statistical Analysis of Required Measurements Data

Perhaps the most obvious method for selection of a suitable bandwidth for an instrumentation system, the method immediately suggested by the communications engineer, would be to analyze the data statistically, find out what frequencies are present, and apply the sampling theorem to determine the sampling rate. This is, of course, not possible in advance of the acquisition of data; but perhaps the missile engineer could specify what frequencies he expects to find present in the data. Unfortunately, this type of information, if it exists, has not been available to the instrumentation-system designer.

Some progress can, however, be made with this approach in a way which elucidates some of the other methods. A trajectory condition which would contain higher frequencies than one would expect to encounter in practice is the following: The missile is perturbed by a random series of positive and negative accelerations (linear or angular) of an amplitude equal to the maximum which the system is capable of sustaining. If maximum zero crossings of the acceleration wave just described are Poisson distributed, with an average number of k per second, then the power-density spectrum of the wave has the form

$$\frac{2A}{\pi}\,\frac{2k}{(2k)^2+\omega^2},$$

where A is the maximum acceleration. k may be chosen very large with the result that the spectrum of acceleration is nearly flat with a value of

$$\frac{A}{k\pi}$$

out to any frequency of interest.

The spectrum of position is related to the spectrum of acceleration by a factor of ω^{-2}, *i.e.*, the position spectrum is

$$\frac{A}{k\pi}\,\frac{1}{\omega^2}.$$

The errors caused by dropping off the spectrum at some value ω_m are the familiar aliasing errors. At some particular frequency ω_0, $0<\omega_0<\omega_n$ the error caused by the omission of the higher frequencies is

$$\frac{A}{k\pi}\left\{\frac{1}{(2\omega_n-\omega_0)^2}+\frac{1}{(2\omega_n+\omega_0)^2}+\frac{1}{(4\omega_n-\omega_0)^2}+\cdots\right\}=\frac{A}{k\pi}\sum_{n=1}^{\infty}\frac{1}{(2n\omega_n\pm\omega_0)^2}.$$

At $\omega_0=0$ the error would be

$$\frac{A}{k\pi}\sum_{n=1}^{\infty}\frac{1}{4\omega_n{}^2n^2}=\frac{A}{4k\pi\omega_n{}^2}\sum_{n=1}^{\infty}\frac{1}{n^2}=\frac{A}{4k\pi\omega_n{}^2}\left(\frac{\pi^2}{6}\right).$$

If this error is equated to the permissible error in the quantity x, a formula for band limit is

$$\omega_n=K\sqrt{\frac{A}{\sigma_x}},\qquad K=\sqrt{\frac{\pi}{24k}}$$

which is very much like previous formulas for bandwidth of position-measuring systems.

VII. An Approach Based on Control-Systems Design

There are broad similarities between instrumentation systems and control systems. Both are, ultimately, devices for processing information in the case of a control system with power gain. This last fact causes stability to be of major concern in the case of control-system design, but not in the case of instrumentation-system design. After suitable means are found to introduce stability criteria, it is possible to use control-system design methods to arrive at frequency-domain specifications for instrumentation systems.

An input function which is chosen for this analysis is a symmetrical step function of acceleration. If the amplitude of this step function is chosen as the maximum which the system is capable of sustaining, it represents the most severe transient which could actually occur short of a complete malfunction, such as an explosion.

The Fourier integral representation of such a step function is

$$F(t)=\frac{A}{\pi}\int_{-\infty}^{\infty}\frac{\sin\omega t}{\omega}\,d\omega,$$

where A is the acceleration amplitude. The contribution of each small band of frequencies to the function is

$$dF(t)=\frac{A}{\pi}\,\frac{\sin\omega t}{\omega}\,d\omega.$$

Thus the amplitude of the acceleration spectrum as a function of frequency is

$$\frac{A}{\pi}\,\frac{1}{\omega}\,d\omega.$$

The position and velocity would have spectra

$$\frac{A}{\pi}\,\frac{1}{\omega^3}\,d\omega\quad\text{and}\quad\frac{A}{\pi}\,\frac{1}{\omega^2}\,d\omega,$$

respectively, because these quantities are related to the acceleration by factors of $-\omega^{-2}$ and $-\omega^{-1}$, respectively.

If σ_x and σ_v are the permissible errors in x and v (the velocity of x), then the open loop gain required may be written

$$G_x=20\log\frac{A}{\pi\omega^3\sigma_x}\text{ decibels for a system measuring }X,$$

and

$$G_v = 20 \log \frac{A}{\pi\omega^2\sigma_v} \text{ decibels for a system measuring } \dot{x}.$$

These gain expressions may be expanded as

$$G_x = 20 \log \frac{A}{\pi\sigma_x} - 60 \log \omega$$

$$G_v = 20 \log \frac{A}{\pi\sigma_v} - 40 \log \omega.$$

The first term fixes the gain at unit-angular frequency and the second term fixes the maximum permissible attenuation rate at intermediate frequencies.

Required degree of stability criteria must still be derived. This will be done by fixing the maximum permissible closed-loop gain for intermediate frequencies. For sinusoidal behavior of the quantity x with maximum allowable acceleration A, the maximum amplitudes possible for x and $\dot{x}$ at frequency ω are A/ω^2 and A/ω, respectively. If errors of σ_x and σ_v are permissible for x and $\dot{x}$, then fractional errors in x and $\dot{x}$ are

$$m_x = \frac{\sigma_x}{\frac{A}{\omega^2}} = \frac{\omega^2\sigma_x}{A} \qquad \text{for } x,$$

and

$$m_v = \frac{\sigma_v}{\frac{A}{\omega}} = \frac{\omega\sigma_v}{A} \qquad \text{for } \dot{x}$$

The ratio of output to input, or gain, k, is related to the fractional error by the expression

$$m = k - 1.$$

The closed-loop gain as a function frequency may not exceed the following values:

$$k_x = 1 + \frac{\omega^2\sigma_x}{A} \qquad \text{for } x,$$

and

$$k_v = 1 + \frac{\omega\sigma_v}{A} \qquad \text{for } v.$$

With these data, a trial and error control-system design procedure may be followed. Bode diagrams and Nichols charts may be used to obtain closed-loop frequency-response characteristics from which a band limit specification is obtainable.

VIII. Use of Information Theory

Thus far, the methods suggested for obtaining the bandwidth have been based on sine-wave response. Another, somewhat different, approach involves the use of information theory concepts.

If an observation of a measurand x is made giving a result x_1, with an error standard deviation of σ_1 on a system for which the value of x is thought to be x_0, with an error standard deviation of σ_0, a certain amount of information is gained. To determine how much, consider the error distributions to be Gaussian. First, if the measurement x_1 were exact, the information gained would be

$$-\log p_0(x_1),$$

where

$$p_0(x_1) = \frac{1}{\sqrt{2\pi}\,\sigma_0} e^{-(x_1)^2/2\sigma_0^2}.$$

From this amount of information must be subtracted an amount to account for the uncertainty associated with the measurement x_1, *i.e.*, the entropy of the distribution. The information gained is, therefore,

$$-\log p_0(x_1) - \log (\sigma_1\sqrt{2\pi e}).$$

But x_1 can supposedly, on the average, have any value, so this expression should be averaged over the p_0 distribution. When this is done, the average information gained is found to be

$$\Delta I = \log (\sigma_0\sqrt{2\pi e}) - \log (\sigma_1\sqrt{2\pi e}) = \log \frac{\sigma_0}{\sigma_1}.$$

In observations made on a missile while in flight, σ_1 is the one-sigma error associated with successive measurements of some quantity. σ_0 would be the error associated with knowledge of the same quantity before a measurement is taken. For a very short time after a measurement, σ_1 is almost equal to σ_0. The way in which σ_0 grows with time depends on the uncertainties of parameters associated with the dynamics of the system.

For external ballistics measurements the motion of the missile can be described by the equations of motion. Uncertainties in the parameters of these equations then causes σ_0 to grow with time. A sufficiently general formulation of the equations of motion is the Lagrangian set of equations:

$$\frac{d}{dt}\left(\frac{\partial T}{\partial \dot{x}_i}\right) = Q_i(x_i, \dot{x}_i, t),$$

where T is the kinetic energy of the system, $\dot{x}_i$ a generalized velocity, and Q_i a generalized force. The kinetic energy will be a homogeneous quadratic form in the generalized velocities

$$T = \sum_{i,k} a_{ik}\dot{x}_i\dot{x}_k.$$

Formally,

$$\frac{\partial T}{\partial \dot{x}_i} = \int Q_i dt + \text{const.} = \sum_k a_{ik}\dot{x}_k.$$

The constant term of integration is a total initial momentum term, say, μ_{0i}. Rewriting,

$$\sum_k a_{ik}\dot{x}_k = \int Q_i dt + \mu_{0i}.$$

In case the kinetic energy contains no cross-product terms the summation has only one term and a formal integration can again be performed:

$$\dot{x}_i = \frac{1}{2a_{ik}} \int Q_i dt + \frac{\mu_{0i}}{2a_{ik}},$$

$$x_i = \int \frac{dt}{2a_{ik}} \int Q_i dt + \int \frac{\mu_{0i}}{2a_{ik}} dt + x_{0i}.$$

If there are cross-product terms in the kinetic energy, a formal expression for $\dot{x}_i$ could be obtained by solving the set of simultaneous equations. Under most conditions the equation for x_i above would satisfactorily describe the behavior of a quantity associated with missile motion, at least for a limited time. Uncertainty about x_i will be connected with uncertainty about: 1) x_{0i}, which is the uncertainty in the quantity x_i at the time of a measurement, σ_x using the previous notation; 2) $\mu_{0i}/2a_{ik}$, which can be identified as a velocity so that σ_v will be used to symbolize this uncertainty; and 3) $Q_i/2a_{ik}$, which can be identified as an acceleration, so σ_A will be used to denote this uncertainty. Therefore, the way μ_0 grows with time follows from the equations of motion

$$\sigma_0 = \int dt \int \sigma_A dt + \int \sigma_v dt + \sigma_x.$$

The formula for information gain may be written

$$\Delta I = \log \frac{\sigma_v}{\sigma_1} = \log \frac{\sigma_0}{\sigma_x}$$

$$= \log \left\{ 1 + \int \frac{\sigma_v}{\sigma_x} dt + \int dt \int \frac{\sigma_A}{\sigma_x} dt \right\}.$$

For samples taken at intervals of time S the information rate is

$$I = \frac{1}{S} \log \left\{ 1 + \int \frac{\sigma_v}{\sigma_x} dt + \int dt \int \frac{\sigma_A}{\sigma_x} dt \right\}.$$

σ_x is certainly a constant, and likewise σ_v. However, σ_A may explicitly contain coordinate or velocity terms and perhaps time. If σ_A is set equal to the maximum possible acceleration which can occur, as has been done in previous arguments, a formula for information rate as a function of sampling interval may be written

$$I = \frac{1}{S} \log \left\{ 1 + \frac{\sigma_v}{\sigma_x} S + \frac{1}{2} \frac{A}{\sigma_x} S^2 \right\}.$$

It is easily shown that

$$\lim_{s \to 0} I = 0,$$

and

$$\lim_{s \to \infty} I = 0,$$

so that I has at least one maximum value. An analytic expression for this maximum or for the value of s at this maximum has not been obtained because of mathematical difficulties associated with handling transcendental equations; however, for a particular case, computation of these data can be done numerically or graphically. A graph of I for a typical case of missile-position measurement is shown in Fig. 1. The sampling rate giving a maximum information rate under the assumptions mentioned would be selected for use by the instrumentation system.

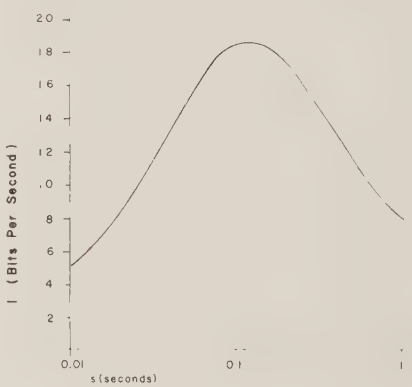

Fig. 1—Information rate.

IX. Conclusions

Under the assumption that missile performance and instrumentation-system required accuracy interact in a way which limits the bandwidth required in the instrumentation of a missile flight, several ways of examining the relationship to establish a bandwidth figure are possible. Of these, the use of control-system design techniques and information theory, as outlined above, is recommended for establishing the bandwidth parameter.

Some Considerations Concerning the Measurement of the Atmospheric Temperature Field by Electromagnetic Means*

D. FRYBERGER†, MEMBER, IRE, AND E. F. URETZ†, MEMBER, IRE

Summary—**A system for determining atmospheric temperature structure by using an electromagnetic radiometer probe is described. The relationship between the electromagnetic sensor reading and atmospheric conditions is developed for both the microwave and infrared sensor utilizing a unified approach for the two cases. It is shown that, with the assumption of horizontal homogeneity, several alternate procedures for inversion of sensor readings to yield the spacial-temperature field are possible. One of these procedures which was used to invert theoretical radiometer readings from an assumed atmospheric structure is described in detail. The results of the inversion which was accomplished with the aid of a UNIVAC 1105 computer are included.**

I. Introduction

ONE of the basic limitations to obtaining adequate meteorological data, for both synoptic and prediction purposes, is the inability to place sensors into regions of interest throughout the atmosphere. This limitation is mainly a result of two factors. First, the mechanics of sensor placement are such that accurate positioning of the sensor is difficult and expensive, *e.g.*, balloon position is at the mercy of prevalent winds. And second, air space restrictions are imposed by the cognizant local and national authorities.

This paper discusses the problem of determining atmospheric temperature without introducing physical probes into the region being investigated.[1] The methods investigated utilize narrow beam electromagnetic probes to obtain integrated temperature function readings. It is shown how, with the assumption of horizontal stratification, these integrated temperature function readings may be inverted to yield the spatial temperature field.

A UNIVAC 1105 was used to simulate the readings of an infrared radiometer and subsequently invert these readings to yield the spatial temperature field. The procedures for these computations and their results are included.

II. Relationship Between Sensor and Atmospheric Temperature Functions

In order to determine a means of calculating the spatial atmospheric temperature field from measurements furnished by an electromagnetic sensor, it is first necessary to determine how this field influences the measurement of that sensor. For the purposes of this derivation, consider an ideal lossless antenna matched to a load resistor R and imbedded in an absorbent atmosphere of infinite extent. It is assumed that the only significant energy transfer between them occurs by the radiative process. Practically speaking, it is reasonable to neglect energy transfer by conduction and convection but corrections must be made to take into account radiation from other thermodynamic entities such as the earth and losses in the antenna and transmission line or waveguide components. It is convenient to consider radiative power transfer as a cycle and label the powers associated with the appropriate points in this cycle. Fig. 1 is included to aid in visualizing the cycle of power transfer.

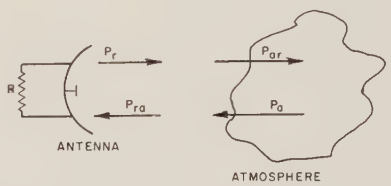

Fig. 1—The cycle of radiative power transfer.

P_r is the power generated by the resistor and radiated from the antenna, and P_{ar} is the power (which was radiated from the antenna) absorbed by the atmosphere. P_a is the power radiated by the atmosphere as a whole, and P_{ra} is the power (which was radiated by the atmosphere) absorbed by the load resistor. Thus by definition $P_{ar}=P_r$ and $P_{ra}=P_a$, and the distinction between the powers related by these qualities is the physical entity with which they are associated.

One can now define the incremental quantities of power dP_{ar} and dP_a which are analogous to P_{ar} and P_a, except that they are associated with the incremental atmospheric volume dV. From the above definitions it follows that

$$P_{ar} = \iiint_V dP_{ar}. \tag{1}$$

In order to obtain a more explicit expression for dP_{ar}, consider the matched antenna to be located at the origin of a spherical coordinate system (s, ξ, η). The antenna is assumed to radiate in all directions, having its direction of maximum gain in the direction $\xi=0$. This configuration is depicted in Fig. 2. Assuming the

* Received by the PGMIL, June 6, 1961.
† Armour Research Foundation, Chicago, Ill.
[1] Many of the results described in this paper were produced while working under Contract No. DA-36-039 SC-80328 for the Meteorological Dept. of the Signal Corps at Fort Huachuca, Ariz.

near field region of the antenna to be negligible,[2] the radiated power density from the antenna at point (s, ξ, η) will be

$$p(s, \xi, \eta) = \frac{P_r G(\xi, \eta)}{4\pi s^2} \exp\left[-\int_0^s \alpha ds\right], \tag{2}$$

where $G(\xi, \eta)$ is the relative antenna power gain over an isotropic radiator as a function of the angles ξ and η, and $\alpha = \alpha(s, \xi, \eta)$ is the power attenuation factor per unit distance due to absorption.

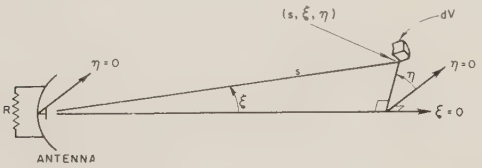

Fig. 2—The coordinate system (s, ξ, η).

The incremental power dP_{ar} absorbed in the incremental atmospheric volume $dV = s^2 \sin \xi d\eta d\xi ds$ at (s, ξ, η) is simply

$$\begin{aligned} dP_{ar} &= \alpha p(s, \xi, \eta) s^2 \sin \xi d\eta d\xi ds \\ &= \frac{\alpha P_r G(\xi, \eta)}{4\pi} \exp\left[-\int_0^s \alpha ds\right] \sin \xi d\eta d\xi ds. \end{aligned} \tag{3}$$

It is important to note that (2) and (3) only include that power which travels directly from the antenna to the point (s, ξ, η) and which is actually absorbed (converted into another energy form) in the incremental volume. Hence, if at the frequency of operation the atmospheric attenuation due to scattering is significant when compared to that due to absorption, the conclusions of this derivation should be regarded as approximations.

Substitution of (3) into (1) yields

$$\begin{aligned} P_{ar} = \frac{1}{4\pi} \int_0^\infty \int_0^\pi \int_0^{2\pi} &\alpha P_r G(\xi, \eta) \\ &\cdot \exp\left[-\int_0^s \alpha ds\right] \sin \xi d\eta d\xi ds. \end{aligned} \tag{4}$$

If at this point the antenna and the atmosphere are considered to be at thermal equilibrium, it follows that $P_r = P_{ra}$, and $P_a = P_{ar}$. These equalities permit the interchange of these quantities in (4) which then becomes the expression for the power absorbed by the antenna as a function of that radiated by the atmosphere, or

$$\begin{aligned} P_{ra} = \frac{1}{4\pi} \int_0^\infty \int_0^\pi \int_0^{2\pi} &\alpha P_a G(\xi, \eta) \\ &\cdot \exp\left[-\int_0^s \alpha ds\right] \sin \xi d\eta d\xi ds. \end{aligned} \tag{5}$$

[2] This assumption will be true if the frequency used allows an effective radiation path length much longer than the antenna dimensions.

The powers appearing in (5) may be associated with temperature by the equation for thermal noise power in a microwave circuit.

$$P = k\theta B, \tag{6}$$

where

k is Boltzmann's constant,
B is the bandwidth under consideration,
θ is a function of the absolute temperature T of the real part of the circuit impedance such that

$$\theta = \frac{h\nu}{k(e^{h\nu/kT} - 1)} \tag{7}$$

where

h is Plank's constant
ν is the frequency under consideration.

It can be seen that θ, appropriately, has the dimensions of degrees. For microwave frequencies and temperatures of over about 10°K, $h\nu/kT \ll 1$ and (7) reduces to $\theta = T$.

However, when considering frequencies in the infrared region, equating the temperature function θ to T is no longer valid.[3] It is also important to note that for any given frequency, θ is a single-valued monotonically-increasing function of temperature. This fact is important in the inversion techniques discussed below.

Eq. (6) may be used to convert (5) into an equation relating the integrated antenna temperature function defined by

$$\theta_i = \frac{P_{ra}}{kB} \tag{8}$$

to the atmospheric temperature function defined by

$$\theta_a = \frac{P_a}{kB}. \tag{9}$$

This relationship is

$$\begin{aligned} \theta_i = \frac{1}{4\pi} \int_0^\infty \int_0^\pi \int_0^{2\pi} &\alpha \theta_a G(\xi, \eta) \\ &\cdot \exp\left[-\int_0^s \alpha ds\right] \sin \xi d\eta d\xi ds. \end{aligned} \tag{10}$$

As was first suggested by Prévost, the radiation mechanism depends only upon conditions of the radiating body and not those of the environment. Consequently, it is found empirically that the radiation from each incremental atmospheric volume is a function of the local temperature and attenuation constant and is not dependent upon the equilibrium condition. Therefore, θ_a need not be considered a uniform constant over all space but may be replaced by $\theta_a(s, \xi, \eta)$, which is a local atmospheric temperature function as a function of

[3] For example, if $\nu = 20\mu$ and $T = 300$°K, then $h\nu/kT = 2.4$, and the higher-order terms of the exponential in (7) are not negligible.

spatial position. This generalization of (10) is

$$\theta_i = \frac{1}{4\pi}\int_0^{\infty}\int_0^{\pi}\int_0^{2\pi} \alpha\theta_a(s,\xi,\eta)G(\xi,\eta) \cdot \exp\left[-\int_0^s \alpha ds\right]\sin\xi d\eta d\xi ds. \quad (11)$$

If the case is considered in which the beam-width of the antenna is narrow enough so that significant contributions to θ_i come from a single direction, then $\theta(s,\xi,\eta)$ and α may be considered to be functions only of the distance coordinate s out along the beam. As a result (11) may be integrated over the angular coordinates. It follows from the definition of $G(\xi,\eta)$ that

$$\int_0^{\pi}\int_0^{2\pi} G(\xi,\eta)\sin\xi d\eta d\xi = \int_0^{\pi}\int_0^{2\pi}\sin\xi d\eta d\xi = 4\pi \quad (12)$$

and (11) reduces to

$$\theta_i = \int_0^{\infty}\alpha\theta_a(s)\exp\left[-\int_0^s \alpha ds\right]ds. \quad (13)$$

Although the essence of the above development is valid in the infrared region, a change in form is required since the concept of antenna gain is not applicable, and as a consequence (12) may not be used. In order to eliminate G in favor of a parameter which has an infrared analog, consider the relationship

$$G = \frac{4\pi A_e}{\lambda^2}, \quad (14)$$

where

A_e is the effective area
λ is the wavelength of the radiation.

The effective area of a lossless, high-gain, highly directional antenna [which would be necessary to reduce $\theta_a(s,\xi,\eta)$ to $\theta_a(s)$] is essentially equal to the actual physical area of the antenna aperture. Thus the concept of effective area is analogous in the two frequency ranges, whereas that of gain is not. However, since an infrared sensor receives radiation of arbitrary polarization while a microwave antenna receives only that component with a specific polarization, the power reception capability per unit area of an infrared sensor is twice that of a microwave antenna, and a factor of two must be used in conjunction with (14). Following this line of reasoning to eliminate gain in favor of the more appropriate concept, effective area, (11) yields

$$\theta_i = \int_0^{\infty}\int_0^{\pi}\int_0^{2\pi}\alpha\theta_a(s,\xi,\eta)\frac{2A(\xi,\eta)}{\lambda^2} \cdot \exp\left[-\int_0^s \alpha ds\right]\sin\xi d\eta d\xi ds, \quad (15)$$

where A is now the effective area of the infrared sensor when viewed from the direction (ξ,η).

If, as before, it is assumed that the beamwidth is sufficiently narrow such that α and θ are not functions of the angular coordinates within the beam, and that $A(\xi,\eta)$ is constant at A_0 for sources within the beam and zero for those elsewhere, then (15) may be integrated over the angular coordinates yielding

$$\theta_i = \frac{2A_0\Omega}{\lambda^2}\int_0^{\infty}\alpha\theta_a(s)\exp\left[-\int_0^s \alpha ds\right]ds, \quad (16)$$

where Ω is the solid angle of the radiometer beam.

By again considering the atmosphere and the sensor at a uniform temperature and using (6) and (7), it may be shown that (16) reduces to Planck's radiation law.

Thus it has been shown that for a narrow beam radiometer, the temperature along the beam contributes to an integrated temperature function according to the relation

$$\theta_i = K\int_0^{\infty}\alpha\theta_a\exp\left[-\int_0^{\infty}\alpha ds\right]ds, \quad (17)$$

where

$K=1$ for the microwave case, and
$K=2A_0\Omega/\lambda^2$ for the infrared case.

The value of θ_i associated with a radiometer measurement is found by use of (8), which is its relation to the power entering the sensor. It would, of course, be necessary to calibrate any given sensor, taking into account extraneous inputs, losses, reflections, etc., so that an accurate assessment of P_{ra} and thus θ_i may be made from the sensor output.

It can be seen that the integrated temperature function of the radiometer is composed of a contribution from each point along the beam. This contribution is proportional to the local temperature function and attenuation factor diminished by the total attenuation between that point and the radiometer. In this context, the absorption attenuation factor may be considered to be a kind of coupling coefficient which couples each point in the beam to the radiometer. The mechanism of scattering, which was not taken into account above, will diffuse the beam allowing radiation emanating from points outside the beam to contribute to θ_i. Consequently, if the technique of remote temperature measurement described herein is attempted at a frequency at which attenuation by scattering is significant, the accuracy of the results will be deteriorated. This deterioration can be minimized by using the total attenuation factor in (17), but in this case the resultant solution for θ_a at each point will, in reality, be an average of the temperature function at that point and an integral similar to (15) which will include θ_a at all other points within scattering range. The fact that the two components of this average will be weighted in proportion to the ratio of the attenuation factors due to these two processes affords a means of estimating the amount of deterioration due to scattering.

III. Requirements for Solution

Eq. (17) forms an integral relationship between the field of atmospheric temperature function $\theta_a(s)$ and the integrated temperature function θ_i. The desired information is a profile of atmospheric temperature T_a vs distance s out along the beam. This temperature profile may be obtained directly from a profile of θ_a vs s by the explicit solution of (7) for T_a, which is

$$T_a = \frac{h\nu}{k \ln\left(1 + \frac{h\nu}{k\theta_a}\right)}. \tag{18}$$

However, in order to obtain the θ_a-s profile it is evident that a profile of θ_i vs some new parameter, say ϕ, is necessary. It is shown in the next section how, if it is assumed that the atmospheric temperature field is horizontally stratified, the elevation angle of the radiometer beam may be used as the parameter ϕ. It may also be possible to use other variables, such as the radiometer frequency ν, as the data profile parameter. The use of ν would relax the requirement for the assumption of stratification, but due to the additional complications in the functional relationships and consequently in the mathematical solution, this approach has not yet been investigated.

There are several possible approaches which may be used to solve for a θ_a-s profile given a θ_i-ϕ profile. One possibility is a demonstration that the integral is in the form of an integral equation for which the solution is already known. Another possibility is the selection of N points, for example a set of N data points, from the θ_i-ϕ profile and the solution of the resultant N equations for N selected points on the θ_a-s profile. This latter approach offers a considerable variety of options since there is an infinite number of possible sets of the N points on the unknown θ_a-s profile, as well as several solutional forms which may be assumed for the θ_a-s profile. For example, it may be assumed that there are N homogeneous layers each of constant θ_{an}, or it may be assumed that θ_{an} is continuous throughout, but allowed to vary in a linear fashion in each layer.

For solution by any of these approaches it must be assumed that $\alpha(s)$ is not a function of $\theta_a(s)$ if the mathematics are to be tractable. However, since the parameter $\alpha(s)$ is, in fact, a function of $\theta_a(s)$, it is necessary initially to assume an expected $\theta_a(s)$ structure, determine the resultant $\alpha(s)$ structure, and then solve for $\theta_a(s)$. If necessary, this solution for $\theta_a(s)$ can then be used to correct the assumed $\alpha(s)$ structure and a second more accurate solution for $\theta_a(s)$ may be found. The number of successive approximations which must be made in this fashion in order to obtain a final solution of sufficient accuracy depends upon the accuracy of the initial assumption for the $\theta_a(s)$ structure and the sensitivity of α to variations in θ_a. Another limitation on the accuracy of the profile solution is, of course, the number and accuracy of the original data points in the θ_i-ϕ profile. A further consideration concerning the accuracy of the final result is the requirement for a complete θ_i-ϕ profile. If the θ_i-ϕ profile is continuous but not complete, then the solution for the θ_a-s profile is not uniquely determined, but is dependent upon the assumptions made about the unknown segments of the θ_i-ϕ profile. These aspects of the problem are covered in more detail in the next section.

IV. Procedures for Solution

As discussed above, the elevation angle of the radiometer beam may be used as a profile parameter of θ_i. The geometry of the radiometer beam and the division of the atmosphere which is used for the solutional techniques discussed below is depicted in Fig. 3.

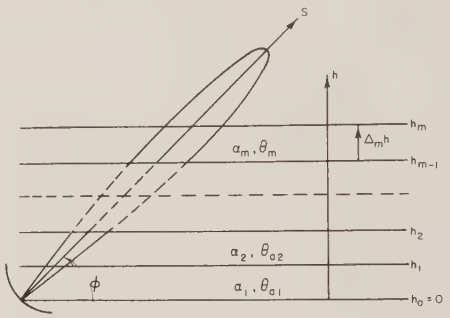

Fig. 3—Orientation of the radiometer beam in the atmosphere.

A. Integral Inversion

Given a profile of θ_i vs ϕ, an integral solution of (17) may be effected as follows. If horizontal stratification of atmospheric temperature is assumed, we may express (17) in terms of the variable of h instead of s. This makes possible a simplification in (17) which will lead to a solution for the atmospheric temperature θ_h at the height h feasible.

For the case of horizontal stratification, α may be considered to be a function of height which may be expressed as

$$\alpha = \alpha_0 f(h) \tag{19}$$

where α_0 is the attenuation at $h=0$. It will be recalled that θ_h as well as other atmospheric parameters enter into the expression for $f(h)$. However, to include these relationships explicitly in (19) would render a solution for θ_h extremely difficult if not impossible. The most practicable approach is to assume a structure for the pertinent atmospheric parameters and consider $f(h)$ as a function of h alone. Typical variations for atmospheric parameters for heights up to 700 km are published,[4] and these may be used in conjunction with local atmospheric conditions, which will be known at the time of measurement of θ_i, to determine the best pro-

[4] R. A. Minzner, K. S. W. Champion, and H. L. Pond, "The ARDC Model Atmosphere," AF Surveys in Geophysics, AF Cambridge Res. Labs., L. G. Hanscom Field, Bedford, Mass. Rept. No. 115; 1959.

files of θ_h and α vs h which whould be assumed for the operating frequency. After a profile of θ_h vs h is determined, corrections may be made to the α-h profile, if necessary. By the use of successive approximations the accuracy of θ_h may be improved.

From the geometry of the configuration we may say

$$ds = \csc \phi dh. \tag{20}$$

Atmospheric refraction of the beam is neglected since for small ϕ, when the refractive effects are greatest, path attenuation will limit the effective path length so that path curvature will not introduce appreciable error. For larger ϕ, path curvature becomes negligible.

Substituting (19) and (20) into (17) we get

$$\theta_i = \alpha_0 K \csc \phi \int_0^\infty f(h)\theta_h \cdot \exp\left[-\alpha_0 \csc \phi \int_0^h f(h)dh\right] dh. \tag{21}$$

This may be simplified by letting

$$\int_0^h f(h)dh = z. \tag{22}$$

Then

$$dh = \frac{dz}{f(h)}. \tag{23}$$

Substituting (22) and (23) into (21) gives

$$\theta_i = \alpha_0 K \csc \phi \int_0^\infty \frac{f(h)\theta_z \exp\left[-\alpha_0 z \csc \phi\right]}{f(h)} dz$$

$$= \alpha_0 K \csc \phi \int_0^\infty \theta_z \exp\left[-\alpha_0 z \csc \phi\right] dz. \tag{24}$$

Note that the subscript of θ_a has been changed depending upon which variable is considered to be independent. The upper limit of integration is unchanged if we assume all $\alpha > \delta$ where δ is any arbitrarily small fixed value greater than zero. For from this it follows that

$$\int_0^\infty f(h)dh = \infty.$$

By (22) $z=0$ when $h=0$, and the lower limit remains zero.

For further simplification let

$$p = \alpha_0 \csc \phi \quad \text{and} \quad \theta_i = K\theta_p. \tag{25}$$

This gives

$$\theta_p = p \int_0^\infty \theta_z e^{-pz} dz. \tag{26}$$

The subscript p is used in order to denote the angular dependence of θ_p upon the new parameter p.

Eq. (26) is in the form of a p-multiplied Laplace transform. The inverse transform[5] of (26) is

$$\theta_z = \frac{1}{2\pi i} \int_{Br_1} \frac{e^{pz}\theta_p dp}{p}, \tag{27}$$

where $i = \sqrt{-1}$ and Br_1 indicates that the integration is to be performed over a suitable Bromwich contour in the complex plane.

In order to solve (27) θ_p must be expressed as a function of p. An examination of the physical situation will aid in doing this. From (25) when $\phi = 0$, $p = \infty$ and θ_p will be equal to the ground temperature function θ_g divided by K. When $\phi = 90°$, $p = \alpha_0$. Thus it can be seen that θ_p as a function of p can be determined empirically for real p in the range of $\alpha_0 \leq p \leq \infty$, but θ_p is undefined in the range $0 \leq R_e(p) < \alpha_0$. Since (27) must be integrated over a Bromwich contour in the complex plane, in order to obtain a solution it is desirable to choose ν such that α_0 is as close to zero as possible to minimize the effects of approximating the function θ_p for values of $R_e(p) < \alpha_0$. However, if α_0 is chosen to be too small, the effective path length for $\phi = 0$ will be too long to neglect the effects of the earth's curvature and atmospheric refraction. For these reasons, a tentative minimum α_0 of about 1 db/km is suggested.

From physical considerations a graph of $K\theta_p$ vs p would be expected to be similar to the plot in Fig. 4. $K\theta_p$ approaches θ_g asymptotically as p increases to ∞. For $p > p_1$, $K\theta_p = \theta_g$ may be assumed true with negligible error.

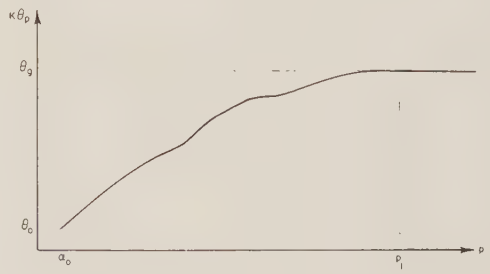

Fig. 4—Typical profile of $k\theta_p$ vs p.

The θ_p-p profile along the real p-axis which is obtained from a θ_i-ϕ profile using the appropriate relationships above can be used to define a general θ_p function in the right half of the complex p-plane. This function used in (27) will result in a solution for θ_z from which may be extracted the desired solution for θ_h. Care must be exercised, however, in the extension of θ_p as a function of complex p if convergent solutions are to be obtained. The authors have devised a technique using a power series expansion of θ_p, a discussion of which would go beyond the intended scope of this paper.

B. Matrix Inversion

If N readings of θ_i vs ϕ are taken, then by the use of appropriate approximations to the form of the θ_a-s

[5] N. W. McLachlan, "Complex Variable Theory and Transform Calculus," University Press, Cambridge, England, p. 135; 1955.

profile, N equations in N unknowns will result. If, for example, it is assumed that there are N homogeneous layers of thickness $\Delta_m h = h_m - h_{m-1}$ as depicted in Fig. 3, each with a constant temperature θ_{am} and attenuation factor α_m, then an equation relating the N unknown θ_a's to the nth measurement of θ_i may be written

$$\theta_{in} = \sum_{m=1}^{N} A_{nm}\theta_{am}, \tag{28}$$

where A_{nm} is approximated by

$$A_{nm} = K \csc \phi_n \alpha_m \Delta_m h \cdot \exp\left[- \sum_{j=1}^{m-1} \csc \phi_n \left(\alpha_j \Delta_j h + \frac{\alpha_m \Delta_m h}{2} \right) \right]. \tag{29}$$

The N equations corresponding to the N measurements of θ_{in} vs ϕ_n are linear and may be written in the matrix form

$$\Theta_i = A\Theta_a, \tag{30}$$

where Θ_i, A, and Θ_a represent the matrix arrays of θ_i, A_{nm}, and θ_a, respectively. The solution of (30) is, of course, obtained by inversion of the matrix A.

$$\Theta_a = A^{-1}\Theta_i. \tag{31}$$

Although the matrix solution of (31) is mathematically straightforward, as N is increased the quantity of the mathematics rapidly becomes unwieldy, and the use of computers for calculations is highly desirable.

Another assumption which may be made concerning the form of the unknown θ_a-h profile is that

$$\theta_a \big|_{h=0} = \theta_g,$$

the ground temperature function, and θ_a varies linearly throughout each layer and is continuous between layers. This approach was used in an atmospheric temperature structure simulation and inversion investigation that was programmed for a UNIVAC 1105 computer. The details of this analysis are outlined in the next section.

V. Profile Inversion Using a Computer

In order to test the practicality of this kind of profile inversion, several typical T_a-h profiles were assumed. These profiles were then converted to θ_a-h profiles and integrated to obtain simulated radiometer profiles of θ_i vs ϕ. In order to have a practical integral for evaluation, a distance D, within which 99.9 per cent of the atmospheric power contribution to θ_i would be emitted, was chosen for the upper limit of the main integral in (17). This distance was determined by examining the appropriate expected profile of α. The radiometric profile simulation equation then becomes

$$\theta_i' = \int_0^D \theta_a \alpha \exp\left[- \int_0^s \alpha ds \right] ds, \tag{32}$$

where $\theta_i' = \theta_i / K$. By letting $h = s \sin \phi$ this becomes

$$\theta_{in}' = \int_0^{D \sin \phi_n} \alpha \csc \phi_n \theta_a \exp\left[- \int_0^h \alpha \csc \phi_n dh \right] dh. \tag{33}$$

For each T_a-h profile which was assumed, twenty data points (θ_{in}', ϕ_n) were found by integrating (33) for values of ϕ_n such that

$$\sin \phi_n = \frac{2000n}{D}, \qquad n = 1, 2, 3, \cdots 20. \tag{34}$$

In order to invert the θ_i'-ϕ profile, the θ_a-h profile was divided into 500-foot increments, and θ_a was assumed to be the function of height given by the following set of equations:

$$\theta_a = \begin{cases} \theta_{a1} = \theta_g + k_1 h & 0 \le h < 500 \\ \theta_{a2} = \theta_g + k_1 500 + k_2(n - 500) & 500 \le h < 1000 \\ \cdots\cdots\cdots\cdots & \\ \theta_{aj} = \theta_g + k_1 500 + \cdots + k_{j-1} 500 + k_j[h - (j-1)500] & (j-1)500 \le h < j500 \\ \cdots\cdots\cdots\cdots & \\ \theta_{a20} = \theta_g + k_1 500 + \cdots + k_{19} 500 + k_{20}(h - 9500) & 9500 \le h < 10{,}000, \end{cases} \tag{35}$$

where θ_g is computed from ground measurement.

The k_j, then, are the constants describing the θ_a-h profile which were to be evaluated.

As the first step in the computation of the k_j, a temperature-density structure was assumed based on standard atmospheric profiles. With this temperature-density structure, the value of α as a function of height was approximated from theoretical considerations. (The values of α have been tabulated as a function of T, p, and ν with the aid of a UNIVAC 1105 computer.) Since ϕ_1 and D were chosen in such a fashion that the contribution from the layers $n \ge 2$ is negligible, the first evaluation of the value of k_1 was straightforward. Thus

$$\theta_{i1}' = \int_0^{D \sin \phi_1} \alpha \csc \phi_1 (\theta_g + k_1 h) \cdot \exp\left[- \int_0^h \alpha \csc \phi_1 dh \right] dh \tag{36}$$

or

$$k_1 = \frac{\theta_{i1}' - \int_0^{D \sin \phi_1} \alpha \csc \phi_1 \theta_g \exp\left[- \int_0^h \alpha \csc \phi_1 dh \right] dh}{\int_0^{D \sin \phi_1} \alpha h \csc \phi_1 \exp\left[- \int_0^h \alpha \csc \phi_1 dh \right] dh}. \tag{37}$$

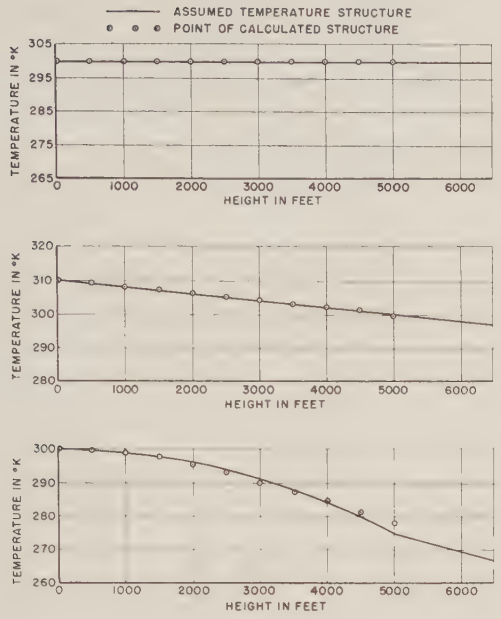

Fig. 5—Comparison of computed and actual temperature-height profiles.

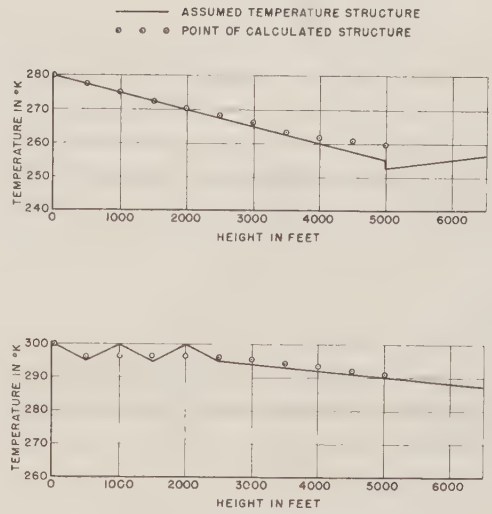

Fig. 6—Additional comparison of computed and actual temperature-height profiles.

The value of $\theta_{a1}=\theta_g+k_1h$ was then converted to the temperature profile in the range $0\leq h<500$, and new values for p and α corresponding to this temperature structure were found. Approximate values for p and T corresponding to a standard profile from 500 feet up were used to compute α in the range $500\leq h<D\sin\phi_2$. Then the value k_2 was found as

$$k_2=\frac{\theta_{i2}'-\int_0^{500}\alpha\csc\phi_2(\theta_g+k_1h)\exp\left[-\int_0^h\alpha\csc\phi_2dh\right]dh-\int_{500}^{D\sin\phi_2}\alpha(\theta_g+k_{1500})\exp\left[-\int_0^h\alpha\csc\phi_2dh\right]dh}{\int_{500}^{D\sin\phi_2}\alpha\csc\phi_2(h-500)\exp\left[-\int_0^h\alpha\csc\phi_2dh\right]dh}. \quad (38)$$

Proceeding in this fashion a first approximation to the values of k_j was obtained. From these values of k_j, T_a-h profiles which could be compared to the originally assumed profiles were derived. This comparison is given in Figs. 5 and 6.

VI. Conclusions

The above analysis has shown that if the temperature of the atmosphere is assumed to be horizontally stratified, that a profile of radiometer measurements vs elevation angle can be inverted into a profile of atmospheric temperature vs height. The assumption of horizontal stratification is a reasonable one for a first approximation and is quite often used in meteorological analysis. But it should be kept in mind that although the vertical temperature gradients are generally the largest, there are horizontal gradients which, for better approximations to the atmospheric temperature field, should not be neglected. The possibility of using frequency as a profile parameter is suggested as a means of relaxing the assumption of horizontal stratification, but it is evident that this would lead to practical difficulties such as radiometer calibration, etc., as well as to mathematical complexity.

The first approximate solutions to the profile inversions which were accomplished with the aid of a UNIVAC 1105 computer show a fairly good correlation to the originally assumed profiles and, indeed, detect atmospheric inversions. Although this gives an indication of the mathematical feasibility of a profile inversion of this type, there are still practical considerations concerning the radiometer and the errors inherent in its data which have not yet been investigated. For example, it is expected that scattering in a hazy atmosphere, especially at infrared wavelengths, could be a limitation to the usefulness of this technique. Despite these limitations, it is felt that continued investigations, both theoretical and experimental, offer promise of the development of a useful technique for the remote measurement of temperature.

Improvement in Tracking Accuracy of Pulse Radar by Coherent Techniques*

S. KAZEL†, ASSOCIATE MEMBER, IRE, AND J. N. FARAONE†, MEMBER, IRE

Summary—**The theory of optimum linear prediction and filtering is applied to determine the optimum system response of pulse (noncoherent) and pulse-Doppler (coherent) radars for target motions consisting of 1) random steps of velocity, and 2) random steps of acceleration. The rms error in velocity data is calculated for each system, and the improvement factor of pulse-Doppler over pulse radar is obtained. The improvement factor is considerably greater in the case of random steps of acceleration, demonstrating that the relative accuracy of the two systems depends on the nature of the target motion, as well as on the radar parameters. Although the errors in both systems are reduced somewhat by allowing large delays in output data, the relative accuracy is found to be unchanged.**

I. Introduction

ATTEMPTS to improve on the accuracy of velocity data obtainable from ordinary, noncoherent pulse tracking radars have led to the development of coherent, pulse-Doppler techniques. The purpose of this paper is to demonstrate that the degree of improvement of pulse-Doppler over pulse radar depends considerably on the type of target motion, as well as on the radar parameters. The theory of optimum linear filtering is applied to obtain the design for the pulse and pulse-Doppler systems that will, in each case, minimize the mean-square-tracking error. The errors for the two systems are then compared. The analysis is carried through in detail for a target motion consisting of random steps of velocity, and results are also presented for the case of random steps of acceleration. Although all target motions are not random processes, as are the two examples above, the use of random inputs simplifies the analysis and demonstrates clearly that the degree of improvement in tracking accuracy due to coherent techniques depends on the type of target motion.

II. Pulse and Pulse-Doppler Radar Tracking Systems

In radar tracking systems, the RF echo pulses are modulated by the motion of the target, both in their time of occurrence and in their radio frequency. The latter effect is the Doppler-shift phenomena. The time displacement of the echoes is proportional to the range of the target, while the frequency, or Doppler, shift is proportional to the target velocity. In ordinary (noncoherent) pulse radar, target position or range is obtained by means of a feedback loop that tracks the time of occurrence of the echo pulses. Radial velocity, acceleration, etc., are obtained by successive differentiation of range data. In pulse-Doppler (coherent) radar, target velocity is obtained directly by means of a feedback loop that tracks the frequency of the echo pulses. Integration and differentiation of the velocity data, respectively, provide range and acceleration data. The two types of tracking loops are shown in Fig. 1(a) and (b). The response of both loops is linear, over the normal operating range, with respect to the quantity they track. This linearity justifies the representation of the tracking loops as linear-feedback networks, as shown in Fig. 1(c). The feedback network, in turn, may be replaced by a single block representing the closed-loop transfer function of the feedback network, as in Fig. 1(d).

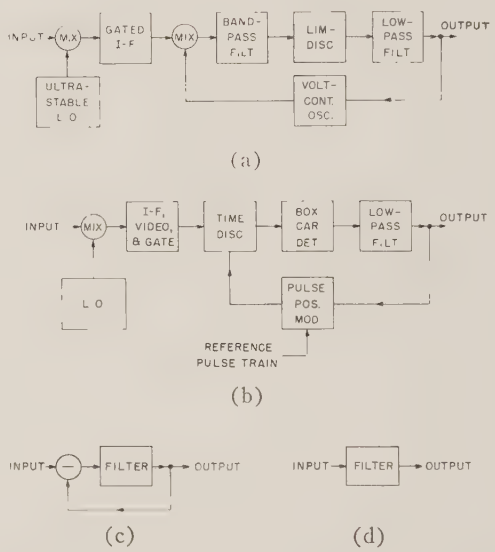

Fig. 1—Representation of pulse and pulse-Doppler tracking loops. (a) Pulse-Doppler radar velocity tracking. (b) Pulse-radar range tracking. (c) Equivalent feedback network. (d) Equivalent filter.

Thus, the problem of designing tracking loops for minimum error is equivalent to the problem of determining the optimum linear filter or transfer function that passes the waveform corresponding to range or velocity with minimum error. The error criterion applied is the total mean square error due to signal distortion (lag errors) and system noise.

III. Optimum Linear Filtering

The optimum filter effects the best compromise between errors due to signal distortion (lag errors), and errors due to system noise. The criterion of performance

* Received by the PGMIL, May 29, 1961. This work was conducted under Contract No. DA-36-039-SC-85318.

† Armour Research Foundation, Illinois Inst. Tech., Chicago, Ill.

is commonly taken as the total mean-square-error σ^2 and is given by[1]

$$\sigma^2 = \int_0^\infty \{ | Y(\omega) |^2 \Phi_n(\omega) + | Y(\omega) - Y_d(\omega) |^2 \Phi_s(\omega) \} d\omega \quad (1)$$

for the usual case of uncorrelated signal and noise.[2] Here

$\Phi_s(\omega)$ is the signal power spectrum,
$\Phi_n(\omega)$ is the noise power spectrum,
$Y_d(\omega)$ is the desired operation on the signal,
$Y(\omega)$ is the actual transfer function,
ω is the frequency variable.

The first term in the integrand of (1) is the spectral density of the output noise, and the second term is the spectral density of output signal distortion. It is assumed that the radar PRF is large compared to the spectrum of target motion, so that no significant components of target motion are lost because of the sampled nature of the data.

The optimum filter for mimimization of the mean-square-error is given by[3,4]

$$Y(s)_{\text{opt}} = \frac{1}{\psi(s)} \left[\frac{Y_d(s)\Phi_s(s/j)}{\psi(-s)} \right]_+, \quad (2)$$

where $\psi(s)$ and $\psi(-s)$ result from factoring the total input spectrum. That is, total input spectrum,

$$\Phi(s/j) = \Phi_s(s/j) + \Phi_n(s/j) = \psi(s)\psi(-s), \quad (3)$$

where $\psi(s)$ has poles only in the left half s plane. The operation $[\ ]_+$ indicates picking the realizable part of the expression in brackets (*i.e.*, the part having poles only in the left-half plane). It is thus seen that the form of the optimum filter for performing a specified operation on its input depends only on the spectra of signal and noise.

This paper is concerned primarily with the problem of obtaining velocity data from the pulse and pulse-Doppler radars. It is assumed that no delay in the velocity data output is allowable.[5] Thus, for the pulse radar, which tracks a range signal, the desired operation on the signal is differentiation. For the pulse-Doppler radar which tracks a velocity signal, the desired operation is pure smoothing, corresponding to an operator of unity.

IV. Signal and Noise Spectra

Pulse Radar

Assume that the target motion is specified in terms of its velocity spectrum $\Phi_v(\omega)$. Since range is the integral of velocity, a factor of $1/\omega$ relates the magnitude of the two components, and a factor of $1/\omega^2$ relates the magnitude of their power spectra. Thus, the corresponding range spectrum is

$$\Phi_r(\omega) = \frac{1}{\omega^2} \Phi_v(\omega). \quad (4)$$

The spectrum of the equivalent signal in the range tracking loop is proportional to $\Phi_r(\omega)$, or

$$\Phi_s(\omega) = c_1 \frac{\Phi_v(\omega)}{\omega^2}, \qquad c_1 = \text{a constant}. \quad (5)$$

If the input noise has the spectrum $N(\omega)$, the equivalent noise in the range tracking loop has the same form, or

$$\Phi_n(\omega) = c_2 N(\omega), \qquad c_2 = \text{a constant}. \quad (6)$$

The optimum filter for differentiating the range signal (thus giving the desired velocity data) could be obtained from the signal and noise spectra of (5) and (6), setting $Y_d(s) = s$ in (2). This corresponds to designing a filter that differentiates and smooths the input, all in one step. Mathematically, however, it makes no difference if we differentiate the input first, and follow this with an optimum smoothing filter. Differentiation of the input multiplies the range signal and noise spectrum of (5) and (6) by ω^2, so that the spectra of signal and noise to be smoothed, are

$$\Phi_s = c_1 \Phi_v(\omega), \quad (7)$$

$$\Phi_n = c_2 \omega^2 N(\omega). \quad (8)$$

Pulse-Doppler Radar

The spectrum of the equivalent signal in the Doppler-frequency tracking loop is proportional to the spectrum of target velocity, or

$$\Phi_s(\omega) = c_3 \Phi_v(\omega), \qquad c_3 = \text{a constant}. \quad (9)$$

The effect of the limiter-discriminator combination in the frequency-tracking loop is to multiply the input noise spectrum $N(\omega)$ by $c_4\omega^2$, (see Appendix IV), giving:

$$\Phi_n(\omega) = c_4 \omega^2 N(\omega), \qquad c_4 = \text{a constant}. \quad (10)$$

The desired operation of the loop is pure smoothing. Comparing (9) and (10) with (7) and (8), it is apparent that the signal and noise spectra have the same form, apart from constant factors. Thus, the optimum-filter design problem is essentially the same in the two cases, except for the values of the constants, noting that the pulse radar, in addition, differentiate the input. The essential design problem may be restated as follows,

[1] H. W. Bode and C. E. Shannon, "A simplified derivation of linear least square smoothing and prediction theory," Proc. IRE, vol. 38, pp. 417–425; April, 1950.

[2] The integral extends only over positive frequencies because we have chosen to combine spectral components at positive and negative frequencies.

[3] N. Wiener, "Extrapolation, Interpolation and Smoothing of Stationary Time Series," John Wiley & Sons, Inc., New York; 1949.

[4] H. S. Tsien, "Engineering Cybernetics," McGraw-Hill Book Co., Inc., New York, N. Y., p. 238; 1954.

[5] In many tracking problems, no significant delay in data can be tolerated. The effect of allowing large data delay is considered later.

Find the optimum filter, given

$$\text{Signal spectrum, } \Phi_s(\omega) = c_a^2\Phi_v(\omega)$$

$$\text{Noise spectrum, } \Phi_n(\omega) = c_b^2 N(\omega)$$

$$\text{Desired operation, } Y_d(\omega) = 1 \text{ (pure smoothing),} \quad (11)$$

where c_a^2 and c_b^2 are constants.

V. Optimum Tracking of Random Steps of Velocity

The target motion is assumed to be a series of alternate and equal positive and negative steps of velocity occurring at random with a Poisson distribution of spacings, and having an average switching interval $\overline{T}$. The power spectrum of this waveform is given by[6]

$$\Phi_v(\omega) = \frac{d^2}{1 + \dfrac{\omega^2}{K^2}}, \quad (12)$$

where

$$K = 2/\overline{T}, \qquad d^2 = \frac{2}{\pi}\frac{{V_{\text{rms}}}^2}{K}, \quad (13)$$

and V_{rms} is the rms target velocity, neglecting any constant velocity component.

The input noise to the radar will be assumed to be of constant power density η or

$$N(\omega) = \eta. \quad (14)$$

Other noise spectrums can be readily treated; however, (14) is the most common in practice.

It should be pointed out that other processes and waveshapes may have the same power spectrum as (12). For example, the output of a low-pass, single-section RC filter, has the same form as (12), when the input is a flat noise spectrum. The solution of our present problem is applicable to all other problems having the same signal and noise spectra.

Substituting (13) and (14) in (11) gives the following optimum filter design problem.

$$\text{Signal spectrum, } \Phi_s(\omega) = \frac{\phi^2}{1 + \dfrac{\omega^2}{K^2}}, \quad (15a)$$

$$\text{Noise spectrum, } \Phi_n(\omega) = k^2\omega^2, \quad (15b)$$

$$\text{Desired operation, } Y_d(\omega) = 1 \text{ (pure smoothing),} \quad (15c)$$

where

$$\phi = c_a d \quad \text{and} \quad k^2 = c_b^2\eta. \quad (16)$$

The solution of this problem, given formally by (2), is carried out in Appendix I. The result is

$$Y(s)_{\text{opt}} = \frac{1}{(1 + b + a)}\cdot\frac{1}{1 + bs + as^2}, \quad (17)$$

[6] Tsien, *op. cit.*, p. 123.

where

$$a = k/\phi K, \qquad b = \frac{k}{\phi}\sqrt{1 + 2\frac{\phi}{Kk}}. \quad (18)$$

At high signal-to-noise ratios (small k), which are required for high-accuracy tracking, the optimum filter approaches the form

$$Y(s)_{\text{opt}} = \frac{1}{1 + \sqrt{2a}\,s + as^2}. \quad (19)$$

Having obtained the optimum filter, the minimum mean-square-error in the tracking loop may be determined from (1). The integral of (1) is evaluated in Appendix II, for the $Y(s)$ given in (19). The result is

$$(\sigma_v^2)_l = \sqrt{2}\pi(K\phi)^{3/2}k^{1/2}. \quad (20)$$

The subscript l indicates that the error is in the loop analog of target velocity. The notation σ_v indicates rms velocity error. This result applies to both the pulse and pulse-Doppler systems, except that the values of ϕ and k (corresponding, respectively, to effective input signal and noise levels) differ in the two systems. It therefore remains to evaluate ϕ and k for both systems.

The constant ϕ is evaluated in Appendix III with the result:

$$\text{Pulse radar:} \qquad \phi^2 = \frac{8}{\pi c^2}\frac{{V_{\text{rms}}}^2}{K}, \quad (21)$$

$$\text{Pulse-Doppler radar:} \quad \phi^2 = \frac{8}{\pi}\left(\frac{f_0}{c}\right)^2\frac{{V_{\text{rms}}}^2}{K}, \quad (22)$$

where c is the propagation velocity, and f_0 is the transmitted RF frequency.

The constant k is evaluated in Appendix IV with the result:

$$\text{Pulse radar:} \qquad k^2 = \frac{1}{3\pi}\frac{\tau^2\eta}{P_{\text{av}}}, \quad (23)$$

$$\text{Pulse-Doppler radar:} \quad k^2 = \frac{2}{3\pi}\frac{\eta}{P_{\text{av}}}, \quad (24)$$

where τ is radar pulse width (at the half-amplitude points, assuming a triangular pulse). P_{av} is average received power, and η is system noise power density referred to the input.

Substituting the values of ϕ and k from (21)–(24) into (20) gives the mean-square-error in the loop velocity signal:

$$\text{Pulse radar:} \qquad (\sigma_v)_l{}^8 = \frac{2^{12}}{6}\left(\frac{V_{\text{rms}}}{c}\right)^6\frac{K^3\eta\tau^2}{P_{\text{av}}}, \quad (25)$$

$$\text{Pulse-Doppler radar:} \quad (\sigma_v)_l{}^8 = \frac{2^{12}}{3}\left(\frac{V_{\text{rms}}}{c}\right)^6\frac{K^3\eta f_0{}^6}{P_{\text{av}}}. \quad (26)$$

In order to obtain the actual velocity errors of the target, the loop-velocity errors $(\sigma_v)_l$ must be expressed in terms of corresponding target-velocity errors σ_v as

$$\text{Pulse radar:} \qquad \sigma_v = \frac{c}{2}(\sigma_v)_l, \tag{27}$$

$$\text{Pulse-Doppler radar:} \quad \sigma_v = \frac{1}{2}\frac{c}{f_0}(\sigma_v)_l. \tag{28}$$

These two relations follow from the considerations in Appendix III. Substituting (27) and (28), respectively, into (25) and (26) gives, the final result for σ_v, the rms error in target velocity:

$$\text{Pulse radar:} \qquad \sigma_v^8 = \frac{8}{3}c^2 V_{\text{rms}}{}^6 K^3 \tau^2 \eta / P_{\text{av}}, \tag{29}$$

$$\text{Pulse-Doppler radar:} \quad \sigma_v^8 = \frac{16}{3}c^2 V_{\text{rms}}{}^6 K^3 \eta / P_{\text{av}} f_0. \tag{30}$$

The improvement factor F of pulse-Doppler over pulse radar, defined as the ratio of their rms velocity errors, is then found to be

$$F = \frac{\sigma_v(\text{pulse})}{\sigma_v(\text{pulse-Doppler})} = \left(\frac{1}{\sqrt{2}} f_0 \tau\right)^{1/4}. \tag{31}$$

As a numerical example for a C-band radar with $f_0 = 5$ kMc and $\tau = 0.25$ μsec, the improvement factor of pulse-Doppler is $(884)^{1/4}$ or 5.45. In the following section, results are presented for a target motion consisting of random steps of acceleration to demonstrate the marked dependence of the improvement factor on the type of target motion.

VI. Optimum Tracking of Random Steps of Acceleration

The optimum system response of pulse and pulse-Doppler radars for tracking a target motion consisting of random steps of acceleration has been derived, using the same procedure as in the case of random steps of velocity. To avoid repetition, only the highlights and main results of the analysis are presented.

The power spectrum of target acceleration, analogous to (12), is given by

$$\Phi_a(\omega) = \frac{d^2}{1 + \dfrac{\omega^2}{K^2}}, \tag{32}$$

where

$$K = 2/\overline{T}, \qquad d^2 = \frac{2}{\pi}\frac{A_{\text{rms}}{}^2}{K}, \tag{33}$$

and A_{rms} is the rms target acceleration neglecting any constant component of acceleration.

For low noise levels (the usual condition in a high-accuracy tracking system), the optimum response of the pulse-Doppler system for pure smoothing (no data delay) is

$$Y(s)_{\text{opt}} = \frac{1 + 2as}{(1 + as)(1 + as + a^2 s^2)}. \tag{34}$$

This response is multiplied by s for the optimum pulse-radar response, corresponding to differentiation of the input. The parameter a is given by

$$a = (k/K\phi)^{1/3}, \tag{35}$$

where k and ϕ are given by (21)–(24), replacing V_{rms} by A_{rms}.

The rms error in target velocity σ_v is found to be

$$\text{Pulse radar:} \qquad \sigma_v^4 = \frac{3}{2}c^2 A_{\text{rms}}{}^2 K \eta \tau^2 / P_{\text{av}}, \tag{36}$$

$$\text{Pulse-Doppler radar:} \quad \sigma_v^4 = 3c^2 A_{\text{rms}}{}^2 K \eta / P_{\text{av}} f_0{}^2. \tag{37}$$

The improvement factor F of pulse-Doppler over pulse radar is

$$F = \frac{\sigma_v(\text{pulse})}{\sigma_v(\text{Doppler})} = \left(\frac{1}{\sqrt{2}} f_0 \tau\right)^{1/2}. \tag{38}$$

This expression involves the *square*-root of the quantity in parenthesis. For the previous case of random steps of velocity, the improvement factor was the *fourth*-root of the same quantity. Since the quantity $(1/\sqrt{2} f_0 \tau)$ is in practice always much greater than unity, it follows that the improvement factor for pulse Doppler for tracking random steps of acceleration will be greater than for the case of random steps of velocity. For the same numerical example used previously, $f_0 = 5$ kMc and $\tau = 0.25$ μsec, the improvement factor becomes $(884)^{1/2} = 29.7$, compared to the previous value of 5.45. It is apparent that the nature of the target motion has considerable effect on the capability of pulse Doppler to increase tracking accuracy.

VII. Effect of Allowing Data Delay

In theory, the accuracy of output data can be improved by allowing a delay in the processing of the data. Essentially, this allows interpolation of the data from part of the succeeding signal values as well as from past values, rather than from past values alone as in pure smoothing. The output errors decrease monotonically with increasing delay, but approach an irreducible minimum even for infinite delay. Whether a given amount of delay is acceptable depends on the particular application. For command or guidance purposes, little, if any, delay is tolerable. In fact it may be necessary to have negative delay, *i.e.*, a prediction system. For purely measurement purposes, considerable delay may be allowed; however, it may be more practical to obtain such delays by post-data reduction rather than attempting to incorporate the delay in the radar. One reason for this is that for large delays, the instantaneous difference between input and output may be quite large, possibly exceeding the linear range of operation of the tracking system.

The systems analysis is essentially the same if delay is allowed, except that the desired operation $Y_d(s)$ becomes $e^{-\alpha s}$ rather than unity, where α is the delay. The irreducible mean-square-error, corresponding to infinite delay, can be calculated directly by means of the relation[1]

$$\sigma^2 = \int_0^\infty \frac{\Phi_s(\omega)\Phi_n(\omega)}{\Phi_s(\omega) + \Phi_n(\omega)}\, d\omega, \tag{39}$$

where $\Phi_s(\omega)$ and $\Phi_n(\omega)$ are the power density spectra of signal and noise, respectively.

Evaluation of the infinite-lag-error integral of (39) for the target motions considered in this paper, under conditions of low noise, shows that the rms velocity tracking error with no lag can at most be reduced by a factor of two for the case of random steps of velocity, and by a factor $3\sqrt{2}$ for the case of random steps of acceleration. The reduction in error is the same for both pulse and pulse-Doppler systems, so that the improvement factor of pulse-Doppler is unchanged.

VIII. Conclusions

The optimum design of pulse and pulse-Doppler tracking loops in accordance with a mean-square-error criteria has been carried out for two random target motions. Comparison of the resultant tracking errors demonstrates that the improvement of pulse-Doppler (coherent) radar over pulse (noncoherent) radar depends considerably on the type of target motion. Although tracking errors can be reduced somewhat by allowing delay in the output data, the improvement factor of pulse-Doppler over pulse radar was unaffected by the delay, for the target motions considered.

It appears very likely that similar results would be obtained for nonrandom target motions, such as ballistic trajectories. Further work in this area is recommended to obtain specific results.

Appendix I

Calculation of Optimum Smoothing Filter

Given a signal of power spectrum Φ_s,

$$\Phi_s(\omega) = \frac{\phi^2}{1 + \dfrac{\omega^2}{K^2}}, \tag{40}$$

and a noise power spectrum Φ_n,

$$\Phi_n(\omega) = k^2\omega^2 \tag{41}$$

uncorrelated with the signal, the optimum filter is given by

$$Y(s) = \frac{1}{\psi(s)}\left[\frac{Y_d(s)\Phi_s(s/j)}{\psi(-s)}\right]_+, \tag{42}$$

where $Y_d(s)$ is the desired operation on the signal, and is equal to unity for pure smoothing, and

$$\Phi(s/j) = \Phi_s(s/j) + \Phi_n(s/j) = \psi(s)\psi(-s). \tag{43}$$

The operation $[\ ]_+$ indicates picking the realizable part of the expression in brackets. Thus,

$$\Phi(\omega) = \Phi_s(\omega) + \Phi_n(\omega) = \frac{\phi^2}{1 + \dfrac{\omega^2}{K^2}} + k^2\omega^2$$

$$= k^2 \frac{(\phi^2K^2/k^2) + K^2\omega^2 + \omega^4}{K^2 + \omega^2}, \tag{44}$$

$$\Phi(s/j) = k^2 \frac{(\phi^2K^2/k^2) - K^2s^2 + s^4)}{K^2 - s^2}. \tag{45}$$

Factorization of $\Phi(s/j)$ in (45) such that

$$\Phi(s/j) = \psi(s)\cdot\psi(-s)$$

yields

$$\psi(s) = k \frac{s^2 + K\sqrt{1 + 2(\phi/Kk)}\, s + (\phi K/k)}{K + s}, \tag{46}$$

with $\psi(s)$ having zeros and poles only in the left-hand plane, as required. From (40),

$$\Phi_s(s/j) = \frac{\phi^2}{1 - \dfrac{s^2}{K^2}} = \frac{\phi^2K^2}{K^2 - s^2}. \tag{47}$$

Thus,

$$\frac{Y_d(s)\Phi_s(s/j)}{\psi(-s)}$$

$$= 1\, \frac{\phi^2K^2}{K^2 - s^2}\, \frac{1}{k}\, \frac{K - s}{s^2 - K\sqrt{1 + 2(\phi/Kk)}s + (\phi K/k)}$$

$$= \frac{\phi^2K^2}{k}\, \frac{1}{K + s}\, \frac{1}{s^2 - K\sqrt{1 + 2(\phi/Kk)}\, s + (\phi K/k)}. \tag{48}$$

The realizable part of (48) is obtained by expanding the right-hand side in partial fractions and picking the part having poles only in the the left-hand plane. It is evident that only the fraction with $(K+s)$ in the denominator is realizable. Evaluating the coefficient for this term gives

$$\left[\frac{Y_d(s)\Phi_s(s/j)}{\psi(-s)}\right]_+$$

$$= \frac{\phi^2K^2}{k}\, \frac{1}{1 + K\sqrt{1 + 2(\phi/Kk)} + \phi(K/k)}\, \frac{1}{K + s}. \tag{49}$$

The optimum smoothing filter is then given by

$$Y(s) = \frac{1}{\psi(s)}\left[\frac{Y_d(s)\Phi_s(s/j)}{\psi(-s)}\right]_+$$
$$= \frac{\phi^2 K^2}{k^2}\,\frac{1}{1 + K\sqrt{1 + 2(\phi/Kk)} + (\phi K/k)}\left(\frac{1}{s^2 + K\sqrt{1 + 2(\phi/Kk)}s + (\phi K/k)}\right). \quad (50)$$

For small k (low noise) this reduces to

$$Y(s) \cong \frac{1}{1 + \sqrt{2k/\phi K}\,s + \frac{k}{\phi K}s^2}$$
$$= \frac{1}{1 + \sqrt{2a}\,s + as^2}, \quad (51)$$

where $a = k/\phi K$.

Appendix II

Calculation of Mean Square Error in Filtering

The mean square error E may be expressed as

$$E = \int_0^\infty \{\,|\,Y(\omega)\,|^2\,\Phi_n(\omega) + |\,Y(\omega) - Y_d(\omega)\,|^2\Phi_s(\omega)\}\,d\omega, \quad (52)$$

where $Y_d(\omega)$ and $Y(\omega)$ are the desired and actual filter operations, respectively, and $\Phi_s(\omega)$ and $\Phi_n(\omega)$ are the input-signal and noise-density spectra, respectively. Because all the terms in the integrand are even functions, (52) may be written as

$$E = \frac{1}{2}\int_{-\infty}^\infty \{\,|\,Y(\omega)\,|^2\Phi_n(\omega) + |\,Y(\omega) - Y_d(\omega)\,|^2\Phi_s(\omega)\}\,d\omega. \quad (53)$$

For the problem in Appendix I.

$$\Phi_s(\omega) = \frac{\phi^2}{1 + \frac{\omega^2}{K^2}}, \quad (54)$$

$$\Phi_n(\omega) = k^2\omega^2, \quad (55)$$

$$Y(\omega) = \frac{1}{1 + c_1 s + c_0 s^2} = \frac{1}{1 + jc_1\omega - c_0\omega^2}\left(\begin{matrix}\text{Low noise}\\ \text{approximation}\end{matrix}\right), \quad (56)$$

where

$$c_1 = \sqrt{2k/K\phi} \quad \text{and} \quad c_0 = k/K\phi, \quad (57)$$

$$Y_d(\omega) = 1 \text{ (pure smoothing, no delay)}. \quad (58)$$

The two terms in the integral of (53) will be treated separately. The noise term is

$$E_n = \frac{1}{2}\int_{-\infty}^\infty |\,Y(\omega)\,|^2\Phi_n(\omega)\,d\omega = \frac{1}{2}\int_{-\infty}^\infty \frac{k^2\omega^2\,d\omega}{|\,1 + jc_1\omega - c_0\omega^2\,|^2}. \quad (59)$$

Integrals of the above type can be evaluated directly by the "method of residues,"[8] or by the use of integral tables based on this method.[9] The result is

$$E_n = \frac{\pi}{2}\,k^2/c_0c_1. \quad (60)$$

Substituting for c_0 and c_1 from (57) gives

$$E_n = \frac{\pi}{2\sqrt{2}}\,(K\phi)^{3/2}k^{1/2}. \quad (61)$$

The error due to signal distortion is

$$E_s = \frac{1}{2}\int_{-\infty}^\infty |\,Y(\omega) - Y_d(\omega)\,|^2\Phi_s(\omega)\,d\omega = \frac{1}{2}\int_{-\infty}^\infty \left|\frac{1}{1 + jc_1\omega - c_0\omega^2} - 1\right|^2 \frac{\phi^2}{1 + \frac{\omega^2}{K^2}}\,d\omega. \quad (62)$$

After some manipulation, this leads to

$$E_s = \frac{\phi^2}{2}\int_{-\infty}^\infty \frac{(c_0^2\omega^4 + c_1^2\omega^2)\,d\omega}{|\,1 + j[c_1 + (1/K)]\omega - [c_0 + (c_1/K)]\omega^2 - j(c_0/K)\omega^3\,|^2}. \quad (63)$$

This integral may be evaluated using the method of residues or integral tables, with the result

$$E_s = \frac{1}{2}\,\pi\phi^2K^2\,\frac{\left(K + \frac{1}{c_1}\right)\frac{c_0}{c_1} + 1}{K\left(\frac{c_0}{c_1}K + 1\right) + \frac{1}{c_1}}. \quad (64)$$

[8] E. C. Titchmarch, "Theory of Functions," Oxford University Press, New York, N. Y.; 1932.

[9] H. M. James, *et al.*, "Theory of Servomechanisms," M.I.T. Rad. Lab. Ser., McGraw-Hill Book Co., Inc., New York, N. Y., vol. 25; 1947. See Appendix.

Substituting for c_0 and c_1 from (57), and taking k small as assumed, gives

$$E_s = \frac{3}{2}\frac{\pi}{\sqrt{2}}(K\phi)^{3/2}k^{1/2}, \qquad \text{for small } k. \tag{65}$$

The total mean square error in filtering is obtained by adding (61) and (65), giving

$$E = E_n + E_s = \sqrt{2\pi}\,(K\phi)^{3/2}k^{1/2}. \tag{66}$$

Appendix III

Evaluation of Loop Signal Level Coefficient, ϕ

The constant ϕ in (15a), corresponding to loop signal level, is evaluated as follows. Since the tracking loop signal spectrum,

$$\Phi_s(\omega) = \frac{\phi^2}{1 + \dfrac{\omega^2}{K^2}}, \tag{67}$$

is the analog of target velocity spectrum,

$$\Phi_v(\omega) = \frac{d^2}{1 + \dfrac{\omega^2}{K^2}}, \tag{68}$$

it follows that $\phi_0{}^2$ is the loop analog of $a^2{}_0$. Therefore, since

$$d^2 = \frac{2}{\pi}\frac{{V_{\text{rms}}}^2}{K}, \tag{69}$$

it follows that

$$\phi^2 = \frac{2}{\pi}\frac{(V_{\text{rms}})_l{}^2}{K}, \tag{70}$$

where $(V_{\text{rms}})_l$ is the rms input signal, corresponding to velocity, in the loop.

Range Tracking Loop

In the range tracking loop, a change of target range Δr produces a time displacement in the loop Δt_l given by

$$\Delta t_l = \frac{2}{c}\Delta r, \tag{71}$$

where c is the velocity of propagation.

A target velocity V produces a loop "velocity" V_l of

$$V_l = \frac{(\Delta t)_l}{\Delta t} = \frac{2}{c}\frac{\Delta r}{\Delta t} = \frac{2}{c}V. \tag{72}$$

In terms of rms values,

$$(V_{\text{rms}})_l = \frac{2}{c}V_{\text{rms}}. \tag{73}$$

Substituting (73) in (70) gives the desired evaluation of the constant ϕ for pulse radar:

$$\phi^2 = \frac{8}{\pi c^2}\frac{{V_{\text{rms}}}^2}{K}. \tag{74}$$

Doppler Tracking Loop

In the Doppler, or frequency, tracking loop, the Doppler-shift frequency f_d produced by a target velocity V is

$$f_d = 2f_0\frac{V}{c}, \tag{75}$$

where f_0 is the transmitted RF frequency. Since Doppler shift is the loop equivalent of target velocity, we have

$$V_l = f_d = 2f_0\frac{V}{c}. \tag{76}$$

In terms of rms values,

$$(V_{\text{rms}})_l = 2f_0\frac{V_{\text{rms}}}{c}. \tag{77}$$

Substituting (77) in (70) gives the desired evaluation of the constant ϕ for pulse-Doppler radar:

$$\phi^2 = \frac{8}{\pi}\left(\frac{f_0}{c}\right)^2\frac{{V_{\text{rms}}}^2}{K}. \tag{78}$$

Appendix IV

Evaluation of Loop Noise Level Coefficient, k^2

Pulse-Radar

The effect of input noise on the range tracking loop of the pulse radar is to produce a jitter in the detected time of arrival of the echo pulses. It has been shown that the rms time jitter, $\overline{\Delta t}$, with optimum demodulation, cannot be less than[10]

$$\overline{\Delta t}^2 = \frac{1}{2\beta^2}\frac{\eta_d}{\epsilon}, \tag{79}$$

where η_d is the noise spectral density at the time discriminator (referred to the input); ϵ is the signal energy (referred to the input); and β is the effective signal bandwidth, given by

$$\beta^2 = \frac{\displaystyle\int_0^\infty (2\pi f)^2 \left| F_s \right|^2 df}{\displaystyle\int_0^\infty \left| F_s \right|^2 df}. \tag{80}$$

[10] A. J. Mallinckrodt and T. E. Sollenberger, "Optimum pulse-time determination," IRE Trans. on Information Theory, vol. PGIT-3, pp. 151–159; March, 1954.

Here, F_s is the Fourier spectrum of the input pulse. For the triangular pulse shape assumed in this analysis, the Fourier spectrum is of the form

$$F_s(2\pi f) = C\left[\frac{\sin(2\pi f\tau/2)}{2\pi f\tau/2}\right]^2. \tag{81}$$

Substituting (81) in (80), and making the substitution $x = 2\pi fT/2$, gives

$$\beta^2 = \frac{4}{\tau^2}\frac{\int_0^\infty \frac{\sin^4 x}{x^2}\,dx}{\int_0^\infty \frac{\sin^4 x}{x^4}\,dx} = \frac{3}{\tau^2}. \tag{82}$$

The received signal energy ϵ is

$$\epsilon = P_{av}T, \tag{83}$$

where P_{av} is average received power and T is the PRF period. Due to foldover of the noise sidebands in detection, the noise density at the time discriminator (referred to the input) is twice the input noise density η or

$$\eta_d = 2\eta. \tag{84}$$

Substituting (82), (83), and (84) into (79) gives the final expression for time jitter of the received pulses:

$$\overline{\Delta t}^2 = \frac{1}{3}\frac{\tau^2\eta}{P_{av}T}. \tag{85}$$

The output of the range tracking loop time discriminator, for each pulse, is stretched to the full PRF period T using a "boxcar" detector. The effective loop noise is then a random amplitude square wave of period T and rms magnitude $\overline{\Delta t}$ given by (85). The power spectrum of this noise signal can be shown to be of the form $[\sin(\omega T/2)/(\omega T/2)]^2$ with low frequency density k^2 given by[11]

$$k^2 = \frac{1}{\pi}T\,\overline{\Delta t}^2. \tag{86}$$

When the PRF is large relative to the signal spectrum (as assumed in this paper), only the low-frequency noise components are of significance. Thus, for purposes of analysis, the loop noise density may be considered flat, having the value k^2 of (86). Combining (85) and (86) gives

$$k^2 = \frac{1}{3\pi}\frac{\tau^2\eta}{P_{av}}. \tag{87}$$

[11] G. G. MacFarlane, "On the energy spectrum of an almost periodic succession of pulses," Proc. IRE, vol. 37, pp. 1139–1147; October, 1949.

Pulse-Doppler Radar

For low level noise inputs, the noise spectrum out of the FM discriminator of the Doppler tracking loop is quadratic in ω, and is given by[12]

$$\Phi_n(\omega) = \frac{1}{\pi}\frac{\eta_d}{A_c^2}\omega^2 \tag{88}$$

where η_d is the effective input noise density (assumed constant) into the discriminator, and A_c is the (peak) magnitude of a sinusoidal intput signal.

The signal input, prior to the band-pass filter of the tracking loop, is a pulsed carrier having an assumed triangular shape. The band-pass filter isolates the carrier component A_c which is then tracked in frequency. A Fourier analysis of the trangular wave gives the magnitude of the carrier component as

$$A_c^2 = 3P_{av}\frac{\tau}{T}, \tag{89}$$

where P_{av} is average received power, τ is pulse width (at the half-amplitude points), and T is the PRF period.

The effective input noise density η_d is much less than the actual input noise density η, because of the gating of the input. A close approximation for the effect of gating on the low-frequency noise component is that it reduces it by the duty cycle of the gate.[13] Since the gate must be of width 2τ to accept the entire triangular pulse, we obtain

$$\eta_d = \frac{2\tau}{T}\eta. \tag{90}$$

Substituting the above values of A_c and η_d in (88) gives the final expression for the noise spectrum in the Doppler tracking loop:

$$\Phi_n(\omega) = k^2\omega^2 \tag{91}$$

where

$$k^2 = \frac{2}{3\pi}\frac{\eta}{P_{av}}.$$

Acknowledgment

The authors are grateful for helpful suggestions from J. E. McManus of the Armour Research Foundation, and to P. White and D. Samuelson, U. S. Army White Sands Signal Agency, N. Mex.

[12] M. Schwartz, "Information, Transmission, Modulation, and Noise," McGraw-Hill Book Co., Inc., New York, N. Y., p. 301; 1959.

[13] Z. Jelonek, "Noise problems in pulse communications," *J. IEE*, no. 94, pt. IIIA, pp. 533–545; 1947.

Integrated Missile Flight Safety System at Vandenberg/Point Arguello*

K. E. BAILEY† AND J. K. MOLLER‡, SENIOR MEMBER, IRE

Summary—**The background for the present safety system is outlined in a review of the original Air Force plans and installations and subsequent Navy-Air Force agreements for the coordinated use of the Pacific Missile Range, considering the expanded scope of operations in the area.**

A description is given of the ground stations in the unified acquisition and tracking system for range safety as well as the auxiliary equipment for missile monitoring during early parts of its flight trajectory. A review is made of the associated data transmission and processing equipment including operational direct voice circuits. The corresponding safety equipment in different types of missiles is discussed in connection with both command, tracking, and telemetry functions. The implementation of the flight termination command requirements is outlined in the main transmitting station and missile checkout apparatus. The support areas of status reporting, telemetry, timing, and communications are discussed in detail. Finally, new requirements for precise downrange impact prediction and vehicle thrust termination are described.

I. Background

IN March, 1958, the Chief of Staff, USAF, and the Chief of Naval Operations signed an Agreement for the Coordinated Peacetime Operation of the Pacific Missile Range. This agreement assigned the Navy certain responsibilities, among them, "Range Safety precautions within the Pacific Missile Range."

Prior to the agreement, an Instrumentation and Range Safety System was designed, installed, and operated by USAF at Vandenberg AFB to serve the planned training launches of operational ballistic missiles.

In September, 1959, the Agreement for the Coordinated Peacetime Operation of the PMR was rewritten. The new agreement increased the Navy responsibility in range safety to include "Establishment of range safety criteria and the review and approval of range safety plans, procedures and equipment for all missiles, satellites, and space vehicles launched at or into the Pacific Missile Range." This agreement was further modified in December, 1960, giving the National Range Commanders the responsibility and authority for actuating inflight destruction devices when required for safety on all missiles.

In the meantime, the scope of missile operations in the Vandenberg/Point Arguello area (Fig. 1) had been increased to include polar-orbit satellites and R and D and target-type vehicles as well as a more comprehensive ballistic missile training program. To meet the added responsibility and greater requirements by range users in all services, PMR established a plan for an Integrated Missile Flight Safety System covering both USAF and Navy requirements. The instrument systems and equipment available to meet these requirements including the existing USAF system were studied to determine suitability for present and future programs, considering the functions of the Vandenberg/Point Arguello area and the Pacific Missile Range as a whole.

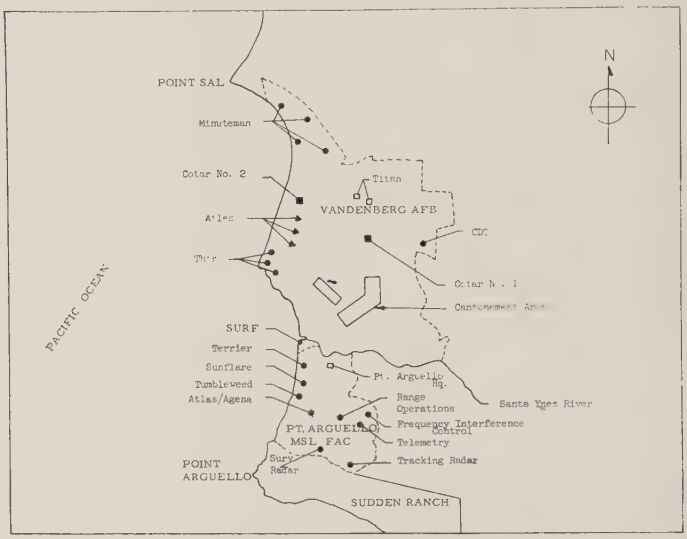

Fig. 1—Outline of Vandenberg/Point Arguello area.

Economy and total launch schedule dictated that only one integrated center should be provided. After extensive study, it was decided to locate the permanent range safety center at Point Arguello rather than expand the Instrumentation Control Center building at Vandenberg AFB. This decision was based on the extent and capability of existing facilities and those being installed as well as cost factors. Also, the integrated center could be developed and checked out without interruption to the Vandenberg safety system, and could be demonstrated in a "monitor" status on actual missile flights.

II. Integrated Missile Flight Safety System (IMFSS)

The Integrated System (Fig. 2) basically consists of four radar stations, one BI-COTAR system, an IBM-709 computer, trajectory display equipment, and a command destruct transmitter. For close-range work,

* Received by the PGMIL, June 1, 1961. The opinions or assertions provided herein by LCDR Bailey are not to be construed as official or reflecting the views of the Navy Department or the Naval service at large.

† Lt. Commander, U. S. Navy, Pacific Missile Range Headquarters, Point Mugu, Calif.

‡ Space Systems Tech. Group, the Siegler Corp., Inglewood, Calif.

the System also uses optical, wire, and radar skyscreens. Supporting this equipment is an extensive voice, status reporting, and remote control wireline network. Microwave and radio voice equipment terminating in the Range Operations (RO) building, Point Arguello. links the IMFSS with the remainder of the Pacific Missile Range and allows for a greater flexibility in operations and instrumentation tie-ins. It is, for instance, quite feasible to use data from a radar station on San Nicolas Island, compute it on the IBM-709, and display the results for the Missile Flight Safety Officer (MFSO) at Point Arguello. Of the above equipment, the radars are located on Point Arguello, while the BI-COTAR and the command destruct transmitter are on Vandenberg. Communications, control and display equipment, and the IBM-709 are in the RO building on Point Arguello. The skyscreens are mobile and located as required in relation to each launch pad.

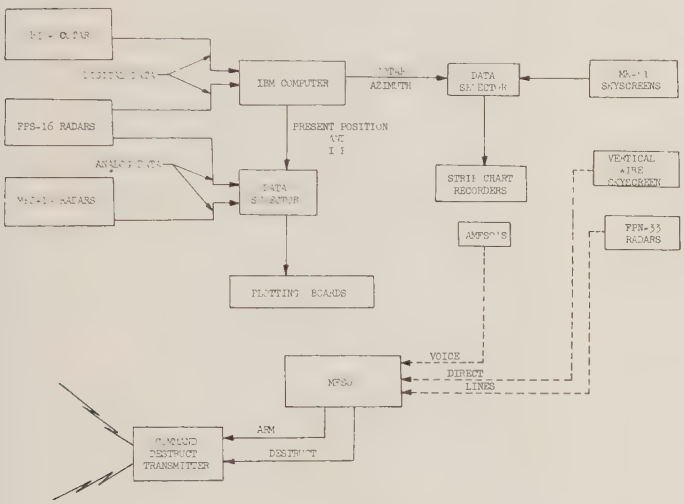

Fig. 2—Block diagram of IMFSS.

The primary tracking radars (Fig. 3) are two *C*-band AN/FPS-16 by RCA, superbly located on top of a 2000-ft mountain. These provide a practical tracking accuracy of 0.2 mil in azimuth and elevation, and 15 feet in range. One unit is set up for a maximum range of 200 and the other for 500 nautical miles. Peak power is 1000 kw with pulse widths of 0.25 to 1.0 μsec. Data output is both 17 bit digital and dc analog. CUBIC digital distribution units and COLLINS Kineplex equipment are used to transmit the digital data by wire to the IBM-709. To aid target acquisition each FPS-16 uses a MK-51 gun director, manually operated, for remote synchro designation to its antenna. The MK-51 has proved very useful in directing the radars at Vandenberg during the first seconds of missile flight until automatic track is established. In addition, each FPS-16 can be slaved to the other for antenna and range gate positioning. The secondary tracking radars are two *S*-band AN/MPS-19, located on a small hill near the RO building. These are 250-kw modified SCR-584 units, one designated as Master for independent or Master/Slave connected operation with a maximum range of 200 nautical miles. A MK-51 director, positioned adjacent to the radar vans, is shared by the two radars for remote antenna designation. Data output is dc analog transmitted by wire to the RO building.

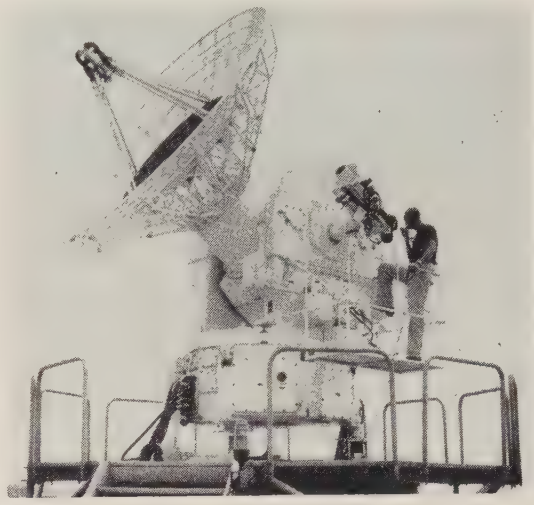

Fig. 3—AN/FPS-16 radar.

The primary radars skin track the average IRBM or ICBM to a slant range of 200 nautical miles. Range restrictions for beacon tracking are set by the equipment range gate limits for targets equipped with radar beacons. The secondary radars provide good tracking out to 100 nautical miles slant range against passive missile targets.

The CUBIC BI-COTAR system (Fig. 4) was originally intended as the primary long-range tracking system at Vandenberg and provides precise real-time position to 50 nautical miles, and missile flight azimuth out to 700 nautical miles. The system measures phase differences on the telemetry carrier radiated from the missile, and from these develops direction cosines. Two extremely flat, four-acre antenna fields are used, each with two perpendicular baselines containing three pairs of antennas for coarse, intermediate, and fine track. Near each field is a building with data receivers, signal strength and frequency monitors, which connect with the IBM-709 computer over wirelines through Kineplex equipment. The BI-COTAR is unique in being the first equipment of its kind with all-electronic phase measurements and binary digital output. The system performs well and tracks regularly beyond 1000 nautical miles slant range. Normal acquisition altitude (due to antenna field radiation patterns) is 1000 ft over the launch pad, but the system has frequently locked on to the missile before lift-off and provided useful early trajectory data, thanks to a multiple-point data smoothing program in the computer.

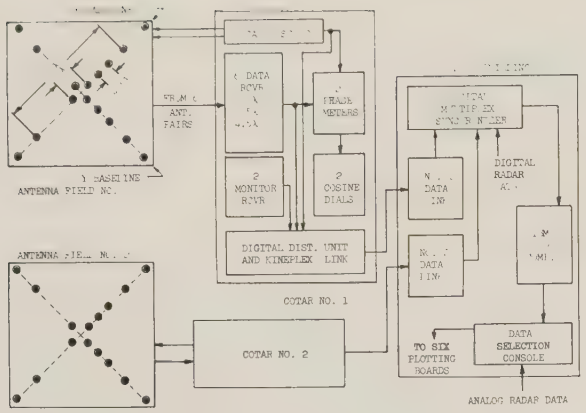

Fig. 4—BI-COTAR systems diagram.

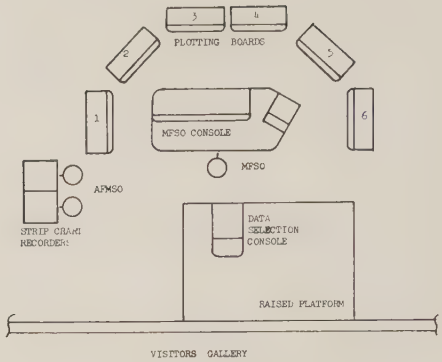

Fig. 5—Layout of Range Safety Center.

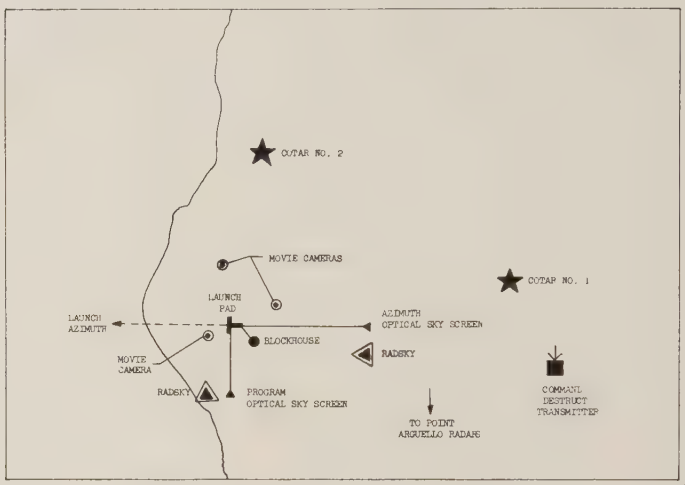

Fig. 6—Equipment deployment at launch site.

In the RO building, the IBM-709 computer accepts data from the FPS-16 radars and the two COTAR fields, and provides present position and instantaneous impact prediction outputs which are displayed on MILGO 30-inch vertical plotting boards in the Range Safety Center (RSC). COTAR data from either field alone provides a direction angle to the missile and this output from the computer is displayed on a constant-speed stripchart recorder in the RSC. The data from the AN/MPS-19 radars and the analog data from the AN/FPS-16 radars passes through coordinate converters and axis rotators before being plotted on the 30-inch boards. All radar and COTAR data can be displayed on any one of the six plotting boards and a data selection console behind the MFSO (Fig. 5) has the capability of controlling and displaying the data from any source on any board with instantaneous switching. This console has provisions also for operational direct voice communications to radars and COTAR field stations, and a control panel for program directions to the IBM computer is planned for the near future.

During the period of time from lift-off until the electronic tracking-devices have "lock-on" track, the missile flight is monitored (Fig. 6) by optical and radar skyscreens. The optical skyscreen system consists of MK-51 and vertical wire skyscreens. The MK-51 skyscreens are telescopic devices which transmit angular deviation in the horizontal (ground) plane over analog dc circuits to constant-speed stripchart recorders located in the RSC. The MK-51's are located so that one is on the reciprocal of the launch azimuth and the other normal to the launch azimuth. These instruments then provide angle deviation relative to the intended course and the "up-range, down-range" direction. Assistant MFSO's observe the stripchart recorders for COTAR and skyscreens, and report to the MFSO by voice.

The vertical wire skyscreen (Fig. 7 opposite) is located normal to the launch azimuth, and by sighting along two vertical wires the operator has a vertical plane reference. The wire is so oriented that the vertical plane will pass through the missile on the pad. The data from this instrument is in the form of a voice report of missile performance as described by the skyscreen operator to the MFSO by voice direct line.

The radar skyscreens (RADSKY) were developed to replace the optical skyscreen during periods of reduced visibility. Originally a 50-kw GILFILLAN AN/FPN-33 *X*-band radar, this apparatus has been modified mainly by stepping up the scanning rate, increasing the scan angle, and adding a beamsplitter mirror system to its indicator unit (Fig. 8) so that trajectory limits may be superimposed on the radar presentation. Its accuracy is satisfactory up to 5000-ft altitude for the relatively coarse observations necessary; extensive field tests have given very good results. In addition to all-weather capability, the positioning of RADSKY is not as critical as that of optical skyscreens, since trajectory contours are more easily adaptable to the radar presentation. This system recently met the supreme test when an ATLAS/AGENA vehicle was successfully launched in dense fog which completely obscured the missile from view by the optical skyscreens. This was a significant step toward an all-weather safety system.

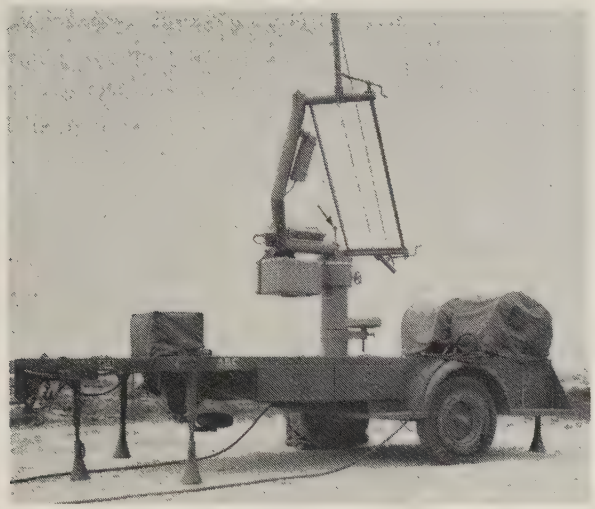

Fig. 7—Wire skyscreen.

Fig. 9—Command destruct transmitter.

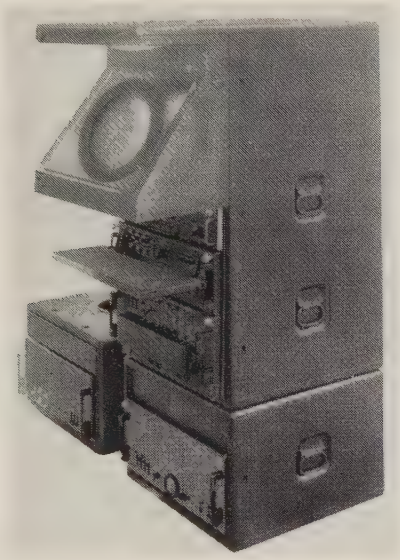

Fig. 8—Presentation unit for RADSKY.

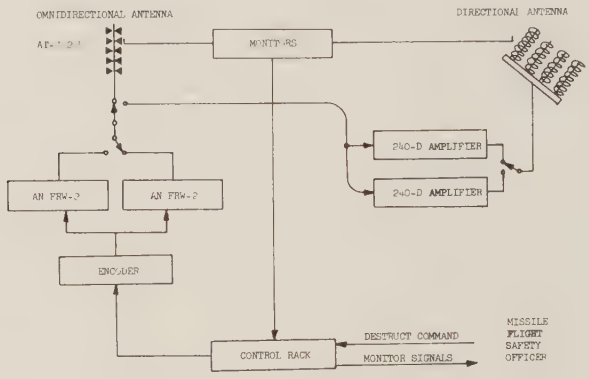

Fig. 10—Block diagram of command destruct transmitter.

For flight termination of errant missiles, the MFSO over duplicate and differently routed wirelines remotely controls the command destruct transmitter (Fig. 9) located on a 750-ft hill at the rear of Vandenberg. The 60-ft tower supports an omnidirectional UHF antenna for close-in work and a four-helix directional UHF antenna for long distance coverage. Dual AN/FRW-2A FM transmitters driving two COLLINS 240D 10-kw amplifiers (Fig. 10) are used for maximum reliability. The FRW-2A is used to feed 500 w into the omnidirectional antenna during the early portion of a missile's flight, after which a pre-set timer switches over to 10 kw into the four-helix antenna. Power level is controlled also by the MFSO who can remotely override the timer as well as monitor the transmitter output and initiate destruct commands. Automatic monitors at the station will select standby units if RF power drops or modulation fails. Field tests indicate that the station has a satisfactory cylindrical radiation pattern 10 miles high with a 50-mile radius from the omnidirectional antenna and a 17° by 55° beam from the directional unit that produces good RF fields to 750 nautical miles.

III. Missileborne Equipment

To comply with economy considerations and USAF requirements for operational missile training, the IMFSS requires only command destruct capability and a telemetry transmitter (to function as a passive tracking beacon) on board ICBM's launched into the PMR. In IRBM's, the latter instrument could conceivably be omitted, as existing radars are capable of tracking an IRBM beyond the point where it could no longer return and impact on the mainland and coastal islands. However, the importance of gross vehicle performance data exceeds the value of a small telemetry set and a unit (Fig. 11) such as a UED AN/DKT-15 with 25 w of PAM/FM/FM around 250 Mc, and about 60 measurements is always carried. A typical command destruct receiver is the modified AVCO AN/ARW-62, a 21-tube dual conversion UHF superheterodyne with decoder. Of course, R and D vehicles carry considerably more

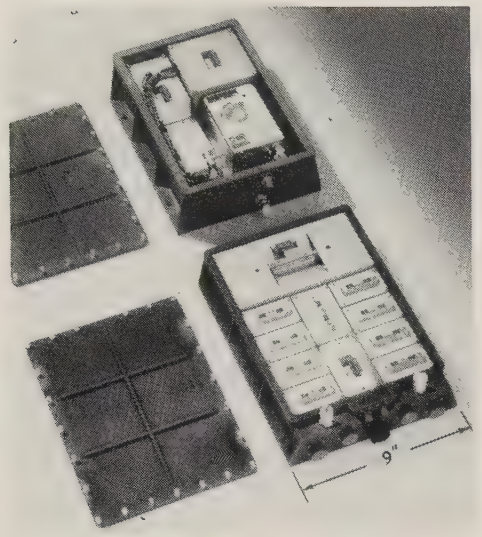

Fig. 11—Telemetry transmitter AN/DKT-15.

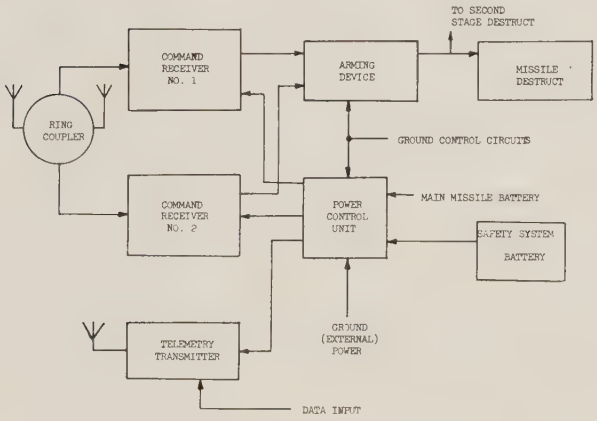

Fig. 12—Missileborne safety equipment.

telemetry, as is reflected in the PMR telemetry ground station installations for the area.

The control and monitoring of the missileborne safety equipment (Fig. 12) is accomplished by an operations and checkout (O and C) console in the blockhouse associated with each launch pad. This console is connected independently to the missile over umbilical cables and has the following main functions:

1) Checkout and monitoring of command destruct missile subsystem.
2) Arm and safe missile destruct ordnance.
3) Selection of internal/external power to command receivers and telemetry set and activation of safety system battery.

Therefore, in addition to power supplies, switching devices and status lights, this console has a special RF signal generator capable of synthesizing commands to the command destruct receivers.

The use of the O and C console during a launch operation is an outstanding example of the interservice working relationship in the Vandenberg/Point Arguello area. The console operator is a senior Air Force Sergeant provided by the First Missile Division to support Air Force sponsored launches. He operates the O and C console when directed by the MFSO, a Naval Officer located in the RO building at Point Arguello. Only through this cooperative atmosphere of interservice coordination have many launches been executed without delay because of missileborne safety equipment with all components performing properly during the flight.

IV. Supporting Range Instrumentation

Functions pertaining to range instrumentation which were not part of the range safety system have been assumed by the Range Operations Department, Naval Missile Facility, Point Arguello. This includes the operation of telemetry fixed ground stations, communications, and range timing. The telemetry station has, however, a safety function in that the existence of the telemetry carrier is necessary for the functioning of COTAR.

The PMR telemetry facility consists of two stations and ancillary equipment. One station, which is a Receiver and Tape Recording Station, includes 1) Six NEMS-CLARKE 1401A FM receivers, 2) Six NEMS-CLARKE 1411A FM receivers, 3) One AMPEX FR 107A tape recorder/reproducer and 4) One AMPEX FR 107A tape recorder. This equipment has the capability to record six RF's per tape deck, but has no display capability. It will be augmented by the addition of another station containing similar equipment.

The second PMR telemetry station includes a Receiver and Display set-up containing 1) Two NEMS-CLARKE 1411A FM receivers, 2) Three BRUSH model RD2661 six-channel pen recorders, 3) One R. M. Parsons 5201-2058-1 PAM/PDM decommutator station and 4) 18 subcarrier discriminators. This station has the capability to display 18 continuous channels of telemetry data by means of pen recorders. An additional Receiver and Display Station is planned using NEMS-CLARKE model 1432 receivers which will permit over 100 per cent increase in displayed channels and data.

The present facility utilizes two ANDREW model No. 50110 tri-helix antennas and an RF patch-bay to permit patching of any receiver to any multicoupler or receiver to any antenna. By use of NEMS-CLARKE type MC-406 multicouplers, and NEMS-CLARKE type 203 preamplifiers, a highly sensitive receiving system is obtained in which up to six receivers can be operated from one antenna. The system has the further capability of selecting the signal with the highest signal-to-noise ratio for display and/or recording.

Range timing is presently provided from a central timing generator containing a one Mc crystal oscillator with a stability of one part in 100 million and synchronized with WWVH. Pulse-rate dividers and time-code circuits produce a 12-digit binary timing code on a 100 and 20 and a 13-digit code on one pulse/second basis as well as 1000, 100, and one-cps reference frequencies. Timing signals are distributed to all launch

complexes and camera stations as well as within the IMFSS over the special direct-line communications system that is required for the range safety operations. A 17-digit system is under installation to allow for future coordinated missile experiments with the Atlantic Missile Range and other national ranges.

Communications for IMFSS is furnished by a special network, designed primarily from the viewpoint of range safety. Direct lines for the handling of critical operational information such as voice communication and countdown, remote control, status reporting, and digital time display are isolated circuits, not connected through the main facility switchboard. Noncritical general business traffic is handled over additional standard dial phones. This allows for complete control over operational traffic and permits the installation of simple visual-aural signaling devices as well as arbitrary and pre-set conference circuits.

Status reporting is done with three-lamp modules containing low-voltage transistor switches. Green, amber, and red lights indicate READY, IN PROCESS and NONOPERATIONAL during a countdown, while after missile lift-off, these colors mean SAFE, DOUBTFUL, and UNSAFE, as applicable to each subsystem. All reporting lines, as well as remote control, monitor, and critical direct voice lines outside the RO building have 100 per cent back-up. With the exception of the lines terminating in the MFSO and data selection consoles as mentioned above, all voice and status reporting lines terminate in an instrumentation control room, adjacent to the RSC.

V. Planned Additions

With range users establishing requirements for instrumented impact areas located near inhabited islands downrange in the PMR, the need for long-range impact prediction is essential for range safety. The Navy is presently installing a General Electric Range Safety Instrumentation System (GERSIS) to provide impact prediction from lift-off to target. GERSIS is essentially the tracking portion of a GE MOD III guidance system tied in with an IBM-7090 computer, which computer will replace the present IBM-709. All missiles launched toward targets located near inhabited islands will be required to carry a transponder compatible to the GERSIS.

Also, in the planning stage is a television system to be used primarily by ground safety for pad and area surveillance, but with two cameras so arranged that they can be used by range safety as television skyscreens. They will be located approximately in the same manner as the MK-51 skyscreens with monitors at RSC. This instrumentation will give the MFSO instant indication of gross malfunctions in the early flight phase, which is particularly important during launches of solid propellant missiles since the increased initial velocities do not allow enough time for a vertical wire or MK-51 verbal report.

A new requirement on the range user has been established by PMR range safety in that certain missiles must have thrust termination capability by a means other than destruction. In some instances, it is possible to increase hazards by the shot-gun effect of missile destruction rather than by letting a "bad bird" go. Also, thrust termination provides positive prevention of overflying the target without interfering with the missile system. This feature is highly beneficial to both the project and range safety.

VI. Conclusion

The assimilation of the original range safety system at Vandenberg AFB into the present integrated missile flight safety system was an orderly transition commencing in early 1960. By mid-June, 1960, when a launch was fully supported from the new safety center at Point Arguello, the IMFSS had been demonstrated on several actual launches without interference to the Vandenberg system supporting the launch. No subsystem was accepted unless it provided the same degree, or better, of range safety and protection to a good missile as the system it replaced.

The Digital Data Processor for the Skytop Static Test Facility*

K. M. ROEHR†, MEMBER, IRE, AND R. D. COLEMAN‡

Summary—The Digital Data Processor implements a new data-acquisition concept which permits self-adaptive, accurate, real-time digitizing and editing of a large number of high-frequency data channels. The system was designed to meet the constantly changing requirements of a high-energy propulsion engine research and development program.

The centrally located processor basically samples 127 channels of analog information from any one of several 1-million-pound static test stands, and produces a digital tape. Before a new test the sampling scheme of the data channels is quickly set for any desired selection sequence that will best fit the new test situation. During a test the data processor can monitor preselected channels. Based on their performance, sampling priority can be shifted from one channel group to another, thus automatically optimizing the data-acquisition process. Immediate digitizing of the multiplexed analog data preserves its original accuracy. Record lengths on the output tape are programmable, and the tape format is compatible with the IBM 7090 computer.

Introduction

THE cost of testing high-energy propulsion engines in static test stands makes it desirable to acquire as much data as possible from any one firing. These large quantities of data can be most efficiently reduced and analyzed by use of a high-speed digital computer. The Digital Data Processor was designed to receive the meaningful data, to preserve its accuracy, and to store it in a form which can be used for direct computer entry. The more detailed requirements for the device can be stated as follows:

1) The transmission error from the sensing element to the final data shall not exceed 0.1 per cent. Allowing for errors during transmission and amplification, the modulation equipment should introduce less than 0.03 per cent of error.

2) A maximum of 127 data channels shall be acquired simultaneously.

3) The sum of all intelligence frequencies on the different data channels will not exceed 5 kc.

4) One centralized control room will serve several test bays. Therefore:

   a) the acquisition equipment shall be easily connectable to one bay or another,
   b) sampling schemes shall be quickly changeable.

5) The data should be in a format suitable for direct input into a large universal-purpose digital computer.

6) During the test, basic maximum-minimum computations on selected data channels shall be performed. The results will be used to optimize the data acquisition process and to perform closed-loop test control.

Historical Solutions

The classical way to acquire propulsion test data is to record the frequency-modulated and mixed signal onto magnetic tape. After completion of the test, the data is fed through filters and demodulators into a time-multiplexed analog-to-digital converter and finally into a digital computer. This method has two main disadvantages:

1) Achievable over-all accuracies are less than 1 per cent because the sequence of modulation, mixing, recording, reading, filtering, and demodulation invariably introduces errors.

2) Every data channel needs separate modulation and demodulation equipment, which is very costly for a large number of data channels.

A better approach is to digitize the data as soon as possible, in order to preserve its accuracy. Many successful systems have been built using this approach. Their shortcomings for our particular application were primarily in three areas:

1) Their analog sampling schemes were relatively inflexible, permitting channel-sequence or sampling-frequency changes during a test only at the expense of losing data points.

2) Their output tapes were not directly intelligible to and compatible with a large computer and required special editing.

3) Their computing capabilities were usually not adequate for self-adaption and closed-loop control.

The DDP Approach

The Digital Data Processor represents an evolutionary step beyond the best-known historical approach. The fixed-rate commutator was replaced by a randomly addressable gating structure, which is actuated by instructions from an internally stored program. The format buffer was enlarged to a random-access memory for simultaneous data and instruction storage. A directly-compatible IBM 729 tape is written. A Flexowriter serves for checkout and maintenance, and high-speed program read-in is accomplished via photoelectric cardreader. In addition, computing capabilities were provided to monitor preselected channels. All actions in the analog input, in the digital input-output, and in the arithmetic unit are initiated from the instruction-interpreting central control unit.

The logical design of the Digital Data Processor has much in common with a general-purpose digital com-

* Received by the PGMIL, May 29, 1961.
† IBM Federal Systems Div., Communications Systems Center, Rockville, Md. Formerly with U. S. Naval Ordnance Test Station, China Lake, Calif.
‡ U. S. Naval Ordnance Test Station, China Lake, Calif

puter. This general-purpose design concept is considered ideal, since the test stand has, as part of its mission, the experimental and developmental advancement of instrumentation state-of-the-art.

The Skytop Acquisition Concept

Fig. 1 shows how the transducer-generated signals from the test bay are fed through the nearby blockhouse into 800 feet of twisted-pair shielded cable. In the centrally located instrumentation building the signals are amplified to a maximum of ± 5 volts and are used for different ways of recording. Direct-writing oscillographs and stripchart recorders provide quick-look information. High-frequency but low-accuracy data channels, such as those which record vibration, are used for wide-band recording on magnetic tape. The most important and the most accurate data is fed into the Digital Data Processor via low-pass filters in order to cut out high-frequency noise. To back up the digitizing process in case of failures, the same channels are also frequency-modulated, mixed, and written onto magnetic tape. After the test, data from the high-frequency channels can be digitized through DDP.

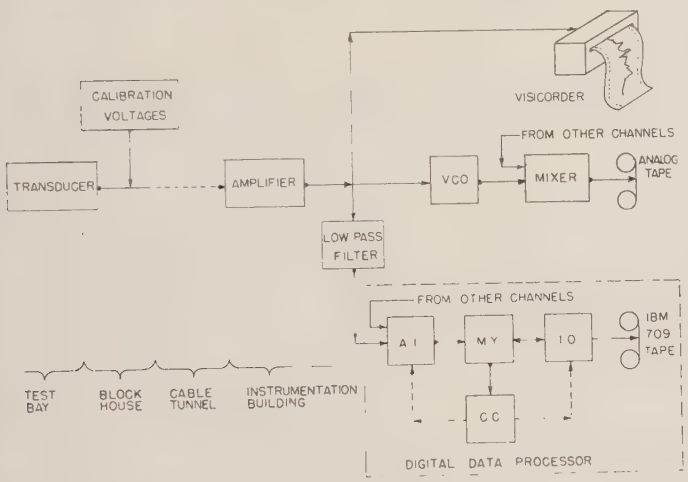

Fig. 1—Typical data-acquisition channel.

The Digital Data Processor

The main characteristics are given in Table I. A more detailed discussion follows.

Data Flow

The 127 channels of analog data from the test stand are connected to the electronic commutator,[1] which is capable of feeding one of the 127 input voltages into the sample-and-hold amplifier every 80 μsec (see Fig. 2). The channels to be sampled and the sampling sequence are determined by the instruction arrangement chosen in the sampling program. The sample-and-hold amplifier samples a selected channel for 2 μsec and holds this value during the conversion time. The sampled voltage level is fed to the analog-to-digital converter[2] and is converted into a 12-bit binary data word. After serial-to-parallel conversion and assembly of two data words, 24 bits are transferred, in parallel, to the ferrite core memory.[3] This process continues until the number of words specified by the program have been written into the memory.

TABLE I
DDP Characteristics

Mode of Operation:	serial
Number system:	binary
Word length:	24 bits
Operation speed:	24 μsec per instruction cycle
Core memory:	2048 words, 1 read-write cycle per 8 μsec
Index registers:	7
Analog input:	19 channels, 1 sample = 12 bits per 80 μsec
Digital input:	Flexowriter: 1 octal word per 0.8 sec Cardreader: 400 cards per minute
Digital output:	magnetic tape: 1 word per 144 μsec Flexowriter: 1 octal word per 1.1 sec

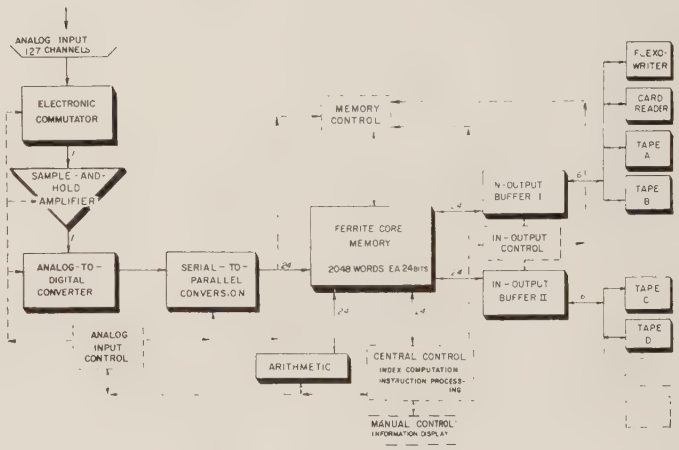

Fig. 2—DDP block diagram.

At this point the program initiates a write-tape instruction which transfers the data from the memory, one memory cell after another, into the input-output buffer. Six bits at a time are shifted in parallel into the tape-write circuitry, which in turn writes the six data bits, together with one parity bit, onto the $\frac{1}{2}$-inch mag-

[1] J. Millmann and A. E. Puckett, "Accurate linear bidirectional gates," Proc. IRE, vol. 43, pp. 29–37; January, 1955.

[2] "The Multiverter System Application Manual," Packard-Bell Corp., Los Angeles, Calif.

[3] "Instruction Manual for Coincident Current Random Access Memory Systems," Computer Control Co., Inc., Wellesley, Mass., Contract 3917, Navy Contract N123(60530)20833A(FBM); July 8, 1959.

netic tape.[4] The spacing between words, the end-of-record gap, the longitudinal parity, and the end-of-file indication all follow the IBM-tape format so as to permit automatic processing of the data in the IBM 7090 computer.

Instruction Flow

Instructions can be entered from a set of switches in the central control panel, from the Flexowriter, from the cardreader, or from one of several magnetic tape units via the input-output buffer. Once the program has been read into the memory, the automatic program-cycling can begin. After start has been manually initiated, the contents of the program counter, located in central control, are transferred in parallel to memory control, where they determine the first instruction word to be read out from memory into the central control section. In the continuous-start mode, contents of the program counter are incremented by one after every instruction cycle, unless a counter-set instruction is given.

Depending on the operation part of the instruction word, action in the different control sections of analog input, arithmetic, or digital input is initiated. The address part of all standard instructions (see Fig. 3 and Table II) can be modified by the contents of any one of seven index registers before it is routed into the proper control counter. The instructions LDX and INX are used to load and to increment the contents of the index register. The indexing capability provides a powerful tool for relative addressing and makes it easy to generate complex sampling scans.

The address part of the channel-select instructions contains the next channel address to be sampled. As soon as the analog input has finished its last selection, this address is transferred in parallel to the analog input.

Two instructions must be sent to the input-output section to control an input-output operation. The first, a counter-set instruction, specifies how many words are to be read from or written into the memory. The second, an input-output instruction, specifies the first memory location to be operated on, the input-output device to be used, and the operation to be performed. Once these instructions are sent, the entire operation is performed under input-output control until the specified number of words have been read or written. Analog input and central control operations proceed independently during the input-output operation.

Conditional transfers of the program counter can be made on the basis of the result of a compare instruction, the sign of the data word in the accumulator, or other externally derived conditions. For ease of programming the program counter is unconditionally transferred with either the instruction STU or CTS, which also initiate selection of one data channel.

[4] "Ampex Digital Tape System, Series FR-300 Digital Tape Handler," Ampex Corp., Redwood City, Calif.

TABLE II
DDP Instructions

Abbreviation	Instruction designation
HPR	Halt and proceed
STU	Set counter unconditionally
STC	Set counter conditionally
COM	Compare
SUB	Subtract
LDA	Load Accumulator
STA	Store Accumulator
LDX	Load index
INX	Increment index
CSS	Channel select single
CSD	Channel select dual
CTS	Channel transfer select
WRT	Write tape
RWT	Rewind tape
RDF	Read Flexowriter
WRF	Write Flexowriter

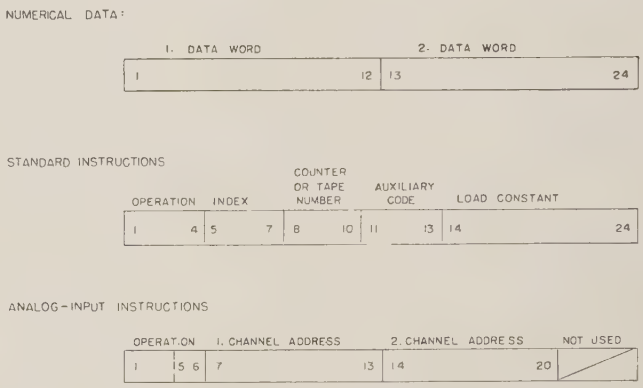

Fig. 3—DDP word format.

Timing

To accommodate time-shared memory access of central control, analog input, and digital input-output, a synchronous clock system was employed. This consists of a 12-μsec ($A_0 \cdots A_{11}$) and 8-μsec ($B_0 \cdots B_7$) clock (see Fig. 4). The 12-μsec clock is used for timing of operations with the 12-bit data word, while the 8-μsec clock corresponds directly to the 8-μsec read-write-cycle time of the memory. Out of these two clocks a 24-μsec clock is generated which controls the functions during an instruction cycle. After central control has once had access to the memory, another 24 μsec can elapse until it needs a new instruction. In between the memory is free to handle two more 8-μsec memory requests, which are allocated to analog input and digital input-output.

Analog-input timing consists essentially of a repetitive 80-μsec start-of-conversion pulse, which is synchronized with the central 8-μsec clock. The analog-to-digital conversion is completed in 52 μsec, and the remaining 28 μsec, before the next conversion, is used for changing to a new channel address. Program-counter C1 cannot proceed to a new instruction if central control has a new analog-input instruction ready before the analog input has finished the old instruction. By this means, time interlock between analog input and central

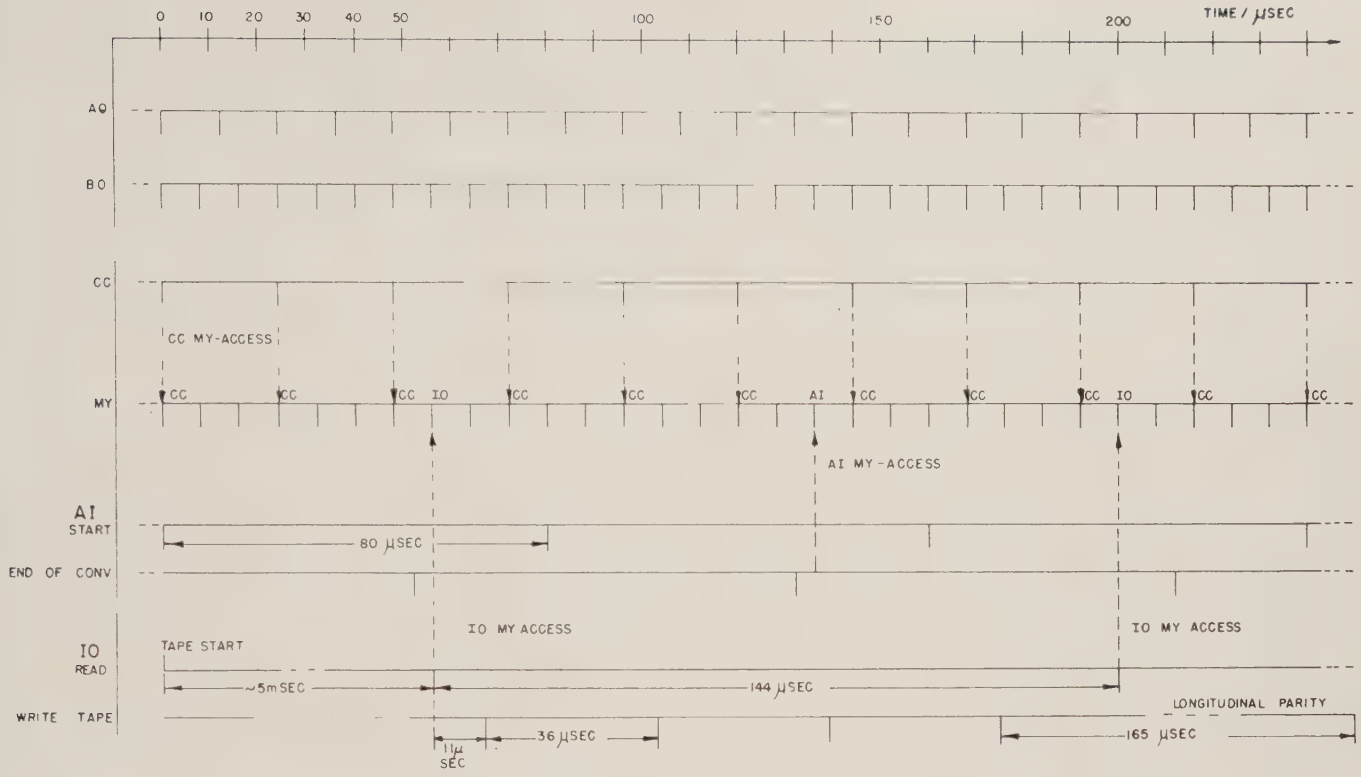

Fig. 4—DDP timing.

control is accomplished. During sampling, at intervals of every 160 μsec, one 24-bit data word is assembled in analog input and read into memory.

After receiving a tape-read instruction, the digital input-output control starts the tape transport. After 5 msec the tape is at full speed. When an input-output memory access cycle occurs, a start-read pulse initiates the first in a series of information transfers from memory to tape. This process repeats four times, once every 36 μsec, for every memory word written on tape. Every 144 μsec a new word is requested from memory, until a number of words determined by the contents of counter no. 4 have been written on tape; 165 μsec after the last recorded bit of data, a longitudinal parity bit is produced.

The timing diagram shows that many memory access times are not used. The unused times may be employed to initiate and execute operations in the arithmetic unit. After a dual-channel select instruction, for instance, five arithmetic instructions can be given without interference. The execution of these instructions utilizes free memory cycles between analog input or digital input-output accesses.

Sampling Scheme

In compatible sampling a number of input lines are sampled at different time intervals, but only one channel at a time can be selected and connected to the analog-to-digital converter. This can be done if the larger sampling-time intervals are integral multiples of all the smaller ones. Starting with the shortest sampling-time interval, To, (determined by the basic analog-to-digital conversion time), longer compatible time intervals are derived as follows:

$$\begin{aligned} T1 &= K1 \cdot To \\ T2 &= K2 \cdot T1 \\ &\vdots \\ Tn &= Kn \cdot Tn - 1, \end{aligned} \tag{1}$$

where $K1, K2, \cdots, Kn$ can be any one integer, 1, 2, 3, $\cdots$, etc.

By transformation, the different sampling times can be expressed by products of K's:

$$\begin{aligned} T1 &= K1 \cdot To \\ T2 &= K2 \cdot K1 \cdot To \\ T3 &= K3 \cdot K2 \cdot K1 \cdot To \\ &\vdots \\ T4 &= Kn \cdot Kn - 1 \cdot Kn - 2 \cdots K2 \cdot K1 \cdot To. \end{aligned} \tag{2}$$

The selection of sampling-time intervals according to (1) is a necessary but not a sufficient condition for compatibility. Also the number of samples must not exceed the capacity of the system. For instance, when the longest chosen sampling-time interval is Tn, and the shortest possible one is To then a maximum number of Tn/To samples can be taken between two Tn samples:

$$\frac{Tn}{To} \geqq \frac{Tn}{T1} + \frac{Tn}{T2} + \cdots + \frac{Tn}{Tn - 1} + 1. \tag{3}$$

If the equal sign in (3) is true, it is called a complete scan; if the scan is incomplete (>sign applies), we easily fill out the scan by adding sampling events of insignificant data (zero channel selects). Using (2), (3) finally becomes

$$\begin{aligned}\frac{Tn}{To} \geqq\ & K2\cdot K3\cdot K4\cdots Kn-1\cdot Kn \\ & + K3\cdot K4\cdots Kn-1\cdot Kn \\ & + \quad \cdot \\ & + \quad \cdot \\ & + \cdot \\ & + Kn-1\cdot Kn \\ & + Kn+1. \end{aligned} \tag{4}$$

With the derived formulas a sampling program can be effectively produced on a general-purpose computer. The limitations on scan complexity are far beyond what is practically necessary and desirable. In order to illustrate the program-generating mechanism, a simple example is given in the Appendix.

Self Adaptation

Tests, especially on new developments, frequently do not perform as expected. The parameters of amplitude and frequency may vary more than anticipated. The amplitude range of present analog-to-digital converters is fairly wide, so that variations of about ± 2 orders of magnitude are allowed. Frequency variations in a time-multiplex system are more critical. If the signal frequency gets smaller than expected, little harm is done except that redundant data is acquired, which has to be edited out. However, if the frequency gets much larger than the sampling frequency, essential data can be lost and the benefits of the whole test are questionable. Increasing the sampling frequency to cover the entire expected range proves to be very costly because parallel techniques have to be used. Even when economical high-speed serial analog-to-digital converters and data-storage devices become available, this approach is questionable because of the immense amount of data that would have to be handled in order to obtain even a small amount of meaningful information.

Another method, which would appear more practicable, is to adapt the sampling frequency to the frequency content of the sampled signal. In this way the time assigned for sampling the various channels would be optimized, and the system could fail only if the over-all input frequency exceeds the available sampling capacity. However, the problems arising from implementing such an ideal self-adapting scheme would be manifold. One critical factor, for instance, would be the time required to identify the input frequency and to change the sampling rate accordingly. Another problem is that low-pass input filters are required in order to cut out disturbances resulting from high-frequency noise. With increasing signal frequencies and correspondingly higher sampling rates, the cutoff frequencies of these filters would have to be raised.

During a normal static firing of a propulsion system, the frequency limits of the different test parameters are well known beforehand. Only in case of a blow-up will the change of voltage at distinct test channels be too fast to be properly sampled. To provide for these cases it is desirable to shift sampling priority to preselected characteristic channels, sacrificing data from other less important channels.

The arithmetic unit is used to determine whether the sampling scheme should be changed. As soon as the difference of successive samples from selected channels exceeds a programmed limit, for instance, an automatic program transfer to other pre-stored sampling loops can be initiated. At the beginning of these alternative loops, write-out instructions are sandwiched in between channel selections. Thus, data write-out is initiated, while the new sampling process immediately feeds new information into other parts of the memory.

Test Control

Propulsion engines are getting more and more sophisticated. During firing, parameters that influence either the amount or the direction of thrust can be changed. To test the performance of these controls, a predetermined sequence of monitoring signals is fed from external generators to the control organs. In case the response of the test motor does not stay within distinct desirable limits, the monitoring capability of the Digital Data Processor can be used to exercise closed-loop control. By storing the necessary control steps, the test can be successfully finished and evaluated. One other test-control application would be to preprogram the desirable values of thrust, for instance, and let the DDP derive the control functions that are necessary to achieve these values. During the test the generated control signals are recorded and can be used to compute the control characteristics of the motor.

Conclusion

The Digital Data Processor implements a new data acquisition concept which permits self-adaptive, real-time digitizing and editing of a large number of high-frequency data channels.

The DDP conversion process, from the analog input to the final magnetic tape, introduces less than 0.02 per cent error into the acquired data. Any number of channels up to 127 may be acquired and digitized to cover a wide range of test data. The basic analog-to-digital conversion rate permits a wide range of sampling rates on all channels.

The DDP may be switched to serve any one of several test bays by removing and replacing one connection. The entire sampling scheme for the device may be readily changed before a test by reading in a new program, or during a test by shifting to a new control loop in a

program. The DDP output tape is suitable for direct input into a large general-purpose computer.

The computing capabilities of the DDP permit it to examine incoming data and change the sampling scheme to fit test requirements during a test, or exercise closed-loop control on a test in progress.

The DDP minimizes the time needed for before-test preparation and after-test evaluation. The flexible sampling scheme, high data rate, and ease of changing the sampling schemes make this device unique in its ability to handle widely variable test situations.

Future Developments

Advances in the state-of-the-art of propulsion systems will call for real-time data acquisition and test-control concepts even more effective than the ones that can be provided at present. For these future needs a DDP will be supported by a large universal-purpose computer having a program-interrupt feature (currently the IBM 7090). A two-way wide-band microwave link is being installed to provide a closed-loop system. Thus the Digital Data Processor will be most useful for the time-consuming pretest checkout and calibration operations, where there is no need to tie up the expensive large computer. Shortly before the test firing the large computer will be interrupted, and after transmission of calibration data the real-time data acquisition and evaluation can begin. The significant test data will be available shortly after the finished test. By sending only short control words the central computer can easily initiate change of the original sampling pattern.

It is felt that the combination of a low-cost but flexible, predominantly off-line operating system with large, powerful, centrally located computers that are otherwise economically utilized, presents an optimum solution for the problem of data acquisition and real-time test control of high-energy propulsion systems.

Appendix

Examples of Compatible Data Scans

For Table III (1) was used to generate four different arrays of sampling times. The time intervals are given in multiples of the basic conversion time To. For the DDP case they must therefore be multiplied by 80 μsec. We restrict ourselves to only three values of Ki, namely 2, 3, and 5.

Starting from any point of the array, compatible sampling-time intervals can be found by going either to the right or to values below the original ones. In (a), (b) and (c) of Table III, the same Ki values were used for generating horizontal rows or vertical columns; in (d), horizontal Ki's are alternately 3 or 5, to illustrate the variety possible.

In order to show the use of (3) we choose a practical example shown in Table IV. The sampling time intervals, Ti/To, were selected from (b) in Table III. The longest chosen relative sampling time is $Ti/To = 100$

TABLE III

Some Compatible Sampling-Time Intervals in Multiples of Shortest Sampling Time To

Ki	5	5	5	5	5	
	1	5	25	125	625	3,125
3	3	15	75	375	1,875	9,375
3	9	45	155	1,125	5,625	28,125

(a) $Ki = 3$ or 5

Ki	5	5	5	5	5	
	1	5	25	125	625	3,125
2	2	10	50	250	1,250	6,250
2	4	20	100	500	2,500	12,500

(b) $Ki = 2$ or 5

Ki	3	3	3	3	3	3	
	1	3	9	27	71	243	729
2	2	6	18	54	162	486	1,458
2	4	12	36	108	324	972	2,916
2	8	24	72	216	648	1,944	5,832
2	16	48	144	423	1,296	3,888	11,664

(c) $Ki = 2$ or 3

Ki	3	5	3	5	3	5	
	1	3	15	45	225	675	3,375
2	2	6	30	90	450	1,350	6,750
2	4	12	60	180	900	2,700	13,500

(d) $Ki = 2$, 3 and 5

TABLE IV

Example of Practical Scan

Channel designation	No. of channels	$\frac{Ti}{To}$	$\frac{Tn}{Ti}$	$\sum \frac{Tn}{Ti}$
1 · · · 6	6	10	10	60
7 · · · 12	6	20	5	30
13 · · · 19	7	100	1	7
				$\sum 97 \leq \frac{Tn}{To}$
01 · · · 03	3	100		3
				$\sum 100 \equiv \frac{Tn}{To}$

$= Tn/To$. Therefore,

$$\frac{Tn}{Ti} = \frac{\frac{Tn}{To}}{\frac{Ti}{To}} = \frac{100}{\frac{Ti}{To}}$$

has to be multiplied by the number of channels that have the same sampling rate. These values are used in accordance with (3) to determine if the scan is complete. In order to achieve a complete scan, three channel-select zero instructions were inserted to satisfy the equal condition of (3).

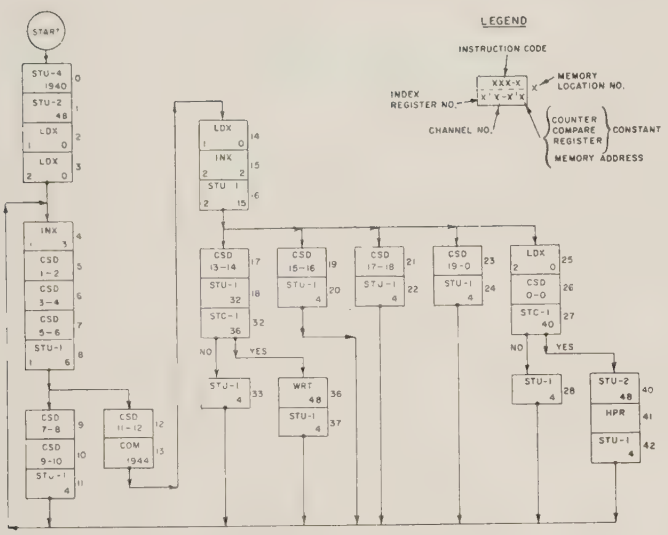

Fig. 5—Example of DDP instruction flow.

The next step during a manual-program preparation is to develop a timing diagram that shows the different sample events and their sequence. From there it is a short step to the instruction-flow diagram, a simple example of which is shown in Fig. 5.

Acknowledgment

Part of this paper was extracted from the authors' manual on the Digital Data Processor.[5] The authors wish to acknowledge the work of R. W. Herman and H. V. Hilker, now with Decisional Control Inc., Anaheim, Calif., who did essential parts of the original planning for the Processor. F. Haymaker, U. S. Naval Ordnance Test Station, provided valuable editorial help.

[5] K. M. Roehr and R. D. Coleman, "Interim Digital Data Processor for the Skytop Static Test Facility," U. S. Naval Ordnance Test Station, China Lake, Calif., NOTS TP 2546; September, 1960

Determination of Satellite Trajectories from Track-While-Scan Radar Measurements*

R. B. BARRAR†, MEMBER, IRE, AND R. DEUTSCH‡, SENIOR MEMBER, IRE

Summary—**Classical methods for determining satellite orbits were limited to the use of angle information and only rough estimates of distance. With radar, it is possible to obtain good range information, but poor angular accuracy. Three approximate schemes are described which are ideally suited to track-while-scan radar observations. The accuracy obtained with these techniques has been demonstrated by the numerical evaluation of some typical cases.**

I. Introduction

IT is well-known that a set of radar observations can be employed in several ways to determine the complete trajectory of an object in free-space fall.[1] Although there is really no simple "best" method of computing the trajectory parameters from the observations, practical limitations of numerical analysis make some schemes more difficult to implement than others. For the class of trajectories under consideration, the measurements can be reduced to obtain solutions for the parameters without resorting to approximating techniques. However, in the interest of saving computational time and required computer capacity, it is often essential that exact-solution techniques be replaced by a suitable computational method which will provide results arbitrarily close to the true solutions.

The approximation schemes described in this paper are based upon a method of Gibbs.[2] The principal departure from Gibbs is that reliance is made on the fact that while optical observational systems provide accurate angular information and no direct distance measurement, radar observations provide good distance measurements coupled with poor angular information. The proposed solution methods carefully avoid the solution of transcendental equations and produce answers for which the computational errors are more than masked by the original observational errors.

The analysis is restricted to the simple two-body problem with no disturbing forces. Thus, the observed object is assumed to be moving in free-space throughout its entire trajectory. Various secondary effects such as the sun and moon influence, continental shelves, and air drag are neglected. No corrections are included in the simplified analysis for the nonhomogeneity of the earth's

* Received by the PGMIL, May 24, 1961.
† System Dev. Corp., Santa Monica, Calif.
‡ Hughes Aircraft Company, Culver City, Calif.

[1] I. I. Shapiro, "The Prediction of Ballistic Missile Trajectories from Radar Observations," McGraw-Hill Book Co., Inc., New York N. Y.; 1958.

[2] J. W. Gibbs, "On the determination of elliptic orbits from three complete observations," *Mem. Natl. Acad. Sci.*, vol. 4, pt. 2, pp. 79–104; June, 1889.

gravitational field of the nonsphericity of the earth. The effect of perturbing forces can be included in the analysis for those cases in which the application of the calculations and the measurement accuracies warrant their consideration.

II. Prediction

Using a set of observations from a scanning radar, the problem is to extract values of trajectory parameters that completely describe the simple orbital motion. For present purposes, it is assumed that no measurement errors exist. Therefore, since the object's motion can be completely specified by six trajectory parameters at a given time, discussion will be limited to nonredundant radar data sets of six distinct measurements at known time. Problem of data-smoothing using over-determined data sets, although related to trajectory determination, are not treated in this paper.[1,3]

The trajectory is completely specified by knowledge of the object's position and vector velocity at a stated time. There are several other sets of trajectory parameters which can just as well be employed. For example, the elements of the ellipse such as the eccentricity, semilatus rectum, and the inclination of the major axis form a specification suited for computation of quantities in the plane of the orbit.

Fig. 1 illustrates a system of geocentric coordinates that are convenient for computation in the plane of the orbit. The free-space trajectory, under the assumed conditions, is an ellipse with a focus located at the center of the earth. ρ is the geocentric radius vector from the center of the earth to a point P on the trajectory. Angles in the plane of the orbit are measured from a reference line that is chosen as the intersection of the orbital plane with the earth's equatorial plane.

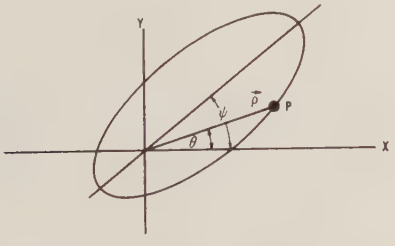

Fig. 1—Geocentric coordinates.

There are several techniques for determining the trajectory from a scanning radar; however, this paper will be restricted to the use of two positional measurements at known times. The use of rate-of-change information is not considered. By the use of a simple coordinate transformation, the original radar coordinates of the object in flight provide values of the geocentric polar coordinates ρ_i, θ_i $(i = 1, 2)$, in the plane of the orbit. These values can be directly substituted into the polar elliptic equation,

$$\rho_i = \frac{a(1 - e^2)}{1 - e \cos(\theta_i - \psi)}; \qquad i = 1, 2. \tag{1}$$

A solution for the unknown quantities a, e, ψ requires an additional relationship. An equation that can serve as the required third relation is a statement of Lambert's theorem.[4] This relation can be written in the form

$$(t_2 - t_1)\rho_0 g^{1/2} a^{-3/2} = (m - \sin m) - (n - \sin n), \tag{2}$$

where

$$\sin\frac{m}{2} = \frac{1}{2}\left(\frac{\rho_1 + \rho_2 + c}{a}\right)^{1/2},$$

$$\sin\frac{n}{2} = \frac{1}{2}\left(\frac{\rho_1 + \rho_2 - c}{a}\right)^{1/2},$$

and

$$c^2 = \rho_1^2 + \rho_2^2 - 2\rho_1\rho_2 \cos(\theta_2 - \theta_1).$$

ρ_0 is the earth's radius and g the gravitation acceleration constant. Eq. (2) is a transcendental relation that can be solved to find a value of the major axis $2a$. With this value of a, (1) can be solved for the remaining parameters ψ and e. The solutions are:

set

$$F = a/\rho_1 \qquad G = a/\rho_2 \qquad H = 1 - F \qquad J = 1 - G,$$

then

$$e^2 = (-B - \sqrt{B^2 - 4AC})/2AC \tag{3}$$

with

$$A = F^2 + G^2 - 2FG \cos(\theta_1 - \theta_2)$$

$$B = -2[FH + GJ - \cos(\theta_1 - \theta_2)(FJ + GH)] + \sin^2(\theta_2 - \theta_1)$$

$$C = H^2 + J^2 - 2HJ \cos(\theta_1 - \theta_2).$$

Now, set

$$k = a(1 - e^2) \qquad D = (1 - k/\rho_1) \qquad E = (1 - k/\rho_2), \tag{4}$$

then

$$\tan\psi = (E \cos\theta_1 - D \cos\theta_2)/(D \sin\theta_2 - E \sin\theta_1). \tag{5}$$

[The derivation is messy but straightforward, for example, squaring and adding (38), (39) with $k = a(1 - e^2)$ gives a quadratic equation for e^2 solved by (3); now writing out the linear equation for $e \sin\psi$ and $e \cos\psi$ in (37) and dividing the solutions yields (5).]

[3] R. Deutsch, "Estimation of Trajectory Parameter Vector from Radar Observations: Hortonote 24," Sys. Dev. Corp., Santa Monica, Calif., Tech. Memo-483; May, 1960.

[4] E. T. Whittaker, "A Treatise on the Analytical Dynamics of Particles and Rigid Bodies," Dover Publications, New York, N. Y.; 1944.

III. Velocity Approximation

The main objective of this paper is to introduce computational schemes which will circumvent the necessity of solving transcendental equations. Although many approximate solutions can and have been employed for the stated problem, the solutions that follow have a certain elegance in that they are founded on dynamical principles rather than on numerical approximations.

The key to the first solution method is obtained by noting that for motion in a central force field, conservation of energy provides a relation between the length of the orbit's semi-major axis, and the scalar velocity at any orbital point. This classical relationship is

$$a = \frac{2}{\rho} - \frac{v^2}{K}, \tag{6}$$

where

$$\begin{aligned} K &= \rho_0{}^2 g \\ &= 1.41008 \times 10^{16}\ \text{ft}^3/\text{sec}^2. \end{aligned} \tag{7}$$

Eq. (6) permits one to substitute a determination of the scalar velocity at any given point on the orbit for the problem of determining the length of the semi-major axis.

Following Gibbs, assume that the geocentric radius vector $\boldsymbol{\varrho}(t)$ can be represented by a third-degree vector polynomial. Thus,

$$\boldsymbol{\varrho}(t) = \boldsymbol{A} + \boldsymbol{B}t + \boldsymbol{C}t^2 + \boldsymbol{D}t^3. \tag{8}$$

This relation has a simple physical interpretation. $\boldsymbol{A}$ represents the initial vector, $\boldsymbol{B}$ its velocity, $\boldsymbol{C}$ its acceleration, and $\boldsymbol{D}$ its jerk.

If (8) is evaluated for the two given values of $\boldsymbol{\varrho}_i$, t_i, the result is simply two equations containing four unknown constants. The trick is to observe that because the motion takes place under the influence of a central force field, the vector acceleration supplies the two remaining required equations. That is,

$$\begin{aligned} \boldsymbol{f} = \frac{d^2\boldsymbol{\varrho}}{dt^2} &= -K\frac{\boldsymbol{\varrho}}{\rho^3} \\ &= 2\boldsymbol{C} + 6\boldsymbol{D}t, \end{aligned} \tag{9}$$

where

$$\rho = |\boldsymbol{\varrho}|.$$

Eqs. (8) and (9) can be combined to derive the following expression for the vector velocity:

$$\boldsymbol{V} = \frac{d\boldsymbol{\varrho}}{dt} = \boldsymbol{B} + 2\boldsymbol{C}t + 3\boldsymbol{D}t^2$$

$$\boldsymbol{V}(t_2) = \frac{1}{T}(\boldsymbol{\varrho}_2 - \boldsymbol{\varrho}_1) - \frac{KT}{3}\left(\frac{\boldsymbol{\varrho}_2}{\rho_2{}^3} + \frac{1}{2}\frac{\boldsymbol{\varrho}_1}{\rho_1{}^3}\right), \tag{10}$$

where

$$T = t_2 - t_1. \tag{11}$$

The magnitude of $\boldsymbol{V}$ can be obtained from (10) and substituted in (6) to find the required value of the semi-major axis. It is interesting to reflect on the two terms on the right-hand side of (10). The first term is a velocity expression that is equivalent to assuming rectilinear motion between the two observed points. The second term can be thought of as being a correction induced by the fact that the motion is under the influence of a central force field:

IV. Gibbs' Method

The procedure for computing the major axis of the trajectory as presented in the preceding section is probably more than adequate considering the errors contained in conventional radar measurements. It is interesting, though perhaps academic, to show with the same input data that there exist other rather simple methods for computing the trajectory elements with even greater accuracy. Before describing these refinements, it is convenient to reproduce some of Gibbs' results which will be needed.

Assume, for the present, that three radar observations have been made at distinct times for an object in a free-fall trajectory. Corresponding to (8), let the geocentric radius vector be represented in the form

$$\boldsymbol{\varrho}_i(t) = \boldsymbol{A} + \boldsymbol{B}t_i + \boldsymbol{C}t_i{}^2 + \boldsymbol{D}t_i{}^3 + \boldsymbol{E}t_i{}^4; \quad i = 1, 2, 3. \tag{12}$$

For convenience, choose the time origin at $t_2 = 0$ and define

$$\begin{aligned} \tau_1 &= t_3 - t_2 \\ \tau_3 &= t_2 - t_1. \end{aligned} \tag{13}$$

The appropriate expression for the acceleration is

$$\frac{d^2\boldsymbol{\varrho}_i(t)}{dt^2} = -K\frac{\boldsymbol{\varrho}_i}{\rho_i{}^3} = 2\boldsymbol{C} + 6\boldsymbol{D}t_i + 12\boldsymbol{E}t_i{}^2. \tag{14}$$

Eqs. (12) and (14) are a set of six equations in five unknowns. A solution of this system will exist if the augmented determinant of the coefficients vanishes. That is,

$$\begin{vmatrix} \boldsymbol{\varrho}_1 & 1 & -\tau_3 & \tau_3{}^2 & -\tau_3{}^3 & \tau_3{}^4 \\ \boldsymbol{\varrho}_2 & 1 & 0 & 0 & 0 & 0 \\ \boldsymbol{\varrho}_3 & 1 & \tau_1 & \tau_1{}^2 & \tau_1{}^3 & \tau_1{}^4 \\ \dfrac{-K\boldsymbol{\varrho}_1}{\rho_1{}^3} & 0 & 0 & 2 & -6\tau_3 & 12\tau_3{}^2 \\ \dfrac{-K\boldsymbol{\varrho}_2}{\rho_2{}^3} & 0 & 0 & 2 & 0 & 0 \\ \dfrac{-K\boldsymbol{\varrho}_3}{\rho_3{}^3} & 0 & 0 & 2 & 6\tau_1 & 12\tau_1{}^2 \end{vmatrix} = 0. \tag{15}$$

The evaluation of the determinant produces Gibbs' fundamental equation

$$n_1\boldsymbol{\varrho}_1 - n_2\boldsymbol{\varrho}_2 + n_3\boldsymbol{\varrho}_3 = 0, \tag{16}$$

where

$$n_1 = A_1(1 + B_1/\rho_1^3)$$
$$n_2 = (1 - B_2/\rho_2^3)$$
$$n_3 = A_3(1 + B_3/\rho_3^3)$$
$$A_1 = \frac{\tau_1}{\tau_1 + \tau_3}$$
$$A_3 = \frac{\tau_3}{\tau_1 + \tau_3}$$
$$B_1 = \frac{K}{12}(-\tau_1^2 + \tau_1\tau_3 + \tau_3^2)$$
$$B_2 = \frac{K}{12}(\tau_1^2 + 3\tau_1\tau_3 + \tau_3^2)$$
$$B_3 = \frac{K}{12}(\tau_1^2 + \tau_1\tau_3 - \tau_3^2). \tag{17}$$

Perform vector multiplication on (16) to obtain

$$n_1\varrho_1 \times \varrho_3 - n_2\varrho_2 \times \varrho_3 = 0$$
$$-n_1\varrho_1 \times \varrho_2 - n_3\varrho_3 \times \varrho_2 = 0, \tag{18}$$

or

$$\frac{\varrho_2 \times \varrho_3}{n_1} = \frac{\varrho_1 \times \varrho_3}{n_2} = \frac{\varrho_1 \times \varrho_2}{n_3}. \tag{19}$$

Hence, the fundamental equation (16) may be regarded as signifying that the three vectors, ϱ_1, ϱ_2, ϱ_3, lie in one plane, and that the three triangles, each determined by a pair of these vectors, have areas usually denoted by $[\varrho_2, \varrho_3]$, $[\varrho_1, \varrho_3]$, $[\varrho_1, \varrho_2]$, which are proportional to n_1, n_2, n_3, respectively. Evidently, the fundamental equation is equivalent to Keppler's law on equal areas.

Define

$$s_i = n_i\rho_i; \qquad i = 1, 2, 3. \tag{20}$$

If s_i is defined to be a line lying along ϱ_i, then s_1, s_2, s_3 form a triangle. Eq. (1) can be thought of as a linear equation in the three unknowns $k=a(1-e^2)$, $e\cos\psi$ and $e\sin\psi$. Substitute $x_i=\rho_i\cos\theta_i$ and $y_i=\rho_i\sin\theta_i$ and solve for k. The result is

$$k = \frac{\begin{vmatrix} \rho_1 & x_1 & y_1 \\ \rho_2 & x_2 & y_2 \\ \rho_3 & x_3 & y_3 \end{vmatrix}}{\begin{vmatrix} 1 & x_1 & y_1 \\ 1 & x_2 & y_2 \\ 1 & x_3 & y_3 \end{vmatrix}}. \tag{21}$$

Eq. (21) can be simplified to the form

$$k = \frac{\rho_1[\varrho_2, \varrho_3] - \rho_2[\varrho_1\varrho_3] + \rho_3[\varrho_1, \varrho_2]}{[\varrho_2, \varrho_3] - [\varrho_1, \varrho_3] + [\varrho_1, \varrho_2]}. \tag{22}$$

Insert (19) and (20) in (22). Whence,

$$k = \frac{n_1\rho_1 - n_2\rho_2 + n_3\rho_3}{n_1 - n_2 + n_3} = \frac{s_1 - s_2 + s_3}{n_1 - n_2 + n_3}. \tag{23}$$

The expression $(n_1-n_2+n_3)$ and $(s_1-s_2+s_3)$ are small quantities that cannot be very accurately determined from approximate values of their separate terms. The first quantity can be accurately determined by using the relations in (17). Thus,

$$n_1 - n_2 + n_3 = A_1B_1/\rho_1^3 + B_2/\rho_2^3 + A_3B_3/\rho_3^3. \tag{24}$$

To determine the second quantity, $(s_1-s_2+s_3)$, with equal accuracy, employ the trigonometric formula

$$s_1 - s_2 + s_3 = \frac{2(s - s_3)s}{(s - s_1)} \tan^2 \tfrac{1}{2}(\theta_2 - \theta_1)$$
$$= \frac{2(s - s_3)s}{(s - s_1)} \frac{1 - \cos(\theta_2 - \theta_1)}{1 + \cos(\theta_2 - \theta_1)}, \tag{25}$$

or

$$s_1 - s_2 + s_3 = \frac{2(s - s_1)(s - s_3)}{s} \frac{1 - \cos(\theta_3 - \theta_1)}{1 + \cos(\theta_3 - \theta_1)}, \tag{26}$$

where

$$s = 1/2(s_1 + s_2 + s_3). \tag{27}$$

V. Alternate Computation Schemes

Employing the results of Gibbs, two improved techniques have been developed for predicting orbital parameters from radar measurements. Instead of considering the length of the major axis as the unknown, it will now be convenient to consider the length of the semi-latus rectum as the unknown quantity. Of course, these quantities are related by the expression

$$k = a(1 - e^2). \tag{28}$$

Case A

Assume that the radar provides measurement of ϱ_1 and ϱ_2 at a time separation of τ_3. Now choose

$$\tau_1 = \tau_3 \frac{\sqrt{5} - 1}{2}, \tag{29}$$

which is the value that makes $B_3=0$ in (17). With this choice, the remainder of the required coefficients become

$$A_1 = \frac{\sqrt{5} - 1}{\sqrt{5} + 1}$$
$$B_1 = \frac{\sqrt{5} - 1}{12} K\tau_3^2$$
$$B_2 = \frac{\sqrt{5} + 1}{12} K\tau_3^2 \tag{30}$$
$$B_3 = 0$$
$$s_1 = A_1[\rho_1 + B_1/\rho_1^2]$$
$$s_2 = \rho_2 - B_2/\rho_2^2$$
$$s_3 = [s_1^2 + s_2^2 - 2s_1s_2\cos(\theta_2 - \theta_1)]^{1/2}.$$

Substitute the values given in (30) into (23). The expression for the semi-latus rectum can be put into the form

$$k = \frac{\left[\frac{2(s - s_3)s}{s - s_1}\right]\left[\frac{1 - \cos(\theta_2 - \theta_1)}{1 + \cos(\theta_2 - \theta_1)}\right]}{\left[\frac{A_1B_1}{\rho_1^3} + \frac{B_2}{\rho_2^3}\right]}. \quad (31)$$

Case B

A still more accurate procedure can be used to determine k, at the expense of additional computation. Let ϱ_1 and ϱ_3 be obtained from radar measurements at a separation of T sec. Choose $\tau_1 = \tau_3 = T/2$ and find ϱ_2 from (16). B_2/ρ_2^3 is obtained as the real root of the cubic equation; [this equation follows from a simple modification of $n_2\rho_2 = s_2$ after substituting for n_2 via (17)].

$$B_2/\rho_2^3 = \frac{B_2}{s_2^3}(1 - B_2/\rho_2^3)^3. \quad (32)$$

The other required quantities are found to be

$$\begin{aligned} s_1 &= \tfrac{1}{2}\rho_1 + \frac{1}{96}\frac{KT^2}{\rho_1^2} \\ s_2 &= [s_1^2 + s_3^2 + 2s_1s_3\cos(\theta_3 - \theta_1)]^{1/2} \\ s_3 &= \tfrac{1}{2}\rho_3 + \frac{1}{96}\frac{KT^2}{\rho_3^2}. \end{aligned} \quad (33)$$

The solution for k can then be written in the form

$$k = 2G/N, \quad (34)$$

where

$$\begin{aligned} N &= A_1B_1/\rho_1^3 + B_2/\rho_2^3 + A_3B_3/\rho_3^3 \\ G &= \frac{(s - s_1)(s - s_3)}{s}\,\frac{1 - \cos(\theta_3 - \theta_1)}{1 + \cos(\theta_3 - \theta_1)} \\ B_2 &= \frac{10}{96}KT^2 \\ A_1B_1 &= A_3B_3 = \frac{1}{96}KT^2. \end{aligned} \quad (35)$$

VI. Prediction of Impact Point

As an example of use of the results given in the preceding section, consider the problem of computing the impact point of a free-falling body from scanning radar observations. Suppose a value of k is computed using one of the methods of Section V. From the radar observations, the values of (ρ_1, θ_1) and (ρ_2, θ_2) are known.

The first item to compute is the value of $(\theta_0 - \theta_1)$, where θ_0 corresponds to the impact point. Write this as

$$\begin{aligned} (\theta_0 - \theta_1) &= (\theta_0 - \psi) + (\psi - \theta_1) \\ &= (\theta_0 - \psi) + 1/2(2\psi - \theta_1 + \theta_2) \\ &\quad + 1/2(\theta_2 - \theta_1). \end{aligned} \quad (36)$$

Since $(\theta_2 - \theta_1)$ is assumed known, only the other two terms must be determined. Write (1) in the form

$$e\cos(\theta_i - \psi) = 1 - k/\rho_i; \qquad i = 1, 2. \quad (37)$$

Using the two known values in (37), the result is

$$e\sin\tfrac{1}{2}(2\psi - \theta_1 - \theta_2) = \frac{k\left(\frac{1}{\rho_2} - \frac{1}{\rho_1}\right)}{2\sin\frac{1}{2}(\theta_2 - \theta_1)}, \quad (38)$$

and

$$e\cos\tfrac{1}{2}(2\psi - \theta_1 - \theta_2) = \frac{2 - k\left(\frac{1}{\rho_1} + \frac{1}{\rho_2}\right)}{2\cos\frac{1}{2}(\theta_2 - \theta_1)}. \quad (39)$$

Dividing the last two expressions yields

$$\tan\tfrac{1}{2}(2\psi - \theta_1 - \theta_2) = \frac{\frac{1}{\rho_2} - \frac{1}{\rho_1}}{\frac{2}{k} - \frac{1}{\rho_1} - \frac{1}{\rho_2}}\cot\tfrac{1}{2}(\theta_2 - \theta_1), \quad (40)$$

which determines $\frac{1}{2}(2\psi - \theta_1 - \theta_2)$ and, with the knowledge of $\frac{1}{2}(\theta_2 - \theta_1)$, determines $(\theta_1 - \psi)$. [Squaring and adding (38), (39) yields l^2, then $a = k/(1 - l^2)$, thus the methods described as Case A and Case B can also be used to derive a.]

Write (37) with $i = 0, 1$ to obtain

$$\cos(\theta_0 - \psi) = \frac{1 - k/\rho_0}{1 - k/\rho_1}\cos(\theta_1 - \psi). \quad (41)$$

Eq. (41) determines $(\theta_0 - \psi)$ which, together with the previous results, determines $(\theta_1 - \theta_0)$.

VII. Numerical Results

Since analytical expressions for the approximation errors in the three schemes are difficult to formulate, a set of numerical cases were evaluated to illustrate the validity of the methods. These results are shown in Fig 2. The orbit chosen for illustrative purposes is described by the following parameters:

$a_1 = 0.78025389$: eccentricity.
$a_2 = 2.934299 \times 10^3$ nautical miles: semi-major axis.
$a_3 = 0.10416955$, $a_4 = 0.90334339$, $a_5 = 0.41607619$: Cartesian components of normal to orbital plane.

$a_6 = 1.8087277$ radians: angle between the equatorial reference line and major axis.

$a_7 = 1.3407257 \times 10^3$ sec: time between launch and apogee.

In standard astronomical parameters, the reference orbit is specified by

$e = 0.78025389$

$a = 2.9342999 \times 10^3$ nautical miles

$i = 65.5°$

$\Omega = 83.5°$ E

$\omega = 283.6°$.

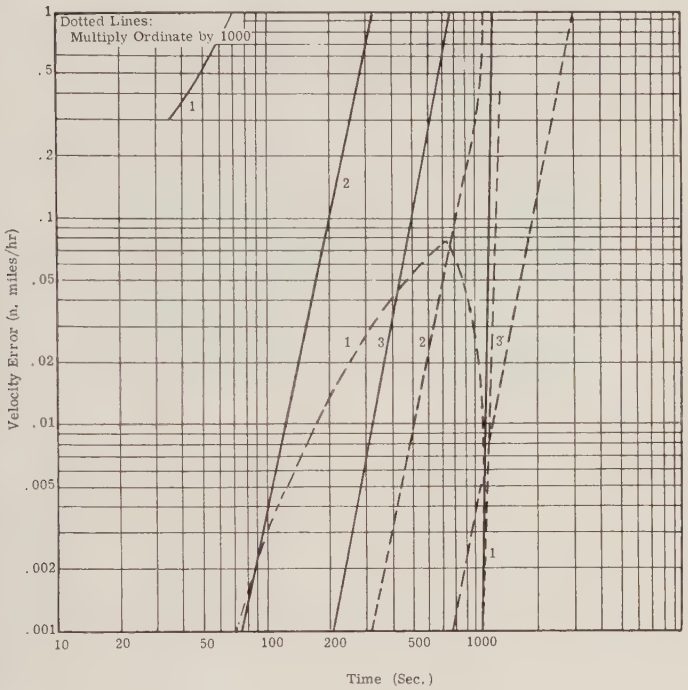

Fig. 2—Error comparison.

In each case, the first observation ϱ_1 is made at apogee. In Fig. 2, curves labeled 1 apply to the velocity approximation method; curves 2 apply to case A and curves 3 to case B. The velocity error ϵ is

$$\epsilon = \left| v_{\text{true}} - v_{\text{approx}} \right| . \tag{42}$$

The interesting result is that, for all three methods, the time separation can be several minutes before either velocity or major axis errors become large. For most scanning radar systems, any of the methods are adequate, and the choice is really determined by the accuracy of the original measurements coupled with the amount of computing time and capacity that is available.

Since the curves cannot really show the true accuracy of the results, some numerical values are listed in Table I.

TABLE I

VELOCITY APPROXIMATION (WITH ASSOCIATED ERRORS)

Time Separation	True Velocity	Approximate Velocity	Velocity Error	Semi-Major Axis Error
(sec)	(nm/sec)	(nm/sec)	(nm/hr)	(nm)
35.265461	5.5386226	5.5385383	0.3031	− 0.0641
52.888752	5.5383344	5.5381416	0.6941	− 0.1469
70.500797	5.5379311	5.5375874	1.2372	− 0.2618
105.67620	5.5367785	5.5360087	2.7714	− 0.5864
140.76200	5.5351647	5.5338067	4.8887	− 1.0342
175.72880	5.5330895	5.5309899	7.5584	− 1.5986
210.54778	5.5305526	5.5275688	10.7414	− 2.2712
245.19069	5.5275536	5.5235562	14.3905	− 3.0416
296.76461	5.5221879	5.5164601	20.6199	− 4.3553
414.82587	5.5056121	5.4951941	37.5050	− 7.9042
512.86383	5.4868680	5.4722762	52.5305	−11.0406
607.39862	5.4639126	5.4457219	65.4864	−13.7139
712.66609	5.4317707	5.4110733	74.5106	−15.5177
812.02428	5.3938027	5.3734903	73.1245	−15.1209
905.13532	5.3499410	5.3338994	57.7498	−11.8359
1003.7011	5.2924919	5.2870519	19.5839	− 3.9639
1104.6101	5.2183516	5.2328152	− 52.0689	10.3605
1204.7425	5.1238652	5.1700428	−166.2390	32.3353
		CASE A		
35.265461	5.5386226	5.5386246	−0.0075	0.0015
42.888752	5.5383344	5.5383356	−0.0042	0.0009
70.500797	5.5379311	5.5379315	−0.0015	0.0003
105.67620	5.5367785	5.5367768	0.0060	− 0.0012
140.76200	5.5351647	5.5351577	0.0251	− 0.0053
175.72880	5.5330895	5.5330712	0.0658	− 0.0139
210.54778	5.5305526	5.5305136	0.1401	− 0.0296
245.19069	5.5275536	5.5274805	0.2628	− 0.0555
296.76461	5.5221879	5.5220260	0.5827	− 0.1230
414.82587	5.5056121	5.5049345	2.4395	− 0.5132
512.86383	5.4868680	5.4851149	6.3109	− 1.3235
607.39862	5.4639126	5.4600085	14.0547	− 2.9363
712.66609	5.4317707	5.4229624	31.7099	− 6.5912
812.02428	5.3938027	5.3754696	65.9990	− 13.6431
905.13532	5.3499410	5.3133439	131.7496	− 27.0899
1003.7011	5.2924919	5.2122173	288.9887	− 59.1713
1104.6101	5.2183516	5.0116931	743.9707	−152.9973
1204.7425	5.1238652	4.4582837	2396.0935	−515.7846
		CASE B		
35.265461	5.5386226	5.5386250	− 0.0087	0.0018
52.888752	5.5383344	5.5383360	− 0.0057	0.0012
70.500797	5.5379311	5.5379323	− 0.0045	0.0009
105.67620	5.5367785	5.5367796	− 0.0040	0.0008
140.76200	5.5351647	5.5351657	− 0.0036	0.0007
175.72880	5.5330895	5.5330906	− 0.0038	0.0008
210.54778	5.5305526	5.5305536	− 0.0038	0.0007
245.19069	5.5275536	5.5275552	− 0.0060	0.0012
296.76461	5.5221879	5.5221906	− 0.0096	0.0020
414.82587	5.5056121	5.5056216	− 0.0341	0.0072
512.86383	5.4868680	5.4868928	− 0.0894	0.0187
607.39862	5.4639126	5.4639688	− 0.2021	0.0422
712.66609	5.4317707	5.4318983	− 0.4591	0.0953
812.02428	5.3938027	5.3940619	− 0.9331	0.1923
905.13532	5.3499410	5.3504250	− 1.7423	0.3562
1003.7011	5.2924919	5.2933989	− 3.2652	0.6602
1104.6101	5.2183516	5.2200350	− 6.0600	1.2080
1204.7425	5.1238652	5.1269230	−11.0077	2.1543

ACKNOWLEDGMENT

The authors wish to acknowledge Roger Cole's work in performing the computations and checking the analytical results.

Infrared Automatic Acquisition and Tracking System*

R. C. BARBERA†

Summary—A technique for accumulating airborne visible and infrared spectroradiometric data from missile plumes and re-entry objects establishes the requirements for a precision tracking front surface mirror. The processing of target radiation, reflected by the tracking mirror into an infrared tracker telescope, to derive target coordinate information, is described. The derivation of transformed target error signals to command the motion of the hydraulically driven tracking mirror is outlined. A description of the servo-electronics system, with selected circuitry, is given. The dynamic characteristics of the system, as determined from preliminary field tests, indicate that the system has a tracking rate capability of 10°/sec with an accuracy better than 60 seconds of arc. The detection sensitivity of the infrared tracker telescope is 1.6×10^{-10} w/cm² in the 2- to 6-μ region, and is sufficient to provide 10-mile tracking ranges against a jet target in a sunlit cumulus cloud background.

In a typical installation, aiming of the tracking mirror is provided by a 7×35, 10° field of view sighting telescope which is automatically slaved by the tracking mirror when acquisition and target tracking occurs, thereby providing continuous observation of the target. As an alternative to visual aiming, an automatic search program is generated by an accurate electro-mechanical programmer, which is described.

Target acquisition, in an automatic mode of operation, is accomplished through the use of a simple logic circuit which provides electronic background discrimination by virtue of signal pulse width.

Introduction

THE problem of accumulating accurate, visible and infrared spectroradiometric data from missile plumes and re-entry objects with airborne equipment, can be solved in either of two ways. The first solution requires that the radiating object be tracked by the analyzing equipment. Although this is a direct solution, it is often impractical. The size, weight, and configuration of the majority of precision spectrometers and radiometers inhibits the direct installation of such equipment in or on conventional tracking gimbal structures. Also, the field of view of such equipment is ordinarily so small (in the order of 7 minutes of arc), that the choice of scanning methods, for achieving reasonable target space coverage, is severely limited by the time available to make the measurements.

The second solution, that of reflecting the target radiation by a high quality front surface tracking mirror into the fixed analyzing equipment, offers many advantages. By such a technique, the designer has control of the size, weight and configuration of the tracking element. In addition, the motion of the tracking mirror can be commanded by information received by a relatively wide field of view optical system, thereby allowing practical target space coverage. In these principles of operation, an Infrared Automatic Acquisition and Tracking System has recently been designed and constructed for the Naval Ordnance Laboratory-White Oak under Contract No. N60291-6313 (FBM). The essential components of the system are shown in Fig. 1.

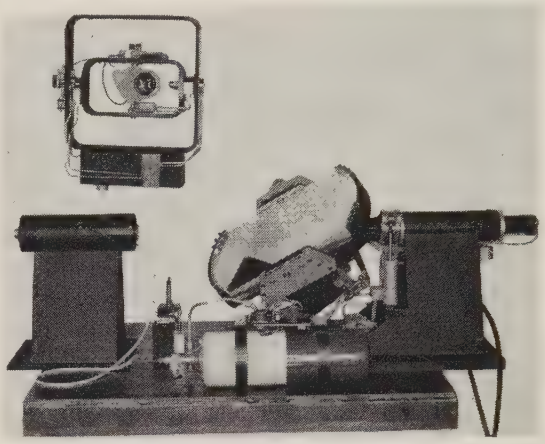

Fig. 1—Infrared automatic acquisition and tracking system.

Description of the System

The system consists of a sighting telescope assembly, an infrared tracker telescope, a 10×16-in front surface tracking mirror assembly, an electronic control system, a detector cooling system and a hydraulic power supply. The system has been designed for operating in an unpressurized cavity at altitudes up to 80,000 ft; the power requirements are 2350 w, 400 cps, 3 phase; the total weight of the equipment is 250 pounds. The maximum continuous operating time of the equipment, established by the infrared detector liquid nitrogen cooling system, is seven hours.

The system has been designed so that motion of the hydraulically driven tracking mirror can be controlled in two search modes of operation. These modes are Manual Search, whereby the operator slaves the tracking mirror by the sighting telescope, and Program Search, whereby the tracking mirror line of sight automatically scans a 15° azimuth by 30° elevation sector of target space. When an acceptable infrared target enters the 3.2° field of view of the fixed tracker telescope, by reflection from the tracking mirror, the system is automatically switched into an Automatic Track Mode of operation. In Automatic Track, the servo system provides the capability of tracking a distant target at rates up to 10°/sec with an accuracy better than 60 seconds of arc. The gimbal limits of the system, as related to the line of sight of the tracking mirror, are −5° to 60° in elevation, and ±45° in azimuth.

* Received by the PGMIL, May 29, 1961.
† Raytheon Co., Bedford, Mass.

In a normal installation, the tracker telescope is mounted on the optical axis of the spectrometer or radiometer so that it intercepts a portion of the reflected target radiation. The diameter of the tracker telescope is 3.5 in, and the obscuration of the projected tracking mirror area, in the limits of the gimbals, is shown in Fig. 2.

Fig. 2—Projected area of tracking mirror and tracker telescope obscuration.

Manual Search Mode

In the Manual Search Mode, the tracking mirror follows the motion of the sighting telescope so that their lines of sight coincide. The sighting telescope is a 7×35, 10° field of view instrument with an illuminated reticle graduated in one-degree increments. The sighting telescope assembly consists of the telescope, gimbal mounts, hydraulics actuators, control functions, and aiming potentiometers. Aiming voltages, which are proportional to the position of the optical axis of the sighting telescope, are derived from a network containing the aiming potentiometers, and supplied to the servo-electronics system to command the motion of the tracking mirror. On the tracking mirror rotation axes, a similar set of aiming potentiometers is mounted, so that a closed command loop, wherein the corresponding aiming voltages are continuously made to cancel, is formed.

Examination of the motions of the lines of sight of the sighting telescope and tracking mirror shows that coincidence will occur along one axis only, unless appropriate rotation axes and amplification factors are provided. This problem is easily solved by providing the same axis for elevation excursions, and a 2 to 1 electrical correction, for azimuth excursions. A coincidence of better than 10 minutes of arc over the complete gimbal limits can readily be obtained.

Program Search Mode

In the Program Search Mode, the line of sight of the tracking mirror is commanded to scan a 15° azimuth by 30° elevation sector of target space at a rate of 30°/sec. The rectangular steps, required to insure complete sector coverage by the 3.2° field of view of the tracker telescope, are supplied to the servo electronics by the electro-mechanical programmer shown in Fig. 3. This programmer generates azimuth switching voltages with a cam-microswitch assembly, and generates a cycling elevation sweep voltage with a synchronous driven precision potentiometer, which is supplied by a regulated voltage supply. The scan pattern is exactly squared at the corners, and the synchronism between the elevation and azimuth commands is better than 0.005 sec.

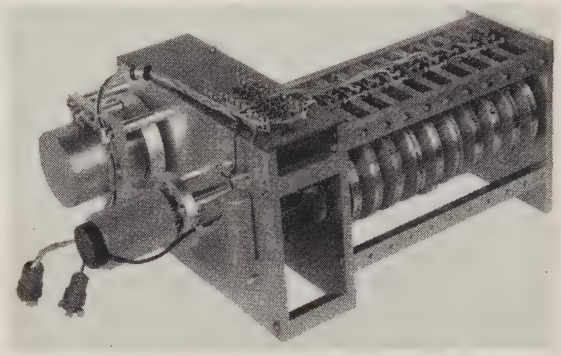

Fig. 3—Electromechanical programmer.

The Program Search command voltages are centered about the aiming voltages derived from the sighting telescope potentiometers. Thus, at any time during the scanning process, the center of the scan pattern can be shifted to a new location in target space by the viewing operator.

Automatic Track Mode

Target radiation, reflected by the tracking mirror, will enter the optics of the tracker telescope, if the target is within the 3.2° field of view of the tracker telescope. The electronics system associated with this optical-mechanical system processes the target signal and provides appropriate signals for the servo electronics to command the motion of the tracking mirror, so as to null the error in the line of sight to the target.

Within the tracker telescope, a rotating wedged plano front surface mirror causes the image of a focused target to rotate in a circle of constant diameter on a sunburst reticle. All radiation passing through this reticle is incident upon a liquid nitrogen cooled lead selenide detector. Thus, when the target is on the optic axis, the output of the infrared detector is an unmodulated wave. When the target moves off the optic axis, frequency modulation of the target signal occurs.

The target signal, thus generated, is amplified, limited and demodulated to provide an error signal at the frequency of the image scan mirror. This error signal is proportional, in amplitude and phase, to the polar coordinates of the target in a plane in target space. Resolution of these polar coordinates into appropriate elevation and azimuth commands for the tracking mirror requires electronic transformation. In the servo

electronics, this transformation is accomplished by comparing the error signal with two phases of a reference voltage generated within the tracker telescope, by the rotation of the wedged plano mirror. Inasmuch as the tracking mirror motion involves rotation about the optic axis (to achieve elevation tracking), the apparent motions of a target, as viewed by the tracker telescope, are reversed. Thus, to eliminate cross coupling and false coordinate transformations, the reference voltage phases are continuously shifted by a two-phase synchro resolver driven by the tracking mirror. For efficiency of design, the synchro resolver is attached directly to the shaft of the tracking mirror drive.

In the Automatic Track Mode, target acquisition and tracking initiates action of the hydraulics system coupled to the visual sighting telescope, causing the sighting telescope to exactly follow the tracking mirror. Thus, the operator can continuously view the target.

This reversal of slave-command roles is simply accomplished. The aiming potentiometers mounted on the axes of the sighting telescope serve, in the Track Mode, as follow-up potentiometers. The voltage appearing across these potentiometers is continuously compared with the voltage appearing across the corresponding tracking mirror potentiometers, and the difference is used to drive the sighting telescope hydraulic actuating system.

The three modes of operation of the system are represented by the block diagram of Fig. 4.

Target Acquisition

Provision has been made for manually or automatically acquiring a target. The viewing operator, through a selector switch, may manually acquire or reject a target, or sensitize the system for automatic acquisition. Two indications of target acquisition are provided at the operator sighting telescope control station. When a target is acquired by the system, an indicator light is illuminated, and an audible distinct tracking tone is generated.

Although spatial and spectral discrimination were incorporated in the tracker telescope design, a requirement for electronic false target discrimination, in the target acquisition phase, existed. An examination of the scanning patterns, generated by the projection of the reticle in target space, indicated that reasonable discrimination could be achieved on the basis of the width of the first pulse produced by a target of any size. Thus, there existed an upper limit on the width of the first pulse generated by acceptable distant targets. Typical natural cloud backgrounds, and the solar disk, could be distinctly characterized by longer pulse widths.

From the design parameters of the tracker telescope, the reticle and the scan times of the programmer, it was determined that an acceptable distant target would generate a first pulse lasting no longer than 2.0 msec. This upper limit establishes the maximum angle subtended by an acceptable distant target at the tracker telescope as 0.32°.

A simple logic circuit has been evolved which determines if such conditions are satisfied. The block diagram of this transistorized circuit is shown in Fig. 5. Prior to $t=0$, gate A_1 is open and A_2 is closed. At $t=0$, the initial pulse rise triggers T_1 through A_1. During this interval ($t=0$ to 2.0 msec), gate A_2 is open, and a fall in the input pulse can be transmitted through A_2 to T_3. The timer T_3 generates a 15 msec pulse which activates the tracking function relay, through the driver D_1. If the initial pulse did not fall prior to 2.0 msec (denoting a false target), T_1 recovers and closes A_2. T_1 also triggers T_2 which closes A_1 for 90 msec, preventing target pulse interrogation. At the end of the 90 msec period of quiescence, T_2 recovers, opens A_1, and the circuit is again ready to examine the input. The 90 msec delay insures that, for this system of scanning, a normal cloud will be rejected during passage of the tracker telescope field of view across it.

The acquisition sensitivity of the circuit is, as to be anticipated, poorer than the tracking sensitivity of the system. In the Program Search Mode, acquisition sensitivity is approximately 1.5×10^{-9} w/cm^2. In the Manual Search Mode, acquisition sensitivity is approximately 7×10^{-10} w/cm^2. Tracking sensitivity of the system, for reasonably smooth tracking, is 4×10^{-10} w/cm^2, and the detection sensitivity of the system is 1.6×10^{-10} w/cm^2. These target radiation densities are

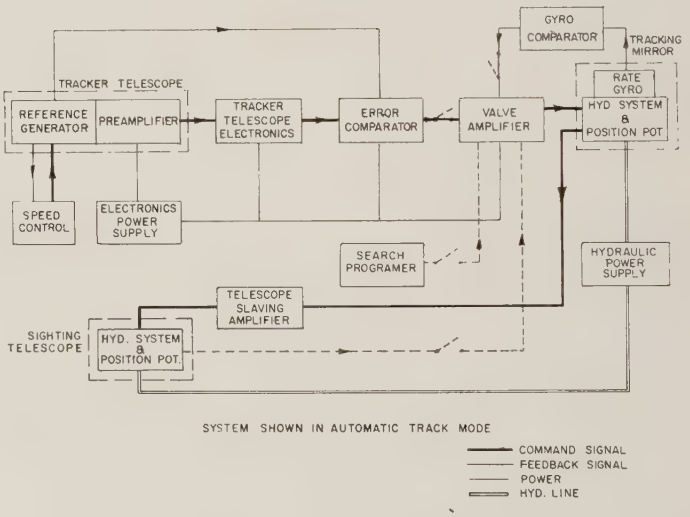

Fig. 4—System block diagram.

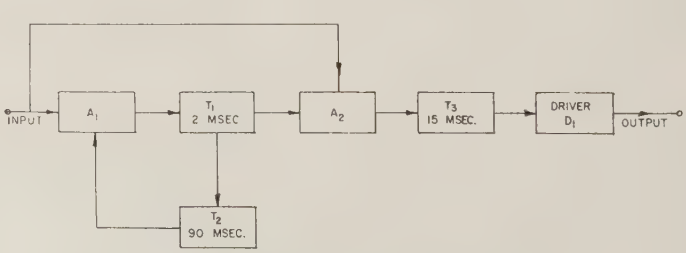

Fig. 5—Automatic acquisition circuit block diagram.

referred to a spectral bandwidth from 2 to 6 μ, as indicated by the spectral sensitivity characteristics of the tracker telescope shown in Fig. 6.

Tracking Mirror Assembly

The tracking mirror is a front surface Pyrex mirror figured, over-all, to five fringes of sodium vapor light. The mirror is 16 in long, 10 in wide, $1\frac{1}{4}$ in thick, and weights $14\frac{1}{2}$ pounds. It is aluminized and overcoated with SiO.

The tracking mirror is rigidly held in an aluminum gimbal structure. This structure provides rotation about the optic axis of the spectrometer or radiometer, for elevation tracking, and rotation about an axis perpendicular to the optic axis and lying in the front surface of the mirror, for azimuth tracking. Through this gimbal action, a maximum projected area of the tracking mirror is provided for all tracking angles, and a minimum of *orange peel* effect is projected in target space.

The moments of inertia of the mirror structure are 0.7 slug ft^2 approximately (elevation), and 0.4 slug ft^2 approximately (azimuth). The hydraulic actuating system which drives the tracking mirror provides 135 lb ft of torque in the elevation axis, and 155 lb ft of torque in the azimuth axis, at a hydraulic system operating pressure of 1600 psi. These torques are more than adequate to provide the angular accelerations required in normal system application.

The tracking mirror is velocity damped, in the servo loop, through the use of rate gyros mounted on the mirror support structure. No complete experimental measurements of loop stability have been made. However, it is estimated that the *close out* frequency of the servo is approximately 12 cps. That is, for normal aircraft maneuvers during a tracking measurement, the tracking mirror will be fixed on the target, and will not follow the motions of the platform to which it is mounted. In field tests against a low flying jet aircraft target at maximum tracking rates of about 6.5°/sec, the support table of the system was subjected to vibrations at approximately 6 cps with no apparent degradation in tracking performance.

Tracker Telescope

The tracker telescope primary optical system is $f/2.3$ Dall-Kirkham with a 7.5-in focal length. The on-axis blur circle diameter does not exceed 0.005 in. The optical schematic diagram is shown in Fig. 7.

The f-m reticle is located at the focal plane of the primary optical system. It is photoetched, in a special design, of beryllium copper. The spoke and center detail were selected to provide a fairly high degree of spatial discrimination against background targets. This discrimination, resulting from off-axis degradation of the image of extended targets, provides reduced sensitivity to background at the edge of the field.

In order to further enhance background discrimination, spectral filtering is incorporated in the optical system. A 3.5-μ cut-on interference filter, located in front of the reticle, has proven effective. In a series of tests with a sunlit cumulus cloud background, tracking ranges in excess of 10 miles were obtained against a jet target.

Concentration of the interrupted radiation on the cooled lead selenide detector is accomplished by a light pipe, rather than by a conventional field lens system. This light pipe, whose curvature was obtained by extensive ray tracing, is sufficiently effective to provide an over-all optical efficiency of about 20 per cent.

The infrared detector and liquid nitrogen cooling system were provided by the Santa Barbara Research Center. The detector has a D^* of 3.7×10^9 cm cps$^{1/2}$/w. The liquid nitrogen cooling system, operating by transferring liquid nitrogen from a heater controlled reservoir, has a capacity of $1\frac{1}{2}$ liters. This is sufficient to provide a continuous operating time of at least seven hours, with the detector at -196°C.

The detector preamplifier circuitry is housed in the tracker telescope in order to reduce microphonic cable noise. The system photograph of Fig. 1 permits a comparative evaluation of the size of the tracker telescope. It measures 3.5 in in diameter and 12 in in over-all length.

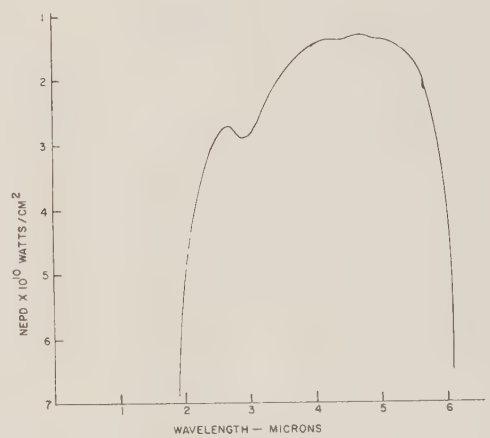

Fig. 6—Tracker telescope spectral sensitivity with Ge. filter and detector No. JW-1297-18.

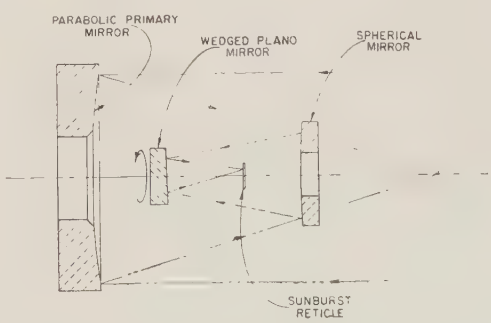

Fig. 7—Tracker telescope optical schematic diagram.

Electronics Control System

The frequency modulated target signal generated in the tracker telescope is amplified, filtered and limited; then converted to a 50-cps amplitude modulated wave by a discriminator circuit. The on-axis target frequency is 800 cps, and the modulation frequency (the frequency of the scanning mirror) is 50 cps.

The filtered error signal is supplied to the error comparator section of the servo electronics where the appropriate electronic coordinate transformations are made. This portion of the servo electronics, by comparison in full wave rectifier bridges, provides dc hydraulic valve command voltages to control the motion of the tracking mirror. These command voltages are precisely adjusted in polarity and amplitude to insure cancellation in the error in the line of sight to the target.

The control valves in the hydraulic system which actuate the tracking mirror are solenoid operated spool valves having a reasonably linear response. The flow rate through the valves is linearly proportional to the target error. This implies that the rate at which the tracking mirror moves to cancel the error will vary with the magnitude of error. Thus, it would be expected that overshoot and oscillation about the null position would be highly probable unless damping were imposed upon the tracking motions.

Such damping is provided by the use of rate gyros attached to the tracking mirror support structure. The rate gyro outputs are supplied to appropriate gyro comparators and compared in amplitude and phase with reference voltages generated at the frequency of the gyro. Thus, as in the error comparator, a rectified voltage is provided for command. This voltage is proportional to the angular velocity of the tracking mirror, and by proper attenuation and summing with the rectified target error signal, is used to provide smooth tracking performance with no overshoot at the null position.

As is characteristic of all infrared f-m scanning systems, the resolved error is linear only over a small portion of the total field of view of the optical system. This characteristic results from the detail of the reticle and the method of scanning, whereby the target image falls off the reticle spoke region even at small target angles. However, in spite of what appears to be a defect, the linearity of the error curves is exceptionally good. Also, beyond the linear region, target sense is always preserved. This feature is illustrated by the error curve of Fig. 8, and implies a high degree of tracking accuracy.

In the previous description of system operation, it was mentioned that the sighting telescope is slaved to the tracking mirror in the Automatic Track Mode, allowing the operator to observe the target continuously. The amplifiers which drive the sighting telescope hydraulic actuators are supplied by voltages which are proportional to the difference in position of the wiper arms of the aiming potentiometers mounted on the tracking mirror and on the sighting telescope. Although

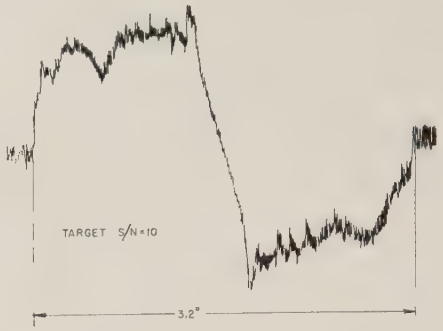

Fig. 8—Typical target dc error curve measured at error comparator.

similar spool valves control the actuation of the sighting telescope, as control the tracking mirror, no separate rate damping is required for the sighting telescope. Since the sighting telescope follows the tracking mirror, the rate damping applied to the tracking mirror is reflected into the motions of the sighting telescope and provides sufficiently smooth visual tracking.

Hydraulic Power Supply

A major advantage of hydraulic actuation systems compared with electrical torquers is apparent by consideration of the size of components located at the site of application of force. This is one reason for the selection of the actuation system for the Infrared Automatic Acquisition and Tracking System. Other technical reasons such as fluid incompressibility, acceleration capabilities, and reliability were extremely important.

The maximum requirements imposed upon the actuation system occur during the Program Search Mode. Calculations indicated that the scan pattern could be achieved with minimum accelerations of 6 rad/sec^2. The final design produces a constant rate for most of the scan, during the elevation passes at 30°/sec, and azimuth steps at maximum acceleration. This was readily achieved with pistons approximately $\frac{3}{4}$ in in diameter and oil flow rates of approximately 0.3 gal/min.

The hydraulic power supply which satisfies the system requirements has a capability of 0.5 gal/min at a maximum delivery pressure of 3000 psi. The power supply, occupying a volume of approximately 5 ft^3 and weighing 75 pounds, is amply protected against overpressures and is designed for a continuous loaded operating period of four hours. Consistent with the electrical characteristics of the other equipment, the hydraulic power supply utilizes 400 cps aircraft power.

Acknowledgment

The system which has been described was designed and delivered in less than 100 calendar days. This accomplishment was made possible through the efforts and ingenuity of a competent team. Particular credit is due to A. Krutchkoff and W. P. Frost of the IR and Optics Branch, Missile and Space Division, Raytheon Company, Bedford, Mass.

High-Precision Angle Determination by Means of Radar in a Search Mode*

E. C. WATTERS†, F. L. REES†, AND R. A. ENSTROM†

Summary—One of the more difficult requirements to meet in the design of radars is that of accurate angular measurement. In tracking radars the azimuth and elevation of a target can be measured to a high degree of accuracy by a nulling method. Two of the most practical methods for obtaining angular accuracy in search radars are discussed in this paper. The first method is an interferometer technique employing either two receiving antennas for each dimension of angular measurement with two frequencies of transmission for the resolution of ambiguities, or three receiving antennas positioned relative to one another so that the equivalent effect is achieved with only one-frequency transmission. The second method is a combination amplitude comparison and interferometer technique in which the ambiguities are resolved by the amplitude comparison system. An analysis of each of these systems has been made using a statistical approach in which equations are developed relating the probability of error for a specified angular accuracy to SNR power in the receiver. Curves are presented which show this relationship for a 100 to 1 beam-splitting ratio.

Introduction

THE problem of accurate angular measurement may be considered from two aspects, practical and theoretical. From a practical point of view, hardware capabilities must be considered. From the theoretical aspect, the problem of achieving a given accuracy can be related to SNR.

From a practical point of view, beam-splitting from a single antenna is dependent upon solving the following problems. First, the shape of the beam (or beams) must be accurately known. Secondly, if a single beam is used, measurements will depend on the target scintillation between pulses. Thirdly, if two or more beams are used, the receiver channels must be accurately balanced. Finally, the accuracy of angular measurement is directly related to the boresight error which would considerably increase the cost of mounting in many cases. On the other hand, these problems can be reduced if two widely spaced antennas are used in an interferometer system. The beam pattern is merely used to resolve gross ambiguities, thus the precise shape of the beam is of reduced importance. Phase-balancing of the receiver channels is not as critical as amplitude-balancing and the boresight problem is transferred to the problem of setting up the baseline which can be done with considerable accuracy by standard surveying methods.

Each of the systems being considered in this paper make use of two or more widely separated antennas. Therefore, the above-mentioned sources of error are secondary when compared to the error caused by noise in the receiving channels. For this reason, the primary consideration in the following analysis of the two systems is the effect of SNR on the accuracy of angular measurement.

* Received by the PGMIL, May 23, 1961.
† Westinghouse Electric Corp., Electronics Div., Baltimore, Md.

Influence of Signal-to-Noise Ratio

The accuracy to which angle can be measured, whether it be azimuth or elevation, is primarily a function of the SNR in the receiver. Prior to the analysis of the two beam-splitting techniques in question, it is of interest to consider the theoretical minimum SNR required to attain the desired angle accuracy. Manasse [1] develops expressions for the optimum SNR for a given angular accuracy for both the monopulse and the interferometer techniques of angular measurement. These have been duplicated independently with somewhat less restrictive assumptions. The analysis involved is presented in the Appendix. For a monopulse system with coincident apertures, the rms error is given by

$$\sigma_{\hat{\theta}} = \frac{\sqrt{1 + P/\sigma_n^2}}{\left(\frac{\alpha}{\beta}\right)(P/\sigma_n^2)\sqrt{2}}, \tag{1}$$

where

P/σ_n^2 = signal to rms noise power ratio, and
$\alpha/\beta = d_0/\lambda$,

d_0 is a measure of the effective length of the antenna aperture and λ is the wavelength of the transmitted frequency.

For large SNR's, $P/\sigma_n^2 \gg 1$

$$\sigma_{\hat{\theta}} \approx \frac{1}{\left(\frac{\alpha}{\beta}\right)\sqrt{2P/\sigma_n^2}} = \frac{\lambda}{d_0\sqrt{2P/\sigma_n^2}}.$$

For a circular aperture of radius R, $d_0 = \pi R$ and

$$\sigma_{\hat{\theta}} \approx \frac{2}{\pi}\left(\frac{\lambda}{R}\right)\frac{1}{\sqrt{2P/\sigma_n^2}}.$$

However, the beamwidth is $\theta_B = (\lambda/R)(1/\sqrt{\pi})$ for small θ_B which yields

$$\frac{\sigma_{\hat{\theta}}}{\theta_B} \approx \left(\frac{\pi}{2}\frac{P}{\sigma_n^2}\right)^{-1/2}. \tag{2}$$

Now, for $\sigma_{\hat{\theta}}/\theta_B = 1/100$, the minimum SNR power is $P/\sigma_n^2 = 38$ db.

Similarly, for an interferometer system, assuming large SNR's, $d_0 \approx \pi D$, where D is the spacing between antennas and

$$\sigma_{\hat{\theta}} \approx \frac{1}{\pi}\left(\frac{\lambda}{D}\right)\frac{1}{\sqrt{2P/\sigma_n^2}}. \tag{3}$$

For the number of ambiguities, $m = D/\lambda\theta_B$. Thus,

$$\frac{\sigma_{\hat{\theta}}}{\theta_B} = \frac{1}{\pi m}\,\frac{1}{\sqrt{2P/\sigma_n^2}}. \tag{4}$$

Again, assuming $\sigma_{\hat{\theta}}/\theta_B = 1/100$ and further assuming $m = 10$, the minimum signal-to-rms noise power ratio is $P/\sigma_n^2 = 7$ db.

It is from these figures that some combination of monopulse and interferometer techniques should allow more reasonable SNR's for a given accuracy while, at the same time, resolving most of the ambiguities.

Two-Frequency Interferometer Theory

General

In the analysis of each of the systems being compared, the major problem is one of resolving the $(D/\lambda)\theta_B$ ambiguities in the single interferometer measurement.

Fig. 1 illustrates the geometry for an interferometer measurement of target azimuth. The points A and B represent two antennas. It is assumed that the radar beam is scanned and that line OC is the axis of symmetry of the amplitude pattern. The beamwidth θ_B is not necessarily the usual 3-db beamwidth. It may be 6 db or any other level beamwidth. The significant point is the assumption that the target is known to lie within the beamwidth.

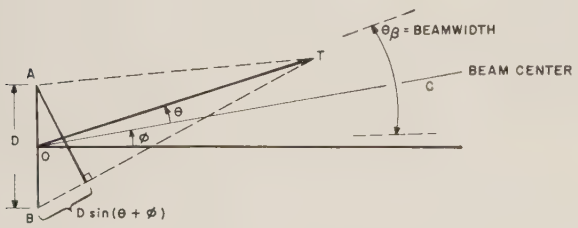

Fig. 1—Interferometer geometry.

In order to obtain an accurate measure of the interpolation angle θ from the beam center, phase comparisons of the signal received at A and B will be made for two frequencies of transmission. Alternatively, three antennas can be used on one baseline with one transmission frequency to achieve the same effect. Whether three antennas are used or different frequencies are employed is immaterial as far as accuracy is concerned. The form of the equations will show this. The ability to perform an accurate measurement will actually depend on the practicality of choosing the proper relation between frequency of transmission and spacing D. For these reasons the following discussion will assume that D is fixed and two different transmission frequencies will be employed.

The analysis which follows will confine itself to the particular case where one frequency is chosen in such a way that the interferometer pattern admits a tenfold ambiguity over the beamwidth θ_B. The other frequency of transmission will then be employed to resolve this ambiguity. It is the choice of this second frequency wherein the difference of performance lies. The second frequency may be chosen so that there is no ambiguity within the beamwidth θ_B or it may be chosen in such a way that there is, perhaps, a ninefold ambiguity. The details will be carried out for both cases and it will be shown that, due to noise, the latter case is less desirable.

Analysis

From Fig. 1, the phase difference in signals received at A and B is

$$\Delta \text{ phase} = \frac{\omega_i D}{C}\,\text{Sin}\,(\theta + \phi) = \frac{2\pi D}{\lambda_i}\,\text{Sin}\,(\theta + \phi), \tag{5}$$

where λ_i $(i = 1, 2)$ is the wavelength of the received signal and ω_i is the radian frequency. Assuming that θ_B, hence θ, is small

$$\Delta \text{ phase} = \frac{2\pi D}{\lambda_i}\,[\text{Sin}\,\phi + \theta\,\text{Cos}\,\phi]. \tag{6}$$

Let

$$\alpha_i = \frac{2\pi D}{\lambda_i}\,\theta\,\text{Cos}\,\phi, \qquad i = 1, 2$$

$$\gamma_i = \frac{2\pi D}{\lambda_i}\,\text{Sin}\,\phi, \qquad i = 1, 2.$$

By the initial assumption that a tenfold ambiguity exists for the frequency ω_1, it is possible to sketch α_1 versus θ as indicated in Fig. 2. Since α_1 may be measured only to within 2π, ω_2 must be chosen to resolve the ambiguity. Two methods suggest themselves:

1) Choose ω_2 such that $-\pi < \alpha_2 < \pi$, $-\theta_B/2 < \theta < \theta_B/2$;
2) Choose ω_2 such that $-\pi < \alpha_1 - \alpha_2 < \pi$, $-\theta_B/2 < \theta < \theta_B/2$.

The first choice involves a sizeable percentage change in transmitted frequency as compared to the second, and there is a difference in the method of data-processing. It will be seen in the analysis to follow that the first method is preferable from a SNR standpoint.

Fig. 3 presents a block diagram of a system to measure θ by either of the two methods described above. In this figure the quantities

$$(X_i + S)\,\text{Cos}\,(\omega_i t + \delta_i) + Y_i\,\text{Sin}\,(\omega_i t + \delta_i)$$

$$(x_i + S)\,\text{Cos}\,(\omega_i t + \delta_i - \alpha_i - \gamma_i) + y_i\,\text{Sin}\,(\omega_i t + \delta_i - \alpha_i - \gamma_i)$$

represent the received signal plus noise in the two channels, respectively. Here the x's denote the in-phase and the y's the quadrature components of noise. They are all independent normally distributed variables with standard deviation σ_n. S represents peak-signal strength and δ_i is absolute target phase. The system is independent of absolute signal and noise levels, but it is important that the gains of the two channels be matched.

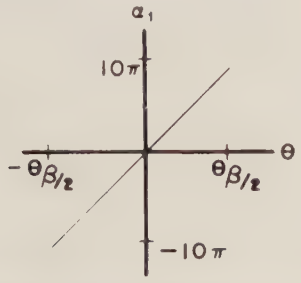

Fig. 2 Phase as a function of angle for wavelength λ_1.

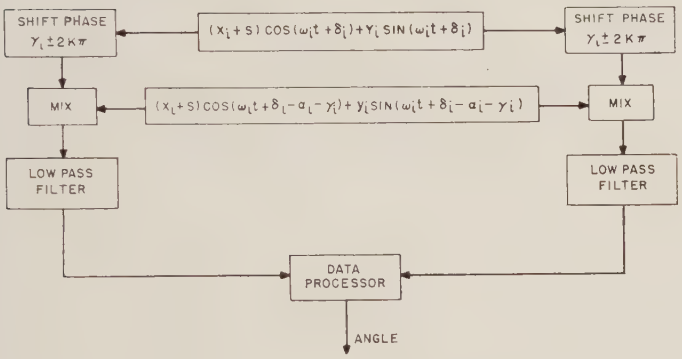

Fig. 3—Block diagram of a two-frequency interferometer system.

Let

$$M_i = [(X_i + S)(x_i + S) + y_i Y_i]\frac{1}{S^2},$$

$$N_i = [(x_i + S)Y_i - (X_i + S)y_i]\frac{1}{S^2}, \tag{7}$$

and

$$a_i = C[M_i \operatorname{Cos}\alpha_i + N_i \operatorname{Sin}\alpha_i],$$
$$b_i = C[-N_i \operatorname{Cos}\alpha_i + M_i \operatorname{Sin}\alpha_i], \tag{8}$$

where C represents an arbitrary gain. Since the data-processing will depend on the technique employed to resolve ambiguities, the analysis will now consider the cases separately.

Analysis of Case 1

$\left.\begin{array}{l}\omega_2 \text{ is chosen so that } -\pi < \alpha_2 < \pi \\ \omega_1 \text{ is chosen so that } -10\pi < \alpha_1 < 10\pi\end{array}\right\} -\theta_B/2 < \theta < \theta_B/2.$

If there were no noise, $M_i = 1$, $N_i = 0$ and

$$a_i = C \operatorname{Cos}\alpha_i,$$
$$b_i = C \operatorname{Sin}\alpha_i. \tag{9}$$

Thus, α_2 could be determined from Fig. 4.

In this case there is no need for further measurement. In practice, however, noise will be present and α_2 cannot be determined precisely. Letting the subscript m denote measured quantities and employing Fig. 4 to determine α_{2m}, yields

$$\alpha_{2m} = \alpha_2 - \epsilon_2 \tag{10}$$

where ϵ_2, the error due to noise, is shown in Fig. 5.

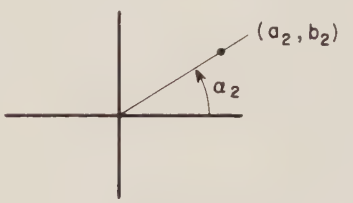

Fig. 4—Polar diagram of the in-phase and quadrature components, at λ_2, relating phase.

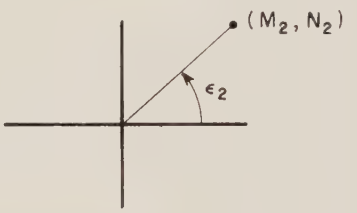

Fig. 5—Polar diagram of the in-phase and quadrature coefficients due to signal and noise, at λ_2, relating phase error.

In order to properly resolve the tenfold ambiguity in the next measurement at frequency ω_1, it is necessary that $|\epsilon_2| < 2\pi/10$. We have assumed $|\alpha_2| < 19\pi/20$ in making this latter statement, which in turn implies the target is not too close to the edge of the beam; *i.e.*, $|\theta| < 19\theta_B/40$. The probability that satisfies the stated inequality is a function of SNR. For large SNR's (exceeding 14 db) the approximate relations hold:

$$M_2 \approx 1 + \frac{x_2 + X_2}{S}$$

$$N_2 \approx \frac{Y_2 - y_2}{S}. \tag{11}$$

Furthermore, the probability that $|\epsilon_2| < \pi/5$ is approximately equal to the probability that

$$\left|\tan^{-1}\frac{N_2}{M_2}\right| < \frac{\pi}{5},$$

where the principal value of the $\tan^{-1}$ is chosen. It is not difficult to show that the probability that this last inequality holds is given by

$$P = \int_{-\pi/5}^{\pi/5} p(x)dx, \tag{12}$$

where

$$p(x) = \frac{1}{\pi} e^{-R^2/4} + \frac{R}{2\sqrt{\pi}} \cdot e^{-(R^2 \sin^2 x)/4} \cos x \operatorname{erf}\left(\frac{R \cos x}{2}\right). \tag{13}$$

R is peak signal to rms noise ratio s/σ_n and

$$\operatorname{erf}(z) = \frac{2}{\sqrt{\pi}} \int_0^z e^{-t^2} dt.$$

Making an approximate evaluation of P yields

$$P \approx \operatorname{erf}\left(\frac{\pi R}{10}\right). \tag{14}$$

Thus, for targets not too far from beam center, 100 P per cent of the time the ambiguity in the second measurement will be correctly resolved and 100 $(1-P)$ per cent it will be incorrectly resolved. Once the ambiguity is resolved, the above analysis can be repeated for the frequency of transmission ω_1. If the probability of error is required to be less than 1/100 beamwidth θ_B, considerable simplification in analysis results if a slightly more restrictive requirement is placed on the first measurements, *i.e.*, require $|\epsilon_2| < 0.9\pi/5$ instead of $|\epsilon_2| < \pi/5$. This permits the immediate statement of the final result: The probability that the resultant error is less than $\theta_B/100$ is given by

$$\operatorname{erf}\left(\frac{0.9\pi R}{10}\right) \operatorname{erf}\left(\frac{\pi R}{10}\right), \tag{15}$$

where $R > 5$ is peak signal to rms noise ratio. The effect of adding the more restrictive requirements described is small. A graph of (15) is presented in Fig. 6.

Analysis of Case 2

$\left.\begin{array}{l}\omega_2 \text{ is chosen so that } -\pi < \alpha_1 - \alpha_2 < \pi \\ \omega_1 \text{ is chosen so that } -10\pi < \alpha_1 < 10\pi\end{array}\right\} -\theta_{B/2} < \theta < \theta_{B/2}.$

In this case, from $\alpha_1 - \alpha_2$ one determines θ to a tenth beamwidth and then refines the measurement as in Case 1 by employing the measured α_1. It is not difficult to show that if

$$\begin{aligned} A &= a_1 a_2 + b_1 b_2 \\ B &= a_2 b_1 - a_1 b_2 \end{aligned} \tag{16}$$

and no noise is present, $(\alpha_1 - \alpha_2)$ is given in Fig. 7. In the presence of noise, however, $(\alpha_1 - \alpha_2)_m$ the measured value of $(\alpha_1 - \alpha_2)$ is determined. More specifically

$$(\alpha_1 - \alpha_2)_m = \alpha_1 - \alpha_2 + \epsilon \tag{17}$$

where ϵ, the error due to noise, is shown in Fig. 8. For SNR exceeding 14 db, ϵ is approximately that given in Fig. 9.

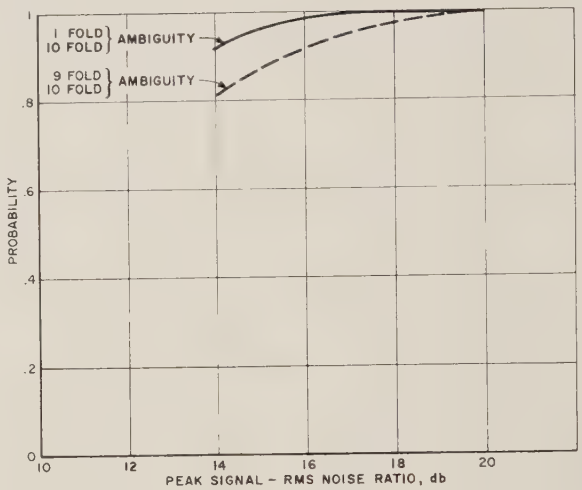

Fig. 6—The probability of measuring angle to within one-hundredth of a beamwidth as a function of SNR.

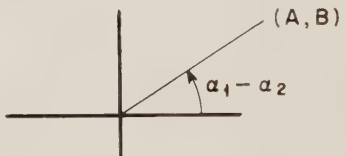

Fig. 7—Polar diagram of the in-phase and quadrature coefficients, at $\lambda_1 - \lambda_2/\lambda_1\lambda_2$, relating phase.

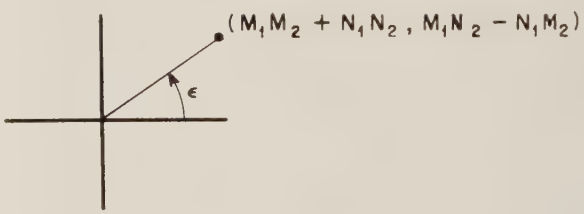

Fig. 8—Polar diagram of the in-phase and quadrature coefficients relating phase error.

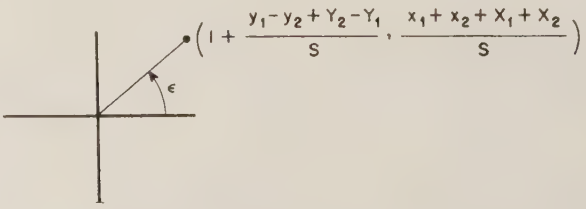

Fig. 9—Polar diagram of the in-phase and quadrature coefficients relating phase error for large SNR.

Comparing this with Fig. 5 and (11), it is clear that the difference between Case 1 and Case 2 lies in the distribution of ϵ_2 and ϵ. For ϵ_2 and ϵ to have the same probability distribution, an increase of 3-db SNR is required in the latter since twice as many noise components are present. Allowing for this increase in SNR the remainder of the analysis is identical to that of Case 1. Thus the result may be stated: The probability that the resultant error is less than $\theta_B/100$ is given by

$$\operatorname{erf}\left(\frac{0.9\pi R}{10\sqrt{2}}\right)\operatorname{erf}\left(\frac{\pi R}{10}\right), \tag{18}$$

where $R>5$ is peak signal to rms noise ratio. A graph of (18) is presented in Fig. 6.

The major difference in the two systems is the initial measurement to a tenth beamwidth which resolves the tenfold ambiguity. Fig. 10 shows the percentage of time the wrong decision is made for the two systems.

Amplitude Comparison-Interferometer System

The second system to be analyzed is one which combines the interferometer technique for fine angular measurement with a monopulse technique for resolving the ambiguities in the interferometer measurement. Fig. 11 shows a block diagram of such a system.

In the monopulse section of the system,

$$y_1(t) = (S_1 + X_1)\operatorname{Cos}\omega t + Y_1 \operatorname{Sin}\omega t$$

and

$$y_2(t) = (S_2 + X_2)\operatorname{Cos}(\omega t + \phi_1) + Y_2 \operatorname{Sin}(\omega t + \phi_1), \tag{19}$$

where

ϕ_1 = phase change due to path differences,
$S_1 = \sqrt{P}e^{-\alpha(\theta-\theta_1)^2}$, $S_2 = \sqrt{P}e^{-\alpha(\theta-\theta_2)^2}$ } P = signal power, θ_1, θ_2 are the angles

corresponding to the peaks of the adjacent beams as shown in Fig. 12. X_1, X_2, Y_1, Y_2. are the in-phase and quadrature components of the noise in channels I and II. They are assumed to be independent, normally distributed variables with average zero and standard deviation σ_n.

These assumptions reduce the problem to one considered by Enstrom [2] in which an expression was developed for the probability density of the estimated angle $\hat{\theta}_M$ as a function of SNR. For large SNR's, this probability density is approximately Gaussian. That is,

$$p(\hat{\theta}_M) \approx \frac{1}{\sigma_M\sqrt{2\pi}} e^{-(\hat{\theta}_M-\bar{\theta}_M)^2/2\sigma_M^2}. \tag{20}$$

The average estimated angle is,

$$\bar{\hat{\theta}}_M = \frac{\theta_T S_1^2 S_2^2}{.312\sigma_n^2(S_1^2+S_2^2)+S_1^2S_2^2} = \theta_T + \beta \tag{21}$$

where θ_T is the actual target angle and β is a bias error.

The mean square angular error is,

$$\sigma_M^2 = \frac{\theta_B^4\sigma_n^2(S_1^2+S_2^2)}{64\theta_S^2(\ln K)^2[.312\sigma_n^2(S_1^2+S_2^2)+S_1^2S_2^2]}. \tag{22}$$

In this expression, θ_S = beam separation angle $(\theta_2-\theta_1)$ and θ_B = beamwidth. The constant K is the level at which the beamwidth is measured.

The estimated angle measurement using the interferometer system will yield ambiguities spaced λ/D apart. For this reason, the estimated angle of the

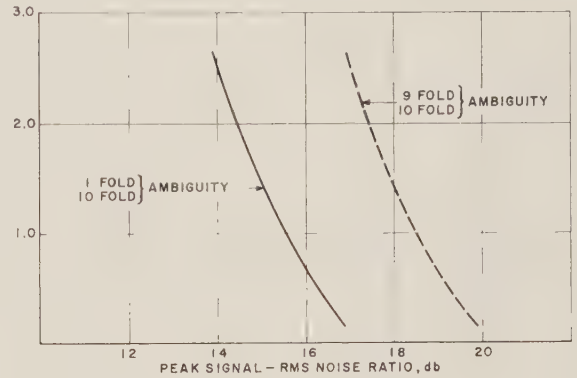

Fig. 10—Percentage of time ambiguity resolution is in error.

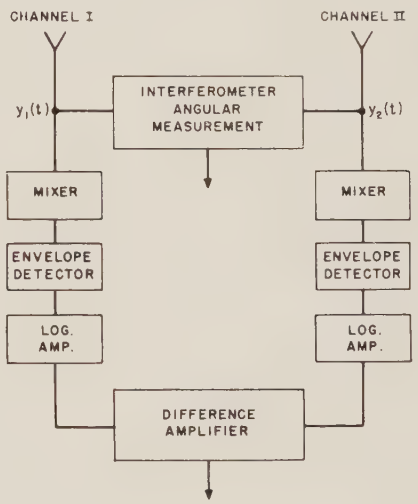

Fig. 11—Block diagram of amplitude comparison-interferometer system.

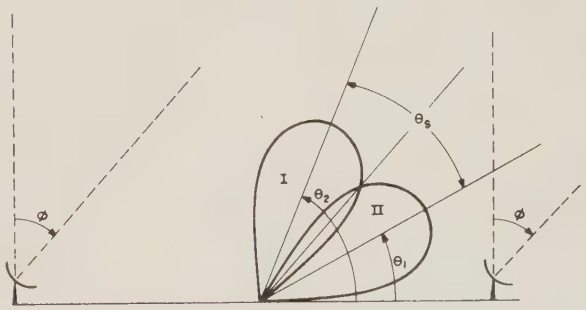

Fig. 12—Beam-splitting geometry with spaced apertures.

amplitude comparison system must be accurate to within $\pm\lambda/D+\beta$ in order to resolve these ambiguities. The probability that this is accomplished is a function of SNR and actual target position and can be found using $p(\hat{\theta}_M)$ as described below.

$$P = \text{Prob.}\,(\beta - \lambda/D < \hat{\theta}_M - \theta_T < \beta + \lambda/D)$$

$$= \frac{1}{\sigma_M\sqrt{2\pi}} \int_{\beta-\lambda/D}^{\beta+\lambda/D} e^{-\epsilon^2/2\sigma_M{}^2} d\epsilon, \qquad \epsilon = \hat{\theta}_M - \theta_T$$

$$= \frac{1}{2}\left[\text{erf}\left(\frac{\beta+\lambda/D}{\sigma_M\sqrt{2}}\right) - \text{erf}\left(\frac{\beta-\lambda/D}{\sigma_M\sqrt{2}}\right)\right]. \tag{23}$$

Returning to the expression for $\sigma_M{}^2$ and substituting the values for S_1 and S_2,

$$\sigma_M{}^2 = \frac{\theta_B{}^4 \dfrac{\sigma_n{}^2}{P}\left[e^{2\alpha(\theta_T-\theta_2)^2} + e^{2\alpha(\theta_T-\theta_1)^2}\right]}{64\theta_S{}^2(\ln K)^2\left[.312\dfrac{\sigma_n{}^2}{P}\left(e^{2\alpha(\theta_T-\theta_2)^2} + e^{2\alpha(\theta_T-\theta_1)^2}\right) + 1\right]}.$$

If

$$e^{-\alpha(\theta_B/2)^2} = \frac{1}{K}, \qquad \alpha = \frac{4\ln K}{\theta_B{}^2}$$

and

$$\sigma_m{}^2 = \frac{\theta_B{}^4\sigma_n{}^2/P\left[e^{8\ln K(\theta_T-\theta_2/\theta_B)^2} + e^{8\ln K(\theta_T-\theta_1/\theta_B)^2}\right]}{64\theta_S{}^2(\ln K)^2\left[.312\dfrac{\sigma_n{}^2}{P}\left(e^{8\ln K\left(\frac{\theta_T-\theta_2}{\theta_B}\right)^2} + e^{8\ln K\left(\frac{\theta_T-\theta_1}{\theta_B}\right)^2}\right) + 1\right]}. \tag{24}$$

Making the same substitutions,

$$\beta = -.312\theta_T\left(\frac{\sigma_n{}^2}{P}\right)\left[e^{8\ln K(\theta_T-\theta_2/\theta_B)^2} + e^{8\ln K(\theta_T-\theta_1/\theta_B)^2}\right]. \tag{25}$$

Furthermore, from the expression for $\sigma_{\hat{\theta}}$ derived in making the maximum likelihood estimate (Appendix),

$$\lambda/D = \sigma_{\hat{\theta}}\pi\sqrt{2P/\sigma_n{}^2}. \tag{26}$$

Now, combining (23), (24), (25) and (26), the probability of correctly measuring an angle as a function of SNR for a specified accuracy can be found. Choosing a probability of correctly measuring the angle and the corresponding SNR (26) can be used to determine the required wavelength to antenna separation ratio λ/D.

As an example of how this is done, assume that the beamwidth is measured at the 3-db points and that the beams cross over at the 3-db level. These assumptions imply that $K=\sqrt{2}$ and $\theta_S=(\theta_2-\theta_1)=\theta_B$. A further assumption that $P/\sigma_n{}^2\gg 1$ (14 db or more) makes possible valid approximations on $\sigma_M{}^2$ and β which yield an approximate form for (23). That is,

$$P = \text{erf}\left(\frac{\lambda}{\sigma_M D\sqrt{2}}\right). \tag{27}$$

Substituting (24) and (26) into (27) yields

$$P = \text{erf}\left\{(P/\sigma_n{}^2)\left(\frac{\sigma_{\hat{\theta}}}{\theta_B}\right)4\pi\ln 2\left(\frac{\theta_S}{\theta_B}\right)\left[e^{-4\ln 2(\theta_T-\theta_2/\theta_B)} + e^{-4\ln 2(\theta_T-\theta_1/\theta_B)^2}\right]^{-1/2}\right\}.$$

If the target angle $\theta_T=\theta_1$ (which, incidentally, is the worst case from a SNR standpoint),

$$P = \text{erf}\left\{(P/\sigma_n{}^2)\left(\frac{\sigma_{\hat{\theta}}}{\theta_B}\right)\frac{16\pi\ln 2}{\sqrt{17}}\right\}. \tag{28}$$

For a probability of accurate angular measurement of 0.98 ($P=0.98$) and 100 to 1 beam-splitting,

$$P/\sigma_n{}^2 = \frac{165\sqrt{17}}{4\pi\ln 2} = 19\,\text{db}.$$

Having found the necessary parameter values for this case, the wavelength to antenna separation ratio (26) is

$$\lambda/D = 0.0196.$$

A general comparison of the performance of the two systems is shown in Fig. 13. These curves indicate that the one- to ten-fold ambiguity solution is the best from a SNR standpoint. However, the frequency difference required in this case is so large that it becomes impractical. The equivalent three-antenna system would eliminate this problem at the expense of hardware. There is little basis for choosing one of the remaining two systems. The boresight error is still a problem in the amplitude comparison-interferometer system but it is of diminished importance since the required spacing D for this system is a little over one-fourth that of the two-stage interferometer system for a common beamwidth.

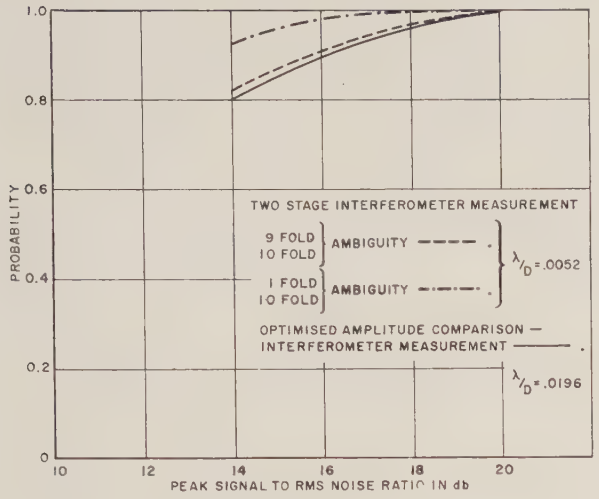

Fig. 13—Probability of measuring angle to within one-hundredth of a beamwidth.

Data Processing for Two-Stage Interferometer

The data processing required to remove the ambiguities associated with a two-stage interferometer system, cascading two maximum likelihood estimates of angle based on phase information alone, would be the following: The phase information due to the path difference at the first frequency is derived by phase detecting an in-phase and quadrature component combined in logic circuitry, in order that a linear output may be obtained between $-\pi$ and π, rather than $-\pi/2$ and $\pi/2$ as obtainable with a conventional phase detector (otherwise, an additional 3-db SNR would be required to resolve ambiguities). This phase information contains all the ambiguities to be resolved. Phase information contained in the returns subjected to a path difference at the second frequency is compared with the first by extracting the phase difference between them. However, this difference does not suffer from multiple ambiguities as it is the difference between a nine- and ten-fold ambiguity parameter and as such lies between $-\pi$ and π. Again, the in-phase and quadrature components have been processed to extend this range unambiguously.

The sequence of operations performed on the data in order that the ambiguities in the system are resolved is contained in the following discussion. First, the unambiguous coarse measurement of angle gained from the phase difference is scaled by 10 and quantized to the nearest π in steps of π from -10π to 10π. Then, after scale adjustment, this quantized analog voltage is added to that representing the phase measurement at the first frequency, being a fine measure of angle with a tenfold ambiguity. The result is that the coarse measurement obtained from the phase difference yields an accurate measure of phase to the nearest π, to which is added the fine interpolation of this π interval to an accuracy determined by the available SNR. Finally, a scale adjustment is performed analog-wise by a secant potentiometer to normalize the resultant voltage, representing phase, to angle about the antenna boresight axis. This scale is $\lambda_1 \sec \phi/2\pi D$, where D is the spacing, λ_1 the wavelength of the first frequency and ϕ the angle between the boresight axis and one normal to the base line.

Fig. 14 shows a block diagram of the steps involved in deriving the final angle using the two-frequency interferometer system.

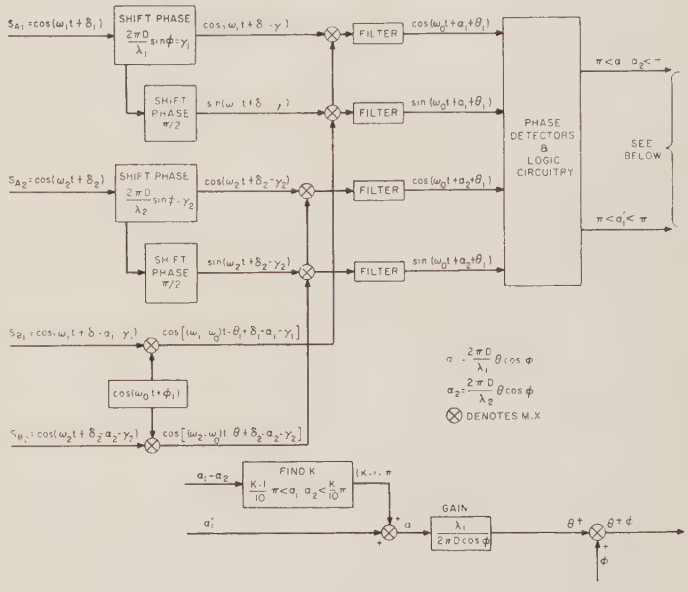

Fig. 14—Data processing in the two-stage interferometer.

Data Processing for Amplitude Comparison-Interferometer

Fig. 15 shows a block diagram of an amplitude comparison-interferometer system including the steps necessary for combining the two outputs in such a way that the final estimated angle $\hat{\theta}_M$ can be determined.

The output of the triangular phase detector will be a voltage proportional to a phase between $-\pi$ and π which represents the phase measurement over one of the theoretical lobe structures of the interferometer pattern. (Again the information is processed so that the phase detector is linear between $-\pi$ and π.)

The voltage output of the difference amplifier is quantized in steps of $\pm 2\pi$ between $-m\pi$ and $m\pi$ where m is the number of ambiguities in the interferometer measurement of angle.

The analog voltage from the phase detector is scaled so that a given level represents the same quantity as that from the difference amplifier. The two quantized outputs can then be added and scaled by the factor $\lambda \sec \phi/2\pi D$ to give the estimated angle θ. In this system, the accuracy also depends upon an accurate knowledge of the beam crossover angle of the amplitude comparison pattern.

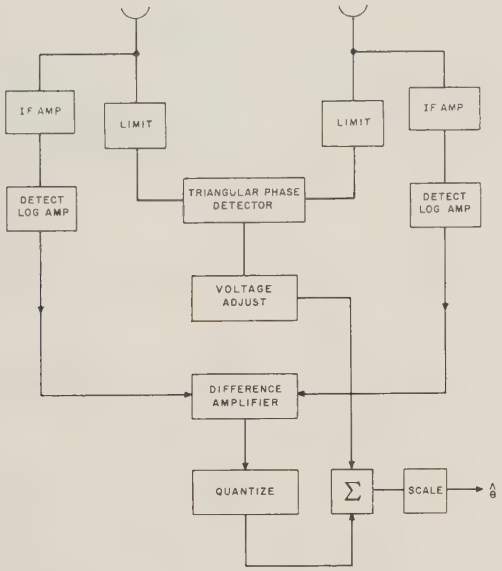

Fig. 15—Data processing in the amplitude comparison-interferometer system.

Appendix

In the following analysis, the method of processing the received information which yields the maximum likelihood estimate of angle using the interferometer technique is determined. In addition, the expression for the minimum SNR for a given angular accuracy is developed. A block diagram of this interferometer system is shown in Fig. 16. The combinations of signal and noise received by the two antennas are,

$$y_1(t) = P_1 \operatorname{Cos}(\omega t + \psi_1) + x_1(t)$$

and

$$y_2(t) = P_2 \operatorname{Cos}(\omega t + \psi_2) + x_2(t), \tag{29}$$

where

$$x_i(t) = x_{ci}(t) \operatorname{Cos} \omega t + x_{si}(t) \operatorname{Sin} \omega t, \qquad i = 1, 2.$$

Although it appears that these expressions for $y_1(t)$ and $y_2(t)$ are not the same as those used in the analysis of the monopulse section, they differ only in form and are otherwise equivalent. From these equations, $y_1(t)$ and $y_2(t)$ can be written,

$$\begin{aligned} y_1(t) &= V_1(t) \operatorname{Cos}[\omega t + \phi_1(t)] \\ y_2(t) &= V_2(t) \operatorname{Cos}[\omega t + \phi_2(t)]. \end{aligned} \tag{30}$$

Passing through the amplitude limiter,

$$y_1(t) = \sqrt{P_1} \operatorname{Cos}[\omega t + \phi_1(t)], \qquad P_1 = \text{signal power.}$$

Davenport and Root [3] show that the conditional probability density is

$$q_1(\phi_1 \mid \psi_1) = \frac{\sqrt{P_1} \operatorname{Cos}(\phi_1 - \psi_1)}{\sigma_n \sqrt{2\pi}} e^{-P_1/2\sigma_n^2 \operatorname{Sin}^2(\phi_1 - \psi_1)} \tag{31}$$

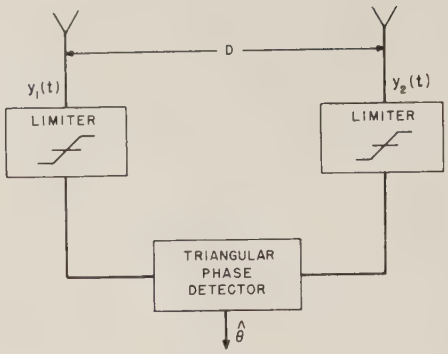

Fig. 16—Block diagram of the maximum likelihood estimator for an interferometer system.

when $\sqrt{P_1} \operatorname{Cos}(\phi_1 - \psi_1) \gg \sigma_n$, which is the case for large SNR's, and $0 \leq \phi_1, \psi_1 \leq 2\pi$. Similarly,

$$q_2(\phi_2 \mid \psi_2) = \frac{\sqrt{P_2} \operatorname{Cos}(\phi_2 - \psi_2)}{\sigma_n \sqrt{2\pi}} e^{-P_2/2\sigma_n^2 \operatorname{Sin}^2(\phi_2 - \psi_2)}. \tag{32}$$

Assuming ϕ_2, ψ_2 independent of ϕ_1, ψ_1 the joint conditional probability density is (likelihood function of Cramer) [4]

$$\begin{aligned} L(\phi_1, \phi_2 \mid \psi_1 - \psi_2 = \alpha) &= q_1(\phi_1 \mid \psi_1) q_2(\phi_2 \mid \psi_2) \\ &= \frac{\sqrt{P_1 P_2}}{\sigma_n^2 \sqrt{2\pi}} \operatorname{Cos}(\phi_1 - \psi_1) \operatorname{Cos}(\phi_2 - \psi_2) \\ &\quad \times e^{-(P_1 \operatorname{Sin}^2(\phi_1 - \psi_1) + P_2 \operatorname{Sin}^2(\phi_2 - \psi_2))/2\sigma_n^2}. \end{aligned} \tag{33}$$

The likelihood function is such that its maximum occurs at the same value of the argument as that of its natural logarithm. Allowing $P_1 = P_2 = P$, taking the natural logarithm and differentiating,

$$\begin{aligned} &\frac{d}{d\alpha} \ln L(\phi_1, \phi_2 \mid \psi_1 - \psi_2 = \alpha) \\ &\quad = \frac{d}{d\alpha} \ln \operatorname{Cos}(\phi_1 - \psi_1) + \frac{d}{d\alpha} \ln \operatorname{Cos}(\phi_2 - \psi_2) \\ &\qquad - \frac{P}{2\sigma_n^2} \frac{d}{d\alpha} [\operatorname{Sin}^2(\phi_1 - \psi_1) + \operatorname{Sin}^2(\phi_2 - \psi_2)] \\ &\quad = \operatorname{Sin}(\phi_1 - \psi_1) - \operatorname{Sin}(\phi_2 - \psi_2) \\ &\qquad - \frac{P}{\sigma_n^2} [-\operatorname{Sin}(\phi_1 - \psi_1) \operatorname{Cos}(\phi_1 - \psi_1) \\ &\qquad\qquad + \operatorname{Sin}(\phi_2 - \psi_2) \operatorname{Cos}(\phi_2 - \psi_2)] \\ &\quad = 0. \end{aligned}$$

This implies that

$$\begin{aligned} &\operatorname{Sin}(\phi_1 - \psi_1)[1 + P/\sigma_n^2 \operatorname{Cos}(\phi_1 - \psi_1)] \\ &\qquad = \operatorname{Sin}(\phi_2 - \psi_2)[1 + P/\sigma_n^2 \operatorname{Cos}(\phi_2 - \psi_2)], \end{aligned}$$

and for $P/\sigma_n^2 \gg 1$

$$\tfrac{1}{2}\,\mathrm{Sin}\,2(\phi_1-\psi_1) \approx \tfrac{1}{2}\,\mathrm{Sin}\,2(\phi_2-\psi_2),$$

hence, the estimated value for alpha, $\alpha=\psi_1-\psi_2$, is

$$\hat{\alpha} = \hat{\psi}_1 - \hat{\psi}_2 = \phi_1 - \phi_2$$

which indicates that phase-detecting yields the maximum likelihood estimate.

Now, the average value of $\hat{\alpha}$ is

$$\begin{aligned}
E_\alpha(\hat{\alpha}) &= E_\alpha(\phi_1-\phi_2)\\
&= \int_0^{2\pi}\int_0^{2\pi}(\phi_1-\phi_2)L(\phi_1,\phi_2\,|\,\alpha)\,d\phi_1 d\phi_2\\
&= \frac{P}{2\pi\sigma_n^2}\int_0^{2\pi}\int_0^{2\pi}(\phi_1-\phi_2)\,\mathrm{Cos}\,(\phi_1-\psi_1)\,\mathrm{Cos}\,(\phi_2-\psi_2)\\
&\quad\times e^{-P/2\sigma_n^2\,\mathrm{Sin}^2\,(\phi_1-\psi_1)}e^{-P/2\sigma_n^2\,\mathrm{Sin}^2\,(\phi_2-\psi_2)}d\phi_1 d\phi_2\\
&= \sqrt{\frac{P}{2\pi\sigma_n^2}}\cdot\left\{\int_0^{2\pi}\phi_1\,\mathrm{Cos}\,(\phi_1-\psi_1)e^{-P/2\sigma_n^2\,\mathrm{Sin}^2\,(\phi_1-\psi_1)}d\phi_1\right.\\
&\quad\left.-\int_0^{2\pi}\phi_2\,\mathrm{Cos}\,(\phi_2-\psi_2)e^{-P/2\sigma_n^2\,\mathrm{Sin}^2\,(\phi_2-\psi_2)}d\phi_2\right\}.
\end{aligned}$$

Using the approximations, $\phi_1-\psi_1=x$, $\phi_2-\psi_2=y\ll 1$ and $P/\sigma_n^2\gg 1$,

$$\begin{aligned}
E_\alpha(\hat{\alpha}) &\approx \sqrt{\frac{P}{2\pi\sigma_n^2}}\left\{\int_{-\infty}^{\infty}(x+\psi_1)e^{-P/2\sigma_n^2x^2}dx\right.\\
&\qquad\left.-\int_{-\infty}^{\infty}(y+\psi_2)e^{-P/2\sigma_n^2y^2}dy\right\}\\
&= \psi_1-\psi_2.
\end{aligned}$$

Also,

$$\begin{aligned}
E_\alpha\{[\phi_1-\phi_2-E_\alpha(\hat{\alpha})]^2\} &= \sigma_\alpha^2(\hat{\alpha})\\
&= \overline{(\phi_1-\phi_2)^2}-(\psi_1-\psi_2)^2\\
E_\alpha[(\phi_1-\phi_2)^2] &= E_\alpha(\phi_1^2+\phi_2^2)-2\psi_1\psi_2.
\end{aligned}$$

If $\phi_1-\psi_1=x$, $\phi_2-\psi_2=y\ll 1$ and $P/\sigma_n^2\gg 1$,

$$\begin{aligned}
E_\alpha(\phi_1^2+\phi_2^2) &\approx \sqrt{\frac{P}{2\pi\sigma_n^2}}\\
&\quad\cdot\left\{\int_{-\infty}^{\infty}(x^2+2x\psi_1+\psi_1^2)e^{-P/2\sigma_n^2x^2}dx\right.\\
&\quad\left.-\int_{-\infty}^{\infty}(y^2+2y\psi_2+\psi_2^2)e^{-P/2\sigma_n^2y^2}dy\right\}\\
&= \frac{2\sigma_n^2}{P}+\psi_1^2+\psi_2^2. \qquad (34)
\end{aligned}$$

Finally,

$$\begin{aligned}
E_\alpha\{[\phi_1-\phi_2-E_\alpha(\hat{\alpha})]^2\}&\\
&\approx \frac{2\sigma_n^2}{P}+\psi_1^2+\psi_2^2-2\psi_1\psi_2-(\psi_1-\psi_2)^2\\
&= \sigma_\alpha^2(\hat{\alpha}) = \frac{2\sigma_n^2}{P} \quad\text{and}\quad \sigma_\alpha(\hat{\alpha}) = \sqrt{\frac{2\sigma_n^2}{P}}.
\end{aligned}$$

Since angle is related to phase by the factor $2\pi D/\lambda$,

$$\begin{aligned}
\sigma_{\hat{\theta}} &\approx \sigma_\alpha(\hat{\alpha})\,\frac{\lambda}{2\pi D}\\
&= \frac{\lambda}{\pi D\sqrt{2P/\sigma_n^2}}. \qquad (35)
\end{aligned}$$

Bibliography

[1] R. Manasse, "Maximum angular accuracy of tracking a radio star by lobe comparison," IRE Trans. on Antennas and Propagation, vol. AP-8, pp. 50–56; January, 1960.

[2] R. A. Enstrom, "The effects of noise on stacked beam height finding radars," *Proc. Conf. on Military Electronics*, Washington, D. C.; June 29–July 1, 1959.

[3] W. B. Davenport, and W. L. Root, "Random Signals and Noise," McGraw-Hill Book Co., Inc., New York, N. Y.; 1958.

[4] H. Cramér, "Mathematical Methods of Statistics," Princeton University Press, Princeton, N. J.; 1946.

[5] M. I. Skolnik, "Theoretical accuracy of radar measurements," IRE Trans. on Aeronautical and Navigational Electronics, vol. ANE-7, pp. 123–129; December, 1960.

[6] P. Swerling, "Maximum angular accuracy of a pulsed search radar," Proc. IRE, vol. 44, pp. 1146–1154; September, 1956.

[7] C. A. Schroeder, "Electronic interferometer tracking," 1960 *Proc. 5th Natl. Symp. on Space Electronics and Telemetry.*

[8] W. N. Christiansen, *et al.*, "The cross-grating interferometer—a new high resolution radio telescope," *Proc. IEE*, vol. 108, pp. 48–58; January, 1961.

An Automatic TV Tracking Theodolite for Range Instrumentation*

ROBERT E. WISNIEFF†

Summary—The factors affecting the design of a gated Automatic TV Tracking System are discussed, and a system mechanization to achieve the design objectives is outlined. Only the composite video of a closed-circuit TV system is required as an input. A study of the dynamic performance of typical targets indicates that the unpredictable target motion in a frame period of 1/30 sec must be an extremely small fraction of the field of view required for initial target acquisition. This permits the use of a small tracking gate in the larger acquisition field, since the target coordinates of the previous frame may be used to position the gate. This small gate permits a signal-to-noise enhancement and effectively rejects extraneous targets outside the tracking gate.

The tracking is effected by subdividing the tracking area into equal early and late video gates in each coordinate. The differential video between these gates is applied to an electronic integrator in such a manner that the integrator output voltage, which is also the reference for the generation of the early-to-late gate transition, changes to place this gate transition on the target. The integrator voltages are, therefore, a measure of the target coordinates in the TV field.

The operation of an experimental system fabricated to determine the feasibility of applying this technique to a range-instrumentation system has produced tracking accuracies of better than 0.05 milliradian in an acquisition field of 10×10 milliradians. Current developments and additional applications of the technique are discussed briefly.

Introduction

During the past decade, television techniques have found increasing acceptance in range-instrumentation systems. Initially, the technique was used to relay a scene to a control console, permitting an operator to command an operation at a distant, inaccessible or high-hazard area. By the addition of a photographic or video tape recorder, a permanent record of the event may be obtained. The television transducer has the property of transforming a scene into an electrical signal. It is the purpose of this paper to outline the means whereby this electrical signal may be employed to provide tracking data for a selected object within the field of view.

Since the TV sensor responds to visible wavelengths, extreme accuracies may be achieved without wavelength limitations. Being a passive system, its response depends on the size and visible contrast of the target relative to the field and is independent of range. With these features, a single optical system devoid of mechanically-scanned elements may be used to provide tracking information, a remote visual display of the target area, and a permanent record of the entire operation. The single optical system and transducer eliminate all possible sources of boresight error which may become a limiting factor in a multimode, high-precision tracking system.

* Received by the PGMIL, June 5, 1961.

† Tracking and Detection Sect., Television and Infrared Branch, Norden Div., United Aircraft Corp., Norwalk, Conn.

Target and Servo Performance Effects

In a typical range installation, the tracking stations are located a mile or more from the targets to be tracked. Tracking accuracy should be limited by the angle sensors of the tracking platform and the random fluctuations in the atmosphere between the tracking station and the target. These considerations indicate that a tracking-error detector should be capable of sensing errors of less than one minute of arc. Examples of the visible targets to be tracked would be the contrast of a missile or aircraft body against a sky background, the plume radiation from a rocket during boost phase, or a satellite reflecting solar radiation. The system must, therefore, be capable of tracking targets that may be either brighter or darker than the background.

An important factor in the design of a tracking system is the dynamics of the object to be tracked. Since the follow-up servo system may be provided with velocity memory, the important quantity in the tracker performance is the vehicle acceleration. With normal RETMA scanning rates, the frame period is 1/30 sec. For a vehicle subjected to 30 g, the displacement resulting from this acceleration in a frame period, as given by

$$S = 1/2at^2, \tag{1}$$

is approximately $\frac{1}{2}$ ft. At a one-mile viewing distance, this represents a displacement of about one-tenth of a milliradian or 20 seconds of arc.

The field of view of the system should not be limited by the target dynamics for several reasons, the most important of which is target acquisition. The operator must be provided with a field sufficiently large that he can recognize known objects and, thus, initially orient the system on the target to be tracked. About $\frac{1}{2}°$ field coverage is a reasonable minimum field for aircraft or missile test ranges. Other contributing factors are the thermal effects on atmospheric refraction and the accuracy of the positioning servos. In any event, the relative displacement of the target between two adjacent TV frames will be an extremely small fraction of the required field coverage.

For viewing a distant object, such as a satellite, a much smaller field may be employed. Fields of view of one or two minutes are appropriate for this application. In this case, the unpredictable target motion in one frame period is still a small fraction of the total field of view.

The task of the TV tracking system is to sense displacements of a target in the order of a few per cent of the field of view in a frame period. If the error sensor is linear over the entire field of view, then the target co-

ordinates may be determined by the vector sum of the base-mount readings of the center of the field of view and the target displacement relative to the field center as determined by the tracking system. The base-mount servo performance, with respect to static and dynamic errors, may be relaxed by an order of magnitude because of the highly accurate target coordinate data obtained within the field.

Signal to Noise

Since the television video signal is generated by a sequential scanning of the transducer mosaic, the video signal may be considered as a series of pulses of variable amplitude but constant width equal to the period of one horizontal resolution element τ. This period is determined primarily by the upper-band limit of the video amplifier.

The lower-band limit of the video amplifier is chosen below the field repetition frequency of 60 cps and is, therefore, sufficiently below the upper-band limit (equal to approximately 5 Mc for $\tau = 0.1$ μsec) that it may be considered as a low-pass amplifier. The noise in the output of the video amplifier will then be a series of pulses of duration τ having random amplitude and occurrence. Noise pulses shorter than τ cannot exist because of the upper-band limit of the amplifier. Pulses wider than τ may be synthesized as a series of pulses of width τ. Consider the output of the TV sensor to be a white-noise source, and let the noise output of the video amplifier be normalized to a one-volt rms amplitude. In a time interval T the number of pulses N, of width τ exceeding a given amplitude b will be given by

$$N = \frac{T}{\tau}\left[1 - \sqrt{\frac{2}{\pi}}\int_0^b e^{-Y^2/2}dy\right].$$

Consider a TV system with 500-line resolution in each coordinate, and let $\tau = 0.1$ μsec. Then $T = (500)^2 (10^{-7}) = 25\times10^{-3}$ sec. For a 30-frame-per-sec system, a frame period of 33.3×10^{-3} sec is indicated. The difference may be attributed to the horizontal and vertical retrace time during which both the signal and noise are blanked. Therefore, the active scanning period per frame is approximately 25×10^{-3} sec. In Table I, column 1, is recorded the level b relative to an rms noise output of one volt. In column 2 the number of noise pulses N that exceed the level b in one active frame period (25×10^{-3} sec) is recorded. It will be observed that the number of noise pulses exceeding a given level falls rapidly as the level is increased. Clearly, the noise pulses will set the lower signal limit that may be tracked. If the number of noise pulses above a threshold level greatly exceeds the number of signal pulses in each frame, the signal pulses will have a secondary effect on the tracking circuits, and many frames will be required before the presence of the signal may be detected.

The objective of the tracking system is to obtain accurate tracking data with the lowest possible SNR. The system must, therefore, be designed to maximize the ratio of the number of signal pulses to the number of noise pulses of equal or greater amplitude. Noise of appreciably smaller amplitude than the signal may be rejected by an amplitude-discriminating device such as an automatic gain control amplifier.

TABLE I

Column	1	2	3
Item	level b relative to 1 volt rms output signal	number of noise pulse exceeding level b in one frame period $T=25\times10^{-3}$ sec $\tau=0.1$ μsec	number of pulses exceeding level b in area of $\frac{1}{10}\times\frac{1}{10}$ of entire frame $T=25\times10^{-5}$ sec $\tau=0.1$ μsec
	0	25×10^4	25×10^2
	1	7.9×10^4	7.9×10^2
	2	1.14×10^4	114
	3	675	6.75
	4	16	0.16
	5	0.14	1.4×10^{-3}
	6	10^{-3}	10^{-5}
	7	10^{-6}	10^{-8}

The first thought of a signal-enhancement technique might be to increase the size of the target on the sensor photocathode and, thus, increase the number of signal pulses. If this is accomplished by increasing focal length of the optical system, then the number of signal elements will increase as the square of the focal length. However, if the aperture is held constant, the energy density at the photocathode (and hence the SNR for a linear transducer) will decrease as the inverse square of the focal length. From Table I, it is obvious that the number of noise pulses per frame increases at a much greater rate than the inverse square of the level. Hence, for constant aperture, the ratio of signal pulses to noise pulses of equal or greater amplitude will decrease with an increase in image size. This leads to the conclusion that a maximum ratio of signal to noise pulses will occur when the target energy is concentrated on a single resolution element of the sensor. This conclusion applies only for low-signal amplitudes where a significant number of noise pulses of equal or greater amplitude appear in a frame. For stronger signals, a larger-area target will effect significant improvement in tracking performance.

It can be seen from (2) that a vast improvement in SNR could be obtained if the active scanning time T per frame could be reduced. Recall that the target will only move a few per cent of the total field between adjacent frames. This implies that the knowledge of the target location from the previous frame may be used to specify the coordinates of a small area of the total field in which the target will appear on the next frame.

For example, in many cases it is possible to predict the target location to within 10 per cent of the total field in each direction. If a gate is placed around the initial target location extending to 10 per cent of the total field in the direction of each coordinate, the remainder of the video information in each frame may be removed from the signal delivered to the tracking data-processing circuits. In effect, the active frame time T in (2) is reduced by a factor of 100, and the number of noise pulses of a given level appearing within the gated area is reduced by the same ratio. This is recorded in column 3 of Table I. Consider a target equal in size to a single-resolution element and having a peak signal equal to four times the rms noise. From Table I column 2 it can be seen that there would be 16 noise pulses of equal or greater amplitude per total active frame. A tracking system would, therefore, require several frames of correlation to determine which of the seventeen pulses (16 noise+1 signal) is the target pulse. If the tracking video is confined to a gated area as outlined above, we note from column 3 that a noise pulse equal to or greater than the target pulse will occur only once in every six frames.

The gating of the field has another important effect on signal enhancement. In many applications, the field of view may contain targets other than the one being tracked. The presence of these targets in the tracking field of view will disturb the tracking, frequently making it impossible. The gating technique permits complete rejection of signals outside the gated area and yet retains them within the view of the operator so that potential sources of tracking interference may be noted and appropriate action (reduction of gate size, manual guidance in the event of target crossing, etc.) may be taken. The gating technique, therefore, will permit tracking a single aircraft in a formation or the main missile body after booster separation.

It remains, therefore, to instrument a gated tracking system in which the center of the gate is always maintained on the target coordinate of the previous frame.

System Mechanization

The design objectives of the TV tracking system are to generate the two coordinate tracking data from the signal available in the composite video of a closed circuit TV chain. The components of the complete TV system would then be

1) A conventional television camera (vidicon or image orthicon sensor) that produces the composite video.
2) A data-processing system that converts the video signal to the real time two coordinate tracking voltages, which are proportional to the displacement of the target from the boresight axis of the TV camera.
3) A visual monitor that displays the TV field with an open-center reticle surrounding the target being tracked.
4) A photographic monitor or video tape recorder that provides a permanent record of the scene and automatic TV tracker performance.

The novel component of the system is the data-processing unit, which produces the two coordinate tracking information. Fig. 1 is a block diagram of these circuits. The method of generating the analog voltages proportional to the two coordinate target displacement is based upon the use of comparison-tracking gates. The use of these gates not only permits the signal-to-noise enhancement and extraneous target discrimination effects previously discussed, but also insures that the proportionality of the signal output will be determined solely by the linearity of the sweep generators and be independent of target size or signal strength.

The horizontal and vertical synchronizing pulses are separated from the composite video in a conventional separator circuit. These pulses synchronize linear horizontal and vertical sawtooth generators. Equal early and late gates are generated in each channel by comparators operating on the sweep generators. The reference for the center of these gates is determined from the best knowledge of target coordinates. In acquisition, this voltage is manually controlled by the operator from observation of the display. During automatic tracking, this reference is provided by the tracker output from the previous frame. The size of the gates is set manually from knowledge of target size and anticipated dynamic performance. These gating circuits divide the target video between early and late gates in the horizontal and vertical scan directions. The respective early- and late-gated video signals in each direction are supplied to the inputs of difference amplifiers. The output of each difference amplifier is delivered to an electronic integrating network with polarity such that the integrator outputs will be modified for target motion in the frame period. The integrator outputs after amplification are then a measure in both polarity and

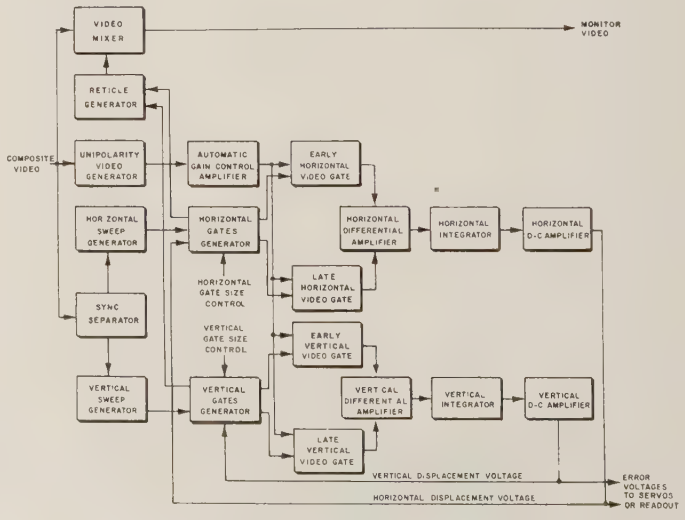

Fig. 1—Data-processing unit, block diagram.

magnitude of the horizontal and vertical target displacements. These voltages are fed back to the gate generation circuits to reflect changes in the best knowledge of target coordinates in the frame.

To assure that the system will be capable of tracking targets of positive, negative, or mixed contrast (with respect to the background), a diode bridge is included to convert any departure from the background video level to a unipolarity signal for delivery to the video-comparison circuits.

In order to compensate for variations in target aspect and contrast, the video delivered to the comparison circuitry is processed by an automatic gain control amplifier which maintains the target at a constant standarized amplitude. Circuitry is also provided to prevent operation of the video-comparison circuits whenever the received target signal falls below a reliable level. This successfully prevents false information from being produced.

The gates generator also provides the necessary signals to generate an electronic reticle on the TV monitor. The result on the monitor is an open crosshair centered on the tracking-gate position which, under proper operation, is centered on the target. The gate size may be restricted by manual control to enhance the SNR and to increase the usefulness of the equipment when looking at areas containing false or undesired targets.

The design of the circuits to accomplish the functions outlined above follows well-known techniques of pulse- and video-circuit design and need not be discussed in detail.

The gated tracking system combines the advantages of a large-field-acquisition viewing device with the performance of a small-field-of-view tracking system. It is interesting to compare its performance with that of a unit employing separate acquisition and tracking transducers.

In the system employing separate transducers, the maximum static and dynamic errors tolerable in the servo system are set by the small field of view of the tracking sensor. In the gated TV-tracking system, the servo performance is set by the large acquisition field, since the gates are free to move to any position within the larger area. In the separate acquisition-track system, the field of the tracking system is fixed by the original design and cannot be readily changed to accommodate a different target size or changes in dynamic performance. In the gated system, the tracking field may be readily adjusted to suit the particular problem at hand. Indeed, it is possible to vary the gate size during a tracking run in order to obtain maximum performance at all points on the trajectory. For example, a missile at launch being viewed from a nearby tracking station may require a large field of view. As the missile range increases, the target becomes smaller and the signal weaker. Reducing the tracker field of view will, then, enhance the SNR for accurate tracking in midcourse.

In multimode tracking systems of extreme accuracy, alignment errors of the various systems can be appreciable. Also, careful alignment at one point may be disturbed when the mount is shifted and the mass distribution changed or when the systems are subject to dynamic forces. In the gated TV-tracking system, a single optical system and transducer are used so that boresight errors are eliminated. In addition, the obvious optical system simplicity and the need for only one sensor results in appreciable reduction in over-all system complexity, even though the tracking data reduction may be somewhat more complex than for a separate single-element tracking system.

Applications

In order to test the feasibility of the concepts outlined above, experimental equipment was fabricated for use in the range-instrumentation system at Eglin Air Force Base under contract AFO8(603)-4574. The design objective of the equipment, known as Tracking Error Measuring Device, was to provide real time readout of the tracking error of a Contraves Cinetheodolite tracking system. This equipment consisted of a Zoomar "Reflectar 40" optical system with a vidicon TV camera rigidly attached to the optics barrel of the manually operated theodolite. The data processing was accomplished in a remotely located instrument console shown in Fig. 2. Since the equipment did not control the tracking servos directly, two output terminals were provided to monitor the output voltages. These voltages were analogs of the azimuth and elevation displacement of the target from the center of the TV field, which was aligned with the boresight axis of the Cinetheodolite. In addition, a special photographic monitor and recording camera were provided within the console to provide a permanent record of the sys-

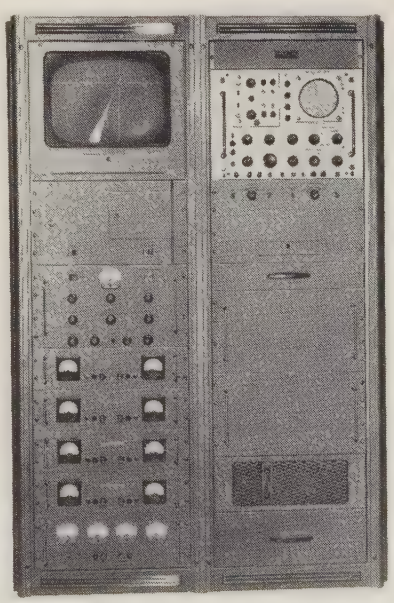

Fig. 2—Tracking-error measuring device console.

tem operation. The field of view of the equipment was 10×10 milliradians. Reproducible error readout was obtained to better than 0.05 milliradian or approximately 10 seconds of arc. Under dynamic operation, the chief contributing source of error was the distortion of relative line of sight between the theodolite and TV optics. Future plans for this program provide for the use of the main theodolite optics for the TV system to eliminate this source of error.

A second system is currently under development for the White Sands Missile Range under Contract DA-36-039 SC-87146. In this system, the camera and optical system are mounted on, and boresighted with, an AN/FPS-16 range-tracking radar. The two coordinate tracking data are then reduced to a form compatible with the radar-tracking servos. The TV-tracking information will be used when the radar system is incapable of operation as, for example, in the initial acquisition of a missile when the radar signal is lost in ground clutter but the visible signal from the booster plume may be clearly discerned. It is anticipated that this system will also be capable of operation during midcourse, since the experience with the Eglin Air Force system indicates tracking capability with contrast ratios as low as 10 per cent.

In general, the system may be applied to any tracking problem where a visible signal can be reduced to TV video information. The technique may be directly applied to the tracking of satellites illuminated by solar radiation. Other applications would include passive fire control in land-based, shipboard or airborne applications. To date, no effort has been made to miniaturize the data processing circuits, although it appears entirely possible to package a miniaturized version of these circuits in a 250 cubic inch package with a weight of approximately 6 pounds and a power consumption of 30 watts.

Acknowledgment

The author is indebted to many co-workers at Norden for assistance in the system development program and to D. Edwards of Eglin Air Force Base, and H. Lambeth of White Sands Missile Range, for their helpful suggestions and comments.

The Future of Pulse Radar for Missile and Space Range Instrumentation*

DAVID K. BARTON†, SENIOR MEMBER, IRE

Summary—An account of instrumentation radar development is given, and advantages and disadvantages of radar as compared to other instruments are discussed. Capabilities of present monopulse radars are described, based upon actual test data from the AN/FPS-16. This radar has a range of 200 miles on echo targets of one-square-meter cross section and can track to an accuracy of 0.1 mil in angle and 5 yards in range. The next generation in instrumentation radar is represented by the AN/FPQ-6, now under development, which will extend accurate tracking to ranges in excess of 500 miles on echo targets and will track existing beacons beyond the moon. An important capability not yet exploited in pulsed-instrumentation radars is the coherent pulsed-Doppler velocity-measurement channel which will equal the accuracy of microwave CW systems in radial-velocity data. Provisions for adding this fourth tracking channel to both AN/FPS-16 and AN/FPQ-6 are being made, and suitable beacons are being designed. An important advantage of pulsed-Doppler radar is the ability to share a single coherent beacon in multiple-station operation, providing highly accurate, three-coordinate velocity and position data without special interstation communication links over ground paths.

Beyond the immediate developments of the AN/FPQ-6, there are three major areas of improvement which will greatly extend radar performance. Solid-state maser preamplifiers will increase sensitivity of microwave radars by a factor of nearly one hundred within one or two years. Microwave antennas are already under construction in the 100- and 300-ft diameter class. Multiple-tube transmitters will make available ten to one hundred times the presently used average power, and signal-processing techniques are available to code the transmissions for accurate measurement of range and velocity. As a result of these developments, the improvement in radar performance should proceed at a more rapid pace even than that of the past ten years.

The unique ability of radar in acquiring and tracking uncooperative objects has been appreciated for some years, and examples of actual tracks are presented to show some of the interesting data which can be extracted from satellite echo signals.

* Received by the PGMIL, June 2, 1961.

† RCA Missile and Surface Radar Dept., Moorestown, N. J. Development and production of the AN/FPS-16 was carried out under cognizance of the Navy Dept. on Contracts NOas-55-869c and NOas-56-1026d. The AN/FPQ-6 and AN/TPQ-18 are currently being developed under cognizance of the Navy Bureau of Weapons, Contract NOw-61-0428.

I. Background and Status of Instrumentation Radar

THE future needs of space-range instrumentation will be filled by evolution of present missile-instrumentation systems and by introduction of new equipment and techniques made possible by the many scientific programs in the areas of radar, communications and astronomy. Pulsed-tracking radar instruments can be expected to play a major role in future systems, just as they have in the past. Before discussing the lines along which instrumentation radar evolution is taking place, it is appropriate to review briefly the history of present radar systems, and establish the status and capabilities of the equipment now in use.

Early U. S. Systems

The development of high-altitude research rockets and guided missiles in the United States brought together instrumentation methods from many fields. From the aircraft test field came internal instrumentation, radio telemetry and recording devices. Anti-aircraft artillery evaluation has made extensive use of theodolites, and these were brought to bear on missiles in the earliest stages of development. Various fixed-camera methods were derived from other ordnance projects as well as from the field of astronomy, which also contributed the long focal-length telescope. Electronic instrumentation came from the fields of navigation, direction finding, fire control, close-support bombing, and from specialized methods such as the Doppler radio techniques used by the Germans in the V-2 program. Since the program got under way toward the end of World War II, it was logical that military equipment, surplus and captured, would play a significant role, and this was certainly true in the case of radar equipment.

The SCR-584 Radar

One radar in particular, the SCR-584, proved particularly valuable to the test ranges and has maintained its usefulness to this day. The primary reasons for this were its availability (some fifteen-hundred sets had been built by the end of the war), reliability (a tremendous production and field engineering effort had followed the original MIT Radiation Laboratory development work), and flexibility. Designed for control of 90-mm AA guns and similar weapons, the SCR-584 was equipped with alternate forms of data output, an oversized modulator and power supply, and ample space for additions and modifications that proved necessary. Furthermore, development of instantaneous electronic-plotting boards (operating in rectangular coordinates) had already been carried out for use in close-support bombing and in mortar location. Transponder beacons were also available from the close-support bombing program, as was a standard radar modification for long-range tracking of beacons. Thus, the SCR-584 was ready for the earliest V-2 and Wac Corporal firings at the White Sands Proving Ground and was in use at other rocket ranges. Along with the radar, of course, there were used the famous German Askania theodolite, Bowen-Knapp fixed cameras, and Doppler radio system.

Modifications and Refinements

The flexibility of the original SCR-584 has already been mentioned. Dozens of important field modifications were made in order to incorporate design advances to this radar at various times in the range instrumentation programs. These were concerned primarily with extending the range of tracking and range rates, synchronizing adjacent radars for reliability of operation without interference, recording of position and signal-strength data and providing control links to the missile through modulation of radar pulse rate or pulse code. Ultimately these and other improvements were incorporated through factory modification in the AN/MPQ-12 radar, which first became available in 1949, and in the improved AN/MPQ-18, which followed the MPQ-12 in design and has been operational since late 1954. These radars have been used primarily at the White Sands Missile Range, but similar modifications have been applied to the SCR-584 for use at the Pacific Missile Range, NOTS (China Lake), the Atlantic Missile Range, Edwards Air Force Base, and the Gulf Test Range. Other nomenclature applied to modified SCR-584 radars includes AN/MPG-2 (referring to an *X*-band set using the MC607 kit on a standard SCR-584), tracking radar Mod II (similar to the MPQ-18), and AN/MPS-25 (a *C*-band version used at the Pacific Missile Range). In each case the basic SCR-584 pedestal, modulator and power supply, and 30-cycle conical scan is employed, while most other major components have been replaced or extensively modified. In some cases, the cost of modification has run to two or three times the original cost of the radar.

Parallel to evolution of improved radars has been a great effort in system design, involving chain radar operation, real-time computing, plotting and data transmission, precision data recorders, communications systems, transponder beacons, and control and telemetry equipment The effect of this effort, which will not be described in detail here, has been to provide further uses for radar data and to keep a continuing pressure towards development of radars with greater precision and range, so that significant data can be supplied to the instrumentation system as a whole.

The AN/FPS-16 Instrumentation Radar

By 1953, military development programs had made possible the design of highly precise tracking radars using the "monopulse" method [1], with adequate range and accuracy to serve as primary missile-range instrumentation. Development of such radars was carried out on a triservice program under cognizance of the Navy Bureau of Aeronautics. The first experimental model, designated AN/FPS-16 (XN-1), was completed

and tested by June, 1956, and installed early in 1957 at Patrick Air Force Base for use on various missile and satellite programs. This model (see Fig. 1) was housed in a trailer, with the antenna on a solid base nearby. A second model, designated AN/FPS-16 (XN-2), was built as a fixed-station radar and served as a prototype for subsequent production of 46 sets for use in all parts of the world. The XN-2 equipment (Fig. 2) was installed at Grand Bahama Island in June, 1957, and has served since that date in support of all test programs at the Atlantic Missile Range. The distribution of production models of the AN/FPS-16 is shown in Fig. 3. Major characteristics of the radar already described in the literature [2] are repeated in the Appendix for reference.

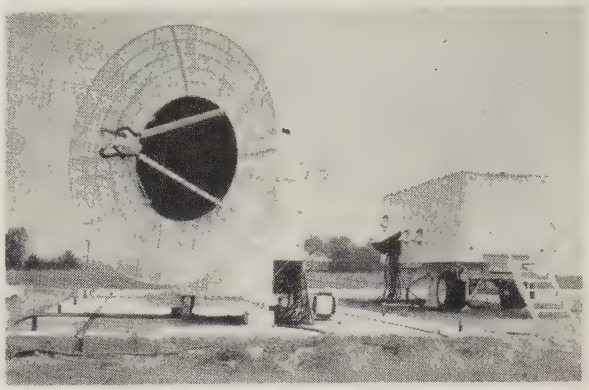

Fig. 1—Instrumentation radar AN/FPS-16 (XN-1).

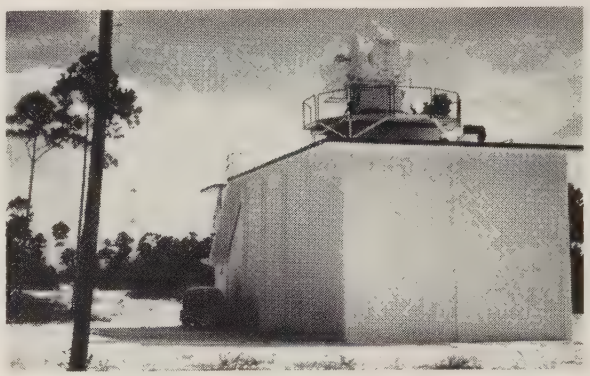

Fig. 2—Radar set AN/FPS-16 (XN-2) at Grand Bahama Island.

Fig. 3—Location of AN/FPS-16 instrumentation radars.

AN/FPS-16 Modifications

As with the venerable SCR-584, the new AN/FPS-16 has been modified successively to increase its range, accuracy and adaptability to new requirements. Some of the major modifications will be listed here to indicate the current status of different versions of the radar.

1) *AN/FPS-16 (XN-3).* A fairly extensive modification program was initiated by the Signal Corps soon after the AN/FPS-16 program began. The changes involved the use of a 3-Mw tunable klystron to replace the original magnetron transmitter, addition of a circularly-polarized mode of operation to supplement linear polarization in beacon tracking, replacement of the boresight camera with a closed-loop TV system, and inclusion of a data corrector to overcome mechanical limitations of the antenna pedestal and extend the bandwidth of the data system to 20 cps. The XN-3 radar remains in operation at Moorestown, N. J., as a base for further modifications, and three field radars, designated AN/FPS-16 A-X, are operating at the White Sands Missile Range. The circular polarizer and data correction provisions have also been applied to several PMR and AMR radars.

2) *Range System Modifications.* Field modifications to provide continuous tracking to 500 miles have been installed in several radars, and such trackers are standard equipment on the later production sets. In addition, a digital range tracker with a 5000-mile range and provision for automatic resolution of 500-mile ambiguities has been developed and installed in five radars. The digital range tracker makes possible the acquisition of beacon-equipped satellites and missiles as soon as they rise above the horizon, and provides for continuous tracking as long as the target stays within line-of-sight range. Tracking can proceed without interruption beyond 5000 miles, on strong enough signals, with ambiguities at intervals of 8192 miles.

3) *16-ft Reflector.* Using the original pedestal, the reflector size has been increased from 12 to 16 ft on five radars, and the 16-ft reflector is standard on late production units.

4) *AN/MPS-25.* A new trailerized model of the radar, using the same basic circuits as the AN/FPS-16, has been built, and seven units are in use.

5) *Acquisition Console.* Added acquisition displays and controls have been placed in eleven sets, primarily to assure rapid acquisition on programs such as Mercury.

6) *Improved Receivers.* Improved crystal mixers giving a 7-db system noise figure and parametric amplifiers giving 4–5 db have been developed for use with the various models of the AN/FPS-16 radar.

Although the possibilities of further piecemeal modification of the AN/FPS-16 are far from exhausted, a program for a major step forward in an integrated design was undertaken late in 1960. This program calls for

combining the major modifications developed for the AN/FPS-16 with a newly-developed antenna and pedestal, to produce both fixed-station equipment (AN/FPQ-6) and transportable units (AN/TPQ-18). These developments will be discussed more fully in a later portion of this paper.

Advantages and Disadvantages of the Pulsed Radar Method

Pulsed tracking radars, starting with the SCR-584 and proceeding through AN/FPS-16 to AN/FPQ-6, have been adopted as standard instrumentation on all the world's missile ranges. The reasons for this choice, along with some of the negative factors to be overcome, can be discussed in a general way here. The principal advantages of the radar method are as follows:

1) Complete data are obtained at a single station.
2) Data are available in electrical form.
3) Reduction of data to rectangular coordinates (or other three-coordinate system) is simple.
4) As a result of 2) and 3), very rapid data processing is possible with small-analog computers, and real-time reduction of precise data is feasible with large-scale digital machines.
5) Operation is possible in all weather conditions.
6) Operation is possible either by reflection from a noncooperating target, or by use of a transponder carried by the target. In the latter case, range is usually limited only by line-of-sight.
7) Interference and multipath propagation troubles are minimized by the narrow angular beam and the narrow range tracking gate.
8) The measured coordinates always intersect at right angles, minimizing geometrical dilution of precision as found in triangulation and base-line systems.
9) Ionospheric effects are negligible if frequencies above 3000 Mc are used.
10) Measurements do not depend upon availability of continuous past history of the trajectory, as with CW Doppler systems.
11) Control and telemetry channels are available when a transponder is used.
12) Reliable equipment is available in production quantities with a high degree of standardization.
13) The radar can be operated and maintained by as few as two men, and maintenance personnel are available from both commercial and military organizations. Manpower required for data transmission and processing is also reduced to a minimum.

Chief limitations of radar methods as currently used are as follows:

1) The radar may be a large, complex and rather expensive instrument.
2) Mechanical error in the antenna pedestal and noise in the tracking servo loop must be contended with.
3) Power consumption of the radar is relatively high.
4) Velocity is generally obtained from differentiated position measurements, with resulting errors depending on smoothing.
5) Tropospheric refraction introduces error in the radar measurement.
6) Tropospheric attenuation is present at the higher radar frequencies.
7) No information is normally obtained on target aspect (attitude).
8) Tracking at low altitudes is affected by ground-clutter reflection in the antenna beam and sidelobes, and line-of-sight limitations apply.

In many cases, these limitations may be overcome by improved siting, operational procedures, or refinements in design, as will be discussed later. Many of the above limitations also apply with equal or greater force to instrumentation systems other than radar.

Performance of Monopulse Radars

The post-war development of monopulse tracking radars has led to a number of highly-refined types of equipment, used in both tactical and instrumentation systems. The AN/FPS-16 is in many ways typical of all such radars, and since it is an unclassified equipment, as well as the only such radar designed specifically for range instrumentation, its performance will be discussed here as indicating the current capability of field radar equipment. In a later section, some of the experimental advances leading to much longer-range radar of comparable accuracy will be covered.

In the AN/FPS-16 development, significant advances were made toward easing the following limitations of the radar method:

1) *Mechanical and Servo Error.* Completely new pedestal design, based on analysis of errors in radar pedestals previously developed, brought total mechanical error below the 0.1 mil level. Careful electrical design reduced servo and target scintillation errors to negligible factors, while the rms extent of target glint for echo tracking is held to about one-fourth the extent of the target itself. Test data substantiating this is given in [2] and [3].

2) *Velocity Data.* The spectrum of position errors was controlled to permit the use of lower smoothing time in derivation of velocity. This was made possible by achievement of servo bandwidths up to 5 cps in angle and 10 cps in range.

3) *Tropospheric Refraction.* Correction formulas were derived to minimize this error.

4) *Tropospheric Attenuation.* A medium frequency (5400 to 5900 Mc) was found to reduce effects of attenuation and masking in clouds, rain, and moist atmosphere, as compared with higher frequencies. At the same time, beamwidths in this band can be made narrow enough, with reasonable antenna size, to reduce error at low-elevation angles, as compared to *S*-band operation.

5) *Low-Altitude Tracking.* Sidelobes were reduced to the point where accurate tracking was possible within 3° of the ground. Below this angle, use of special screens or radar fences may further extend the tracking range.

The net result of these developments was to make possible radars for instrumentation which are capable of a full order of magnitude improvement in instrumental accuracy over that obtained with modified SCR-584's. Range at which precise tracking is possible on similar targets is improved almost 10:1 over the original SCR-584, and 3:1 over the most advanced modifications of this radar used in range instrumentation. Angular precision of 0.03 mil and absolute accuracy of 0.1 mil are available after correction for propagation effects. Range precision of 1 to 2 yards rms and absolute accuracy of 5 yards rms are available after correction of propagation effects. Table I gives the results in terms of space positions.

Analysis of Errors in Monopulse Radar

Within the past few years a great deal of work, both theoretical and practical, has gone into the analysis of radar tracking errors. References [2], [3] and [4] present the results of such analysis on the AN/FPS-16 radar, and the following discussion summarizes these results and illustrates the type of data obtained in verification of the theoretical findings.

It has been common practice to represent radar-angle errors as the sum of three components, as shown in Fig. 4. As radar development proceeded and tracking range was extended, it became necessary to break the errors down into a large number of small components, analyze how each one varied with operating conditions, and devise tests to verify each such relationship. This has been accomplished for the AN/FPS-16, with the error breakdown in angle shown in Table II.

TABLE I

Errors in Monopulse Radar Position Measurement

Range from Radar (n.m.)	Precision (ft rms)	Accuracy (ft rms)
5–10	5	15
10–20	7	20
20–40	10	30
40–100	15	50
100–200	30	100
200–400	60	200
400–1000	150	400
1000–2000	300	1000
2000–4000	600	2000
4000–10,000	1500	4000

Note: Based on coordinate having largest error.

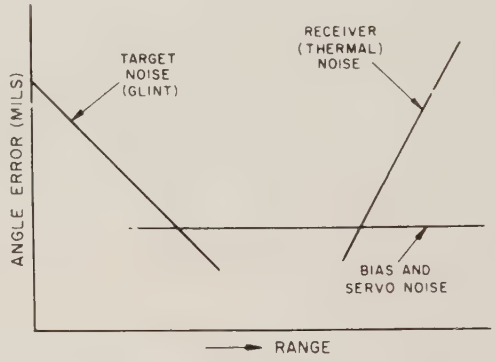

Fig. 4—Theoretical radar errors vs range.

TABLE II

Inventory of Angle Error Components

	Bias	Noise
Radar-dependent tracking errors (deviation of antenna from target)	Boresight axis collimation Axis shift with: RF and IF tuning Receiver phase shift Target amplitude Temperature Wind force Antenna unbalance Servo unbalance	Receiver thermal noise Multipath (elevation only) Wind gusts Servo electrical noise Servo mechanical noise
Radar-dependent translation errors (errors in converting antenna position to angular coordinates)	Levelling of pedestal North alignment Static flexure of pedestal and antenna Orthogonality of axes Solar heating	Dynamic deflection of pedestal and antenna Bearing wobble Data gear nonlinearity and backlash Data take-off nonlinearity and granularity
Target-dependent tracking errors	Dynamic lag	Glint Dynamic lag variation Scintillation Beacon modulation
Propagation errors	Average refraction of troposphere Average refraction of ionosphere	Irregularities in tropospheric refraction Irregularities in ionospheric refraction
Apparent or instrumentation errors (for optical reference)	Telescope or reference instrument stability Film emulsion and base stability Optical parallax	Telescope, camera or reference instrument vibration Film-transport jitter Reading error Granularity error Variation in optical parallax

Detailed measurements of the "fixed" components (those whose rms values are the same for most operating conditions) were made and verified by over-all system measurements under controlled conditions. The results were as follows:

Component	Bias (mils)	Noise (mils)
Mechanical	0.04	0.025
Electrical	0.04	
Data system	0.01	0.035
Total (rms) "fixed" error	0.06	0.04

In order to evaluate those components whose values vary with operating conditions, a series of equations was derived to describe the dependence of error upon various radar, target and environmental factors. A summary of these equations for radar angle measurement is given in Table III. Experimental data were taken under conditions simulating missile tracking, as well as during aircraft tracking. For simulation of missile- and space-tracking conditions and beacon operations, a series of tracks were run on small reflective targets carried by free balloons. Fig. 5 shows the results of a typical tracking run made with the AN/FPS-16 on a 6-in metal sphere carried aloft inside a free balloon. In this figure, azimuth tracking noise is plotted against range (the elevation error plot is similar). The boresight film was analyzed to determine the standard deviation of the error, which is defined as the difference between the radar-pointing direction and the optical line-of-sight to the center of the balloon. Each of the points plotted on the graph represents a sample analyzed over a period of 30 seconds at intervals during the run. The circles and triangles represent two different servo bandwidths.

The lines which have been drawn in on the graph represent theoretical limits or explanations of the results. The left portion of the plot is well-fitted by a straight line of negative slope representing inverse proportionality to range. The explanation of this lies in the fact that the metal sphere is not rigidly supported inside the balloon, but can wander around a bit. Since the radar sees the sphere and the camera sees the balloon, there is an error. The line drawn at the left of Fig. 5 corresponds to a linear error of $1\frac{1}{2}$ in at the balloon.

The line rising to the right has a slope representing proportionality to the square of the range. This is the theoretical lower limit of error due to thermal noise in accordance with the formula appearing in Table III. The points are in fairly good agreement with this line.

Running horizontally at about 0.01 mil is a line which represents the lower limit set by the error in recording and reading the data. In some of the runs, it has been found that the points in the center region did, in fact, closely approach this line. In Fig. 5, this is not the case. This run has been purposely selected because it illustrates another interesting and important effect, namely, random errors due to propagation anomalies or atmospheric blobs of varying index of refraction.

Muchmore and Wheelon [16] have derived the propagation-noise formula given in Table III. If the following typical values are taken:

$$\overline{\Delta N} = 0.5$$
$$L_0 = 50\,\text{ft}$$
$$L = \text{total range to target},$$

TABLE III
SUMMARY OF TRACKING ERROR EQUATIONS

Thermal Noise (for $S/N>1$)	$\sigma_t = \dfrac{\theta}{\sqrt{\dfrac{2S}{N}\dfrac{f_r}{\beta_n}}}$ radians	(1)
Multipath	$\sigma_m = \dfrac{\theta_p}{\sqrt{8A_s}}$ radians	(2)
Target Glint	$\sigma_g \cong \dfrac{1}{4}\dfrac{L_t}{R}$ radians	(3)
Servo Lag	$\sum = \dfrac{\omega_t}{K_v} + \dfrac{\dot{\omega}_t}{K_a}$ radians	(4)
Propagation noise	$\sigma_p \cong 2\Delta N \times 10^{-6}\sqrt{L/L_0}$ radians	(5)

Symbols:

θ = radar beamwidth (rad)
S/N = signal-to-noise power ratio
f_r = repetition rate (pps)
β_n = servo bandwidth (cps)
ρ = ground reflectivity (voltage ratio)
A_s = sidelobe attenuation (power ratio)
L_t = span of target, R = range of target } (any consistent units)
ω_t = target angle velocity (rad/sec)
$\dot{\omega}_t$ = target angle acceleration (rad/sec²)
K_v = velocity error constant (1/sec)
K_a = acceleration error constant $\cong 2.5\beta_n^2$ (1/sec²)
ΔN = rms variation in tropospheric refractivity (N-units, or $[n-1]\times 10^6$)
L = length of tropospheric anomalies, L_0 = scale length of anomalies } (any consistent units)

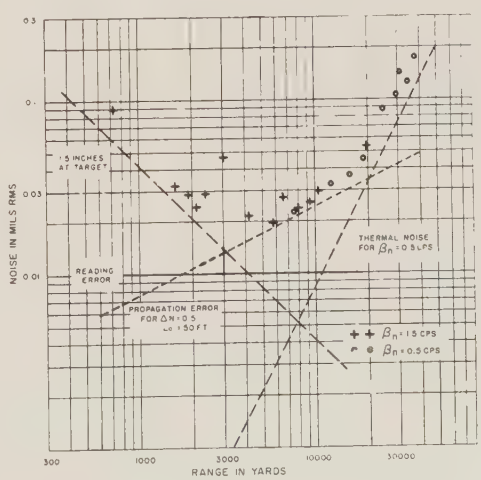

Fig. 5—Measured angle tracking noise vs range.

the straight line which appears in the center portion of Fig. 5 is obtained; this line has a positive slope indicating proportionality to the square root of range. This sets a lower limit of precision in the center region of the graph.

In this explanation is correct, it is believed that this is the first time the effect of atmospheric propagation anomalies has been observed with a single radar. This suggests the possible use of a tracking radar for observation and measurement of this effect.

Fig. 5 extends out only to a range of about 25 miles. This limitation is due, not to the radar, but to inability of the camera to see the balloon at longer range. The radar has tracked these balloons (or rather the 6-in metal spheres inside) out to 70 nautical miles. The maximum range on a target of one-square-meter radar cross section is 150 miles for the unmodified radars, and 200 miles for those currently in production.

Plots obtained from aircraft tracking runs are similar to the one shown for a metal sphere, except that the glint or wander of the electrical center of the target is greater (about $\frac{1}{4}$ of the target dimension in each coordinate), and the thermal noise line moves out further to the right (that is, toward longer range), because of the larger echoing area.

A large amount of additional experimental data is available in [2] and [3].

Range of Echo Tracking

The classical radar equation can be used to calculate the ratio of the received signal power to the radar-receiver noise, and from this ratio the ability of the radar to detect, lock-on and track may be estimated. In its generally used form, the radar equation gives the SNR in the IF amplifier (after the first stage or two) as follows:

$$S/N = \frac{P_t G_0^2 \lambda^2 \sigma}{(4\pi)^3 R^4 K T_0 B \overline{NF_0} L}, \tag{6}$$

where

S/N is the IF SNR during reception of the pulse,
P_t is peak transmitted power in watts,
G_0 is antenna gain along the axis of the beam,
λ is wavelength,
σ is effective radar cross section of the target,
R is range to the target,
K is Boltzmann's constant,
T_0 is ambient temperature at the receiver in degrees Kelvin,
B is receiver bandwidth in cps,
$\overline{NF_0}$ is operating receiver noise figure, and
L is the total system loss, arising from atmospheric attenuation, plumbing losses, transmitter power outside the receiver bandwidth, and degradation of previously listed radar parameters from their assumed values.

Note that λ, σ and R must use the same units of length, while G_0, $\overline{NF_0}$ and L are dimensionless ratios. The applicable AN/FPS-16 radar parameters in the wide-pulse mode are

$P_t = 1.0$ Mw
$G_0 = 44.5$ db
$\lambda = 5.3$ cm (at midband)
$B = 1.6$ Mc
$\overline{NF_0} = 11$ db
$L \cong 4$ db (known loss in plumbing and duplexer).

To calculate values of S/N to be expected at a given range R (in nautical miles) on a given target σ (in square meters), a number of conversion factors must be applied along with the constants $(4\pi)^3$, $K = 1.37 \times 10^{-23}$ watts/degree/cps and $T_0 = 291°$ K. By coincidence, the combined value of all conversion and other constants multiplies out to unity (actually 1.08) when λ is expressed in cm, σ in m^2, R in nautical miles, and B in cps. The resulting simplified form of the radar equation can be written

$$S/N = \frac{P_t G_0^2 \lambda^2 \sigma}{R^4 B \overline{NF_0} L}. \tag{7}$$

Substituting the AN/FPS-16 radar parameters, as given above, we obtain

$$S/N = \frac{\sigma}{R^4} \times 4.4 \times 10^8 \tag{8}$$

or, in logarithmic form,

$$S/N = 10 \log \sigma - 40 \log R + 86.5 \text{ db} \tag{9}$$

(σ must be in m^2, R in nautical miles). Fig. 6 is a plot of (9) showing the calculated SNR for various target cross sections as a function of range. The SNR attainable using the 0.25-μsec pulse and 8-Mc bandwidth, is almost exactly 7 db lower than values given in Fig. 6. Using the 0.5 μsec pulse and 8 Mc bandwidth, the SNR is also down 7 db from Fig. 6, but the longer pulse provides an improvement in visibility on the display. If the 250 kw transmitter is used, the SNR's will be reduced 6 db from the values obtained with the 1.0 Mw transmitter under similar conditions.

Beacon Tracking

For beacon tracking, two separate equations describe the ability of the radar to interrogate the beacon and its ability to detect and track the beacon response. The radar signal available at the beacon receiver is given by

$$S_b = \frac{P_t G_r G_b \lambda^2}{(4\pi)^2 R^2 L_1}, \tag{10}$$

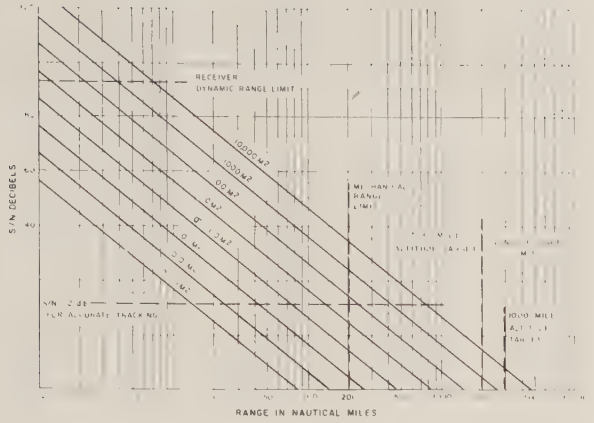

Fig. 6—Calculated values of SNR vs range for echo track for AN/FPS-16.

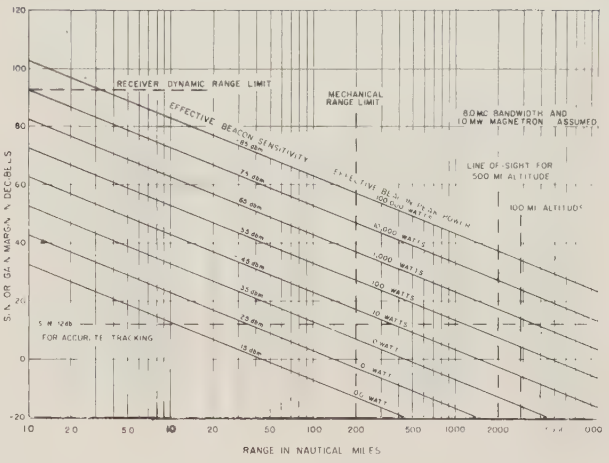

Fig. 7—Theoretical beacon tracking range AN/FPS-16.

where

G_r is the radar antenna gain,
G_b is the beacon antenna gain,
L_1 is one-way system loss for interrogation, and other symbols are as defined for (6).

If P_t is replaced by P_b, the beacon transmitter power, and L_1 by L_2, the one-way loss in response, the equation will give beacon signal available at the radar receiver. Then, since noise power referred to the radar receiver input is

$$N = KT_0B\overline{NF_0}, \tag{11}$$

the resulting SNR at the radar is

$$S/N = \frac{P_bG_rG_b\lambda^2}{(4\pi)^2R^2L_2KT_0B\overline{NF_0}}. \tag{12}$$

Fig. 7 is a plot of gain margin for interrogation (defined as the ratio of available S_b to $S_{\min}$, the minimum power required to trigger the beacon) and SNR at the radar, for AN/FPS-16 radar parameters and various effective values of $S_{\min}$ and P_b. The curves may be used directly for omnidirectional, unity-gain beacon antennas. For antennas with gain G_b, the effective power may be found by the product P_bG_b, while effective sensitivity will be $S_{\min}/G_b$.

Of the radar parameters used in these calculations, only λ and B can be measured directly with high accuracy. Transmitter power can be measured to within a fraction of a decibel using calorimetric procedures, but this is not done as a regular maintenance test, and at any given time the power may be 1 db off in either direction. Similar considerations apply to $\overline{NF}_0$, which is influenced by crystal aging and damage, and G_0, which is originally calculated from beam patterns.

II. Current Development Programs

The first major step beyond the AN/FPS-16 class of instrumentation radars is the AN/FPQ-6 (along with the transportable AN/TPQ-18). The major characteristics of this radar, compared to those of the AN/FPS-16, are given in the Appendix. The performance is basically the same in tracking accuracy (with some improvement in precision), but the range is extended by a factor of four over the AN/FPS-16. An artist's sketch of the new radar is given in Fig. 8. Other than the new antenna and pedestal, it can be seen that the new radar represents a combination of the 3-Mw klystron transmitter, the digital-ranging system (extended to 32,000 miles), complete acquisition features, and updated designs for receivers, data handling and peripheral equipment. The AN/FPQ-6 and AN/TPQ-18 class of radars provides both an extension of missile range coverage and a major step into space instrumentation. Existing beacons can be tracked to the moon with these radars, and beacons now under development will provide wide safety margins in the application [5]. The added performance of the AN/FPQ-6 is largely due to the new and larger antenna. A Cassegrainian design has been used (Fig. 9) to combine high-aperture efficiency, low sidelobes, short waveguide runs and minimum mechanical difficulty. The mechanical resonance is to be above 15 cps to preserve the servo-bandwidth capability of the AN/FPS-16. At the same time, the design should make possible very low antenna noise pickup from the surrounding ground, looking forward to the time when low-noise receiver preamplifiers become available. Delivery of these radars to the initial sites is scheduled for March, 1962, with full operation four months later.

Pulse-Doppler System

An important capability not yet exploited in operational pulse-radar range instrumentation systems is the refined measurement of radial velocity through the Doppler effect. Search radars have used coherent MTI since the end of World War II, and numerous tracking and navigation systems have since been designed to select targets and perform measurements on the basis of Doppler shifts in the spectrum of pulsed signals. The

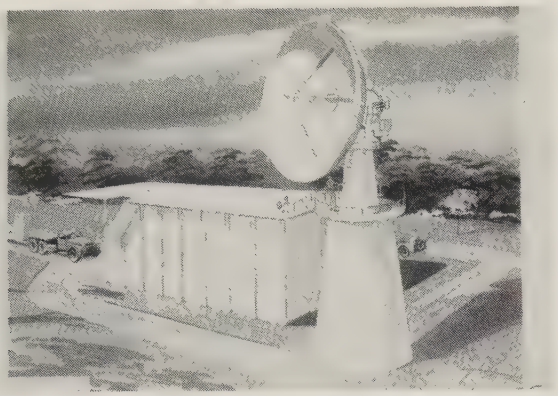

Fig. 8 Artists sketch of AN/FPQ-6 instrumentation radar.

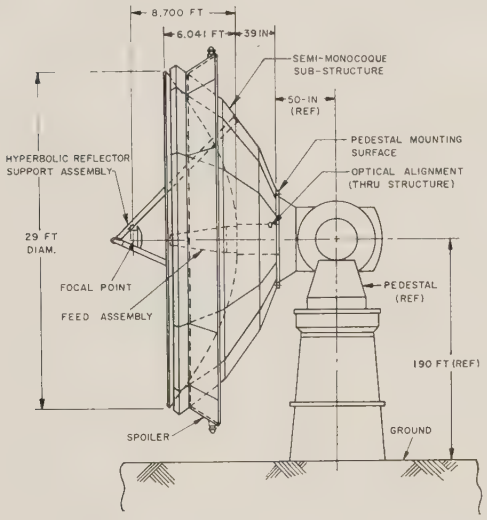

Fig. 9—Cassegrain antenna for AN/FPQ-6.

importance of applying this technique to range instrumentation stems from four major factors:

1) Accurate three-coordinate velocity data is needed for impact prediction, orbit determination, probe guidance, etc.

2) Accuracy of data based on conventional range and angle data is limited by the extreme ranges required.

3) Solutions based upon range-only (trilateration) operation are effective (see discussion in a later section) but are limited by the precision of range measurement.

4) Solutions based upon combined range and Doppler data from three-station nets will meet present and projected requirements for velocity data.

Alternate approaches to solving this problem have been proposed using CW techniques, but the pulse-Doppler system possesses unique advantages:

1) It will operate on noncooperative targets within the echo-range limitations of the pulsed radar.

2) It permits a single transponder beacon to be shared by three or more stations on a time-multiplexed basis, with each station performing a continuous track in all coordinates.

3) The ground equipment consists almost entirely of existing radar sets.

4) The ground radar provides high-system gain and permits the system to expand and extend its range continuously as radar equipment is added and improved.

5) Communications, data links and support equipment are those presently used with the radar.

6) No critical measurement links over ground paths are used in three-station radar trilateration, due to the independent echo or beacon response to each station.

The pulse-Doppler approach is, of course, subject to the same fundamental limitations on accuracy as apply to CW systems: uncertainty in the velocity of light, atmospheric refraction, stability of the basic reference oscillator, acceleration and higher derivative errors, and need for good baseline surveys. In addition, the pulsed system at conventional instrumentation radar-repetition rates is very ambiguous in its Doppler readings. At 640 pps, for instance, a *C*-band radar will have Doppler ambiguities at intervals of about 50 ft/sec, corresponding to the spacing between successive lines in the signal spectrum. Thus, it is necessary to measure independently the target radial velocity with sufficient accuracy to define the velocity intervals being observed. For the case cited, a measurement of 8 ft/sec rms will give 99.7 per cent assurance of unambiguous results, and this is easily within the capability of differentiated range data.

The current development program in coherent pulse-Doppler instrumentation has, as a primary objective, the design of circuits for use with the AN/FPS-16 or AN/FPQ-6 to measure Doppler velocity to the order of 0.1 ft/sec. Secondary objectives include the exploitation of velocity resolution for overcoming thermal noise (predetector integration), for reduction of ground clutter at launch, and for selection of the desired target component as stages are separated in multistage vehicles. Some additional benefits which will be derived incidentally from the coherent system modification are the assurance of exact transmitter and receiver frequency control (through use of ultra-stable oscillator and frequency synthesizer), adequate stability for wide-pulse, narrow-band operation on both echo and beacon tracks, and adaptability of both transmitter and receiver to pulse-compression schemes such as "chirp."

The initial modification for velocity measurement will involve only the addition of a stable exciter and a Doppler channel to the klystron transmitter already available in some of the AN/FPS-16's (see Fig. 10). The existing receivers, angle-tracking circuits and ranging circuits will be undisturbed, except for substitution of a STALO (stable local oscillator) signal from the exciter in place of the existing local oscillator. Ambiguity resolution for the Doppler channel will be provided by processing of range-difference data, and the Doppler circuit will go into operation only after a target has been acquired and tracked by the ranging system. Subsequent modification (Fig. 11) will provide narrow-band filters in all tracking channels to exploit the secondary objectives mentioned above. This Doppler de-

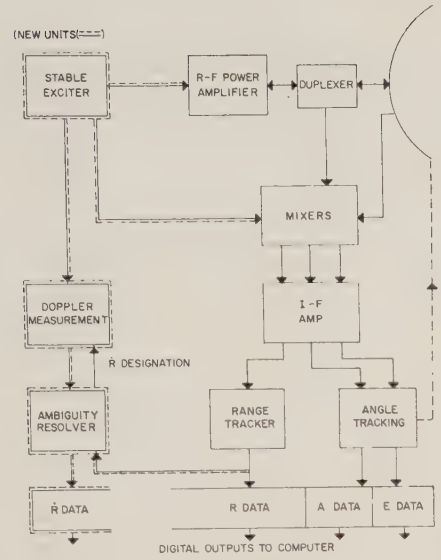

Fig. 10—AN/FPS-16 velocity measurement modification.

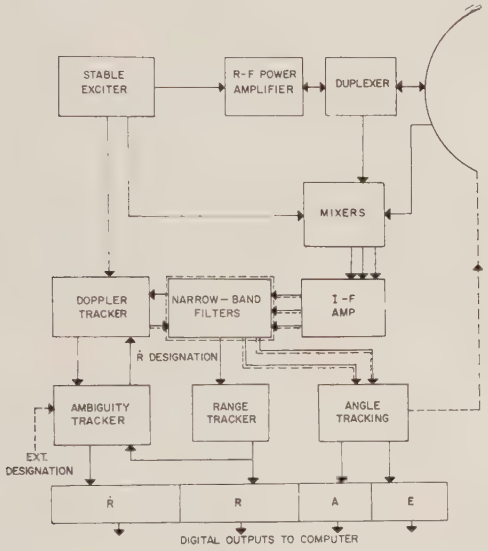

Fig. 11—AN/FPS-16 velocity tracking modification.

velopment program is now proceeding, and the stable exciter will be included as standard equipment with the klystron transmitters of the AN/FPQ-6. Coherent beacons are also under development.

Other Current Modification Programs

Going beyond the AN/FPQ-6 and the Doppler-measurement programs, there are several areas of pulsed-radar-system development which are being followed and which can be expected to result in later modifications to radars after installation in the field. In the antenna area, improved monopulse feeds are under development which will provide complete polarization diversity in reception and flexible control of transmitted polarization. Use of the Cassegrainian antenna permits the extra waveguide components to be added and provides a place for multiple-receiver preamplifiers near the feed assembly. Design of larger antennas and suitable pedestals is being carried out under several radar and communication programs and then may be applied directly where economic considerations permit. For the larger antennas, the combination of equipment for two or more radar bands on a single pedestal and reflector becomes economical, and multiband feed development is going forward.

In the transmitter area, the most significant developments are concerned with building up greater average power and pulse energy. This is done principally through the use of parallel klystron amplifiers with moderate peak-power capabilities per tube, but with cathodes designed for long-pulse operation. Where the range resolution of the present short-pulse systems must be preserved, pulse-compression circuits may be used to combine the pulse-energy advantage of the long pulse with the high-range resolution inherent in a wide spectral bandwidth. A similar advantage might be gained through coherent (predetector) integration of short pulses at high-repetition rates, but this approach is limited by the presence of ground clutter or other short-range targets, which tend to mask the desired echo from extended range in a multiple-time-around tracker.

Developments in the receiver area are chiefly concerned with improved sensitivity through use of parametric amplifiers and masers. Super-cooled paramps are under development which offer significant noise reduction as compared to the present paramp design. Ultimately, the microwave maser will eliminate receiver noise as a significant contribution to system noise, leaving sky noise, antenna noise and waveguide loss as the limiting factors in sensitivity. These developments will be discussed in more detail later.

Also under development are data-processing devices to match the capabilities of the new radars and to permit flexible-net operation in missile- and space-range applications. The details of such equipment are beyond the scope of this paper, but the general system requirements and expected performance will be covered in a later section.

III. Development of Radar for Space Instrumentation

Basic Problems and Limitations

Radar may be used in solution of three major problems in space instrumentation. First, it is applicable to surveillance and tracking of all objects in orbit around the earth, using skin return or whatever cooperative devices may be available on the satellites. Second, use of radar or radar-type ground equipment is mandatory in tracking lunar and deep space probes at ranges from 250,000 miles to the limits of the solar system, using cooperative transponders. Lastly, the radar astronomers employ radar equipment to measure directly the surface characteristics of the moon and planets. This discussion will be limited to use of tracking radar for measurement of position and velocity of satellites and probes and for

obtaining other data on these targets through reception of telemetering signals or analysis of signal-strength records.

The limitations on radar performance in space applications arise from two sources: the extreme range over which the signals must travel and the necessity of operating from beneath the atmospheric blanket which covers the earth. The range limitation, coupled with limited transponder power or reflection area of practical space vehicles, forces the space radar to extremes in transmitter power, antenna gain and receiver sensitivity which go far beyond past designs in radar equipment. The atmosphere acts directly to limit the accuracy of measurement, the sensitivity of the system (through "sky noise" contributions), and the physical size and configuration of antennas which must withstand the assaults of local weather. In addition to these two types of problems, there are the force of gravity which places mechanical limits on antenna design; the presence of the earth, which obstructs line of sight and radiates noise toward the antenna; high-voltage breakdown and personnel-safety limitations on generated and radiated power; man-made, galactic, and solar noise; and many practical equipment design problems. Brief summaries of all these limitations will be given.

Range and Radar Parameters

As a background for discussion, assume that the radar is to track by skin echo a small satellite (≈ 1.0 m^2 cross section) in a synchronous orbit around the earth. A radar which achieves a single-pulse SNR of unity at 30,000 n.m. is suitable for this task. The basic radar equation may be rewritten as

$$R_0 = \left[\frac{P_t \tau G^2 \lambda^2 \sigma}{\overline{NF}_0 L}\right]^{1/4} \text{n.m.}, \tag{13}$$

where R_0 is the range at which unity IF SNR is achieved and the other terms are as used in (7), with pulse width $\tau = 1/B$.

From this equation, the resulting requirement on radar parameters for $R_0 = 30{,}000$ miles on 1.0 m^2 may be expressed as

$$P_t \tau G^2 \lambda^2 / \overline{NF}_0 L = 8 \times 10^{17} \tag{14}$$

or, if the antenna is limited to a diameter D in feet,

$$P_t \tau D^4 / \lambda^2 \overline{NF}_0 L = 10^{10}. \tag{15}$$

If a minimum repetition rate f_r for satisfactory acquisition and measurement is established, the product $P_t \tau f_r = Pav$ specifies the average power required of the transmitter. Values of f_r between 10 and 100 would be typical, depending upon the exact requirements, and there might be some trade-off between higher repetition rate and reduced single-pulse S/N to perform a given function.

Another measure of required radar parameters could be obtained by assuming transponder operation to a 500 million mile range, or approximately to Saturn's orbit The beacon-to-radar path will normally limit range in such a case, due to power output limitations in the beacon. The beacon equation (for the response link) is

$$S/N = \frac{P_b \tau G G_b \lambda^2}{R^2 \overline{NF}_0 L} \times 5 \times 10^7 \tag{16}$$

for the mixed system of units used above. At a range of 5×10^8 miles, for unity SNR at the radar, the beacon equation gives

$$P_b \tau G G_b \lambda^2 / \overline{NF}_0 L = 5 \times 10^9 \tag{17}$$

or, for a beacon antenna of restricted diameter D_b in feet,

$$P_b \tau G D_b^2 / \overline{NF}_0 L = 5.5 \times 10^5 \text{ (independent of } \lambda). \tag{18}$$

Consider now a beacon pulse energy $P_b \tau$ of 0.01 w-sec, and an effective antenna diameter of three feet. The radar requirement becomes

$$G / \overline{NF}_0 L = 6 \times 10^6 \text{ (independent of } P_t \text{ and } \lambda). \tag{19}$$

In certain applications where tracks must be continued for protracted periods, a radar reflector provides better performance than an active beacon (it is certainly superior in long life and reliability). The equation for maximum cross section of a corner reflector is

$$\sigma_{\max} = \frac{4}{3} \pi \frac{a^4}{\lambda^2}, \tag{20}$$

where a is the side length (in the same units as σ and λ^2). A Luneberg lens may have a cross section

$$\sigma_{\max} = \frac{\pi^3 d^4}{4\lambda^2}, \tag{21}$$

where d is the diameter. If the value of $\sigma_{\max}$, for a limited to one meter, is used in calculation of parameters for 30,000 n.m. echo tracking, the equation becomes

$$P_t \tau G^2 / \overline{NF}_0 L = 3.7 \times 10^{13} \text{ (independent of frequency)} \tag{22}$$

(for a Luneberg lens, $d = 3$ ft and the factor is 7.4×10^{13}).

Projected State-of-the-Art in Radar

The peak and average power capabilities of single transmitter tubes, past and present, are shown in Fig. 12. Extrapolating from this into the near future, and taking into account the factors of equipment size and cost and possible use of parallel tubes, the figures of Table IV were arrived at as reasonable limits for the next generation of radar equipment in several frequency bands. It becomes increasingly difficult to use higher peak and average powers at available radar sites, and even the levels shown may be difficult to achieve and use in some cases.

Advances in antenna development have proceeded rapidly over the years, and radio telescopes in the 250- to 1000-ft class have been built or started. It appears possible to build antennas with directive gains approaching 80 db, at which point the atmospheric anomalies begin to limit gain. The economic aspects of tracking antennas impose stricter limits in most cases, however, and the following comparison will be based on the general features of the "Haystack Hill" class of antennas [6], rather than on any "ultimate" limitations. Table V shows the assumed diameters, efficiencies and gains achievable with antennas which might be used on this type of tracking pedestal. The beamwidth is also included to emphasize two points: first, that the higher-frequency radars must receive accurate designation from search radar or computation based on prior tracking data and second, that the angular accuracy will be much better for the higher-frequency systems.

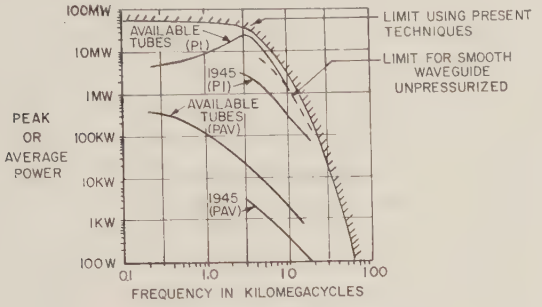

Fig. 12—Power capabilities of transmitting tubes.

TABLE IV
ESTIMATED RADAR POWER

Radar band	UHF	*L*	*S*	*C*	*X*	*K*
Wavelength (cm)	75	25	12	6	3	1.5
Peak power (Mw)	10	25	25	10	3	0.5
Average power (kw)	600	300	100	50	20	3
Pulse energy (w-s)	20,000	12,000	7500	1000	300	50
Pulse width (μsec)	2000	500	300	100	100	100

TABLE V
ESTIMATED ANTENNA PARAMETERS

Radar Band	UHF	*L*	*S*	*C*	*X*	*K*
Wavelength (cm)	75	25	12	6	3	1.5
Ant. diameter (ft)	200	150	120	120	120	100
Efficiency (percent)	50	50	50	50	50	40
Gain (db)	45	52	56.5	62.5	68.5	71.5
Bandwidth (degree)	0.9	0.4	0.24	0.12	0.06	0.04

TABLE VI
ESTIMATED INPUT NOISE (AT 10° ELEVATION)

Radar band	UHF	*L*	*S*	*C*	*X*	*K*
Wavelength (cm)	75	25	12	6	3	1.5
Sky temp. (°K)	50	10	15	18	20	100
Receiver temp. (°K)	10	10	10	10	10	10
Input temp. (°K)	60	20	25	28	30	110
$\overline{NF_0}$ (db)	−7	−12	−11	−10.5	−10	−4.5

Table VI shows the limit to antenna temperature imposed by cosmic noise and the troposphere, disregarding sidelobe effects, and the resulting operating noise figure for a system using a maser. Actual sidelobe effects may add between 20 and 50 degrees to the input temperature.

The data used in Table VI was derived from curves in [7], assuming a constant receiver system temperature of 10°K as would represent a practical maser and its input circuit. The elevation angle of 10° was chosen to indicate the sensitivity which could be attained over a substantial volume of coverage around the radar site. An additional loss factor L of 2 db will be assumed in further calculations to account for plumbing loss, filter matching, and excess noise temperature at the input.

Table VII shows the radar range on a target of 1.0 m² cross section and on a corner reflector of 1.0 m side length, using the radar parameters from the three preceding tables. It can be seen that the considerably higher powers available at the lower frequencies, along with somewhat larger antennas, provide skin-tracking ranges equal to or slightly less than the *S*-, *C*- and *X*-band radars, on noncooperative targets. On cooperative targets, the higher frequencies are considerably better. On beacons (using the earlier assumptions) the higher frequencies have an even greater advantage in that the reduced transmitter power of the radar does not reduce the amplitude of the response.

This tabulation should not be taken as a prediction of "ultimate" performance possible from radar, but as an indication of the relative difficulty of achieving a particular level of performance at different frequencies. Furthermore, as stated earlier, the search and acquisition problem has not been covered, although it obviously favors the lower-frequency bands. For skin tracking, the microwave bands offer significant advantages in equipment size for all targets, and greater range as well on corner reflectors. For beacon tracking, the earlier as-

TABLE VII
RADAR RANGE FOR S/N = UNITY

Radar band	UHF	*L*	*S*	*C*	*X*	*K*
Wavelength (cm)	75	25	12	6	3	1.5
R_0 on 1.0 m² (mi)	20,000	30,000	30,000	27,000	28,000	22,000
R_0 on corner (mi)	60,000	100,000	120,000	140,000	220,000	200,000
σ of corner (m²)	6	60	250	1000	4000	16,000
R_0 on beacon (10^6 mi)	125	500	750	1400	2600	2000

sumption of 0.01 w-sec pulse energy, independent of frequency, should be revised to indicate the relatively higher efficiency of power generation at lower frequencies. This would approximately double the range at UHF and cut in half the range at *K* band, relative to *S* band as a reference, with intermediate effects on *L*-, *C*- and *X*-band operation. Even so, the relative economy and effectiveness of microwave operation is obvious.

Examples of Tracking Radar Systems for Space Research

As examples of possible tracking radar configurations for use in space research, two systems will be discussed, one at 435 Mc and one at 5800 Mc. Both will be based upon the Haystack Hill class of antenna and pedestal, and upon currently available tubes and components or those under development. The full parameters of the two systems are shown in Table VIII, as compared with AN/FPS-16 and AN/FPQ-6. Obviously the step from AN/FPQ-6 to these proposed trackers is a much greater one than between the original SCR-584 and AN/FPS-16, or between AN/FPS-16 and AN/FPQ-6. For this reason, although antennas are now being built even bigger than the Haystack class, it seems probable that one or more intermediate steps will be implemented between AN/FPQ-6 and the space trackers listed in Table VIII. One such step is an experimental space tracker now under construction at the Moorestown RCA plant. Its characteristics are shown in the last column of Table VIII.

The beacons required for the ranges listed in the table are well within the current state of the art, but are not necessarily desirable items for inclusion in space vehicles with small payload capacity. A 40-kw beacon has been described [5], which would weigh 40 lbs and require 150 watts of input power. This would be suitable for use in a lunar probe with the AN/FPQ-6, but would impose considerable burdens on a space probe of longer life, which would use solar cells as a source of prime power. For such vehicles, further development of tunnel-diode oscillators appears to offer a solution. Present experimental diodes have provided CW output powers of 0.2 mw at 5500 Mc, with efficiency of a few per cent [8]. In the near future, a power level of 10 mw appears attainable, with pulse lengths of 100 μsec. Range on such a beacon would be one-hundredth that shown in Table VIII, or about 6 million miles for the *C*-band tracker. Until higher-power solid-state oscillators become available, it appears that longer response pulses will be necessary, accompanied by narrower-receiver bandwidths in the radar, to achieve sufficient range for probes to Venus and Mars. A tunnel-diode beacon producing 10-mw pulses of 10 msec length would provide a 60-million mile range with the *C*-band tracker of Table VIII. Since the radar-ranging system can interpolate to within about 5 per cent of the received pulse width, a range precision of about forty miles would still be possible for independent measurements taken twenty seconds apart. More accurate data in the vicinity of the planet could be obtained by intermittent operation of a higher-power beacon transmitter, using a pulsed triode at the 100-watt level.

For the UHF space tracker, the 5-watt beacon power listed is only slightly higher than now available from solid-state devices, and ranges of 50 million miles ap-

TABLE VIII
SPACE RANGE RADAR PARAMETERS

Radar type		AN/FPS-16	AN/FPQ-6	Proposed Space Trackers		
Radar band		*C*	*C*	UHF	*C*	(Exp) *C*
Radar frequency	Mc	5600	5600	435	5600	5600
Peak power	Mw	1.0	3.0	10	10	3
Pulse width	μsec	1.0	2.4	2000	100	5
Repetition rate	pps	1000	640	30	50	300
Average power	kw	1.0	4.5	600	50	5
Antenna size	ft	12	30	200	120	50
Antenna gain	db	44	52	45	62.5	58
Beamwidth	mils	20	8	16	2	5
Bandwidth	kcps	1600	500	0.5	10	250
Operating noise figure	db	10	8	−7	−10.5	−10
Beacon peak power	w	10,000	4000	5	100	2000
Beacon av. power	w	10	7	0.3	0.5	3.3
R_0: on 1.0 m²	n.m.	150	750	21K	27K	5K
on corner*	n.m.	800	4000	26K	140K	28K
on beacon	n.m.	100K	350K	16M	11M	5.6M
beacon, 3-ft ant.	n.m.	5.6M	20M	90M	600M	300M
Range precision†	ft	5	15	60K	2000	50
Angle precision†	mils	0.2	0.1	1.0	0.1	0.1

* Based on corner reflector with side length $a = 1.0$ m.
† Based on observation for 10 sec at S/N = unity, or for 1 sec at $S/N = 10$.

pear feasible for the near future with parallel tunnel diodes or transistors. The over-all accuracy of range measurement would be comparable to the forty-mile figure for the microwave system.

The tracking precision of the radars listed in Table VIII is shown in Figs. 13 and 14. It may be assumed that the angular accuracy is 0.1 mil in all cases, and the range accuracy is limited to the values shown. When using beacons, a serious limitation to be overcome is the uncertainty in the vacuum velocity of light. This can be relieved if the velocity is defined in terms of a molecular standard [9] rather than by the meter bar and the sidereal second.

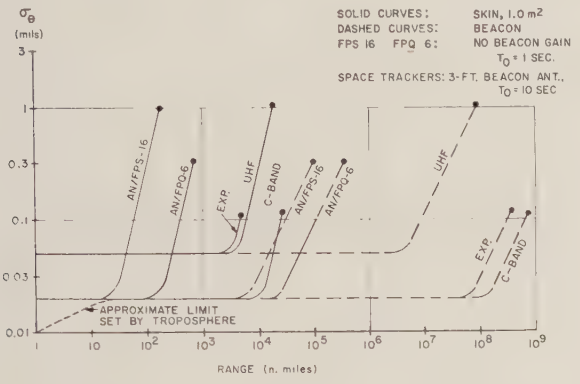

Fig. 13—Angle precision vs range.

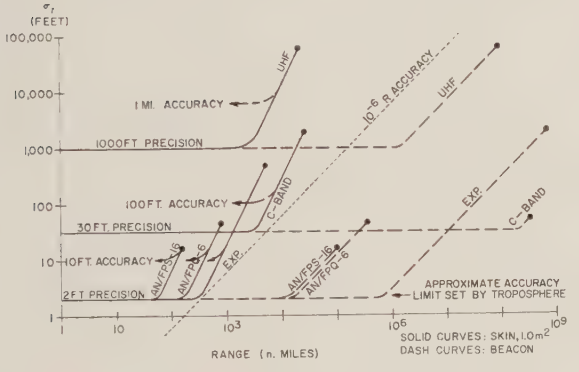

Fig. 14—Range precision and accuracy vs range.

IV. System Applications of Instrumentation Radar to Space Range, Angle and Rate Measurements

The precision and accuracy attained in modern monopulse radars has already been discussed. In space tracking applications, the most important sources of error will usually be receiver noise (at long ranges), atmospheric propagation effects, knowledge of the velocity of light, and systematic errors due to deformation of the large antennas used. Precision figures given in Table VIII were based upon tracking at the maximum range of the radar ($S/N \cong$ unity), with thermal noise as the sole important source of error. In the case of angle tracking, the thermal noise equation from Table III was used with an equivalent servo-noise bandwidth $\beta_n = \frac{1}{2}t_0$ where t_0 is the observation time. An equivalent formula for range precision is

$$\sigma_r = \frac{\tau}{\sqrt{(f_r/\beta_n)(S/N)}} = \frac{\tau}{\sqrt{2t_0 f_r (S/N)}} . \tag{23}$$

Here, τ is the range equivalent of the pulse time (1 μsec = 500 feet) and the other symbols are as used earlier. The equation assumes a matched system ($B\tau$ = unity), but may be extended to systems using short-rise time or pulse compression by substituting for τ the reciprocal of the actual system bandwidth used by the transmitted signal and passed by the receiver. (See [10] for a rigorous derivation and detailed discussion.)

Although there may be other sources of error in the system, a good estimate of error in angle or range rate, derived from radar-position data, may be obtained by considering thermal noise alone. As an approximation, if the position data taken over time t_0 has a standard deviation σ_p, the velocity error will be

$$\sigma_v \cong \frac{\sqrt{3}\,\sigma_p}{t_0} . \tag{24}$$

This equation assumes that the velocity is determined by fitting several raw position readings to a straight line (for a constant-velocity target) or to a line of known curvature (for a target with known acceleration). The equations for angle and range rates become

$$\sigma_{v\theta} = \frac{\sqrt{3}\,\theta}{2\sqrt{t_0^3 f_r (S/N)}} \tag{25}$$

$$\sigma_{vr} = \frac{\sqrt{3}\,\tau}{\sqrt{2t_0^3 f_r (S/N)}} . \tag{26}$$

As an example, for the proposed C-band space tracker at maximum range and for $t_0 = 10$ seconds, the angle-velocity error would be 0.017 mil/sec (17 μrad/sec), while the radial-velocity error would be 380 ft/sec without pulse compression or Doppler measurement.

If radial velocity is measured by observing Doppler shift, much better results are obtained. A relatively crude method involves use of a discriminator system at IF to measure shift of the envelope of the spectrum (noncoherent or single-pulse Doppler measurement). In this case, the frequency error is

$$\sigma_f = \frac{\beta}{\sqrt{(S/N)(f_r/\beta_n)}} = \frac{\beta}{\sqrt{2t_0 f_r (S/N)}} . \tag{27}$$

Applied to the long-pulse UHF tracker, this would yield a Doppler accuracy of 20 cps (corresponding to 23 ft/sec) at maximum range for $t_0 = 10$ seconds. For the C-band tracker, the accuracy would be 316 cps, corresponding to 26 ft/sec. If the system is operated coherently, maintaining consistent phase from pulse to pulse, measurements to within 1 cps are readily achieved, at the expense of ambiguities at the radar-repetition

rate. In the *C*-band tracker, these ambiguities would be at intervals of 4 ft/sec, and would require that velocity be measured to within about one ft/sec before the "vernier" Doppler measurement could be interpreted. This would require about 100 seconds tracking, with the parameters listed, but at the end of that time, the Doppler system would provide data to about 0.1 ft/sec accuracy with independent readings every one second.

Long-Arc Measurements

In position or velocity measurements made over long intervals of time t_0, the importance of thermal-noise errors is reduced, and some of the other terms begin to influence results. The atmospheric terms and other fixed or slowly-varying errors put limits on both accuracy and precision of measurement, and (23)–(27) should be used with great caution for values of t_0 beyond a minute. In addition, the assumptions as to constant velocity in radar coordinates or known acceleration in any coordinate system may not hold to the desired accuracy. There are cases, however, where a long series of measurements can yield estimates of target motion far better than those obtained from brief periods of tracking. Generally, in cases where the laws of motion of the target can be specified exactly, the accuracy of position measurement in all three coordinates can be made to approach that of the best measured coordinate. For example, results on a ballistic missile track of 300 seconds duration have been reported [11] where the rms error in azimuth and elevation data is reduced from 0.01° to 0.0015° (corresponding to reduction in space position error from about 650 to 100 ft) by properly matching the raw data to a set of orbital elements. Accuracy at the midpoint of the track is considerably better.

In measurement of orbital elements of satellites, the same reference shows the results of a 50-second track on Sputnik II, using the AN/FPS-16 (see Table IX). The observed elements agree remarkably well with those given by the Smithsonian Astrophysical Observatory, and are, for the most part, well within the expected variations of the short-term or osculating elements from those averaged over extended periods. In this case, the tracking arc was relatively short and the observed range data could be fit within 10 ft rms by the calculated elements. Over longer arcs, the effectiveness of this method improves markedly. The limiting case is represented by space-probe tracking, where tracks over eight to ten hour periods can be matched to orbital elements involving other bodies in the solar system. In such cases, the position accuracy will be determined almost entirely by the range-bias errors in the system and the knowledge of the equations governing motion of the space vehicle. For this reason, the use of pulse-compression systems to refine precision of range measurement may not be warranted in space tracking, unless extremely long pulses (milliseconds or seconds in duration) are used.

TABLE IX

1957 BETA ONE (SPUTNIK II) ON FEB. 4, 1958

Element	Derived from SO Special Rept. No. 13	Derived from Radar Data
Semi-major axis a, in earth radii	1.106790	1.1070834
Eccentricity, e	0.057406	0.068222497
Inclination i, in degrees	65.29	65.216535
Node, in degrees	217.18	217.23710
Argument perigee, in degrees	20.09	21.564365
Time perigee, in hours, min., sec	$11^h33^m57^s.0240$ UT	$11^h34^m19^s.52149$ UT
Nodal period P, sec	5902.84	5904.31
Time of Node T, hrs, min, sec	$11^h29^m8^s.8454$ UT	$11^h29^m9^s.77019$ UT
Range residual, rms, in ft		9.9687
Elevation residual, rms, degrees		0.02288
Azimuth residual, rms, degrees		0.02238

In discussing space-tracking systems operating over minutes or hours in measuring orbits, it is important to distinguish between those which provide immediate or "real-time" data and long-arc systems. The latter are good for evaluating orbital constants, but cannot provide data for closed-loop guidance and control systems in the usual sense. An error which builds up during the track can be sensed, but the extent of the correction applied by added thrust will not be measured until long after the thrust is applied. The errors in "real-time" measurement may be higher, except for radial position and velocity, but the control thrust may be sensed within seconds or fractions of a second, and the control loop closed within this time. As objects get farther into space, the delay in propagation introduces a time lag which cannot be overcome, and the definition of real-time needs revision. It can be assumed that the time t_0 allowed for measurement can approach the range delay time $t_r = 2R/c$ without compromising system performance in any important respect.

Range and Doppler Trilateration

The inherent accuracy of radial measurements using pulsed radar can best be exploited in long-range trajectory and orbital problems by combining data from three widely-separated radar stations. Each radar makes an independent measurement of range, Doppler, or both, using the reflected echo or the transponder if one is available. Since each range measurement is completed over the path from one station to the target, no high-performance ground communication links are required and propogation errors are minimized. Having made the measurement and placed it in digital form with a time tag attached to represent the mid-point or end of the measurement period t_0, the range or Doppler-velocity data may be transmitted without distortion to a central point. Here it is combined with data from at least two other stations to provide complete three-co-

ordinate output data. Azimuth and elevation data may be carried along for use at short tracking ranges or in case one station's range data is lost.

The error involved in three-station trilateration measurements can be calculated exactly if the individual station range errors and the over-all station and target geometry are known. However, the range errors are known only statistically, and the expected rms error can only be estimated to within a factor of two for practical systems. It is therefore useful to use approximate methods of evaluating system error and neglect the finer points of analysis involved in the rigorous studies on the subject. A two-dimensional case will be discussed and extended to three-dimensional systems by simple geometrical operations. Fig. 15 shows the geometry of the basic measurement for the conventional radar case and for the trilateration case with target range several times the baseline length. The approximate errors in x and y may be expressed in terms of components due to range, range difference, angle and station survey error as shown in Table X. It is assumed that the survey error σ_s applies to both x and y coordinates of the station with respect to the reference system, so that the baseline length is in error by $\sigma_{\Delta s} \cong \sqrt{2}\sigma_s$, its center by $\sigma_s/\sqrt{2}$, and its orientation (with respect to $\theta = 0$) by $\sigma_{\Delta s}/B$. Since there may be systematic errors present in both range and station survey, which are the same at both stations, the difference terms $\sigma_{\Delta s}$ and $\sigma_{\Delta r}$ are introduced to represent the uncorrelated portions of these errors.

It can be seen that the trilateration case is equivalent to a range-angle measurement with a system-range error equal to $1/\sqrt{2}$ times that of the individual station, and a system-angle error in radians equal to $1/B'$ times the error in range difference, where $B' = B \cos\theta$ is the projected length of the baseline normal to the direction of the target. If the range and station survey errors at the two stations are independent, then the error components are approximately as follows (for $\theta \neq 0$):

Component	x error	y error
Range error σ_r	$\sqrt{2}\,\frac{\bar{R}}{B}\,\sigma_r$	$\sqrt{2}\,\frac{\bar{R}}{B}\,\sigma_r \tan\theta$
Station error σ_s	$\sqrt{2}\,\frac{\bar{R}}{B}\,\sigma_s$	$\sqrt{2}\,\frac{\bar{R}}{B}\,\sigma_s \tan\theta$

Similar relationships apply between radial velocity measurements and x and y components of velocity, if the position triangle is already known.

The tracking-error curves (Figs. 13 and 14) provide most of the data needed for calculating performance of the several systems discussed. As an initial example, assume that two AN/FPQ-6 radars are operated with a separation of 50 miles. The equivalent system-angle accuracy (for targets nearly at right angles to the baseline) will be 14 ft/300,000 ft, or about 50 μrad (0.05 mil), and the system precision about 10 μrad. This is no better than the performance of the same radars as range-angle trackers. If coherent Doppler measurements are made, the angular velocity component may be measured to $\sigma_r/B = 0.14/300{,}000$, or about 0.5 μrad/sec. This is a good deal better than the performance with differentiated angle data, unless smoothed over many seconds of track.

For longer ranges when beacons or long-range echo trackers are used, the baseline should be extended to approach the diameter of the earth. A practical limit may be set at about 5000 miles. The predominant systematic error, using any but the UHF radar, will now be in station survey, and may amount to about 100 ft using present mapping procedures. The equivalent angle accuracy of the system would therefore be 140/30,000,000 ft, or about 5 μrad. Better position accuracy will be available as mapping techniques are improved. Fortunately, the Doppler measurement accuracy will not be degraded and will approach 0.005 μrad/sec for distant targets. At the range of the moon, this would give

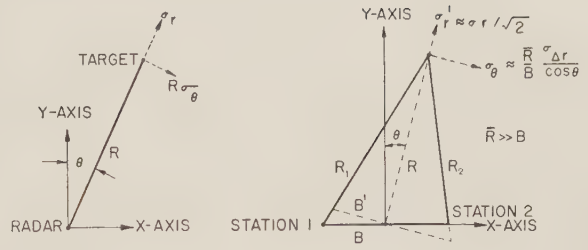

(a) (b)

Fig. 15—Geometry of measurements in two dimensions. (a) Conventional radar solution. (b) Trilateration solution.

TABLE X
COMPARISON OF ERROR COMPONENTS

Component	x error	y error
Radar case		
Range error σ_r	$\sigma_r \sin\theta$	$\sigma_r \cos\theta$
Angle error σ_θ	$R\sigma_\theta \cos\theta$	$R\sigma_\theta \sin\theta$
Station error σ_s	σ_s	σ_s
Trilateration case		
Range error σ_r	$\frac{\sigma_r}{\sqrt{2}} \sin\theta$	$\frac{\sigma_r}{\sqrt{2}} \cos\theta$
Range difference error $\sigma_{\Delta r}$	$\frac{\bar{R}}{B}\,\sigma_{\Delta r}$	$\frac{\bar{R}}{B}\,\sigma_{\Delta r} \tan\theta$
Station error σ_s	$\sigma_s/\sqrt{2}$	$\sigma_s/\sqrt{2}$
Station difference error	$\frac{\bar{R}}{B}\,\sigma_{\Delta s}$	$\frac{\bar{R}}{B}\,\sigma_{\Delta s} \tan\theta$

Assumptions:
$\bar{R} \gg B$
σ_s represents equal but uncorrelated errors in the x and y coordinates, θ in radians,
σ_r equal for two stations.

an accuracy of about six ft/sec in a direction normal to the radar line of sight with a measurement time of one second or less.

The approximate triangulation errors given for two-dimensional operation are readily extended to three dimensions, where a third station is available and removed from the baseline which joins the first two. A simple, approximate way of estimating the results in the third coordinate is to establish a reference plane through the third station and the target and normal to the plane which includes the first baseline B_1 and the target (Fig. 16). The second baseline B_2 may then be drawn at right angles to the first, connecting the third station with an effective station which represents the combined measurement of the original pair. The z-axis error components may then be estimated as the range-difference and station-difference errors multiplied by $\overline{R}/(B_2 \cos\theta)$ where θ is the angle between the target and the normal at the midpoint of B_2.

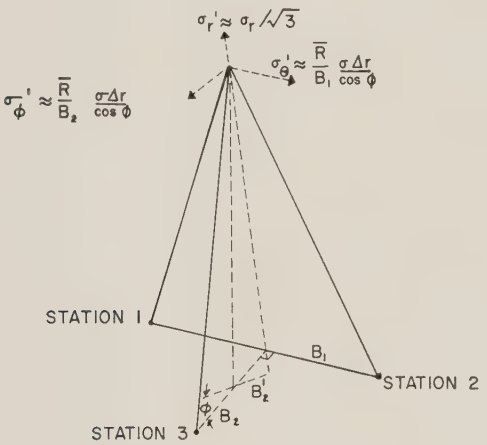

Fig. 16—Extension of trilateration solution to three dimensions.

Target Identification

Before leaving the discussion of radar applications in space tracking, mention should be made of the ability of tracking radar to provide information on target size, shape and motion. Given a record of echo-signal strength taken over a period of a minute or more, it has proven possible to measure, in certain cases, the gross dimensions and the rate and axis of rotation of targets moving through space. Those objects which rotate with periods shorter than the track duration are easiest to evaluate, but stabilized or slowly-tumbling objects may also be measured if long tracks or repeated tracks several hours apart are available.

The general procedure for analyzing a signal-strength record is as follows:

1) Major features in the record are selected and checked for periodicity.
2) Using a crude estimate of target shape, the signal strength and tracking coordinate data are analyzed to relate time to aspect angle, based on an observed constant tumbling rate modified by radar-target geometry.
3) The aspect-angle data is used to establish the widths and separation of lobes in the signal-strength record, and from this information certain dimensions of the object are estimated.
4) Absolute cross-section data is used to estimate other dimensions of the object.
5) All data is reviewed in detail and checked against possible models of the target and its rotational motion to refine the model and establish a consistent explanation for the observed signal-strength variation.

The relationships in Table XI show the major echo characteristics of simple shapes. The application to actual UHF and C-band tracking data on Sputnik II is given in [12] and [13].

Fig. 17 shows the UHF cross-section plot against time, with an aspect angle scale applied. The major features identified by letter correspond to the following:

A) Major lobe, width $2\Delta_a = 1.8°$, peak $\sigma_a = 250$ m², indicating a length $L_a = 70$ ft.
B) Repetitive lobing, width $\Delta_b = 1.0°$, peak $\sigma_b = 30$ m², indicating two equal-amplitude, broad-lobed reflecting elements with peak reflectivity 30° off mainlobe, separated by $L_b = 63$ ft.
C) Shoulders on mainlobe, width Δ_c between 1.0 and 4.0°, peak $\sigma_c = 50$ m², indicating two or more elements separated by L_c between 16 and 63 ft.
D) Lobes early in record, widths Δ_d between 1.0 and 4.0°, peak $\sigma_d = 25$ m², indicating two or more elements with peak reflectivity 30° from mainlobe and separated by L_d between 16 and 63 ft.
E) Lobes late in record, width $\Delta_e = 10°$, peak $\sigma_e = 10$ m², representing extension of one element of the B pattern beyond the other, and corresponding to a length L_e of about 6 ft.

Fig. 18 shows a model which would explain these five features, with two major areas of reflection plus a small corner reflector at one end of a 70-ft object. Detailed discussions of the basis for this model are given in the references. Although target descriptions from radar data are necessarily uncertain and approximate, they are available at any tracking range and may offer data not otherwise available by any means. Similar procedures for evaluating target motion from transponder or telemetry signal strength records are described in [14].

V. Comparison of Radar with Other Instrumentation Systems

Classification of Systems

Before discussing in detail any of the systems which share with radar the field of trajectory measurement, it is useful to consider in general the various methods of position measurement, and to classify systems with

TABLE XI
ECHO CHARACTERISTICS OF SIMPLE SHAPES

Shape	σ_{max}	Major lobe width 2Δ	Number of lobes	σ_{min}
Sphere	πr^2	2π	1	πr^2
Ellipsoid	πa^2	$\approx \frac{b}{a}$	2	$\pi \frac{b^4}{a^2}$
Dipole	$0.9\lambda^2$	π	2	Null
Cylinder	$\frac{2\pi r L^2}{\lambda}$	$\frac{\lambda}{L}$	$\frac{8L}{\lambda}$	Null
Flat plate	$\frac{4\pi A^2}{\lambda^2}$	$\frac{\lambda}{L}$	$\frac{8L}{\lambda}$	Null
Corner reflector	$\left[\frac{4}{3}\pi\frac{a^4}{\lambda^2}\right.$ $\left.+4 \text{ flat plate lobes}\right]$	$\frac{\pi}{4}$	4	—

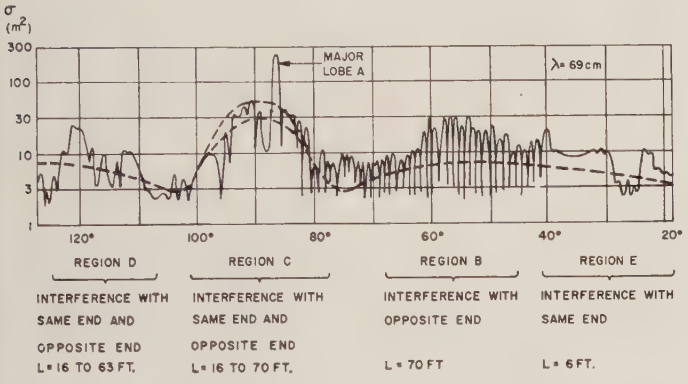

Fig. 17—Comparison of Sputnik II reflection with corner reflector.

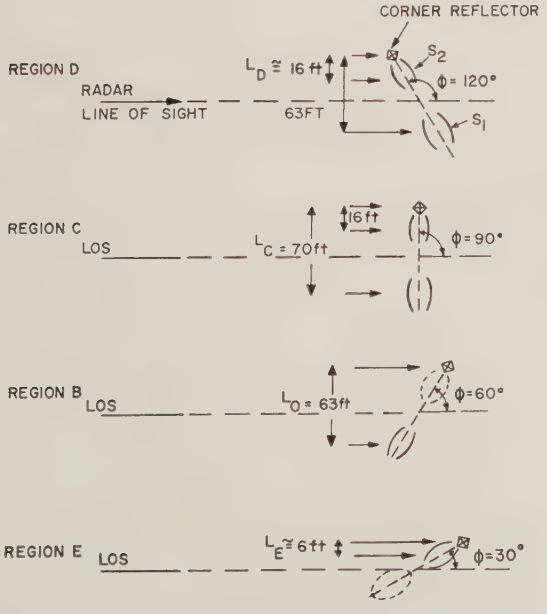

Fig. 18—Location of reflecting surfaces on Sputnik II.

respect to their major characteristics will serve to distinguish between major types of measurement systems:

1) *Frequency:* optical, microwave, or radio. (Infrared and sonic will not be discussed here, and a division between radio and microwave at about 1000 Mc will be used for convenience.)
2) *Coordinate Measured:* angle, range, or a combination of both.
3) *Field of View:* wide (fixed field) or narrow (tracking) angular field of view.
4) *Sensitivity to Motion:* position sensitive, velocity sensitive, or combination of both.
5) *Signal Source:* passive system (receives from target, no transmission) or active (transmits and receives reply).

With the characteristics given above, there are 108 possible combinations that could be considered, but only 15 of these are of immediate interest. The remaining 93 systems can be excluded for various reasons (such as optical systems sensing velocity directly, which are of value to astronomy but too coarse for missile instrumentation). In some cases, the rejected combinations (such as optical ranging systems) appear to merit further investigation for possible future use, but such considerations are beyond the scope of this paper. The 15 systems chosen for comparison are shown in Table XII. Here the five major characteristics are related to practical applications, with specific systems (*e.g.*, AZUSA) given as examples of the technique applicable.

Characteristics of Various Systems

Whenever a choice is made for one of the major characteristics, certain advantages and disadvantages must follow. Tables XIII through XVII outline the chief consequences of choosing among the optional characteristics discussed above. The "right" choice for a particular situation (or choices where more than one system will be used) could be made by assigning a weighting factor to each point given and looking for the system with maximum positive score. No attempt will be made here to assign such factors, but some of the points on which specific information is available will be discussed in more detail and present systems compared in the light of this information.

Propagation Limitations

A tremendous amount of material has been published on the subject of propagation errors and their effects on instrumentation. A survey of much of this material leads to the following conclusions (see [4], [15] and [16] for more detailed discussion and bibliography):

1) Instruments operating over paths longer than 10 miles may make measurements to an accuracy of about 0.05 mil or 2 ft, provided corrections are made for local surface conditions.

TABLE XII

CLASSIFICATION OF FEASIBLE INSTRUMENTATION SYSTEMS

Frequency	Coordinate	Field of view	Sensitivity to motion	Signal source	System example
Optical	Angle	Narrow	Position	Passive	Tracking Theodolite
Optical	Angle	Wide	Position	Passive	Plate Camera
Microwave	Angle	Narrow	Position	Passive	"Radar Theodolite"
Microwave	Angle	Wide	Position	Passive	(Angle portion of AZUSA)
Microwave	Range	Narrow	Position	Active	(Use of 3 radars for ranging)
Microwave	Range	Wide	Position	Active	MIRAN
Microwave	Combination	Narrow	Position	Active	Tracking Radar
Microwave	Combination	Wide	Position	Active	AZUSA
Microwave	Combination	Narrow	Combination	Active	Doppler Tracking Radar
Microwave	Combination	Wide	Combination	Active	(Certain guidance systems)
Radio	Angle	Wide	Position	Passive	COTAR (angles only)
Radio	Range	Wide	Position	Active	DME, LORAN, COTAR (ranging)
Radio	Range	Wide	Velocity	Active	DOVAP
Radio	Range	Wide	Combination	Active	DORAN
Radio	Combination	Wide	Position	Active	COTAR (complete)

TABLE XIII

CHOICE OF FREQUENCY

Choice	Advantages	Disadvantages
Optical	Small, simple equipment High component reliability Proven techniques No frequency allocation problems Attitude and event data available High resolution	Limited range Weather limited Film processing and reading are time consuming and require additional manpower No range data available
Microwave	Medium resolution All-weather use No ionospheric effect Frequencies available Range data available Long-range capability Data in electrical form Small missile antennas	Large complex equipment Relatively new techniques used
Radio	Relatively small, simple and reliable All-weather use Range data available Long-range capability Data in electrical form	Poor resolution Ionospheric effects Frequency allocation difficult New techniques used Missile antenna problems

TABLE XIV

CHOICE OF COORDINATES TO BE MEASURED

Choice	Advantages	Disadvantages
Angle triangulation	Passive system may be used Simple equipment	Geometrical dilution 2 or more stations required Precise timing required Data reduction requires complex processes which are time-consuming and costly in manpower and machine capacity
Range trilateration	Small antennas may be used No mechanical tracking required Minimum propagation error	Geometrical dilution 3 or more stations required Precise timing and wideband communications may be required Data reduction problem (as with angle triangulation) Transponder required
Combination range plus angle	Only one station No precise timing or unusual communications No geometrical dilution except vs range Simple reduction	Equipment is often larger and more complex than required for angle measurement alone

TABLE XV

CHOICE OF FIELD OF VIEW

Choice	Advantages	Disadvantages
Narrow (tracking)	High resolution High antenna gain or magnification Less interference Less multipath problems Shaft data may be in electrical form	Precise mount required Servo noise and tracking errors present
Wide (fixed)	Mechanically simple No tracking or sevo noise	Antenna gain or magnification is low No resolution in angle (electronic system) Susceptible to interference Multipath problem (electronic system) Film or plate reading (optical system)

TABLE XVI

CHOICE OF SENSITIVITY TO MOTION

Choice	Advantages	Disadvantages
Position sensing	Continuous data not necessary Simple recording	Relatively poor velocity data
Velocity sensing (radial)	Velocity data good	Continuous data necessary to integrate position Complex recording or integration device needed 3 or more stations (to get all components)
Combination	Good velocity (radial) Good position without necessity for continuous data	Complex system 3 stations needed to get good velocity in all components

TABLE XVII
CHOICE OF SIGNAL SOURCE

Choice	Advantages	Disadvantages
Passive (receiving only)	Simple Low-power consumption	Source of radiation in target required Accurate range or Doppler-velocity data not available
Active (transmits and receives response)	Range data available Doppler velocity data available May also operate without transponder	More complex High power required for long range if radar is used without beacon

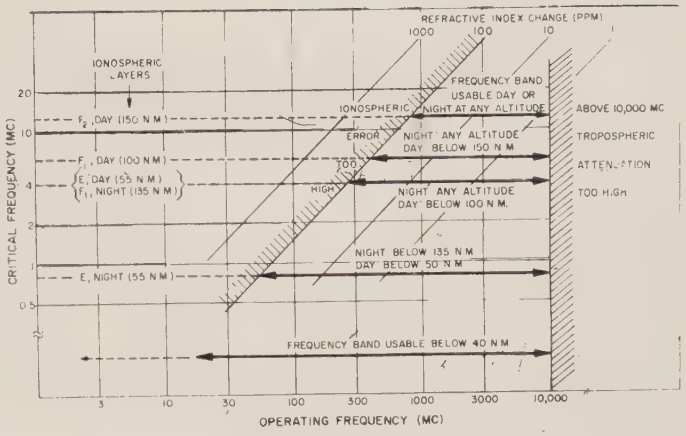

Fig. 19—Frequencies usable for precise instrumentation through ionosphere.

2) Overdetermination by several independent instruments can be used to reduce this propagation error still further.

3) Operating frequencies above 1000 Mc are required to assure 0.1 mil and 100-ft accuracy for targets in or beyond the ionosphere. Errors increase with decreasing frequency, and systems operating at or below 100 Mc are subject to errors of the order of one part per thousand for targets above 50 miles.

4) Only systems operating between 1000 and 6000 Mc can be considered for all-weather operation at ranges extending from 10 miles to beyond 100 miles.

The limitations imposed by tropospheric attenuation and ionospheric refraction are summarized in Fig. 19, which shows the frequency bands usable for precise instrumentation in various altitude regions under daytime and nighttime ionospheric conditions. Critical frequency (the frequency at which total reflection occurs even at normal incidence) is a function of electron density. The refractive-index change is proportional to the square of the ratio of critical frequency to operating frequency. Shown in Fig. 19 are typical values of critical frequency in each ionospheric layer and the operating frequency band satisfactory for operation within or beyond each layer. The criterion used was that the refractive-index change (*i.e.*, the error in incremental position measurement) should not exceed 100 parts per million. This criterion, together with an upper limit of 10,000 Mc due to tropospheric absorption and a maximum critical frequency of 10–14 Mc, defines an operating band of 1000 to 10,000 Mc for long-range precision systems. If the refractive-index change is to be limited to 10 parts per million, the usable frequency band is restricted to 3000 to 10,000 Mc. For operation at low altitudes and/or at night, the lower-frequency limits can be reduced to the extent shown in Fig. 19.

Unpredictable variations in propagation conditions set the ultimate limit to both antenna gain and measurement accuracy. The equation derived by Muchmore and Wheelon [16] and verified approximately by experiments over short tropospheric paths [17], [18], gives the mean square phase variation in propagation through the atmosphere as

$$\overline{\alpha_t^2} \cong \frac{8\pi^2 L_0 L \overline{(\Delta N)^2} \times 10^{-12}}{\lambda^2}, \tag{28}$$

where L_0 is the scale length of the propagation anomalies and $\overline{(\Delta N)^2}$ is the mean square anomaly in N units, or units of $(n-1)\times 10^6$ where n is the refractive index. For the ionosphere, Colin [19] has rewritten (28) in the form

$$\overline{\alpha_i^2} = \frac{2\pi^2 L_0 L \lambda^2}{\lambda_n{}^4} \left(\frac{\overline{\Delta N_e}}{N_e} \right)^2, \tag{29}$$

where λ_n is the plasma wavelength, N_e the ionospheric-electron density, and ΔN_e the variation in electron density. Typical values listed by Colin are

	Troposphere	Ionosphere
L_0	200 ft	5 km (occasionally 100 km)
L (vertical ray)	20,000 ft	65 km
$\overline{(\Delta N)^2}$ (clear day)	0.25	—
$\overline{(\Delta N_e/N_e)^2}$	—	3×10^{-4}

leading to the following values for vertical paths:

$$\overline{\alpha_t^2} = \frac{7.34 \times 10^{-2}}{\lambda^2} \qquad \text{(tropospheric)} \tag{30}$$

and

$$\overline{\alpha_t^2} = 2.51 \times 10^{-4} \lambda^2 \qquad \text{(ionospheric)}, \tag{31}$$

where λ is in cm. At elevations near 10°, the mean-square-tropospheric component will be six times as great and the ionospheric perhaps four times as great. For cloudy conditions, $\overline{(\Delta N^2)}$ and L_0 may each reach 1000, increasing $\overline{(\alpha_t)^2}$ by a factor of 20,000. The resulting values of two-way phase variation, converted to equivalent range variation σ_r in feet, are shown in Fig. 20.

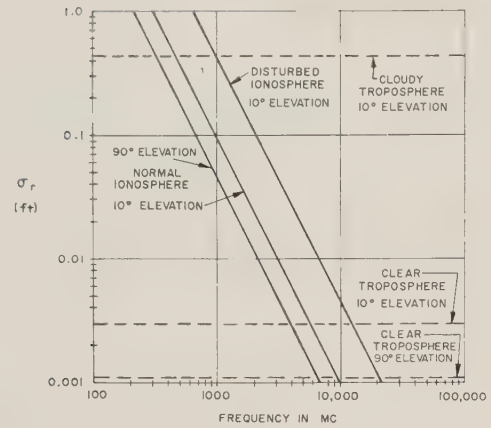

Fig. 20—Range error due to atmospheric fluctuations.

Note that the ionospheric component is appreciable, even at *C* band, and that the worst case (cumulus clouds or thunder storms) causes errors of about one-half foot at all frequencies. These results are particularly important in error analysis of baseline systems, as they set a lower limit an error which is independent of the instrumental precision of the system. Since tropospheric errors will be essentially uncorrelated over paths separated several hundred feet in clear air or several thousand feet under cloudy conditions, the errors shown in Fig. 20 may be considered lower limits to σ_r or $\sigma_{\Delta r}/\sqrt{2}$ in Table X. Ionospheric errors will be uncorrelated for paths spaced tens of miles apart, and will, therefore, affect baseline systems longer than a few miles. In addition to the effects listed, there may be large-amplitude irregularities of very long scale length in both ionosphere and troposphere which will become important where data is smoothed over long tracking periods. The lower limits of error for various baseline lengths are shown in Table XVIII, with the unsmoothed Doppler velocity errors based upon an assumed drift rate of 50 ft/sec for tropospheric anomalies and 1000 ft/sec for ionospheric anomalies (average error periods between 4 sec and 20 sec for both troposphere and ionosphere). It is clear that disturbed conditions of either portion of the atmosphere will drastically affect any of the systems discussed. Only the use of a very long baseline and a frequency above 3000 Mc can provide velocity accuracies approaching one ft/sec in all coordinates at 20,000 miles range.

Factors Favoring Pulsed Radar

The foregoing discussion indicates that pulsed radar should be useful in space-range instrumentation, at least to the same extent that it serves the existing missile ranges. In space work, the use of large, high-gain antennas is mandatory, and at present, the only suitable antennas are of the tracking type. The requirement for low-input noise favors the continued use of such antennas, which require only one maser amplifier (three for monopulse systems) as contrasted with multiple amplifiers for the low-noise electronic-scan types. The required reflector tolerance and pointing accuracy for achieving high gain necessitates the same mechanical design techniques which have been used in the past for precision-tracking radars. Several such radars deployed on two- to four-thousand mile baselines can outperform any of the other schemes described for position and velocity measurements at long range.

Applications Unfavorable to Pulsed Radar

There remain certain applications and requirements in missile and space instrumentation for which pulsed radars are not well suited. At launch, there is a need for very accurate tracking on a well-defined portion of the missile, not subject to disturbing effects of ground re-

TABLE XVIII
TYPICAL VELOCITY ERRORS DUE TO ATMOSPHERIC FLUCTUATION

Conditions	Baseline B (mi.)	Standard Deviation in lateral velocity					
		$\sigma_{\dot\theta}$(μrad/sec)		Equivalent linear vel error (ft/sec)			
				1000 mi range		20,000 mi range	
		L band	*C* band	*L* band	*C* band	*L* band	*C* band
Clear, normal ionosphere, 90° elevation	1	4.0	0.35	25	2.0	500	40
	10	0.7	0.035	4.2	0.2	84	4
	100	0.07	0.0035	0.42	0.02	8.4	0.4
	1000	0.007	0.00035	0.042	0.002	0.84	0.04
Clear, normal ionosphere, 10° elevation	1	8.0	1.1	50	7.0	1000	140
	10	1.4	0.11	8.4	0.7	170	14
	100	0.14	0.011	0.84	0.07	17	1.4
	1000	0.014	0.0011	0.084	0.007	1.7	0.14
Clear, disturbed ionosphere, 10° elevation	1	3.3	1.1	20	7.0	400	140
	10	3.3	0.11	20	7.0	400	14
	100	0.6	0.02	3.5	0.11	70	2.2
	1000	0.06	0.002	0.35	0.011	7.0	0.22
Cloudy, normal ionosphere, 10° elevation	1	100	100	600	600	12,000	12,000
	10	10	10	60	60	1200	1200
	100	1.1	1	6.5	6.0	130	120
	1000	0.11	0.1	0.65	0.6	13	12

NOTE: Velocity error based on use of any smoothing time less than fluctuation period of atmosphere, 4–20 sec.

flections, clutter or glint. Optical and infra-red devices appear advantageous here. During powered flight, exact measurement of attitude and roll, to the order of one degree in angle, requires optical measurement. Throughout the flight, wide-bandwidth command and telemetry channels are used, which do not lend themselves to use of the low-rate pulsed carrier provided by the radar. Although the radar antenna may provide a high-gain transmission path to the vehicle, separate antennas have the advantage of reducing mutual interference. Furthermore, the relative ease with which low-power solid-state CW oscillators can be designed is favorable to use of command, telemetry and measurement systems operating on the CW carrier. With the present state of the art, and in cases where vehicle weight is of extreme importance, it may well prove more economical to build duplicate ground antennas for separated CW transmitter and receivers.

Ultimately, however, the inherent flexibility and economy of the pulsed radar should make it a prime instrument for space research in passive and active tracking of vehicles and active probing of the surfaces of planets.

Appendix

Comparison of AN/FPS-16 and AN/FPQ-6 Parameters

	AN/FPS-16	*AN/FPQ-6*
Antenna size	12 ft	29-ft Cassegrainian
Antenna feed	4-horn monopulse	5-horn monopulse
Antenna beamwidth	1.2°	0.4°
Antenna gain	44 db	51 db
Antenna polarization	Vertical	Vertical, circular
Pedestal drive	Electric	Hydraulic
Antenna-pedestal rotation-azimuth elevation	Continuous −10° to +190°	Continuous −2° to +182°
Antenna-pedestal weight	16,000 lbs	60,000 lbs
Azimuth bearing	Ball	Hydrostatic
Angle-servo bandwidth	0.25 to 5 cps	0.5 to 5 cps
Angle-tracking rate-azimuth elevation	40°/sec 30°/sec	28°/sec 28°/sec
Angle-tracking precision	0.1 mil rms	0.05 mil rms
Frequency	5400–5900 Mc	5400–5900 Mc
Power output-fixed tunable	1 Mw ¼ Mw	3 Mw
Pulse-repetition frequency	Various 341–1707 PPS	160–640 basic, 1707 max
Pulse duration	¼, ½, 1 μsec	¼, ½, 1 and 2.4 μsec
Pulse coding	Up to 5 pulses with duty cycle limits	Up to 5 pulses with duty cycle limits
Receiver noise figure	11 db	8 db
Receiver IF	30 Mc	30 Mc
Receiver bandwidth	Switch with pulse width	1.2 to 1.6/pulse width
Receiver dynamic range	93 db with S.T.C.	110 db with programming
Range-tracking capability	500 nautical miles	32,000 nautical miles Continuous unambiguous
Range-tracking granularity	1 yd	2 yds
Acquisition features	Scan generator variable rep. rates	Scan generator Video integrator "C" scope and joy stick Pulse-coding capability "Aux-track" Multiple-gate array Digital-ranging system
Output—range	20-bit 2-speed binary, dc analog pot	25-bit single-speed binary
Output—angle	17-bit 2-speed binary 16:1 speed synchros Sine-cosine pots	19-bit binary with 8-bit dynamic lag correction 16:1 speed synchros Sine-cosine pots

Bibliography

[1] D. R. Rhodes, "Introduction to Monopulse," McGraw-Hill Book Co., Inc., New York, N. Y.; 1959.

[2] D. K. Barton, "Accuracy of a monopulse radar," *Proc. 3rd Natl. Convention on Military Electronics*, Washington, D. C., June 29-July 1, 1959; pp. 179–186.

[3] D. K. Barton, "Final Report, Instrumentation Radar AN/FPS-16 (XN-2), Evaluation and Analysis of Radar Performance," RCA, Moorestown, N. J., Contract DA36-034-ORD-151, AD212 125; 1957.

[4] D. K. Barton, "Final Report, Instrumentation Radar AN /FPS-16 (XN-2)," RCA, Moorestown, N. J., Contract NOas 55–869c, AD 250 500; 1959.

[5] N. S. Greenberg, "Extending the Range of Radar Beacon Tracking for Lunar Probes," presented at American Astronautical Soc. Lunar Flight Symp., New York, N. Y.; December 27, 1960.

[6] W. W. Ward, "An Account of the Factors that are Important in Tracking of Space Vehicles by Means of Radar," presented at 5th Natl. Symp. on Space Electronics and Telemetry, Washington, D. C.; September 19–21, 1960.

[7] D. C. Hogg and W. W. Mumford, "The effective noise temperature of the sky," *Microwave J.*, vol. 3, pp. 80–84; March, 1960.

[8] F. Sterzer and D. E. Nelson, "Tunnel-diode microwave oscillators," Proc. IRE, vol. 49, pp. 744–753; April, 1961.

[9] M. J. E. Golay, "Velocity of light and measurement of interplanetary distances," *Science*, vol. 131, pp. 31–32; January 1, 1960.

[10] M. I. Skolnik, "Theoretical accuracy of radar measurement," IRE Trans. on Aeronautical and Navigational Electronics, vol. ANE-7, pp. 123–129; December, 1960.

[11] S. Shucker and R. Lieber, "Comparison of short ARC tracking systems for orbital determination," *Proc. 5th Natl. Convention Military Electronics*, Washington, D. C., June 26-28, 1961; pp. 285–301.

[12] D. K. Barton, "Comparison of UHF and *C*-Band Radar Signature Data on Sputnik II," to be published.

[13] D. K. Barton, "Sputnik II as observed by *C*-band radar," 1959 IRE National Convention Record, pt. 5, pp. 67–73.

[14] W. C. Pilkington, "Vehicle motions as inferred from radio-signal strength records," in "Avionics Research, Satellites and Problems of Long Range Detection and Tracking," Pergamon Press, New York, N. Y.; 1960.

[15] G. H. Millman, "Atmospheric effects on VHF and UHF propagation," Proc. IRE, vol. 46, pp. 1492–1501; August, 1958.

[16] R. B. Muchmore and A. D. Wheelon, "Line-of-sight propagation," Proc. IRE, vol. 43, pp. 1437–1458; October, 1955.

[17] J. W. Herbstreit and M. C. Thompson, "Measurements of the phase of radio waves received over transmission paths with electrical lengths varying as a result of atmospheric turbulence," Proc. IRE, vol. 43, pp. 1391–1401; October, 1955.

[18] A. P. Deam and B. M. Fannin, "Phase-difference variations in 9350-megacycle radio signals arriving at spaced antennas," Proc. IRE, vol. 43, pp. 1402–1404; October, 1955.

[19] L. Colin, "The effects of atmospherically induced phase scintillations," pt. IX of final rept., "Upper Atmosphere Clutter Research, Part XIII: Effects of the Atmosphere on Radar Resolution and Accuracy," Stanford Res. Inst., Menlo Park, Calif., RADC-TR-60-44, AD 238 407; April, 1960.

Effects of Atmospheric Turbulence on Optical Instrumentation*

R. A. BECKER†

Summary—The results of research on optical turbulence at White Sands Missile Range are presented. It has been shown that elevating camera stations 33 feet above ground level can yield nearly a threefold increase in optical resolution during periods of atmospheric turbulence. Early research postulated the existence of thermal-induced air lenses as the cause of optical-turbulence effects. Recent research has shown that air lenses can account for most of the observed effects. The "prism" concept of turbulence appears to be unnecessary for explaining turbulence-induced image motion.

The dependence of the optical effects of turbulence upon exposure time and aperture size are discussed qualitatively. The source of optical turbulence in the atmosphere and a method of measuring the turbulence-generating potential of various terrain surfaces are described on the basis of micrometeorology.

This research has been limited to an investigation of optical turbulence during the period from sunrise to sunset. However, many of the results apply to the nighttime turbulence encountered by astronomers.

I. Introduction

EFFORTS to take advantage of the excellent information capacity of optical instrumentation are often frustrated by the presence of optical turbulence in the lower atmosphere. A photographic telescope with a system capability for 40 lines/mm resolution may yield only one-fifth that resolution in the field, especially during midday operation. Furthermore, turbulence-induced random motions of the optical image dilute the accuracy of pointing data sought from the optical instrument. These motions observed in the focal plane amount to apparent angular displacement of the target in object space. The amplitudes of these apparent displacements, in extreme cases, may run as high as 0.5 minute of arc.

The optical effects of atmospheric turbulence have been observed as long as Man has noticed the twinkling of stars. Over the centuries astronomers have had to contend with dancing and blurred images when the "seeing" was poor. However, serious investigation of optical turbulence in the atmosphere during daylight hours has been conducted only during the past two decades. Nearly all of this recent work has resulted from optical instrumentation problems associated with missile flight testing.

II. Early Research at White Sands Missile Range

It was observed during the early years of long-range missile photography at White Sands Missile Range (WSMR) that sharp images of missiles were seldom obtained at long slant ranges during daylight hours with the exception of the period shortly after sunrise and shortly before sunset. Although pitch and yaw data on V-2 rockets were obtained photographically at heights up to 100 miles during early morning and late afternoon shoots, the same data were obtained only to heights of 10 to 20 miles during midday operations. The images recorded during midday were generally blurry and of low contrast (see Fig. 1). Quite frequently two or three closely-spaced images of the missile appeared on the same photograph. These multiple images were at first attributed to vibration in the optical system or camera. However, it was later recognized that they were the result of an out-of-focus condition arising from either the optical defocusing power of optical turbulence in the atmosphere or from the inability to critically focus a telescope when observing a distant target through heavy turbulence.

Attempts to locate a focal plane under conditions of optical turbulence revealed the presence of good images in planes other than the normal focal plane. These images, called "transient images," were of short duration and manifested some degree of periodicity. G. Neeland and R. Roush,[1] under the direction of C. W. Tombaugh, investigated such images under a number of conditions and postulated that optical turbulence might be explained as "air lenses" of various sizes and optical power passing in front of the telescope objective. They demonstrated that thermal inhomogeneities in

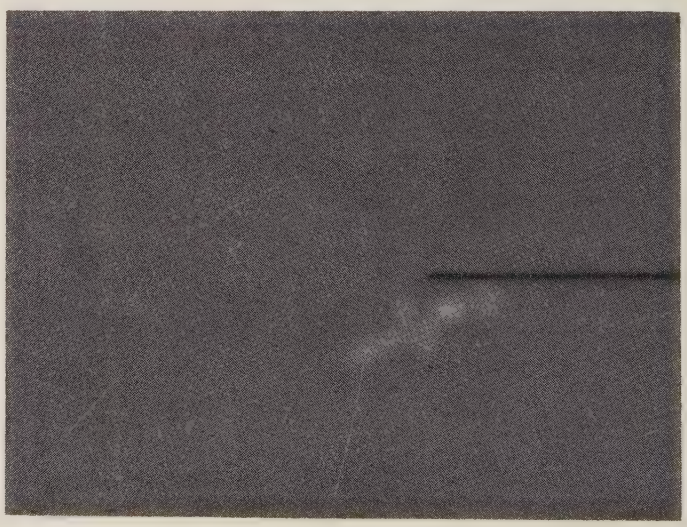

Fig. 1—Image of missile (near right-hand crosshair) shows blurring effect of optical turbulence. This photograph was taken with a 300-inch focal length lens. Focal lengths under 20 inches generally do not give enough magnification to detect effects of turbulence.

* Received by the PGMIL, July 17, 1961.

† Jet Propulsion Laboratory, Pasadena, Calif. Formerly with Optical Systems Branch, Range Instrumentation Dev. Div., Integrated Range Mission, White Sands Missile Range, N. Mex.

[1] G. Neeland and R. Roush, "Atmospheric Turbulence," Ballistic Res. Lab., Aberdeen Proving Ground, Md., Tech. Note No. 514; June, 1951. The work of Neeland and Roush was done at WSMR which, at that time, was operated by Aberdeen Proving Ground.

the atmosphere, rather than wind currents, are responsible for optical turbulence and that turbulence near the telescope objective reduces image quality more than turbulence more distant from the telescope. They were also aware that the type of effect which turbulence produced on the image was related to the relative sizes of the telscope aperture and the turbulence air lenses (turbulence cell size). The duration of most of the transient images reported by Neeland and Roush was about 0.2 seconds; few were longer than that and some were as short as 0.05 seconds. Since they found fewer transient images at large distances from the normal focal plane, they concluded that there are fewer powerful thermal lenses than there are weaker ones in a given period of time.

At this same time, E. P. Martz, Jr.[2] studied the image improvement which might be realized by elevating either the camera, the target, or both above the ground during periods of optical turbulence. He found that elevating the camera above ground gave more improvement than elevating the target and that the greatest improvement came when both target and camera were elevated. Martz's tests were conducted from open steel-framework observation towers over desert terrain typical of WSMR. He was limited in height to 35 feet above ground level. His data indicates that the resolution capability of an optical system may be increased by approximately three times when elevating the lens from a height of 3 feet to 33 feet. However, the resolution obtainable from the top of the tower in the presence of turbulence is only, perhaps, half that which might be obtained if there were no turbulence.

As a result of Martz's work, nearly all camera locations at WSMR are elevated above ground level. Fig. 2 is a photograph of a concrete tower station constructed to rigidly support a tracking cinetheodolite camera approximately 25 feet above the surrounding terrain. Dirt mounds and roofs of small instrumentation buildings are also used to elevate cameras above the region of greatest turbulence.

Fig. 2—Concrete tower station. Roof sections slide down inclined supports to allow tracking camera a full hemispherical view of the sky.

One might expect that the concrete towers, through the effects of solar heating, would become turbulence generators and defeat the purpose of elevating the cinetheodolite cameras. An investigation was conducted in 1958 by J. A. Roth[3] to determine whether or not the resolution obtainable from the top of the towers was as good as that recorded with a camera supported at the same height by a crane approximately 25 feet away from the tower. Roth reports that "no evidence was found that the concrete towers act as turbulence generators." He also investigated the improvement in resolution resulting from the location of a camera at the top of a barren dirt mound 15 feet high (total camera height equals 21 feet), as compared with a camera 5 feet above terrain level near the base of the mound. At midday, the resolution recorded at the top of the mound was nearly twice that recorded at the lower level.

III. Present Research Program

The present research program has a fourfold objective:

1) To investigate the optical effects of turbulence through experimentation with single turbulons.[4,5]
2) To obtain comparative data on the turbulence generating ability of various types of terrain found on the Missile Range.[5]
3) To measure, as a function of telescope aperture, the amplitude and frequency of scintillation and image displacement caused by turbulence under field conditions at WSMR.[6]
4) To conduct experiments in reducing optical turbulence.[6]

Due caution is exercised in this program to avoid duplicating the work of others in this field.[7]

A. Optical Effects of Thermal Turbulence in the Atmosphere

In 1947, it was suggested that the optical effects of turbulence might be explained by the concept of hypothetical prisms of constantly changing power, orientation, and size along the line of sight from the telescope to the target.[8] The air lens, or thermal lens, concept of Neeland and Roush has been previously mentioned. In

[2] E. P. Martz, Jr., "Optical Performance in Elevated Camera Structures," Sys. Engrg. Branch, Flight Determination Lab., White Sands Missile Range, N. M.; November, 1951.

[3] J. A. Roth, "Station Site Turbulence," Range Instrumentation Dev. Div., Integrated Range Mission, White Sands Missile Range, Final Rept. on Sub-Task 1-22-4; September, 1958.

[4] Turbulon—a single elementary parcel of turbulence, an "air lens."

[5] This work was supported in part by the Office of Ordnance Res., Project I-169-P.

[6] Work on these two areas has just commenced and will not be reported in this paper.

[7] It is beyond the scope of this paper to describe all research being done in the field of optical turbulence. A large number of papers have been published since the astronomer, A. E. Douglas, started modern research on the subject in 1892. For a reprint of Douglas' original paper see "Amateur Telescope Making," Book 2, Scientific American, Inc., New York, N. Y., pp. 585–605; 1949.

[8] L. A. Riggs, *et al.*, "Photographic measurements of atmospheric boil," *J. Opt. Soc. Am.*, vol. 37, pp. 415–420; June, 1947.

order to study, under controlled conditions, the optical effect of single turbulons, an experiment was conducted in which both the physical nature of a turbulon and the effect of the turbulon on an optical image could be recorded simultaneously. The optical schematic for this experiment is shown in Fig. 3. A Schlieren-type optical system was used to photograph simultaneously two views of a single turbulon generated in the test area. These two views were oriented at 90° from each other and provided information on the size, shape, and location of the turbulon. At the same time, a target was photographed by a telescope viewing through the turbulon to record its effect on an optical image. The aperture of the telescope was 2 inches, the image distance 72 inches, and the object distance 279 inches. The distance from the test area to the telescope objective was 14 inches. Exposure time for the telescope was determined by an electronic flash unit which transilluminated the target for approximately 175 μsec.

Turbulons were generated one at a time by applying 6 ac volts to a small coil of resistance wire located just below the test area. The shape of the turbulon was generally that of a laminar flow,[9] vertically-oriented column approximately one-half inch in diameter. In order to obtain fairly stable turbulons, it was necessary to block off air inlets to the room and to minimize human movement lest interfering air currents be set up. Schlieren photographs of an artificial turbulon are shown in Fig. 4.

The target pattern photographed by the telescope served two purposes. Standard bar-type resolution patterns in the four quadrants of the target served to indicate the resolution loss introduced in the image by the turbulon. Four space points on the target, one in the center of each quadrant, were used to measure the image displacement and image distortion (differential displacement) produced by the turbulon. A set of fiducial points on the target were independently illuminated and exposed on the telescope film before each turbulon was generated and the main target-pattern photographed. Since the telescope camera shutter was not operated between the fiducial exposure and the target exposure and, further, the camera was not touched during this period, the images of the fiducial points gave a stable frame of reference against which the images of the space points could be measured to determine image displacement and distortion. Also, the measured distance between fiducial point images served to determine the film-shrinkage correction factor to be applied to each photograph taken.

The results of the experiment were as follows:

1) Vertically-oriented column-shaped turbulons reduced the horizontal resolution more than the vertical resolution, thereby acting as astigmatic (cylindrical) lenses.

[9] Laminar flow, since by definition, turbulent flow would not exist *within* a turbulon.

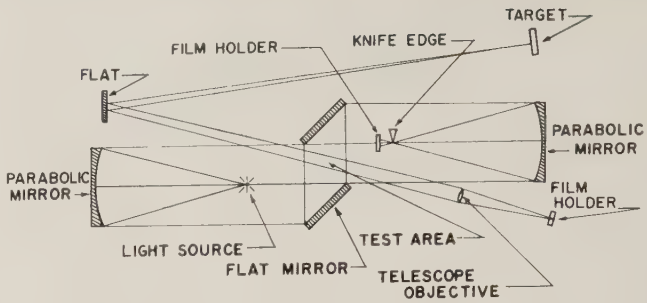

Fig. 3—Optical system used to study the optical effects of single turbulons.

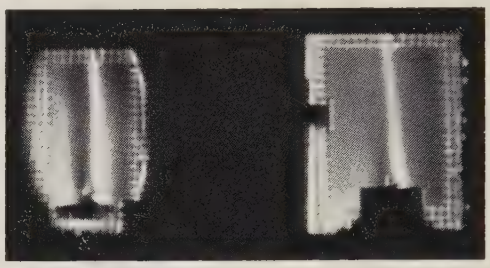

Fig. 4—Schlieren photographs of a column type, warm-air turbulon. These two views are oriented 90° from each other and were photographed simultaneously.

2) Image points in all quadrants of the image were displaced in the same general direction by any given turbulon. The magnitude of displacements among the quadrants was not constant for a given turbulon. Therefore, both image displacement and image distortion resulted from single turbulons.
3) The magnitude and the direction of the image displacement appear to be correlated with the magnitude and direction by which the optical center of the turbulon is displaced from the telescope axis.

(These results were produced by single turbulons which were smaller than the telescope aperture in the horizontal direction and which extended vertically across the aperture. The magnitude of image displacement was generally less than 2.5 seconds of arc.)

The third result enumerated above is of special interest. The data unexpectedly revealed that, if the turbulon was located to one side of the telescope axis, the image was displaced toward the opposite side. It can be shown by geometrical optics that, if a negative lens is located in front of a telescope objective and somewhat off axis, there will be a displacement of the image in the opposite off-axis direction (see Appendix). Thus, the first and third results indicate that the column-shaped, warm-air turbulon acted as though it were a negative-power astigmatic lens. This, of course, should be expected from the fact that the density, hence, the refractive index, of warmed air is less than that of air at ambient temperature. But, it further implies that there is no need for a prism model of turbulence—both

image motion and loss of resolution can be produced by an air lens.

Under field conditions one is confronted not merely with a single turbulon occulting the line of sight but, rather, with a field of turbulence extending both across and along the line of sight. Fig. 5 is a Schlieren photograph showing "effective" cell size[10] of turbulons in the open atmosphere. Cell size is not a constant, but is dependent upon terrain, insolation, and atmospheric conditions. The slightest breeze can completely change the nature of the cell pattern while it is blowing past the objective of the telescope. If the effective cell size is very much smaller than the telescope aperture, each off-axis cell will displace a portion of the image-forming light in a manner similar to that observed in the single turbulon experiment. The net result will be a blurred image which will not manifest any image motion characteristics, but which will have position stability. On the other hand, if the effective cell size is large, or the aperture-size small, so that the effects of many cells are not integrated across the aperture, image motion and distortion will be observed and resolution will be better than that of the blurry image resulting from the many small cells. This suggests that for cinetheodolites, where image stability is of great importance, large optical apertures are required in the presence of optical turbulence. Furthermore, for the large tracking telescopes which provide highly detailed images of missiles at long ranges without great concern over image position stability, small apertures will yield better resolution in the presence of turbulence. The effects of turbulence override the normal aperture-resolution relationship of physical optics. Optimization of aperture size is the subject of future research at WSMR.

There is another type of image-blurring resulting from turbulence. When image motion is caused by relatively large cells and the exposure time of the camera is sufficiently long, a blurred image will result from the fact that the image moved during the exposure. In general, an exposure time of 1/100 second or shorter will prevent this type of blurring. However, it is impossible through the use of short exposures to prevent the type of blurring which results from a large aperture viewing through a field of small turbulons.

The scintillation effect of atmospheric turbulence is directly related to the size of the receiving aperture, the effect being greatest at very small apertures. Scintillation results from distant, optically powerful turbulons, causing light rays to be partially or totally refracted away from a small receiving aperture. Fortunately, nearly all optical instruments used for missile tracking have sufficiently large apertures to avoid scintillation effects. A star which twinkles when observed with the eye does not twinkle when seen through a medium or large sized telescope.

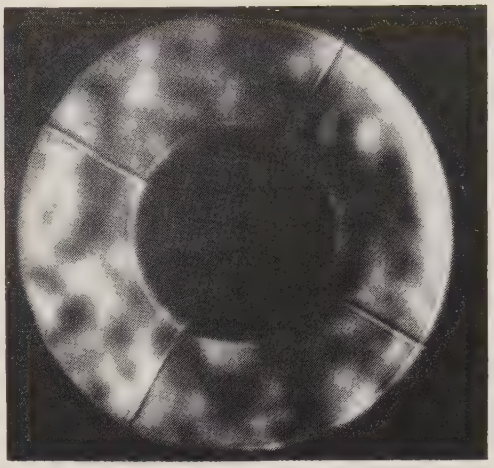

Fig. 5—Schlieren photograph of turbulence cells in the open atmosphere. The light and dark blotches indicate the angular variation with which rays from a point source have impinged upon the telescope objective. The dark area in the center is the shadow of the telescope secondary mirror. Telescope aperture equals 6 inches.

B. The Source of Thermal Turbulence

It was mentioned in Section II of this paper that during the periods shortly after sunrise and shortly before sunset, good images of missiles photographed at long ranges could be obtained. What makes these periods different from the rest of the daylight hours when turbulence is observed and image quality drops off drastically? If, during the periods near sunrise and sunset, one measures the temperature-lapse rate (vertical temperature gradient) of the atmosphere in the first 3 feet above ground level, one will find the lapse-rate to be no greater than adiabatic ($-1°C/m$) or, possibly, inverted (positive slope). Both of these conditions are indicative of a vertically stable air mass. However, during the rest of the daylight hours, the lapse-rate generally becomes super-adiabatic (unstable air) with temperature differences as great as 17°C between ground level and 3 feet above. As the sun illuminates the ground, some of the solar energy is reflected, some absorbed and conducted to subsurface soil, some absorbed and re-emitted at longer wavelengths (infrared), and some absorbed and given up to the boundary layer of air just above the surface by conduction.[11] This very thin, superheated, boundary layer becomes buoyant because of its high temperature and low density and bubbles upward to form turbulons.[12,13] Lapse-rate measurements give an indication of the buoyancy, or turbulence potential, of the lower atmosphere.

[10] The "effective" cell size is smaller than the turbulon size since we are looking in depth at turbulons against a background of randomly spaced turbulons. Boundaries of more distant turbulons may appear in the center of closer ones. However, the effective cell size will be, in some respect, proportional to the turbulon size.

[11] R. Geiger, "The Climate Near the Ground," Harvard University Press, Cambridge, Mass., pp. 1–9; 1957.

[12] *Ibid.*, pp. 51–61.

[13] R. S. Scorer and F. H. Ludlam, "Bubble theory of penetrative convection," *Quart. J. Roy. Meteorol. Soc.*, vol. 79, pp. 94–103; January, 1953.

WSMR, encompassing 4000 square miles, has a variety of terrain surfaces and surface covers ranging from white sand dunes to black lava beds and from sparsely vegetated desert to dense swamp grass. J. A. Roth is conducting a year-long program of measuring lapse-rates from heights of 0.5 foot to 24 feet over white sand, sparsely vegetated desert, and swamp grass.[14] As one might expect from a comparison of reflectivities, the lapse-rate over white sand shows less instability of the atmosphere than that over desert terrain. Somewhat unexpectedly, the highest lapse-rates (greater turbulence potential) were those measured over 10-inch deep, dense swamp grass. It had been previously supposed that the lapse-rates encountered over such grass would be less than those over the desert. The temperature of the air at the top of the grass was actually higher than that of air at the same height above desert sand. Roth's program has been expanded recently to include man-modified surface covers such as commercial crops and close-cropped lawn grass in an attempt to gain a better understanding of lapse-rates over green vegetation. The lapse-rate over a large pond is also being studied.

IV. Conclusions

A systematic research program on optical turbulence has been conducted more or less steadily during the past decade at WSMR. The advantages gained by elevating cameras above ground level have been measured and are now being realized through the use of concrete towers, earthen mounds, and other types of structures. However, elevating the camera stations only reduces and does not eliminate the turbulence problem.

An "air lens" turbulon theory for the optical effects of atmospheric turbulence has been partially developed and can be used to explain some of the observed effects. On the basis of this theory, scintillation, image motion, image blur, and the relationship of aperture size and exposure time to observed turbulence effects are qualitatively understood. The frequently observed undulating appearance of fairly small line images has yet to be explained.

The generation of optical turbulence is understood on the basis of a micrometeorological bubble theory. The turbulence potential of the air near the ground is indicated by a readily measured quantity, the temperature lapse-rate. This potential is being measured over various types of terrain surfaces with the surprising result that dense swamp grass has a higher potential for producing optical turbulence than does sparsely vegetated desert.

Although this research has all been directed toward the optical effects of atmospheric turbulence, the results apply equally well to systems working at radio frequencies. From the general refraction equations, one might expect that humidity inhomogeneities may play an important part in RF turbulence effects, if such inhomogeneities are found in the turbulent lower atmosphere. For the optical problem, only thermal-induced density inhomogeneities are considered important.

[14] The full results of this program will be reported later.

Appendix

The fact that the image displacement produced by a single turbulon is related to the off-axis position of the turbulon was first noticed by L. A. Adams, formerly associated with this program. His explanation for the effect is given below.

Consider two light rays emitted from a point source and focused by a telescope as shown in Fig. 6. Ray 1 passes through the center of the negative lens and, therefore, is not deviated until it strikes the telescope objective. In image space, it will cross the axis at the normal focal plane. Ray 2 is selected as that ray which, in image space, is parallel to the axis. The dashed extension (apparent direction) of this ray in object space will pass through the first focus of the telescope objective and will intersect with Ray 1 defining the apparent location of the point source. Their intersection in image space gives the position of the image of the apparent point source.

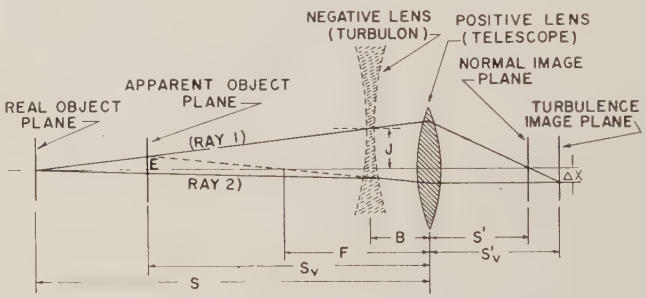

Fig. 6—Image displacement caused by an off-axis negative lens.

From similar triangles, we have

$$\frac{E}{S - S_v} = \frac{J}{S - B},$$

and

$$\frac{E}{S_v - F} = \frac{\Delta X}{F}.$$

Combining the two equations, we have

$$\Delta X = J\left[\frac{F(S - S_v)}{(S - B)(S_v - F)}\right],$$

where J and B depend upon the position of the negative lens, and S_v is a function of the optical power of the negative lens.

When the complete bundle of image-forming rays are considered, it will be found that the centroid of the defocused image observed at the normal image plane will be very nearly $(S'/S_v')\Delta X$ from the telescope axis.

Television in Underwater Weapons Testing*

ALLAN R. METZLER†

Summary—At the Naval Ordnance Test Station sea ranges at San Clemente Island, closed-circuit television is used both over and under water for certain phases of underwater weapons testing. The functions of this instrumentation are to provide: real-time data, engineering surveillance, monitoring, underwater launcher positioning, range surveillance, time-event data, trajectory data, and to assist in underwater search and recovery.

At present, 17 closed-circuit systems are in use above and below the surface of the ocean, and more systems are being built. The new systems include an Image Orthicon camera for underwater search and a Vidicon-type system for operations at a depth of 6000 feet.

THE San Clemente Island Ranges, off the coast of Southern California, serve as a flexible facility for the Naval Ordnance Test Station's testing and evaluation of all types of underwater weapons (Fig. 1). Closed-circuit television is the only practical method of securing real-time information and to provide the essential visual contact with both underwater and topside operations. Technically, it is often better and more flexible than personal observation by divers.

* Received by the PGMIL, June 12, 1961.
† U. S. Naval Ordnance Test Station, Pasadena, Calif.

Complete weapons testing at San Clemente Island requires the observing, monitoring, and recording of events and functions inaccessible to personnel. Closed-circuit television and kinescope-recording cameras provide this means of information storage. Some of the functions performed by television on the San Clemente Island Ranges are: supplying real-time data, engineering surveillance, monitoring, range safety surveillance, time-even data, trajectory information, assistance in search and recovery, and in underwater launcher position.

Although it is often thought that television and film are competitive media, each has a definite area of applicability in our particular tasks. Film cameras in remote positions cannot supply real-time information, and lack the ability to be oriented remotely during underwater tests; also the cameras must be recovered after each operation.

The main disadvantages of television are the present state-of-the-art limitations imposed by its limited applications as compared with film photography. Systems needed to obtain high-speed television data are

Fig. 1—POLARIS Test Range, San Clemente Island, showing FISHHOOK recovery system.

special designs and are costly compared to the innumerable high-speed film cameras available. The complexity and over-all lack of system reliability of television are considered a disadvantage. Another is that present television cameras require video information to be transmitted via cable to the readout system. Multiplexing techniques have alleviated this condition somewhat, but electrical cable still remains a problem in underwater applications.

The Naval Ordnance Test Station uses both film and television for the coverage of events, utilizing the advantages of both. In the examples of the use of television illustrated here, the principal reasons for its application to the particular task will be clearly evident. Having a picture to look at and being able to form real-time conclusions are invaluable to the observer at the remote monitor. Television is not only a data system but a prime tool in underwater surveillance work. Its value is often not realized until after the results are assessed.

At present, the Range Operations Branch (Pasadena Division of the Test Department) operates 17 closed-circuit television systems at San Clemente Island. Two kinescope recorders are used as support for film coverage and data recorders.

The present systems incorporate Hallamore Electronics Company CC400 and CC420 television cameras, each with a low-light level Vidicon-type pickup tube and a cascode preamplifier. The cameras are used with television monitors which combine the functions of camera control and a 14-inch, 17-inch, or 21-inch monitor, depending upon the application (Fig. 2). Master vertical and horizontal oscillators, located in the master monitor, develop the pulses that drive both the camera and monitor-sweep circuits. The master horizontal oscillator is a free-running multivibrator adjustable to 20 kc with a 60-cycle noninterlaced field rate. The 20-kc horizontal sweep frequency theoretically provides 666 scanning lines, although blanking time and field adjustment often reduces the number to 600 television lines. Horizontal deflection for the CRT and Vidicon tube is derived from a common master oscillator source, making it impossible for the camera and master control monitor to lose synchronization.

The television cameras used under water are placed in housings with or without underwater pan and tilt mechanisms (Fig. 3). Most of the housings have corrected windows that provide a relatively distortion-free horizontal field angle of 70 degrees and reduce images to normal size. All these shallow-water housings are so designed that the camera can be submerged to a 1000-foot depth.

Resolution of television systems and film cameras underwater is not limited by the equipment but by the water itself. From earlier work by the writer,[1] later substantiated by experiments in open water by the Naval

[1] While employed at U. S. Naval Photographic Center and contractually assisted by Photogrammetry, Inc., of Silver Spring, Md.

Fig. 2—Typical television monitor.

Fig. 3—Typical underwater television camera and pan-tilt mechanism.

Ordnance Test Station, it is known that the resolution of an optical image in relatively clear water is normally 10 to 15 film lines per millimeter due to the scatter of light in water for distances up to a few feet. The resolution of an optical image underwater is limited primarily by the inherent molecular structure of the water itself and to a lesser degree by water turbidity and frequency of light. It is therefore evident from the resolution characteristics of most film, lenses, and television pickup tubes that the limitations imposed by the water are much more severe than those imposed by the equipment.

The two characteristics of water most troublesome in underwater optical instrumentation are scattering and absorption. Aggravating this condition is the sea-water variable, *turbidity*, which causes visibility to change from a few feet to as much as 100 feet in a few hours. Water turbidity causes variable optical conditions, particularly when artificial light is used. In water depths up to 300 feet at San Clemente Island, artificial lighting is more of a hindrance to Vidicon-type cameras than an aid, except for close subject distances.

The versatility of basic television equipment both in air and in water is increased by remote zoom lenses and pan-tilt controls along with distribution and video line amplifiers, a horizontal vertical synchronizing generator, switching and patching equipment, and kinescope recorders.

Surface Television

On the FISHHOOK recovery system used on some of the POLARIS missile tests, a television camera on the top of the FISHHOOK crane 185 feet above the water is directed toward the water surface for boresight purposes (Fig. 1). In this way it can be determined that the recovery cable is located directly over the launching pad to prevent the transfer of upsetting moments from the cable to the missile.

For range safety, a remotely controlled television camera is located atop the range control blockhouse at San Clemente Island (Figs. 4 and 5). With the zoom lens, the Range Engineer can check small or large areas of the range to ascertain its condition and to assure himself that all personnel have left the area prior to a firing (Fig. 2). The Naval Ordnance Test Station supplies five cameras, utilizing remote control pan-tilt mechanisms, to Lockheed Missiles and Space Division and Westinghouse Electric Corporation for use during POLARIS tests to monitor checkout equipment near the launch site that cannot be remoted to the blockhouse. Here the 600 lines of resolution are important to enable personnel to read meters accurately.

Similarly, the range oceanographic group uses a television camera in the control blockhouse to check performance and view individual records from recorders in the monitor barge at the launch site more than 4000 feet away. The oceanographic group records data from

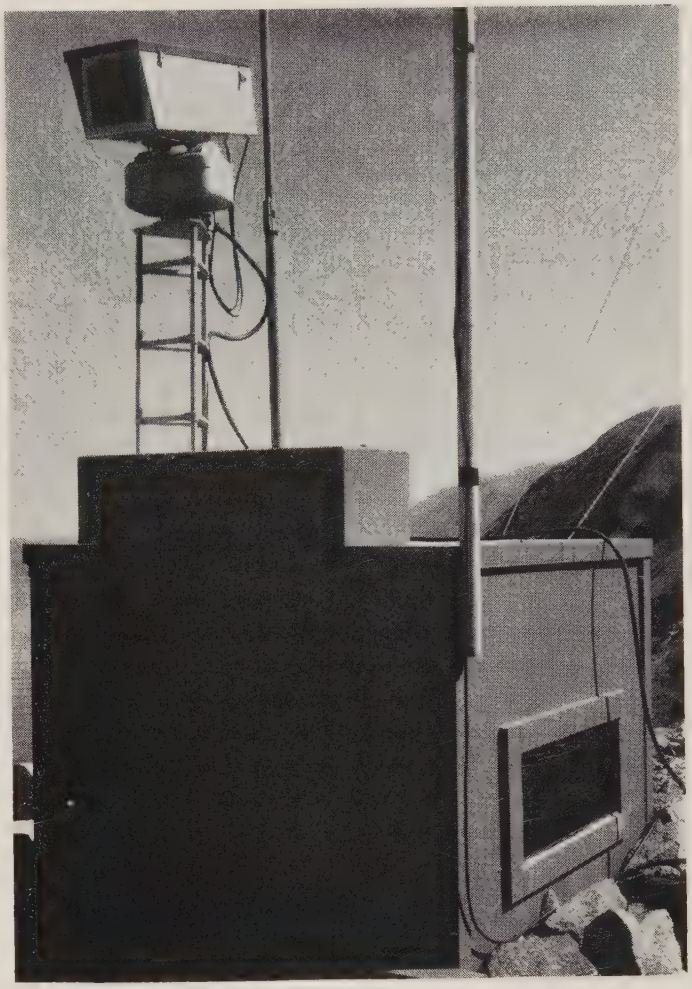

Fig. 4—Range safety surveillance television mounted on command flight termination station atop range control blockhouse.

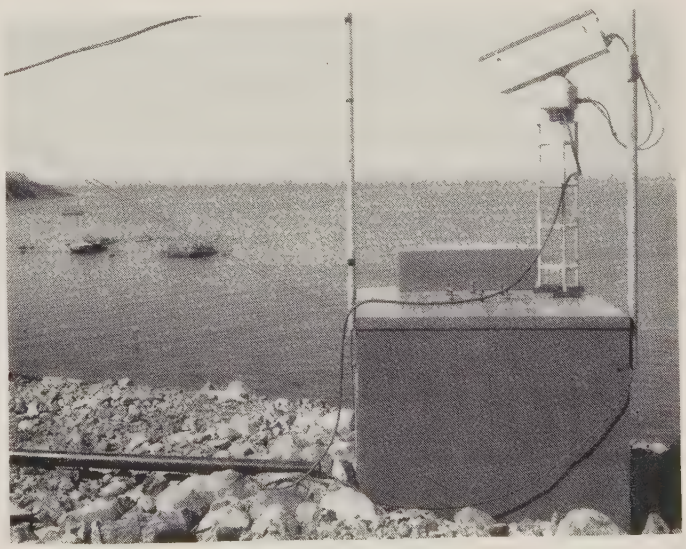

Fig. 5—View of POLARIS range from range control blockhouse.

a thermistor chain (water temperature profiles), Roberts water-current meters, Savonius water-current meter, Litton water-current meter, and Mk 10 bottom-pressure transducers.

The launcher instrumentation group also has a television camera on the monitor barge to check on the performance of the launcher instrumentation. This group, in the blockhouse, calibrates remotely with aid of this television system prior to a firing and records data from pressure transducers in the launcher (Fig. 6). The television also aids the blockhouse instrumentation group in performance of equipment checkout and preflight operations.

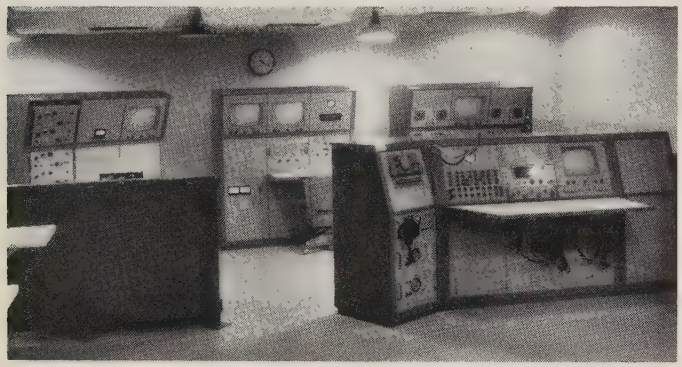

Fig. 6—Internal view of range control blockhouse.

Underwater Television

In shallow water, television is used underwater to observe and position launchers, to read gauges inside the POLARIS submersible launcher, and to observe underwater flight paths. The underwater test observations and the television image of the gauge cameras are recorded on kinescope film recorders as a backup in case of failure of the data equipment or underwater film cameras.

Before launchings, underwater television inspects the ocean floor around San Clemente Island with its many large boulders and other obstacles, in order to prevent damage to the launcher as it is being lowered. When the POLARIS launcher is being pulled down to its pad, the ballasting and winch operators must know if there are any obstructions and how the launcher is oriented with respect to the pad. Submersible winches will presently be monitored in the same manner.

Underwater television cameras are located on the POLARIS submersible launcher to observe its operation. They are of great value in making certain that the hatch is functioning properly before a missile launch is attempted. In ballasting and pressurizing, the operator must know several pressures in the launcher prior to firing in order to give accurate launch characteristics. Accurate gauges in the launcher are observed with television, and special precautions are taken to reduce any error due to parallax.

For missile recovery and oceanographic research, two underwater-search television systems have been developed at the Naval Ordnance Test Station. One system (on the net-tender USS *Butternut* or ASR-type vessel) consists of a tripod that can be set on the ocean floor, a pan and tilt unit, and an underwater television camera. This system allows search of an area from a fixed point. The other system is designed to be towed through the water to observe the ocean floor. Both units can be equipped with four 400-watt, 220 volt underwater mercury-vapor lamps built by Ward Associates, San Diego, California. The towed system has been used on 63-foot vessels (AVR-type) to determine bottom topography.

An underwater tripod-mounted television camera with pan-tilt unit has also been used to observe underwater construction work on the POLARIS program. This enables the inspector, who cannot be under water, to observe the progress of the construction.

A fiberglass and epoxy underwater camera-housing has recently been designed, fabricated, and tested to an operating depth of 1000 feet, and delivered through the cooperation of Summet Industries, Los Angeles, California. It is presently being equipped with a transistorized Vidicon-type television camera for operational evaluation (Fig. 7). The housing represents a corrosion-free, extremely lightweight design with hermetically sealed connectors and a quick-acting, self-aligning rear door (Fig. 8).

The Naval Ordnance Test Station has also completed three new underwater pan-tilt mechanisms designed for 6000-foot depth operations. These are electrically driven, oil filled, and constructed of type 6061 anodized aluminum alloy. They were produced primarily to meet the conditions of greater depth and to be used in areas of high-dynamic pressures created by underwater explosions.

Since underwater cabling is a necessity for underwater television, special nonflooding cables have been designed and procured. Stainless-steel hermetically sealed connectors are used throughout. The aluminum camera-housings have been modified from the example shown in Fig. 3 to provide two additional connectors on the housings for cables to the pan-tilt mechanism and underwater lights.

The most recent application of underwater television at the Naval Ordnance Test Station is an Image Orthicon system built by Vare Industries, Roselle, New Jersey. It is used in conjunction with the Vare Industries underwater self-propelled vehicle (Fig. 9) presently undergoing acceptance testing at San Clemente Island. This underwater television search vehicle will be outfitted with an underwater manipulator claw for recovery work. An underwater automatic computer-type navigation system has been designed and will be installed to aid the television search and to prevent random searching underwater. This vehicle and navigation system are controlled from a mother ship with an X-Y plotter as the navigation readout system.

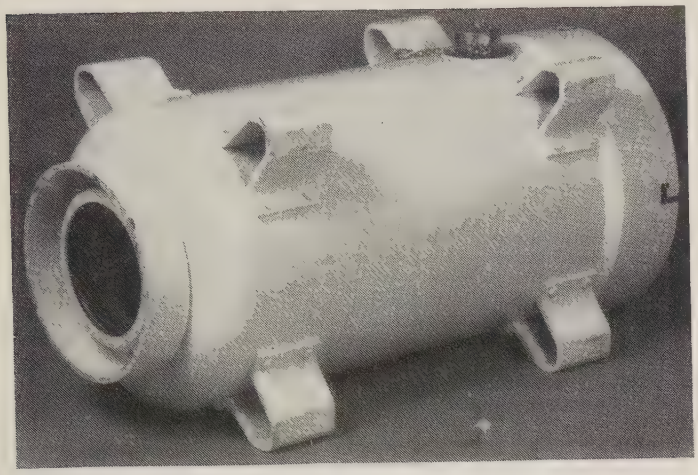

Fig. 7—Fiberglas underwater housing.

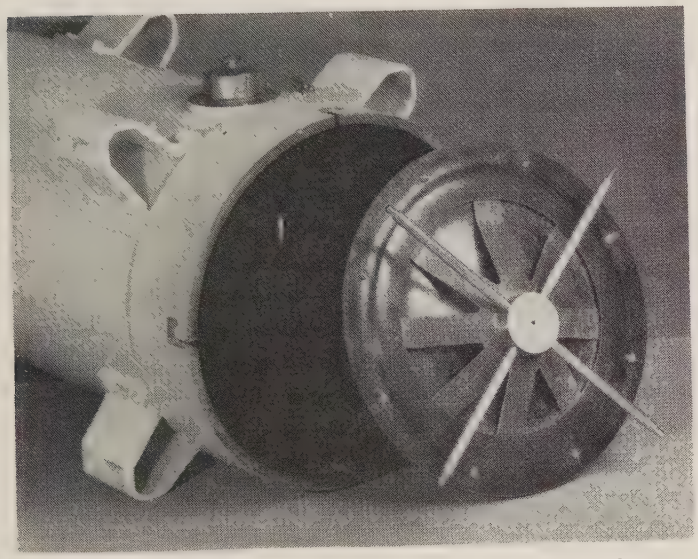

Fig. 8—Fiberglas underwater housing quick-seal rear door.

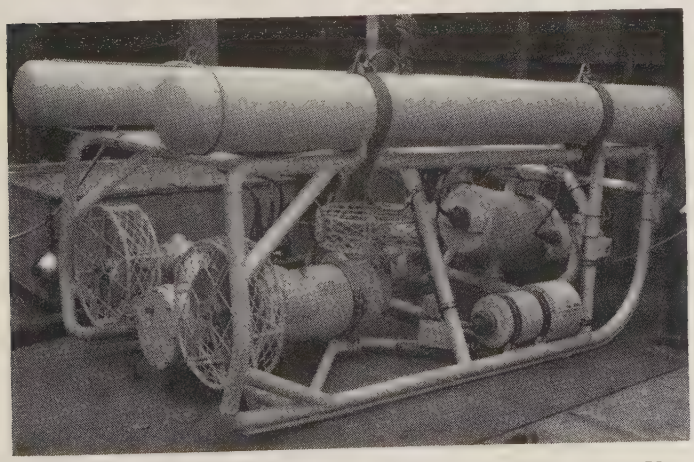

Fig. 9—Underwater search and recovery vehicle produced by Vare Industries, Roselle, N. J.

Future Television

The U. S. Naval Ordnance Test Station, Pasadena Division, of the Test Department, is developing several television systems for various underwater tasks as well as considering the use of television for underwater missile trajectory studies.

Multiplexing four separate television slave monitors over a single coaxial cable is presently planned to eliminate two thirds of the underwater cabling problem for remote monitoring in the control blockhouse.

A new television system is being fabricated to operate at a depth of 6000 feet under water. The camera, built by General Electric Corporation, incorporates a Conrac monitor, and is expected to be used for general deep-water testing and bottom survey. The chief design problem involves the underwater cable that will operate the controls, lighting, television video, power, and contain the tensile member necessary to support the underwater camera and mounting frame. As in all cables of this type, a nonflooding cable is essential. The specifications for most of the underwater electrical cables on the range require that they withstand 300 psi for two hours and do not "hose" or absorb more than 0.1 cubic inch of water in an open cable end. These specifications, which are considered ample even for a 6000-foot depth application, can be met by several manufacturers.

The low frame rate of most commercially available television systems limits them for range operations. Even when resolution is not critical, frame rates up to 500 frames per second are desirable for data output and recording.

Also in the planning stage is a diver-held television. This system requires a lighter and smaller housing and a special buoyant, high-tensile coaxial cable for the camera.

Since the beginning of torpedo development, scientists and engineers have been seeking a practical method for taking underwater trajectory measurements external to the test vehicle. Several acoustic and electronic systems have been proposed and some developed, but all lack the characteristics of optical presentation or picture-type of information on the underwater flight. The Naval Ordnance Test Station is investigating two methods that will possibly result in numerical data and picture-type information. They are underwater acoustic imaging and Image Orthicon underwater television arrays.

A study being conducted at this Station concerns acoustic imaging to produce television-quality data pictures up to 8 frames per second at several hundred feet from a fast-moving underwater test vehicle. Present work is being carried on at 1-mc acoustic frequency and CRT presentations of underwater targets have been produced.

A future television system for underwater trajectory measurements might utilize at least nine Image Orthicon television systems on separate submersible, bottom-

supported mounts, with precision underwater pan-tilt mechanisms instrumented to produce azimuth, elevation, and depth information. These separate video signals, with camera orientation information, could be stored three at a time on video tape-recording equipment for data assessment as well as engineering surveillance playback.

The cameras could be located with the previously described underwater navigation system to aid underwater television search with an accuracy of $\pm 2\frac{1}{2}$ feet, with respect to a fixed bottom reference at a range of 6000 feet from the navigator or plotting station on board ship. Since absorption and scattering affect television and film photography mainly in subject contrast, color television would be very valuable in this area. Shades of grey or tonal contrast are all that conventional black and white television systems can provide.

Conclusion

The future of all underwater television is not limited by the probability that man will some day have complete mobility and freedom under the seas for observation and measurement in yet unthought-of submersible craft. If one accepts the fact that man in space is the most compact of instrumentation packages, optical instruments such as television will never achieve a degree of success equal to that of man's senses. Nevertheless, television-type equipment will always be a necessity underwater, especially in areas of high risk to human life.

Acknowledgment

Special acknowledgment is accorded W. F. Brisch, Head, Range Operations Branch, Pasadena Division of the Test Department, under whose direction the author worked for two years developing television for underwater weapons testing; also to the able complement of electronics personnel under the supervision of Pasqual Mercado who kept the numerous television systems operating under the worst environmental conditions.

The author gratefully acknowledges a most helpful effort on the part of D. Williams, physics student at Harvey Mudd College, on summer assignment with this group, for assistance in the preparation of much of the material comprising this report.

Programmed Search in Adaptive Systems*

NORMAN S. POTTER†, SENIOR MEMBER, IRE

Summary—An investigation is conducted of the programming of search by discrete data systems over a space volume. The distribution of search effort which leads to the greatest attainable information rate on a contact, or probability of its retention by maximizing the probability of a positive interrogation within some designated time interval is determined. An estimate of p, the relative frequency of positive interrogations of an individual contact, is utilized as a basis for adjustment of the sampling rate in accordance with results of the search program optimization study. It is shown that in the case of Rayleigh signal sources, the rate of convergence to a stable estimate of p is greatest if a search program characterized by a rapid sampling rate and a consequent low probability of detection on the individual trial is employed.

If, following a sequence of observations, the statistical distribution of the position of the contact may be ascertained with some confidence, a suitably restricted space volume may be used in the allocation of search. It is shown that, if an extremal exists, the uniformly interrogated search field, which is optimal in the sense that the product of the containment and detection probabilities is greatest, is defined by an equiprobability density of location contour. Further, if a nonuniformly distributed search program is pursued and the errors are determined to be binormally, circularly distributed, the greatest effort should be allocated to the region in the vicinity of the center of the positional distribution, with a parabolic decline to zero in dwell time as the periphery of a bounding, circular region, whose radius is a function of the standard deviation, is approached.

* Received by the PGMIL, June 2, 1961.
† Maxson Electronics Corp., New York, N. Y.

Introduction

THE ADVENT of electronic scanning and high-speed data-processing systems makes the implementation of flexible search-track systems feasible. The contemplated programming of discrete data systems is largely intended to accomplish the distribution of signal integration time in an optimum manner, that is, in such a way that the greatest attainable information rate is generated. As used herein, the information rate upon a contact is said to be greatest when the mean time between successive positive interrogations of it is minimum. Alternately, the probability of effecting a positive interrogation within some designated time interval may be maximized in accordance with other reasonable system performance criteria to be discussed.

To this end, object detectability may first be ascertained upon the basis of a history of successful and nonsuccessful interrogations. Investigation of the convergence of such statistical processes in the case of Rayleigh or strongly fluctuating sources shows that the rate of convergence to a stable probability of success on an individual interrogation is greatest if a program characterized by a rapid sampling rate and a consequent

low probability of detection on the individual trial is employed. The result conflicts in part with the optima indicated earlier and those associated with certain higher order decision processes that might be utilized as criteria for the retention or rejection of a contact.

The preceding programmed distributions concerned themselves with information rate considerations when a space volume is to be interrogated. However, the problem is often one of maximizing the probability of a positive interrogation of a contact if, following a sequence of prior interrogations, its positional distribution over some suitably restricted space volume may be reflected in the allocation of the search over that subspace. It will later be seen that the use of a complex, nonuniform search program provides little improvement above that of the substantially simpler, uniformly distributed search, provided that the space volume has been optimally selected with respect to the latter.

In brief summary, the methods to be developed are of particular consequence in the heavy contact density environments which may largely define modern defensive operations. The confusion arising through the interlacing of trajectories is representative of the factors which dictate a progression to increasingly higher sampling or information rates to facilitate automatic decision processes and reduce computer bandwidths. Further, the compelling possibility exists of implementing multiple purpose detection and tracking equipments that may also effect intelligent control of a counterweapon. The detection and tracking phases largely merge in systems which extensively utilize memory and the correlation of data derived over a series of interrogations in discriminating against system noise and signals from real though extraneous sources. Accordingly, many questions which are similar to those which arise in the tracking phase must be considered in the information handling aspects of detection. However, the optimal system sampling rate for control of a counterweapon is essentially dictated by its over-all time constant of response, thereby leading to more stringent information output requirements. Setting aside the availability of inordinate signal levels, these can only be satisfied by the fuller use of the data available to the composite system.

The Statistical Model of the Detection Process

Let P denote the instantaneous power density of a reception comprising signal and noise, the average of whose fixed and mean fluctuating components are S^2 and S_f, respectively. Following Uhlenbeck, we define the first probability distribution $F(P)dP$ as a stationary distribution leading to the well-known expression

$$F(P)dP = e^{-(P+S^2)/S_f} J_0\left(2i\frac{S}{S_f}\sqrt{P}\right)\frac{dP}{S_f}. \qquad (1)$$

A representative and meaningful discussion of its functional behavior and physical significance may be found in Kerr.[1]

In the most interesting case, that in which the fluctuating component is large, $\rho^2 = S^2/S_f$ vanishes in the limit. If $\overline{P} = S^2 + S_f$ represents the mean signal power,

$$F(P)dP = (1+\rho^2)e^{-[\rho^2 + P/\overline{P}(1+\rho^2)]} J_0\left(2i\rho\sqrt{(1+\rho^2)}\sqrt{\frac{P}{\overline{P}}}\right)\cdot\frac{dP}{\overline{P}} \sim e^{-P/\overline{P}}\frac{dP}{\overline{P}}, \qquad (2)$$

where the asymptotic expression obtains in the situation cited above. It leads to a convenient estimate of the idealized behavior of p, the probability of a detection or positive interrogation since, assuming some threshold P_m, integration of the asymptotic expression over $P > P_m$ leads to $\exp(-P_m/\overline{P})$, an expression which figures prominently in the subsequent analysis. Quantitative analysis indicated that the preceding provides a good approximation to the integration time dependence of $p \equiv p(t)$. By way of a physical rationale, if ϵ represents the signal-to-noise amplitude ratio, assuming an idealized integration process, so that the proportionality $\epsilon = c\sqrt{t}$ obtains, $\overline{P} \propto \epsilon^2$ leads to $p = \exp(-k/t)$. In the above, t is the sampling period for uniform interrogation of the search field.

At the other extreme, if the fluctuating component is small, and ρ large, reason suggests that the statistical aspect of the detection process must decline since detection is then largely contingent upon whether or not the threshold exceeds the mean. This is easily demonstrated since, if ρ is large, one must have $Z \propto S\sqrt{P}/S_f \gg 1$ and $P \backsim S^2$, or $Z \propto \rho^2$. Accordingly, employing the well-known asymptotic expression $J_0(ix) \backsim e^x/\sqrt{(2\pi x)}$, one obtains

$$F(P)dP \sim (1+\rho^2)e^{-[\rho^2+(P/\overline{P})(1+\rho^2)]}\left\{\frac{e^{2\rho\sqrt{(1+\rho^2)}\sqrt{(\overline{P}/P)}}}{\sqrt{(2\pi(2\rho^2)}}\right\}\frac{dP}{\overline{P}} = \frac{1+\rho^2}{2\rho\sqrt{\pi}}e^{-[\sqrt{(1+\rho^2)}\sqrt{(P/\overline{P})}-\rho]^2}\frac{dP}{\overline{P}}, \qquad (3)$$

whence

$$p \sim \frac{1+\rho^2}{2\rho\sqrt{\pi}}\int_{P_m}^{\infty} e^{-[\sqrt{(1+\rho^2)}\sqrt{(P/\overline{P})}-\rho]^2}\frac{dP}{\overline{P}} = \frac{1}{\rho\sqrt{\pi}}\int_{\sqrt{(1+\rho^2)}\sqrt{(P_m/\overline{P})}-\rho}^{\infty} e^{-\phi^2}\phi d\phi + \frac{1}{\sqrt{\pi}}\int_{\sqrt{(1+\rho^2)}\sqrt{(P_m/\overline{P})}-\rho}^{\infty} e^{-\phi^2}d\phi, \qquad (4)$$

where the right hand integral representation follows from the substitution $P/\overline{P} = (\phi+\rho)^2/(1+\rho^2)$. Both integrals exist for all ρ so that the first term, in which the reciprocal of ρ appears as a factor, must vanish in the

[1] D. E. Kerr, "Propagation of Short Radio Waves," M.I.T. Rad. Lab. Ser., McGraw-Hill Book Co., Inc., New York, N. Y., vol. 13, pp. 553–562; 1951.

limit for ρ large. As for the second, it is clear that it approaches unity or vanishes in the limit according as the inequality $P_m < \overline{P}$ or $P_m > \overline{P}$ obtains, and assumes the limit 1/2 in the event that $P_m = \overline{P}$, so that failure or a positive interrogation are then equally likely.

Performing the indicated integrations,

$$p \sim \frac{1}{2\rho\sqrt{\pi}} e^{-(\sqrt{(1+\rho^2)}\sqrt{P_m/\overline{P}}-\rho)^2} + \frac{1}{2}\begin{cases} 1 + E\left(\rho - \sqrt{(1+\rho^2)}\sqrt{\frac{P_m}{\overline{P}}}\right); & \frac{P_m}{\overline{P}} \leqslant \frac{\rho^2}{1+\rho^2} \\ 1 - E\left(\sqrt{(1+\rho^2)}\sqrt{\frac{P_m}{\overline{P}}} - \rho\right); & \frac{P_m}{\overline{P}} \geqslant \frac{\rho^2}{1+\rho^2} \end{cases} \quad (5)$$

in which $E(x)$ denotes the error function. The preceding exhibits the limiting behavior noted above and makes the rapidity of the convergence apparent. One may therefore conclude that the case in which the nonfluctuating component is markedly dominant readily permits large increases in information rate or the selection of other optima before the comparative decline of the integration time, and therefore the nonstatistical portion, reduces it to the Rayleigh signal source case discussed earlier. The further discussion will therefore be confined to the latter, in which the selection of various allocations of search effort is more immediately reflected in terms of various performance criteria, and the optima are more sharply drawn.

Information Handling Subsystem Requirements

The choice of interrogation rates in automatic detection and tracking systems admits of certain conflicting optima. In this instance, data-handling requirements will be principally discussed. However, given *a priori* information relating to anticipated signal amplitudes, it is possible to establish a sampling rate which will yield the greatest attainable cumulative probability of detection. The related theory is developed in Potter,[2] which, subject to frequently applicable constraints upon the observer-contact relative motion, establishes both the existence of a search program that is best in the preceding sense, and the disparity between the resultant search rates and those that will now be investigated. Briefly summarized, the former are substantially lower in that, all else equal, the desired signal integration times which maximize the cumulative probability are seen to lead to probabilities of detection on an individual trial that are of the order of 0.7 to 0.8(+). It is there shown that, in general, the optimum p for a passive system somewhat exceeds that for a system in which the sensor is active, and is a weakly declining function of the rate of information loss by the data handling subsystem.

For purposes of the present discussion, information loss is defined as the failure to effect the correlation of an observation with previously derived data. Due to observation error, the frequent inadequacy of information pertaining to the kinematics and intentions of the contact, and the evident desirability of reducing the region of uncertainty or envelope of its potential predicted positions, it is advantageous to minimize the mean time between successive positive interrogations. Alternately, dependent upon system restrictions on data storage and bandwidth, it may be necessary to reject a contact if a positive interrogation is not received during some predetermined time interval T. In that event, performance may be optimized by maximizing the probability of a positive contact.

If the observed detector performance achieved with a sampling period t, is p, then the dwell or integration time across each element is proportional to t if, as is assumed for the present, search is uniformly conducted. If, then, a sampling period t' is subsequently selected by the system, leading to a different probability $p(t')$ of detection on an individual trial, employing the exponential form developed earlier, $p(t') = p^{t/t'}$. Since they are Bernoullian trials, the number N of detections achieved in time T is $(T/t')p^{t/t'}$, which may then be maximized by making an optimum choice of t'. Examination of the derivative of $N(t')$ with respect to t' shows that $t \ln p^{-1}$ is the desired extremal, whence the minimal mean time between successive positive interrogations is $t'/p(t') = e \ln p^{-1}$. It is apparent that system performance in this sense is the best attainable in the event that the observed $p = e^{-1}$. Fig. 1 displays the ratios of the idealized sampling intervals $t/t' = 1/\ln p^{-1}$ and mean times $(t/p)/(t'/p(t')) = e/p \ln p^{-1}$. The latter provides a meaningful measure of the improvement that may be achieved by adjustment of the sampling interval to that which is indicated by the preceding theory once the observed single glimpse probability is ascertained with some certainty.

Similarly, if one wishes to minimize the probability of large prediction intervals or the inadvertent cancellation of a contact, proceeding as before, the quantity

$$P = 1 - (1 - p^{t/t'})^{T/t'} \quad (6)$$

must be maximized. Differentiating with respect to t', elementary reasoning shows that there is a unique extremal given by $t \ln p^{-1}/\ln 2$. Alternately stated, system performance is optimized in this sense if, given the observed single glimpse probability, the sampling rate is adjusted so that it is equiprobable that an individual interrogation succeed or fail.

To quantitatively appraise the results of an adjustment let it be assumed that system performance corresponding to p is P. Then, following the implementation of a new sampling rate $t' = \ln p^{-1}/\ln p'^{-1}$,

$$P' = 1 - (1 - P)^{\ln p'/\ln p \cdot \ln (1-p')/\ln (1-p)} \quad (7)$$

where the addition of a superscript prime indicates the new value of the designated variable. If, in particular, the initial system performance is marginal, so that

[2] N. S. Potter, "Comparative evaluation and optimization of airborne target detection systems," *Proc. 2nd Natl. Conf. on Military Electronics*, Washington, D. C., June 16–18, 1958, pp. 62–69.

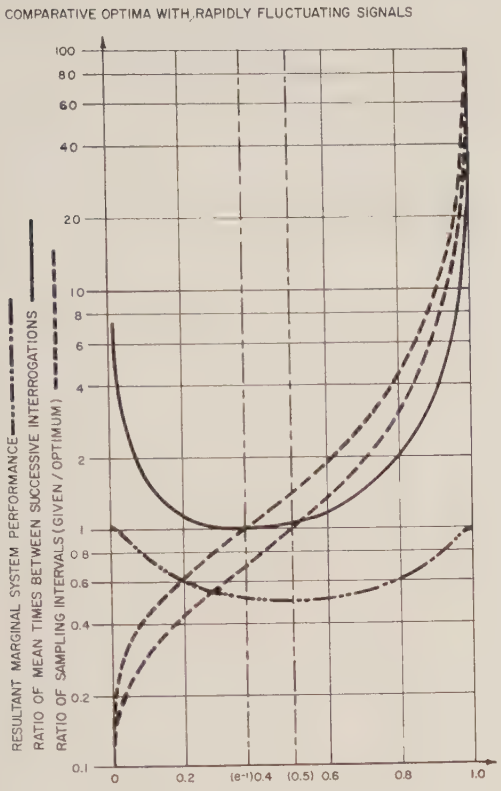

Fig. 1—Relative frequency of positive interrogations.

$P=0.5$, and, following the attainment of an observed estimate of p, the sampling rate is adjusted to the above indicated optimum, the resultant probability P' becomes

$$P' = 1 - 2^{-(\ln 2)^2/\ln p \ln (1-p)}. \tag{8}$$

The latter function and the ratio of sampling intervals t/t' are displayed in Fig. 1.

It is clear that, as in the preceding case, the resultant improvement is substantial if there is a reasonable disparity between the observed and optimal p, and suggests that the conventional desire for a high single glimpse probability may be far from optimal in terms of the composite system. While there is some measure of conflict between the optima derived above, as indicated by the fact that the related sampling rates differ by a factor of ln 2, the flat regions between e^{-1} and 0.5 in the contours that respectively measure system performance suggest that the disparity is not critical, and that it is possible to simultaneously satisfy both criteria. On the other hand, an attempt to maximize the cumulative detection probability in the classical sense by disregarding the realities of the data-handling subsystem may introduce serious and possibly unacceptable degradations in information rate.

Convergence and Stability of the Observed Performance Estimate

The adaptive behavior of the system in appropriately adjusting its sampling rate is contingent upon the availability of a meaningful appraisal of its prior performance. An estimate of the likelihood of the observed probability of a successful interrogation will now be developed and quantitatively analyzed. In effect, the conditional probability P that the relative frequency p of positive interrogations obtained in the sequence of n interrogations will be yielded in a succeeding sequence of length N is required. We consider first a subgroup of ν hypothesized probabilities p_i which are distributed over the closed interval $[0, 1]$ with equal *a priori* probability ν^{-1}. The hypotheses are mutually exclusive and the sample ν will ultimately be taken sufficiently large, infinitely so in the limit, to be exhaustive.

However, Np positive interrogations may result under any of the ν hypotheses and, if the materialization of one of the hypotheses p_i were assumed, that of Np successes would be independent of a prior history of np. Accordingly,

$$P = \sum_{i=1}^{\nu} (\{Np\}\{p_i\}, \{np\})$$

$$= \binom{N}{pN} \sum_{i=1}^{\nu} (\{p_i\}, \{np\}) p_i^{pN}(1 - p_i)^{N(1-p)}, \tag{9}$$

where $(\{Np\}\{p_i\}, \{np\})$ denotes the conditional probability of the simultaneous materialization of Np positive interrogations and the hypothesis of p_i, given np prior successes, and $(\{p_i\}\{np\})$, the occurrence of p_i alone, subject to the same assumption. Applying Bayes' theorem,

$$(\{p_i\}, \{np\}) = \frac{\frac{1}{\nu}\binom{n}{np} p_i^{np}(1 - p_i)^{n(1-p)}}{\sum_{i=1}^{\nu} \frac{1}{\nu}\binom{n}{np} p_i^{np}(1 - p_i)^{n(1-p)}} \tag{10}$$

whence, by substitution and the simplifying, though unrestrictive assumption that the p_i are uniformly distributed, with $p_i = (i-1)/\nu$,

$$P = \binom{N}{pN} \frac{\left\{\frac{1}{\nu}\sum_{i=1}^{\nu}\left(\frac{i-1}{\nu}\right)^{(n+N)p}\left(1 - \frac{i-1}{\nu}\right)^{(n+N)(1-p)}\right\}}{\left\{\frac{1}{\nu}\sum_{i=1}^{\nu}\left(\frac{i-1}{\nu}\right)^{np}\left(1 - \frac{i-1}{\nu}\right)^{n(1-p)}\right\}}. \tag{11}$$

Applying the mean value theorem to the bracketed expressions as ν becomes indefinitely large,

$$P = \binom{N}{pN} \frac{\int_0^1 t^{(n+N)p}(1-t)^{(n+N)(1-p)}dt}{\int_0^1 t^{np}(1-t)^{n(1-p)}dt}$$

$$= \binom{N}{pN} \frac{\beta((n+N)p_1(n+N)(1-p))}{\beta(np, n(1-p))}. \tag{12}$$

Finally, replacing the β functions by their representations in terms of Γ functions and applying Stirling's theorem to the resultant expression, an adequate approximation to P may be readily obtained. That is,

$$P = \left(\frac{\Gamma(N+1)}{\Gamma(Np+1)\Gamma(N(1-p)+1)}\right) \cdot \left(\frac{\Gamma(p(N+n)+1)\Gamma((1-p)(N+n)+1)}{\Gamma(N+n+2)}\right) \cdot \left(\frac{\Gamma(n+2)}{\Gamma(pn+1)\Gamma(n(1-p)+1)}\right), \tag{13}$$

but

$$\binom{m}{mp} = \frac{\Gamma(m+1)}{\Gamma(mp+1)\Gamma(m(1-p)+1)} \sim \left(\frac{m}{e}\right)^m \sqrt{(2\pi m)} \Big/ \left(\frac{mp}{e}\right)^{mp} \sqrt{(2\pi mp)} \left(\frac{m(1-p)}{e}\right)^{m(1-p)} \sqrt{(2\pi m(1-p))} = \{p^{mp}(1-p)^{m(1-p)}\sqrt{(2\pi m(1-p))}\}^{-1}, \tag{14}$$

so that

$$P = \left(\frac{n+1}{N+n+1}\right) \sqrt{\left\{\left(1+\frac{n}{N}\right)\frac{1}{2\pi np(1-p)}\right\}}. \tag{15}$$

It follows then that if the subsequent test interval is a fixed multiple μ of the sampling period during which the relative frequency p was observed, the behavior of P is that of $(np(1-p))^{-1}/\sqrt{2\pi\mu(\mu+1)}$; whence, by this standard, the convergence is best if the variance is least. On the other hand, the stability of the estimate of p over a long sampling interval, as measured by the reproducibility of the prior performance, is of interest. Accordingly, if N is large relative to $n = k^{-1} \ln p^{-1}$, one must consider

$$P \sim \frac{1}{N}\sqrt{\frac{n}{2\pi p(1-p)}} = \frac{1}{N}\sqrt{\frac{1}{2\pi k}}\sqrt{\frac{\ln p^{-1}}{p(1-p)}} \tag{16}$$

With respect to the variance σ^2 as a measure of the stability or convergence rate of the estimate, if n is fixed the variance vanishes at the two extremes of the range of p and is greatest for $p = 0.5$, about which it is symmetric. However, given a particular Rayleigh source, one has $n \propto \ln p^{-1}$, and therefore $\sigma^2 \propto S(P) = p(1-p) \ln p^{-1}$. The latter function is displayed in Fig. 2, and shows the shift in the peak from the center to the near vicinity of e^{-1}. In any event, the optima discussed earlier are in the region of comparatively large dispersion, and one may conclude that the extremes, a very large or small sampling rate, are preferable. This would suggest that it would be best to program the search in such a manner as to initially choose to operate with

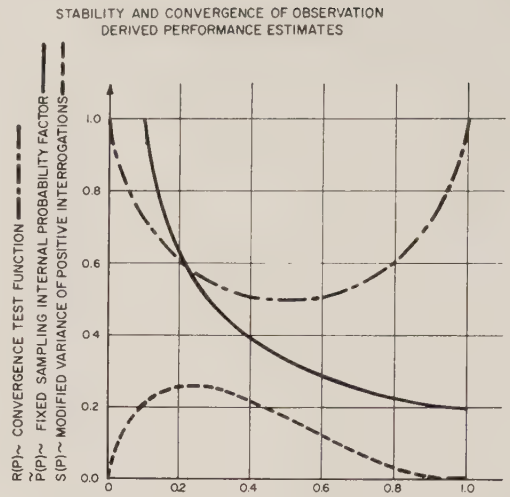

Fig. 2—Estimated or true relative frequency of positive interrogations.

what is presumably one of the extremes, adjusting to the optimal mid-region following the achievement of an estimate of p.

To resolve this issue, one may consider the functional behavior of $\tilde{P}(P) = \sqrt{(\ln p^{-1}/(1-p))}/2\sqrt{(2\pi)}$ which, from the analysis leading to (16), is proportional to the probability that a subsequent extended test period will confirm the estimate. $\tilde{P}(P)$ is displayed in Fig. 2 for a subdomain of p, the extremes of which are not shown since they are not warranted by the degree of approximation involved. It is clear, nevertheless, that small p is preferable in this context though, in point of fact n, and therefore N, must then assume very large values.

These considerations may, perhaps, be made clear by relating the stability of the estimate to the length of the initial period of observation. It will now be shown that the ratio of the probability that the relative frequency of successes will be reproduced is essentially independent of the length of the sampling interval during which the estimate of p was arrived at if p is in the vicinity of zero or unity. Alternately stated, the convergence to a firm estimate is most rapid near the bounds of p. Denoting the probability of the likelihood of the frequency of successes in the event that n or $n+m$ interrogations were involved by the addition of a corresponding subscript,

$$\rho = \lim_{N\to\infty} \left\{ \int_0^1 x^{(m+n+N)p}(1-x)^{(m+n+N)(1-p)}dx \Big/ \int_0^1 x^{(n+N)p}(1-x)^{(n+N)(1-p)}dx \right\} \tag{17}$$

is of interest. Utilizing the gamma function representations and their approximation through Stirling's theorem, as before, one obtains:

$$\rho = \lim_{N\to\infty} \left\{ \frac{\left\{\left(\frac{(m+n+N)p}{e}\right)^{(m+n+N)p} \sqrt{(2\pi(m+n+N)p)}\right\} \left\{\left(\frac{(m+n+N)(1-p)}{e}\right)^{(m+n+N)(1-p)} \sqrt{(2\pi(m+n+N)(1-p))}\right\}}{\left\{\left(\frac{m+n+N+1}{e}\right)^{(m+n+N+1)} \sqrt{(2\pi(m+n+N+1))}\right\}} \right\}$$

$$\left\{ \frac{\left\{\left(\frac{(n+N)p}{e}\right)^{(n+N)p} \sqrt{(2\pi(n+N)p)}\right\} \left\{\left(\frac{(n+N)(1-p)}{e}\right)^{(n+N)(1-p)} \sqrt{(2\pi(n+N)(1-p))}\right\}}{\left\{\left(\frac{n+N+1}{e}\right)^{(n+N+1)} \sqrt{(2\pi(n+N+1))}\right\}} \right\}$$

$$= \left\{p^p(1-p)^{(1-p)}\right\}^m = R^m(P). \tag{18}$$

It is apparent from the above that the parity between the estimates declines rapidly with increasing m, which is to be anticipated. More importantly, as may be seen in Fig. 2, $R(P)$ goes to unity in the vicinity of $p=0$ or 1, which was to be shown.

Programmed Distribution Across the Search Subspace

Specification of the Search Field with Uniform Search

The unavoidable observation errors require that a relative positional search sector of some magnitude be designated to the sensory apparatus when carrying on discrete data track. P_C, the probability of containing the contact under track in the sector, is an increasing function of the latter's size, whereas, all else the same, P_D, the probability of detecting it, if it is so contained, declines as the sector increases. It will be shown that, given the anticipated target distribution, there is a sector size which is dependent upon acquisition system search capability, as well as the observed positional statistics of the contact, which is optimal in the sense that the compounded detection probability, $P=P_CP_D$ on a given interrogation, is a maximum.

In the analysis which follows, the region to be interrogated physically constitutes a cone which, if passive search is involved, is of indefinite altitude. In a more generalized sense, however, the search region is an n dimensional space, only some of whose coordinates are geometric, since, setting aside implementation factors, any *a priori* known signal characteristics may be used for filtering purposes in the detection process. Further, while the major portion of this discussion is confined to the uniform distribution of search over the indicated space volume, as will later be seen, it may be optimally allocated in such a manner as to maximize the signal energy or integration time over those subdomains in which the density of location of the contact is greatest.

In the case of uniformly distributed search, generally applicable theorems may be readily demonstrated. For example, if the area density distribution of the contact is determined over a sequence of discrete observations, the probability of a successful interrogation may be maximized by bounding the search field with an appropriate equidensity contour if, indeed, an optimum does exist. The author[3] discusses elsewhere the related problem when the cumulative probability of detection appears as the factor rather than the probability on a given interrogation. It is there shown that the compounded detection probability is greatest when $P_C=P_D$ if the inferred positional distribution of the contact across the search field is binormal. Further, it graphically displays the results of computations which quantitatively display the magnitude of the consequence of departures from the optimal search field. It is seen that large improvements can be effected through adjustment of the field if, but only if, a reasonable disparity exists between the optimal and given fields.

If the over-all interrogation time is fixed, and A is the angular region to be searched, the admissible integration time is inversely proportional to A so that, from the earlier analysis, $P_D = \exp(-KA)$. Accordingly,

$$P = P_CP_D = \int_0^{2\pi}\int_0^{r} f(\rho,\theta)\rho d\rho d\theta \cdot \exp\left[-\frac{K}{2}\int_0^{2\pi} r^2 d\theta\right], \tag{19}$$

where $f(\rho,\theta)\rho d\rho d\theta$ is the observation determined density function and $r\equiv r(\theta)$ is the required contour, each in polar coordinates. In practice, the functions involved are well-behaved, and the mathematical operations which follow are admissible. Utilizing the customary arguments of the calculus of variations, replacing r by $\tilde{r}=r+\beta\eta$, where $\eta\equiv\eta(\theta)$ is an arbitrary function, and forming $dP/d\beta$, the extremals are given by

$$0 = P_D\int_0^{2\pi} \eta f(r,\theta) r d\theta - P_CK\exp\left[-\frac{K}{2}\int_0^{2\pi} r^2 d\theta\right]\int_0^{2\pi} \eta r d\theta \tag{20}$$

[3] N. S. Potter, "The Controlled Rendezvous of Orbiting Space Stations," (#1483-60), Presented at Fifteenth Annual Meeting, American Rocket Society, Washington, D. C.; December, 1960.

or

$$0 = \int_0^{2\pi} \eta \{ P_D f(r, \theta) - P_C P_D K \} r d\theta. \tag{21}$$

The preceding may vanish for arbitrary η only in the event that the braketed factor is identically null. P_C and P_D are herein interpreted as the values assumed by these functions of r when it is optimally chosen. In any event, the resultant equation $f(r, \theta) = C$ defines an equiprobability contour from which, in theory, r may be found.

It may be formally shown by consideration of the second variation that the solution so defined is indeed a maximum if $\partial f/\partial r$ is negative. However, in that instance, the one most frequently encountered, it is immediately clear that it is a maximum since an equiprobability density contour then describes the minimal region, and thereby the greatest P_D, corresponding to a given containment probability. More generally, it may be shown that the minimal search field is always defined by such a contour when, by way of constraint, the probability of containment is specified. That is, proceeding essentially as above, but using the method of Lagrange to introduce the contraint, the extremals of

$$A = \int_0^{2\pi} r^2 d\theta, \qquad \text{given} P_C = \int_0^{2\pi} f(\rho, \theta) \rho d\rho d\theta \tag{22}$$

are defined as the zeros of

$$0 = \int_0^{2\pi} \eta r (2 - \lambda f(r, \theta)) d\theta, \tag{23}$$

where λ is an undetermined multiplier.

Optimally Programmed Nonuniform Search

The preceding analysis has been primarily concerned with search involving signals of reasonably moderate amplitude. However, factors other than the interplay of signal integration time and the size of the search field may be consequential. In particular, the totality of available search time may be a significant limiting factor. The minimization of the extent of the search interval, to reduce energy consumption, the likelihood of a reliability failure, or system delays, or the reduction of the amount of data to be processed given some meaningful data handling subsystem bandwidth limitation, are representative considerations.

Fixing the total amount of search expended in a given time interval by specifying n, the sum of the interrogations across every element of the field, n is the integral of the search pattern density function $S(\rho, \theta)$. Generally, the angular dimensions of the contact may be expected to be small compared to the scanner resolution unit, where the latter is assumed to be essentially differential in size, so that $S(\rho, \theta)$ is proportional to the expected number of interrogations across the object. The probability of achieving at least one detection, and therefore of accomplishing the acquisition is then $1 - \exp[-S(\rho, \theta)]$. The total probability P of effecting the acquisition is, therefore,

$$P = \int_0^{2\pi} \int_0^{\infty} [1 - e^{-S(\rho, \beta)}] f(\rho, \theta) \rho d\rho d\theta, \tag{24}$$

where $f(\rho, \theta)$ denotes the probability density with which the search field is distributed.

Mathematically stated, the problem is to select $S(\rho, \theta)$ such that, subject to the constraint that the total search involved is fixed, P is a maximum. By the method of Lagrange, the extremals of

$$P = \int_0^{2\pi} \int_0^{\infty} \{ [1 - e^{-S(\rho, \theta)}] f(\rho, \theta) - \lambda S(\rho, \theta) \} \rho d\rho d\theta \tag{25}$$

are required, in which λ is the undetermined multiplier. Forming the first variation by replacing $S(\rho, \theta)$ by $S(\rho, \theta) + \beta\eta(\rho, \theta)$, η being as before an arbitrary function, and equating $dP/d\beta|_{\beta=0}$ to zero, one must have $f(\rho, \theta) \exp(-S[\rho, \theta] = \lambda$, or $S(\rho, \theta) = \ln(f(\rho, \theta)/\lambda)$. Since $S(\rho, \theta)$ is a density function and therefore positive, $S(\rho, \theta)$ must vanish for $f(\rho, \theta) < \lambda$, where λ is determined by the constraint

$$n = \int_D \int \ln \left[\frac{f(\rho, \theta)}{\lambda} \right] \rho d\rho d\theta, \quad \text{or}$$

$$\lambda = \exp\left(-\frac{1}{A} \left[n - \int_D \int \ln f(\rho, \theta) \rho d\rho \right] \right), \tag{26}$$

the integral being taken over that portion of the plane D possessing area A for which the integrand is positive.

To quantitatively appraise this consideration, let it be assumed, as before, that the errors are normally and independently distributed in elevation and azimuth with equal standard deviations σ. Then,

$$f(\rho, \theta) = \frac{1}{2\pi\sigma^2} e^{-\rho^2/2\sigma^2},$$

$$S(\rho, \theta) = -\left\{ \frac{\rho^2}{2\sigma^2} + \ln(2\pi\lambda\sigma^2) \right\} \tag{27}$$

Assuming $2\pi\lambda\sigma^2$ will not exceed unity, the subdomain of the plane for which $S(\rho, \theta)$ is not identically null is the interior of the circle $\rho = \sigma \{ 2 \ln (2\pi\lambda\sigma^2)^{-1} \}^{1/2}$, or no extremal other than $S(\rho, \theta) = 0$ exists. The latter contradicts the constraint on the totality of search unless $n = 0$, and correctly corresponds, therefore, to the trivial minimum $P = 0$ in that instance. From

$$n = -\int_0^{2\pi} \int_0^{\sigma\sqrt{[2 \ln (2\pi\lambda\sigma^2)^{-1}]}} \cdot \left(\frac{\rho^2}{2\sigma^2} + \ln(2\pi\lambda\sigma^2) \right) \rho d\rho d\theta$$

$$= \frac{\pi\sigma^2}{2} \ln^2 (2\pi\lambda\sigma^2) \tag{28}$$

whence $\lambda = (2\pi\sigma^2 e^{(1/\sigma)\sqrt{(n/\pi)}})^{-1}$, and $S(\rho, \theta)$ is given by the two branch functions

$$S(\rho,\theta) = \begin{cases} \frac{1}{\sigma}\left(\sqrt{\frac{n}{\pi}} - \frac{\rho^2}{2\sigma}\right), & [0 \le \rho \le \sqrt{(2\sigma\sqrt{(n/\pi)})}] \\ 0, & [\sqrt{(2\sigma\sqrt{(n/\pi)})} < \rho]. \end{cases} \quad (29)$$

It follows that, as reason suggests, the greatest effort should be allocated to the region in the vicinity of the origin in which the probability density of location is greatest. Further, the desired optimal search effort is seen to decline parabolically to zero.

Substituting λ and the optimal $S(\rho, \theta)$ into (25), the greatest attainable P is found to be

$$P = P_C - e^{-n/A} \cdot \exp\left[\frac{1}{A}\int_D \int \ln f(\rho,\theta)\rho d\rho d\theta\right](A+n) \quad (30)$$

from which it is clear that, in the limit, as n gets large, P approaches P_S, where P_C is the probability that the contact is contained in the search field D.

Applying the preceding analysis, Potter[4] gives a quantitative, comparative evaluation of the case of binormally distributed errors, the results of which establish the fact that optimal uniform search is then very nearly as efficient as is the nonuniformly distributed programmed search discussed above. Since the flexible control of a complex search pattern may introduce substantial implementation problems, particularly with respect to data-handling subsystem bandwidth requirements, it may prove unattractive. One may therefore conclude that, in that instance, the adaptive behavior is best confined to the use of a variable size search field whose dimensions are continuously refined in accordance with the degree of confidence with which the statistics of the predicted position of the contact are regarded.

[4] N. S. Potter, "Guidance-control system integration in satellite rendezvous," *Proc. Natl. Aerospace Electronics Conf.*, Dayton, Ohio, May 8–10, 1961, pp. 428–435.

Conclusions

1) Marked optima exist in the distribution of search effort which can effect large improvements in the information rate concerning a contact or in the probability of retention of its track.
2) In the case of Rayleigh signal sources, the optimum sampling rates with which an extended space volume should be interrogated are readily ascertained and can be selected if the relative frequency of positive interrogations over some time interval is ascertained.
3) The rate of convergence to a stable probability of success on an individual interrogation is greatest if a search program characterized by a rapid sampling rate and a consequent low probability of probability of detection on the individual trial is employed.
4) Given the prior determination of the relative positional statistics of the contact, if an extremal exists the uniformly interrogated search field which is optimal in the sense that the product of the containment and detection probabilities is greatest is defined by an equiprobability density of location contour.
5) If a nonuniformly distributed search program is pursued and the errors are determined to be binormally, circularly distributed, the greatest effort should be allocated to the region in the vicinity of the center of the positional distribution, with a parabolic decline to zero in dwell time as the periphery of a bounding, circular region, whose radius is a function of the standard deviation, is approached.

Acknowledgment

The author appreciatively recognizes the assistance provided by the Maxson Electronics Corporation, in making the use of its personnel and facilities available from the preparation of the final paper.

The Design of a CW Passive Missile Trajectory Measuring System*

R. A. VOSS†

Summary—Several tests have provided data sufficient to demonstrate the feasibility of tracking missiles with a CW passive Doppler system. Initial experiments utilized a local television station as a target illuminator; later tests examined the capability of such a system as a terminal trajectory measuring device. These latter tests showed that the system could be designed to have a multiple-target capability.

An interim high-power system is being installed to determine if the techniques established for a low-power system can be extended to provide reliable coverage of White Sands Missile Range (WSMR). Some improvement of these techniques is anticipated, and, in addition, certain tests will employ spaced receivers operated as radio interferometers.

Introduction

A PASSIVE missile tracking system is here defined as one which requires a ground transmitter to illuminate the missile but does not require an airborne radiator or reradiator. A conventional monopulse radar operating in the skin track mode thus becomes a passive tracking system by this definition. An inherent advantage of a CW passive system, Doppler or interferometer, is high precision.

Passive systems have certain other advantages. Elimination of an active radiator or reradiator from the vehicle provides an obvious gain in system reliability, since phase-locked transponders, for example, are complex devices and operate in a very severe environment.

There appears to be a second significant advantage for systems in which a Doppler cycle count is accumulated from a single reference point. This advantage is that a spinning passive missile is not as likely to introduce extra cycles as is an active missile with anisotropic receiving and transmitting antenna patterns.

These advantages prompted the initiation of a study to investigate the feasibility of a CW passive missile tracking system. The purpose of this paper is to describe the tests which have demonstrated the feasibility of a passive Doppler system and to describe the interim high-power system now being installed, together with the planned tests utilizing this system.

System Parameters

Ideally, any missile tracking system should provide continuous, high-accuracy data from launch to impact. In effecting the design of a CW passive missile trajectory measuring system, many parameters must be examined to insure the fulfillment of this requirement. These are best described by considering the radar equation[1]

$$S = \left(\frac{PG}{4\pi R^2}\right)\left(\frac{\sigma}{4\pi R^2}\right)\left(\frac{G\lambda^2}{4\pi}\right). \tag{1}$$

In the case where the transmitter and receiver are separated, (1) becomes

$$S = \left(\frac{PG_t}{4\pi R_1^2}\right)\left(\frac{\sigma}{4\pi R_2^2}\right)\left(\frac{G_r\lambda^2}{4\pi}\right), \tag{2}$$

where

S = received signal power,
P = transmitter power,
G_t = gain of transmitting antenna,
G_r = gain of receiving antenna,
R_1 = distance between transmitter and target,
R_2 = distance between receiver and target,
σ = target cross section,
λ = wavelength.

To maximize the power incident on the receiving antenna, it is clear that the factors appearing in the numerator should be as large as possible, while those in the denominator are to be minimized. Thus, for example, the power radiated by the transmitting antenna is to be as high as practicable.

The selection of an optimum operating frequency is affected by several principal factors.[2] The effective capture area of the receiving antenna, given by the last parenthesized quantity appearing in (2), is inversely proportional to the square of the frequency. On this basis, the choice of a low operating frequency is indicated.

The signal-to-noise power ratio at the output of the receiver is obtained by multiplying (2) by g_0, the gain of the receiver, and dividing by $N = FgokTB$, the noise power at the receiver output. These operations yield the relation

$$\frac{S}{N} = \frac{PG_tG\sigma\lambda^2}{(4\pi)^3(R_1R_2)^2FkTB}. \tag{3}$$

Another reason for choosing a low operating frequency is demonstrated by (3); the receiver bandwidth, which must increase with frequency, because of correspondingly higher Doppler frequencies, should be minimized.

The equivalent black body temperature of cosmic and galactic noise incident on the receiving antenna is given by[3]

$$t_w = kf^{-2.3}. \tag{4}$$

* Received by the PGMIL, July 17, 1961.

† Electronic Trajectory Systems Branch, Range Instrumentation Dev. Div., Integrated Range Mission, White Sands Missile Range, New Mexico.

[1] L. Ridenour, Ed., "Radar System Engineering," M.I.T. Rad. Lab. Ser., McGraw-Hill Book Co., Inc., New York, N. Y., vol. 1, pp. 21 22; 1947.

[2] BRL Memo. Rept. No. 1220, pp. 78–87; July, 1959.

[3] *Ibid.*, p. 81.

This equation shows that t_w decreases rapidly with frequency. According to (3), it would seem that a high operating frequency might optimize S/N; however, more is lost by the decreased effective capture area than what is gained by the decreased noise temperature.

S/N is seen to decrease with receiver noise figure. Conventional vacuum tube preamplifiers having a noise figure of 2 db are the state-of-the-art; using parametric amplifiers, an improvement of 1 db is possible.[4]

In (3), σ is the radar cross section of the target. As might be expected, the problem of determining σ can be treated analytically in only a few simple cases; *i.e.*, where the target is a simple geometrical figure such as a sphere or a flat plate.[5] It is worthy of note, however, that for a given incident radiation and target configuration, a unique scattering pattern exists, even though it defies analytical treatment. The approach that will be taken here, for the purpose of designing a system, is to assign σ a value sufficiently small so that for the smallest target of interest the capability of the system will not have been overestimated. Such a value is on the order of 0.1 square meter.

The minimum usable S/N ratio is somewhat dependent on the modulation techniques employed; in practical system design, a value of 15 db is considered realistic.[6] If a phase-locked tracking filter is employed, assuming that a tracking bandwidth of 10 cps is adequate, a minimum S/N ratio of approximately -25 db is usable.[7]

Feasibility Tests

The tests conducted initially were designed only to demonstrate the feasibility of a passive Doppler system. A very modest receiver was constructed out of commercially available components; a block diagram of this equipment is shown in Fig. 1. A local television station was utilized as a target illuminator. Numerous recordings were made of signals reflected from aircraft operated near the receiver station. Data were also recorded on several missile firings; Fig. 2 is a portion of one such record. The strength of the reflected signals was on the order of 1 μv at the receiver input, $R_1 \approx 80{,}000$ m, and $R_2 \approx 8000$ m. More extensive tests using this system were not attempted, since using the TV station as a signal source permitted only limited coverage. The test results clearly indicated, however, that the system warranted further investigation.

Investigation of Terminal Trajectory Measuring Capability

After the completion of the feasibility tests, experiments were conducted to investigate the capability of a passive Doppler system used as a terminal trajectory measuring device. For these tests, a transmitter and one receiver, separated by 2370 m, were set up in an impact area. A block diagram of the equipment used in these tests, most of which had been previously used in the DORAN (DOppler RANging) system, is shown in Fig. 3.

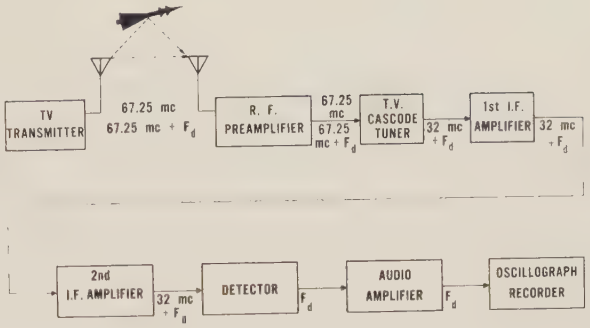

Fig. 1—Equipment used in feasibility tests.

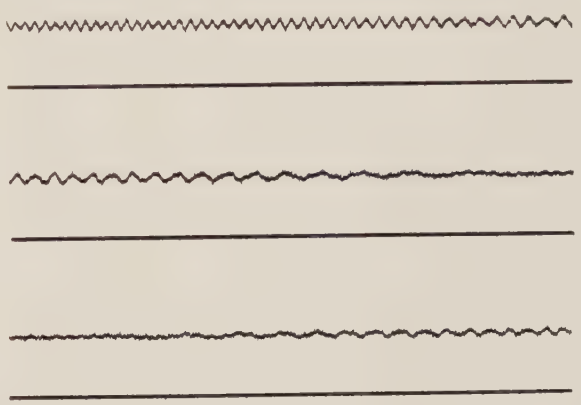

Fig. 2—Sample of Doppler data collected during feasibility tests.

The rate of change of phase difference between the direct signal from the transmitter and that reflected from the target (frequency difference) was recorded on several missiles during the terminal portions of their trajectories. A section of one such record is shown in Fig. 4. The Doppler cycle count was accumulated over one-second intervals; the loop range change during any given interval was calculated from the well-known relationship

$$\Delta L = \lambda n, \tag{5}$$

where

ΔL = loop range change,
λ = wavelength,
n = number of Doppler cycles recorded during the interval.

Comparisons made between these results and DOVAP (DOppler Velocity And Position) data are given in Fig. 5. The greater portion of the difference between the curves has been attributed to errors in the DOVAP system, which was subject to poor geometry and less favorable propagation paths than the passive system.

[4] BRL Tech. Note No. 1354, pp. 8–9; October, 1960.
[5] D. Kerr, Ed., "Propagation of Short Radio Waves," M.I.T. Rad. Lab., Ser., McGraw-Hill Book Co., Inc., New York, N. Y., vol. 13, pp. 445–470; 1951.
[6] L. P. Yeh, "Communicating in space," *Electronic Industries*, vol. 18, pp. 56–57; February, 1959.
[7] BRL Memo. Rept. No. 1173, pp. 5–6; October, 1958.

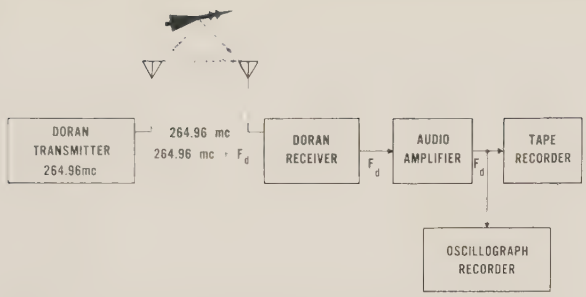

Fig. 3—Equipment used in terminal trajectory measurements.

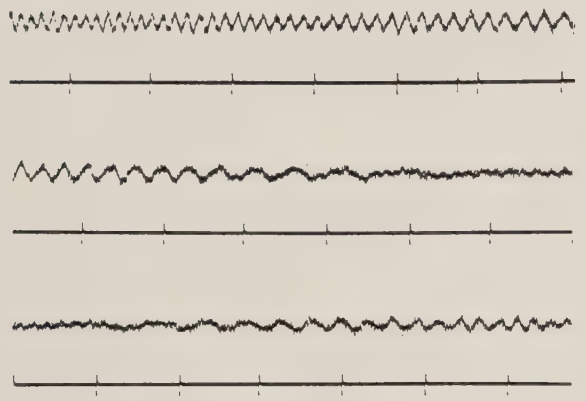

Fig. 4—Sample of Doppler data recorded during terminal trajectory experiments.

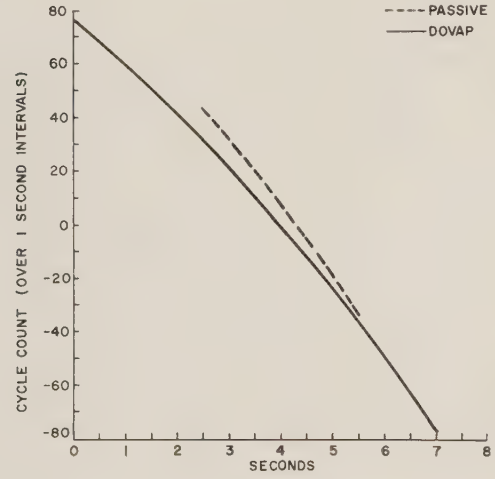

Fig. 5—Comparison of passive and DOVAP data.

Data were also collected on two missiles fired one second apart; Fig. 6 shows a portion of this record. Close inspection reveals the separate signals; it was found that a tracking filter could easily lock on either one. In addition, the passive Doppler data were not noticeably influenced by missile spin.

The conclusion based upon the results of the previous tests is that a passive Doppler system is feasible; further, that it can meet the requirements for a terminal trajectory measuring device, and that it has the capability of multiple-target tracking. The use of an interim high-power system, now being installed at WSMR, will serve

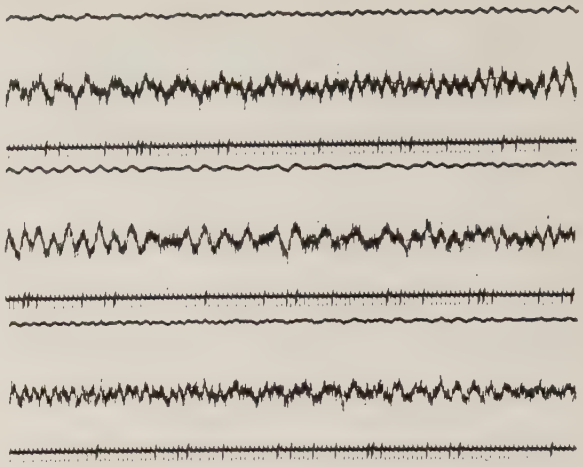

Fig. 6—Superimposition of two Doppler signals.

to extend the techniques developed in the more limited tests to the design of an operational passive Doppler system for the Range.

The Interim System

The target illuminator for the interim system is the 50-kw FM transmitter used previously in the BRL (Ballistic Research Laboratories, Aberdeen Proving Ground, Md.) DOPLOC (DOppler Phase LOCk) system. This transmitter is modified to provide an unmodulated CW output and will be operated at 108 Mc.

The Minitrack antennas, also used in the DOPLOC system, have been redesigned to provide suitable radiation patterns. Fig. 7 is a photograph of the antennas as they were used at Fort Sill, Oklahoma; a drawing of the antenna to be used in the interim system is shown in Fig. 8. Two of these arrays will provide adequate coverage. Radiation patterns, together with the equations on which the pattern computations were based, are presented in the Appendix.

A block diagram of the receiver is shown in Fig. 9. The IF signal, containing the Doppler information, is mixed with a locally generated bias frequency; and through detection action and suitable filtering, the output frequency of the receiver is made to be the sum of the bias and Doppler frequencies. This signal is then recorded on magnetic tape in a format acceptable to automatic cycle counting equipment used by the data reduction facilities at WSMR.

Previous tests have shown that the reflected signal is easily mixed with the direct signal from the transmitter in a single RF channel, yielding the Doppler output. With the present system, it is conceivable that the receiver would be located in a weak transmitter field. In such a situation, mixing the reflected signal with a locally generated signal having exactly the transmitter frequency would enhance receiver performance. At the present time, a receiver having a wide dynamic range, permitting operation in a strong transmitter field, is under development by BRL. This receiver will be considered for use in the passive system.

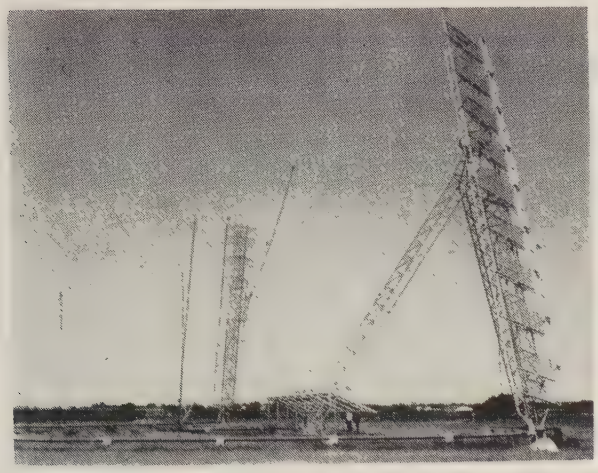

Fig. 7—Minitrack antennas.

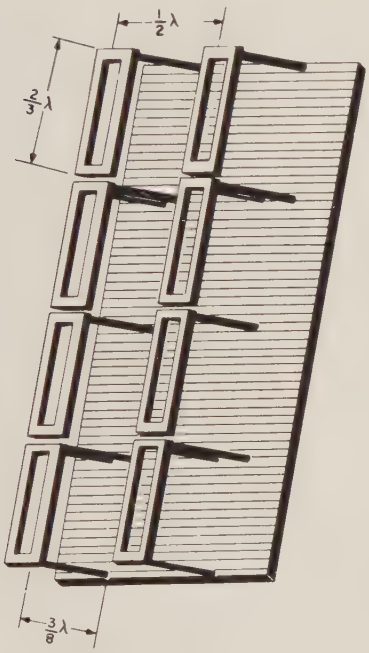

Fig. 8—Interim system transmitting antenna.

The range capability of the system as a function of target cross section can be determined by solving (3) for R_1R_2.

$$R_1R_2 = \left[\frac{PG_tG_r\lambda^2\sigma}{(4\pi)^3FkTB(S/N)}\right]^{1/2}. \qquad (6)$$

For the interim system, this equation reduces to

$$R_1R_2 = 2.9 \times 10^{11}\sqrt{\sigma} \qquad (m^2). \qquad (7)$$

A plot of R_1R_2 vs σ is shown in Fig. 10.

A few tests will be devoted to an investigation of a passive interferometer-type system. Measurement of the phase difference between the reflected signals arriving at two spaced receivers will provide target direction.

Conclusions

Initial tests have proven the feasibility of a passive Doppler system for missile tracking; further, that data

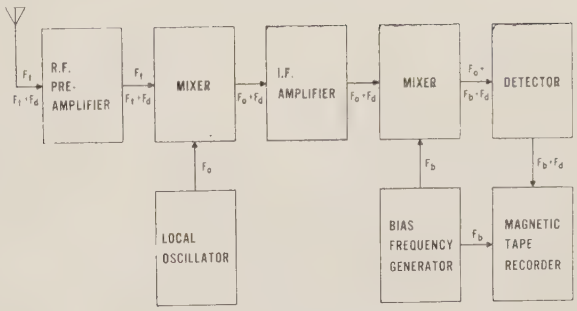

Fig. 9—Interim system receiver.

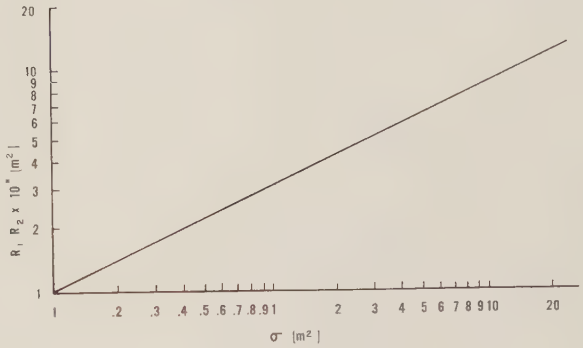

Fig. 10—Range product vs target cross section.

are not appreciably affected by missile spin, and that such a system has multiple-target tracking capability.

Future tests will investigate the workability of a passive interferometer system and will also serve to extend the techniques established in the earlier tests.

The advantages of a passive system are increased reliability and high precision. The major drawback of the system is the high transmitter power that is required.

The product of the effort will be the detailed specifications for an operational CW passive trajectory measuring system.

Appendix

Antenna Array Design

The relative field strength pattern for a rectangular array consisting of a number of identical radiators equally spaced along the x, y, and z axes, carrying equal currents, with constant phase difference between adjacent radiators along any one axis, can be described by[8]

relative field strength

$$= R\left|\frac{\sin\left[n\pi(a\cos\phi\cos\theta + b)\right]}{n\sin\left[\pi(a\cos\phi\cos\theta + b)\right]}\right.$$
$$\cdot\frac{\sin\left[N\pi(A\sin\phi\cos\theta + B)\right]}{N\sin\left[\pi(A\sin\phi\cos\theta + B)\right]}$$
$$\left.\cdot\frac{\sin\left[\eta\pi(\alpha\sin\theta + \beta)\right]}{\eta\sin\left[\pi\alpha\sin\theta + \beta)\right]}\right|. \qquad (8)$$

[8] F. E. Terman, "Radio Engineers' Handbook," McGraw-Hill Book Co., Inc., New York, N. Y., pp. 797–798; 1943.

where

n, N, η = number of radiators along the x, y, and z axes, respectively.
a, A, α = radiator spacing (in wavelengths) along x, y, and z axes, respectively.
b, B, β = phase difference (in cyles) between radiators along x, y, z, respectively.
θ = angle with respect to xy plane.
ϕ = angle with respect to xz plane

In accordance with the method of images, the effect of the ground screen, as shown in Fig. 11, is to produce

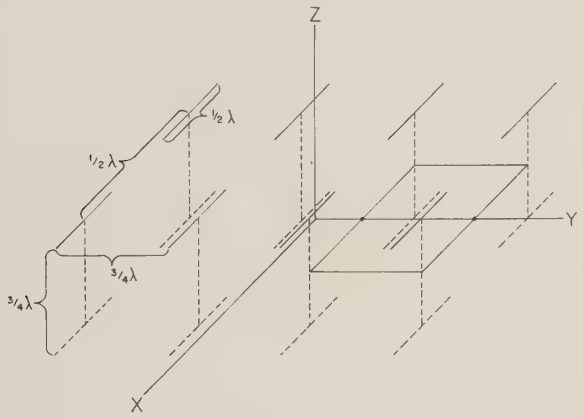

Fig. 11—Equivalent dipole configuration.

an image array of radiators the same distance below the screen as the actual radiators are above it. Moreover, the phase difference between the currents in the image and real radiators is 180°. Setting

$$\begin{array}{lll} n = 2 & N = 4 & \eta = 2 \\ a = 1/2 & A = 3/4 & \alpha = 3/4 \\ b = 0 & B = 0 & \beta = 1/2, \end{array}$$

(8) reduces to

relative field strength

$$= R\left|\frac{\sin\left[\pi\cos\phi\cos\theta\right]}{2\sin\left[\frac{\pi}{2}\cos\phi\cos\theta\right]}\cdot\frac{\sin\left[3\pi\sin\phi\cos\theta\right]}{4\sin\left[3\frac{\pi}{4}\sin\phi\cos\theta\right]}\cdot\frac{\sin\left[\pi\left(\frac{3}{2}\sin\theta+1\right)\right]}{2\sin\left[\frac{\pi}{2}\left(3\sin\theta+1\right)\right]}\right| \tag{9}$$

The individual radiators composing the array are slot antennas. Representing these by equivalent $\lambda/2$ dipoles, the radiation patterns in the xz and yz planes are given, respectively, by (10) and (11).

Relative field strength

$$= \frac{\sqrt{2}\cos\left(\frac{\pi}{2}\cos\theta\right)}{4\sin\theta}\cdot\left|\frac{\sin\left(\pi\cos\theta\right)}{\sin\left(\frac{\pi}{2}\cos\theta\right)}\cdot\frac{\sin\left[\pi\left(\frac{3}{2}\sin\theta+1\right)\right]}{\sin\left[\frac{\pi}{2}\left(\frac{3}{2}\sin\theta+1\right)\right]}\right| \tag{10}$$

relative field strength

$$= \frac{\sqrt{2}\sin\left(3\pi\cos\theta\right)}{8\sin\left(3\frac{\pi}{4}\cos\theta\right)}\cdot\frac{\sin\left[\pi\left(\frac{3}{2}\sin\theta+1\right)\right]}{\sin\left[\frac{\pi}{2}\left(\frac{3}{2}\sin\theta+1\right)\right]}. \tag{11}$$

Plots of these equations are shown in Figs. 12 and 13.

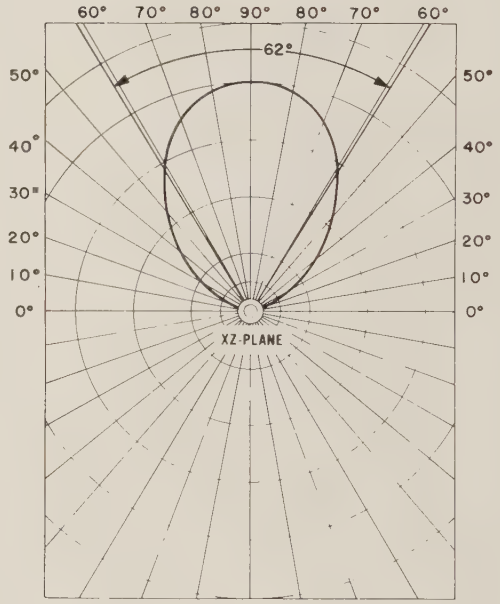

Fig. 12—Relative field strength pattern in xz plane.

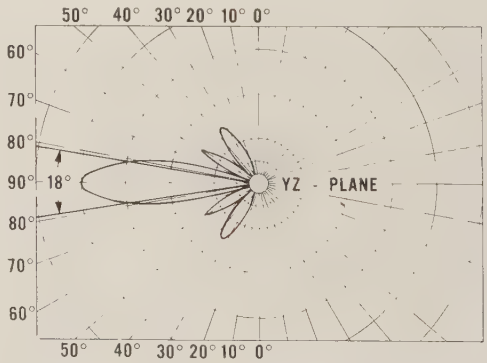

Fig. 13—Relative field strength pattern in yz plane.

Acknowledgment

The author wishes to acknowledge the contributions of R. H. Paul who critically reviewed the draft and of C. W. Williston who formulated the approach to design and directed the project until January, 1961.

Contributors

Keith E. Bailey was born in Winfield, Kan., on April 7, 1924. He received the Naval Aviator Wings and commission in January, 1945. He has performed duties in carrier-based fighter squadrons, air transport squadrons, and airborne early-warning squadrons. Also, he has been a flight instructor in the Naval Air Advanded Training Command.

K. E. Bailey

Upon his graduation from the Naval War College in 1957, he was assigned to the Range Operations Department at Pacific Missile Range Headquarters, Point Mugu, Calif. During the year in this billet, he completed the Pan American Manager's Course at Cape Canaveral and was the Range Operations Liaison Officer for USAF projects conducting operations in the Pacific Missile Range.

In June, 1958, LCDR Bailey was transferred to the Pacific Missile Range Staff as a Missile Fight Safety Officer in the Range Safety Office. His major projects during the past two years have been the Atlas/Agena Satellite System, Atlas ICBM, and Titan ICBM. The primary role in these projects is to conduct the range-safety functions during the countdown, monitor the missile flight, and destroy the missile should it become necessary.

❖

Richard C. Barbera was born in Boston, Mass., on March 26, 1929. He received the B.S. degree in physics from Massachusetts Institute of Technology, Cambridge, in 1948, and the M.A. degree in physics in 1950 from Bryn Mawr College, Bryn Mawr, Pa.

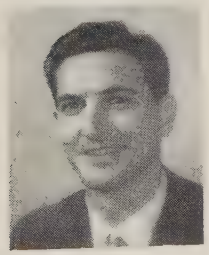

R. C. Barbera

From 1948 to 1950 he was an Instructor in freshman and sophomore laboratory physics at Bryn Mawr College, Bryn Mawr, Pa. From 1950 to 1953 he was Associate Spectroscopist at the University of California at Los Angeles Medical School, where he engaged in infrared absorption and emission spectrographic analyses of biological and mineral samples for assessment of damage due to atomic blasts, radiation and heat. From 1954 to 1956, as a physicist with Tracerlab, Waltham, Mass., he worked on the design and construction of very-high-sensitivity mass spectrometers for heavy-element isotope analysis, and the development of infrared spectroscopic techniques for analysis of deuterated compounds. Since 1956 he has been a Senior Engineer with Raytheon Company, Bedford, Mass., where he has been engaged in the design and evaluation of infrared and optical systems for air to air missiles, AICBM applications, infantry and naval warfare.

Mr. Barbera is a member of Sigma Xi and IRIS.

❖

Richard B. Barrar (M'57) was born in Dayton, Ohio, on October 12, 1923. He received the B.S. and M.S. degrees in physics in 1947 and 1948, respectively, and the Ph.D. degree in mathematics in 1952, all from the University of Michigan, Ann Arbor.

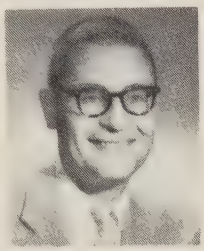

R. B. Barrar

From 1954 through 1957 Dr. Barrar was with the Hughes Aircraft Company, Culver City, Calif. working on electromagnetic theory and antenna and radome design and theory. In 1957 he joined the Hoffman Electronics Corporation, Los Angeles, Calif., where he was engaged in the design of antennas for meteor scattering. Since 1958 he has been with the System Development Corporation, Santa Monica, Calif., applying large-scale digital computers to the solution of physical problems, mainly in the calculation of satellite trajectories.

Dr. Barrar is a member of Sigma Xi, Phi Kappa Phi, the Society for Industrial and Applied Mathematics and the American Mathematical Society.

❖

David K. Barton (S'49–A'50–M'55–SM'59) was born in Greenwich, Conn., on September 21, 1927. He received the B.A. degree in physics from Harvard University, Cambridge, Mass., in 1949.

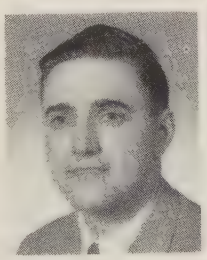

D. K. Barton

From 1949 to 1953 he worked as an electronic engineer with the White Sands Signal Corps Agency in the planning, development and installation of the radar system used in tracking of guided missiles at the White Sands Proving Ground, White Sands, N. Mex. From 1953 to 1955 he was a project engineer with Evans Signal Laboratory in Belmar, N. J., responsible for development contracts on radar beacons and related equipment. In 1955 he assumed his present position as a systems engineer with the RCA Missile and Surface Radar Department in Moorestown, N. J. He has worked on system design and evaluation of several modern search and tracking radars, including the AN/UPS-1, AN/FPS-16, and the AN/FPS-49 tracker for the BMEWS system. In 1958 he received the David W. Sarnoff award for outstanding achievement in engineering, based upon his contributions to precision tracking radar. He has presented papers at national conventions and symposia and was one of the principal lecturers at the 1960 and 1961 Special Summer Course in Modern Radar Techniques, sponsored by the Moore School of Electrical Engineering of the University of Pennsylvania, Philadelphia.

❖

Randolph A. Becker was born in Bowler, Wis., on December 29, 1924. He received the B.S. degree in physics in 1949, and the M.S. degree in physics in 1953, both from the Texas College of Arts and Industries, Kingsville, Tex.

R. A. Becker

In 1950 he was associated briefly with the Department of Astronomy at the University of Chicago, Chicago, Ill., serving as an observing assistant on the 82-inch telescope at the McDonald Observatory, Fort Davis, Tex. In October, 1950, he entered the field of missile instrumentation at White Sands Missile Range, White Sands, N. Mex. In January, 1957, he took charge of the Optical Research Section of the newly formed Range Instrumentation Development Division at WSMR. His work has been concerned with research on long-range visibility of missiles and satellites, optical turbulence, and television and infrared applications to missile instrumentation. He was a co recipient of a WSMR Special Act or Service Award for studies performed on Nike-Zeus instrumentation problems. In 1961, he was employed as a Senior Research Engineer with the Space Optics Group, Jet Propulsion Laboratory, California Institute of Technology, Pasadena.

Mr. Becker is a member of the Optical Society of America.

❖

Gus F. Bigelow (M'58) was born in El Paso, Tex., on July 16, 1932. He received the B.S.E.E. degree from Texas Western College, El Paso, in 1953.

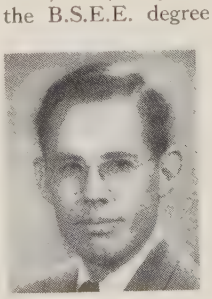

G. F. Bigelow

After graduation he joined the Sperry Gyroscope Company, Great Neck, N. Y., in the Missile Test and Analysis Group.

Since 1954 he has been with the White Sands Missile Range, White Sands, N. Mex., where he has

been engaged in radar and telemetry instrumentation development and research, and where he is presently Chief of Telemetry Research Section.

❖

Robert D. Coleman was born in Lubbock, Texas, on March 6, 1931. He received the B.S.E.E. degree from Texas Technological College, Lubbock, in 1956.

R. D. Coleman

He has been employed since 1956 at the Naval Ordnance Test Station, China Lake, Calif., where his work has included electronic circuit design, servomechanism analysis and analog-computer simulation studies. Since 1958 he has been engaged in the electronic and logical design of digital computer systems for the Data Automation Branch of the Station.

Mr. Coleman is a member of Kappa Mu Epsilon and Tau Beta Pi.

❖

Richard A. Enstrom was born in Pittsburgh, Pa., on March 4, 1930. He received the B.A. degree in mathematics from Washington and Jefferson College, Washington, Pa., in 1952.

R. A. Enstrom

After serving for four years as an electronic technician in the U. S. Navy, he joined Westinghouse Electric Company, Baltimore, Md., in 1956 in the Systems and Analysis Section of Radar Engineering, where he has been engaged in the mathematical analysis of problems arising in the design of radar systems.

❖

Ralph Deutsch (S'41–A'43–SM'54) was born in Boston, Mass., on November 17, 1919. He received the B.S. degree in physics and the M.A. degree in mathematics from the University of Michigan, Ann Arbor, in 1941 and 1950, respectively, and the M.S. degree in physics from George Washington University, Washington, D. C. in 1947.

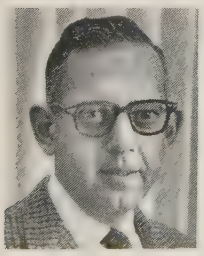

R. Deutsch

He has worked as an applied physicist in radar system research and development at the Naval Research Laboratory, Washington, D. C., the National Bureau of Standards, Washington, D. C., and Sperry Gyroscope Corporation, Great Neck, N. Y. From 1948 to 1952 he served on the Electrical Engineering faculty of the University of Michigan, and headed a Noise and Information Theory Group at the Willow Run Laboratories, Ann Arbor, Mich. In 1952 he joined the Hughes Aircraft Company, Culver City, Calif., where he worked on the application of statistical communication theory to radar system development. Concurrent, he was a lecturer at the University of Southern California, Los Angeles, conducting graduate courses in mathematics and electrical engineering. He was employed by the Philco Research Laboratories, Philadelphia, Pa., in 1957, as research manager for advanced system techniques. In 1958 he joined the System Development Corporation where he was engaged in research on space sciences. He is now a member of the technical staff of the Space Systems Division, Hughes Aircraft Co.

Mr. Deutsch is a member of the American Mathematical Society.

❖

J. N. Faraone (M'60) was born in Berwyn, Ill., on April 5, 1930. He received the B.S.E.E. and M.S.E.E. degrees from the Illinois Institute of Technology, Chicago, in 1951 and 1958, respectively.

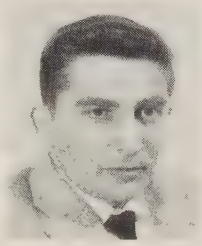

J. N. Faraone

From 1951 to 1954 he was with the Bell Aircraft Corporation, Buffalo, N. Y., and then served two years in the U. S. Army. In 1956 he joined the Armour Research Foundation of the Illinois Institute of Technology, Chicago, where he is Supervisor of the Communications and Radar Section. His major work has been in the field of radar and guidance systems.

Mr. Faraone is a member of Tau Beta Pi and Eta Kappa Nu.

❖

David Fryberger (M'59) was born in Duluth, Minn., on February 22, 1931. He received the B.E. degree in electrical engineering from Yale University, New Haven, Conn., in 1953.

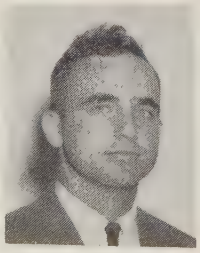

D. Fryberger

In 1954 he joined a carrier-based airborne early-warning squadron where he remained for three years as an electronics officer in charge of operation and maintenance of airborne radar systems. After joining the Armour Research Foundation, Chicago, Ill., he participated in the design of instrumentation for the measurement of low-level RF power and voltage. He has also performed theoretical analyses upon the feasibility of determining profiles of temperature and water vapor vs height from ground measurements. At the present time he is project engineer for a study of atmospheric electricity.

Mr. Fryberger is a member of Tau Beta Pi and an associate member of Sigma Xi.

❖

T. Burr Jackson (SM'55) was born in Penn Yan, N. Y., on January 4, 1919. He received the B.S.E.E. degree from Tri-State College, Angola, Ind., in 1941.

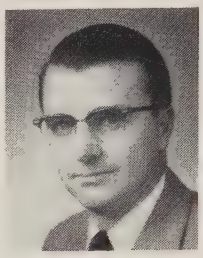

T. B. Jackson

From 1941 to 1942 he was employed by the Eastman Kodak Company, Rochester, N. Y., where he worked on the development of automatic electronic measurement and control equipment related to film processing. He joined the Centimeter Wave Research Section of the U. S. Naval Research Laboratory, Washington, D. C., in June, 1942, and was assigned to the design and development of radar display and control equipment. He became Head of the Indicator Group in 1944, and in 1947 participated in the NRL eclipse expedition into the South Atlantic. In 1948 he transferred to the Instrumentation Division, National Bureau of Standards, Washington, D. C., to become Head of the Telemetry Group, and in 1951 moved with the division to the Corona, Calif., facility of the National Bureau of Standards. The facility was in turn transferred to the Navy in 1952 and became known as the Naval Ordnance Laboratory, Corona, Calif. He was appointed Head, Instrument Application Branch, and Assistant Head, Instrumentation Division, NOLC, in 1952. He has been responsible for the planning and coordination of projects involving the design, development, packaging, evaluation and application of telemetry and automatic data-reduction systems, and is presently working actively in the coordination of telemetry changeover from VHF to UHF operation.

❖

Sidney Kazel (S'54–A'55) was born in Chicago, Ill., on June 22, 1930. He received the A.B. degree from the University of Chicago in 1950, the B.S.E.E. degree from the Illinois Institute of Technology, Chicago, in 1953, and the M.S.E.E. degree from Stanford University, Stanford, Calif., in 1954.

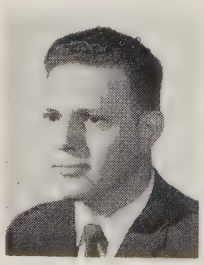

S. Kazel

He has been employed by the Armour Research Foundation of the Illinois

Institute of Technology since 1954, where he has been engaged in the fields of communications and radar theory.

Mr. Kazel is a member of Eta Kappa Nu and Tau Beta Pi.

❖

Robert T. Merriam (A'49–M'57–SM'59) was born in Phoenix, Ariz., on April 23, 1908. He attended the School of Science and Technology, Pratt Institute, Brooklyn, N. Y., from 1933 to 1935.

R. T. Merriam

He has been active in radio communications and electronics since 1927, and in guided-missile telemetry since 1945. From 1945 to 1947, he was a staff assistant in the Telemetry Group at the Applied Physics Laboratory, the Johns Hopkins University, Silver Spring, Md. In 1947, he transferred to the Test Department of the Naval Ordnance Test Station, China Lake, Calif. Since 1956 he has been a member of the Telemetry Working Group of the Inter-Range Instrumentation Group, serving in 1958 as Chairman and in 1961 as Vice Chairman. At present he is Head of the Timing-Telemetry Branch, Test Department, NOTS.

He is a senior member of the Instrumentation Society of America.

❖

Allan R. Metzler was born in Fresno, Calif., on May 15, 1930. He received the B.S. degree in physics from Fresno State College in 1952, then did postgraduate work at the University of Maryland, College Park, until 1955.

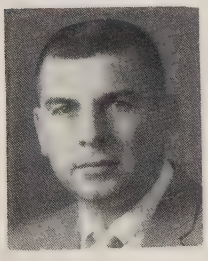

A. R. Metzler

He has been a physicist with the U. S. Government for the past ten years, with the exception of three years of active duty as a Naval officer in diving, underwater photography, and project work. His entire professional career has been concerned with various phases of missile component design and testing, underwater instrumentation, and underwater weapons testing. Recent work of particular interest has been the over-all design philosophy, coordination, and installation of the modified underwater range instrumentation and control complex at San Clemente Island, which culminated in the first successful Polaris live missile firing.

He was associated with the National Bureau of Standards, Washington, D. C., from 1951 to 1953, and the Diamond Ordnance Fuze Laboratory, Washington, D. C., from 1953 to 1955. From 1956 to 1958, he was a Lieutenant in the U. S. Navy stationed at the Naval Photographic Center, Anacostia, D. C. He is presently the Senior Member of the Range Instrumentation Development Branch (Test Department) of the U. S. Naval Ordnance Test Station at Pasadena, Calif.

Mr. Metzler is a member of the Society of Photographic Scientists and Engineers.

❖

William E. Mimmack was born in Eaton, Colo., on August 22, 1926. He received the B.A. degree in physics from the University of Colorado, Boulder, in 1950 and did graduate work at the University of New Mexico, Albuquerque.

W. E. Mimmack

He served with the U. S. Navy from 1944 to 1946. Since 1950 he has been employed with the White Sands Missile Range, N. Mex. He is now a Supervisory Physicist in the Optical Systems Branch of the Range Instrumentation Development Division.

Mr. Mimmack is a member of Sigma Pi Sigma, Alpha Chi Sigma, the American Physical Society and the AAAS.

❖

Jan K. Moller (SM'57) was born in Stockholm, Sweden, on March 25, 1920. He received the M.S.E.E. degree from the Royal Institute of Technology, University of Stockholm, Sweden, in 1945.

J. K. Moller

From 1945 to 1950 he was employed by the Standard Radio Corporation (Swedish ITT subsidiary) in Stockholm as a design engineer. After settling in the United States in 1950, he served as an Electronics Production Engineer with the Philco Corporation and the Electronics Division of the National Cash Register Company until 1955. He then joined Litton Industries at their main branch in Beverly Hills, Calif., to organize instrumentation and environmental laboratory facilities.

Entering the missile systems field in 1958, he was with Space Technology Laboratories until 1960, when he helped form the Space Systems Technology Group of the Siegler Corporation, Inglewood, Calif.

Mr. Moller is a member of the Swedish Association of Engineers and Architects.

❖

Norman S. Potter (SM'58) was born in New York, N. Y., on November 5, 1926. He received his undergraduate training at Brooklyn College, Brooklyn, N. Y., and at the U. S. Naval Academy, Annapolis, Md., where he studied marine and electrical engineering. He received the B.A. degree in mathematical physics from Brooklyn College in 1945, and the M.S. degree in applied mathematics and physics from Massachusetts Institute of Technology, Cambridge, in 1953. He continued supplementary studies at M.I.T. and Columbia University, New York, N. Y., for the Ph.D. degree.

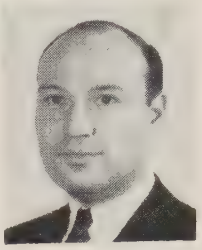

N. S. Potter

As a member of the research staff of Columbia University, he was associated with the Manhattan Project, where he performed analytic studies in radiation propagation. Later, as a member of the research staff of the Department of Electrical Engineering at M.I.T., he worked for some years on SAGE system development, electron digital-computer logic, data-handling in real-time problems, advanced target acquisition techniques, and general air defense systems analyses. Following this, he was affiliated with The Martin Company for several years as a Senior Engineer in the field of advanced design, with primary responsibility for systems studies in several categories of missiles, airborne fire-control systems, missile-guidance techniques, and the analysis of composite airborne electronics subsystems.

He then served as a consultant at USAF Headquarters in Europe in the field of technical evaluation of foreign airborne weapons systems. Following his return from Europe, he was with the Air Arm Division of Westinghouse, Baltimore, Md., where for several years as a Fellow Engineer and Weapons Systems Group Leader he had primary responsibility for systems analyses and development in air-launched guided missiles, bomber detection and penetration techniques, airborne early-warning and interceptor-borne detection and tracking equipments, advanced automatic acquisition techniques in discrete data systems, and operations analysis in large-scale air defense system evaluations.

For some years he was engaged as a consultant on guided missiles systems to the Assistant Chief of Staff, Intelligence, Department of the Army, and is now affiliated with the Maxson Electronics Corporation, New York, N. Y. Initially Manager of the Weapons Systems Research Laboratory, he is now Manager of Systems Analysis, in which capacity he is concerned with advanced systems studies in all phases of military and industrial electronics.

He is a member of the AAAS, ARS, and the IAS.

❖

Frank L. Rees was born in London, England, on November 13, 1931. He received a Higher National Certificate (equivalent to B.S.E.E.) from the South East Essex Technical College, England, in 1954, and is at present completing his M.S. thesis in mathematics at the University of Maryland, College Park.

From 1948 to 1950 he was at the General Post Office, Telecommunications Section, London, England, working on land line repeaters. The next two years were spent in the Royal Air Force, where he was engaged in radar engineering. He then joined Kelvin and Hughes, at their Marine Radar Laboratories, Barkingside, Essex, England, where, until February, 1957, he worked as a Senior Engineer, on microwave equipment and IF receivers. In February, 1957, he joined the Electronics Division of Westinghouse Electric Corporation, Baltimore, Md., and worked, until June, 1958, on a Doppler height-finder channel for a ground radar system. He was then transferred, as a Senior Engineer, to the Radar Systems Development and Analysis Section, where, in April, 1960, he became a Fellow Engineer. His interests are in the area of applied mathematics, in particular, probability calculus and information theory as applied to radar.

F. L. Rees

Mr. Rees is an associate member of the IEE.

❖

Kuno M. Roehr (M'60) was born in Berlin, Germany, on February 9, 1931. He received the Dipl. Ing. degree from the Technische Hochschule, Stuttgart, Germany, in 1956.

K. M. Roehr

He joined the Standard Electric Lorenz A.G. in 1956, where he was involved in the design of a magnetic drum-read system, and circuit and logical design for the ER-56 Computer.

Since December, 1958, he has been with the U. S. Naval Ordnance Test Station, China Lake, Calif. He is responsible for the advanced development of data acquisition equipment for the Naval Ordnance Data Automation Center.

❖

Eugene F. Uretz was born in Chicago, Ill., on February 13, 1929. He received the B.S.E.E. degree from the Illinois Institute of Technology, Chicago, in 1957, and the B.S. and M.A. degrees in mathematics from the University of Chicago, Chicago, Ill., in 1950 and 1951, respectively.

E. F. Uretz

For the past five years he has been employed by the Armour Research Foundation, Chicago, Ill., where he has been working on the development and analysis of systems. Prior to joining the Foundation, he worked for two years as a mathematician at the Ballistics Research Laboratories of Aberdeen Proving Ground, Md.

Mr. Uretz is a member of Eta Kappa Nu and Tau Beta Pi.

❖

Robert A. Voss was born in Davenport, Iowa, on February 14, 1935. He received the B.A. degree in physics and mathematics from Augustana College, Rock Island, Ill., in 1957, and is currently doing graduate work in physics at the New Mexico State University, Las Cruces.

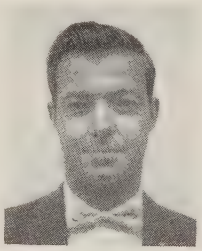

R. A. Voss

He has been associated with the Range Instrumentation Development Division (RID), Integrated Range Mission, White Sands Missile Range, White Sands, N. Mex., since 1957. As a member of the Electronic Trajectory Systems Branch of RID, he has been concerned primarily with the development of trajectory measuring systems.

❖

Edward C. Watters was born in Monroe, Mich., on February 16, 1923. He received the B.S.E.E. degree in 1943, and the M.S. degree in mathematics in 1946, both from the University of Notre Dame, South Bend, Ind. He obtained the Ph.D. degree in mathematics from the University of Maryland, College Park, in 1954, while working as an Assistant Professor of Mathematics at the U. S. Naval Academy, Annapolis, Md.

In 1957 he joined the Electronics Division of Westinghouse Electric Corporation, Baltimore, Md., as a Fellow Engineer in Radar Engineering. A year later he was promoted to supervisor in charge of the Radar Analysis group. In 1959 he was made an Advisory Engineer.

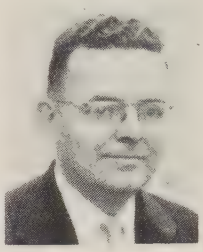

E. C. Watters

Dr. Watters is a member of the American Association of University Professors and The Mathematical Association of America.

❖

Robert Wisnieff was born in Yonkers, N. Y., on May 8, 1924. He received the B.S. degree in engineering physics from the College of Engineering, New York University, N. Y., in 1948, and the M.A. degree in physics from Columbia University, New York, N. Y., in 1950. He is presently a candidate for the M.S. degree in electrical engineering at N.Y.U.

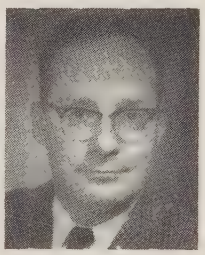

R. Wisnieff

During World War II, he had several years experience as a Crew Chief of U. S. Army Weather Service Radar and Electronic Weather Observation Stations. He also served as a Graduate Assistant at New York University, where he was engaged in developing instrumentation for automatically recording the growth of chromatograms.

In 1951 he joined Norden Division of United Aircraft Corporation, Norwalk, Conn., where he is presently head of the Tracking and Detection Section, Television and Infrared Branch. His contributions have included the design of a high-precision optical system for transmitting angular information about a line of sight, as required in accurate aligning systems and torsion-flexure monitoring. He was responsible for the infrared detection and tracking components of a combined infrared and radar bombing system. Currently he is technically cognizant for the development of the Automatic Television Tracking System.

Mr. Wisnieff is a member of the American Physical Society and Eta Kappa Nu.

Index to

IRE TRANSACTIONS

ON

MILITARY ELECTRONICS

VOLUME MIL 5, 1961

IRE Transactions on Military Electronics

Index to Volume MIL-5, 1961

Contents

Index to Authors

Index to Subjects

INFORMATION FOR AUTHORS

The PGMIL TRANSACTIONS is intended to bridge the gap between the various disciplines contributing to military electronics. Since this includes most of the branches of electronics, of the military services, and of the many fields which are associated with but not actually within the realm of electronics, it is essential that the papers published be of broad interest. The emphasis should be on readable, thought-provoking material that stimulates an attitude of open-mindedness and curiosity.

The major portion of the PGMIL TRANSACTIONS publication program is in the form of special issues designed to bring together the technical achievements of one field or by one group of workers. Topics and guest editors for forthcoming issues are announced regularly nine months in advance of the publication date. Each issue is open to contributions from anyone working in the area covered by that issue. Detailed abstracts of all contributed papers must be submitted for review at least eight weeks prior to the manuscript deadline. Abstracts and manuscripts should be sent in duplicate directly to the guest editor in charge of the issue of interest. Standard IRE practice should be followed in preparation of the manuscript and illustrations. Each manuscript should include a carefully prepared summary of not more than 200 words.

Suggestions are earnestly solicited from the membership on topics for future issues of the PGMIL TRANSACTIONS. Suggested topics should be sent to the PGMIL TRANSACTIONS Editor, Donald R. Rhodes, Radiation Incorporated, P.O. Box 37, Melbourne, Fla.

PUBLICATION SCHEDULE

Publication Date	*Topic*	*Guest Editor*	*Manuscript Deadline*
January, 1962	"Direct Energy Conversion" Processes and devices: photoelectricity, thermoelectricity, thermionics, fuel cells, galvanic batteries, magneto hydrodynamics.	Mr. G. B. Wareham Office of Fuels, Materials, and Ordnance Office of Director of Defense Research and Engineering Washington 25, D. C.	October 1, 1961
April, 1962	"Signal Processing Radar Systems" Electronic scanning, pulse compression, track-while-scan, phased arrays, MTI, monopulse, velocity scanning, Doppler navigation, pseudo-noise modulation.	Dr. A. W. Sissom Radiation Incorporated P. O. Box 37 Melbourne, Fla.	December 1, 1961
July, 1962	"Automatic Testing Techniques" Present and future techniques for automated testing of electronic components, assemblies, and systems.	Mr. D. B. Dobson Systems Support Projects Defense Electronic Products Radio Corp. of America Camden 2, N. J.	March 1, 1962

INSTITUTIONAL LISTINGS

The IRE Professional Group on Military Electronics is grateful for the assistance given by the firms listed below, and invites application for Institutional Listings from other firms interested in the field of Military Electronics

PHILCO CORP., Government and Industrial Div., 4700 Wissahickon Ave., Philadelphia 44, Pa.
Data Processing Systems, Space Communications, Satellites, Radar, Microwave ASW, Guided Missiles

The charge for an Institutional Listing is $75.00 per issue or $225.00 for four consecutive issues. Applications for Institutional Listings and checks (made out to The Institute of Radio Engineers, Inc.) should be sent to L. G. Cumming, Professional Groups Secretary, Institute of Radio Engineers, 1 East 79 Street, New York 21, N. Y.